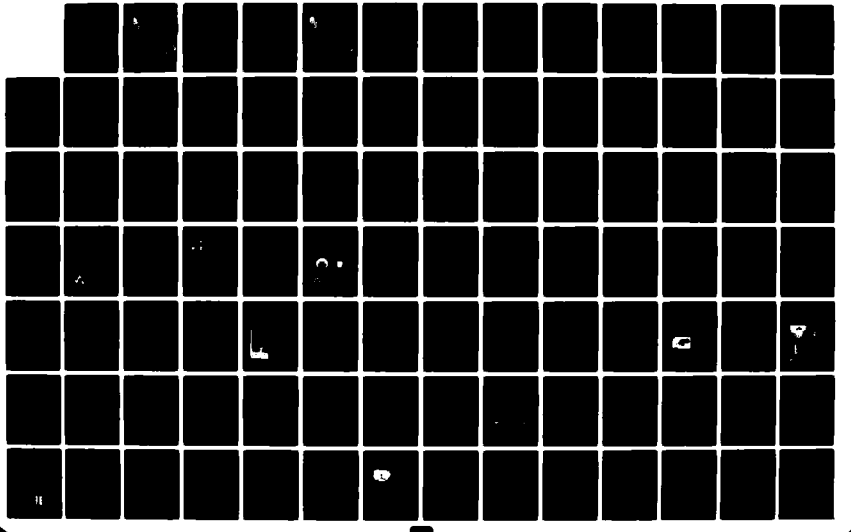

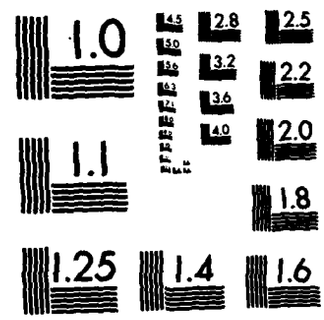

MICROCOPY RESOLUTION TEST CHART
NATIONAL BUREAU OF STANDARDS-1963-A

JHU/APL DST-9
FISCAL YEAR 1981

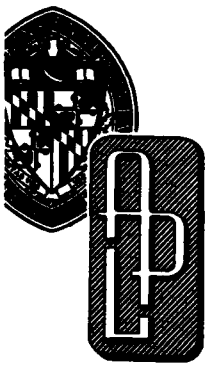

APPLIED PHYSICS LABORATORY

DEVELOPMENTS IN SCIENCE AND TECHNOLOGY

Approved for public release; distribution unlimited.

THE JOHNS HOPKINS UNIVERSITY • APPLIED PHYSICS LABORATORY
Johns Hopkins Road, Laurel, Maryland 20707
Operating under Contract N00024-83-C-5301 with the Department of the Navy

Unclassified

SECURITY CLASSIFICATION OF THIS PAGE

REPORT DOCUMENTATION PAGE

1. REPORT NUMBER	2. GOVT ACCESSION NO.	3. RECIPIENT'S CATALOG NUMBER
JHU/APL DST-9	AD-A125 288	

4. TITLE (and Subtitle)

Developments in Science and Technology

5. TYPE OF REPORT & PERIOD COVERED

Annual Report Fiscal Year 1981

6. PERFORMING ORG. REPORT NUMBER

JHU/APL DST-9

7. AUTHOR(s)

Various

8. CONTRACT OR GRANT NUMBER(s)

N00024-83-C-5301

9. PERFORMING ORGANIZATION NAME & ADDRESS

The Johns Hopkins University Applied Physics Lab.
Johns Hopkins Road
Laurel MD 20707

10. PROGRAM ELEMENT, PROJECT, TASK AREA & WORK UNIT NUMBERS

Various

11. CONTROLLING OFFICE NAME & ADDRESS

Naval Plant Representatives Office
Johns Hopkins Road
Laurel MD 20707

12. REPORT DATE

Fiscal Year 1981

13. NUMBER OF PAGES

239

14. MONITORING AGENCY NAME & ADDRESS

Naval Plant Representatives Office
Johns Hopkins Road
Laurel MD 20707

15. SECURITY CLASS. (of this report)

Unclassified

15a. DECLASSIFICATION/DOWNGRADING SCHEDULE

16. DISTRIBUTION STATEMENT (of this Report)

Approved for public release; distribution unlimited.

17. DISTRIBUTION STATEMENT (of the abstract entered in Block 20, if different from Report)

18. SUPPLEMENTARY NOTES

19. KEY WORDS (Continue on reverse side if necessary and identify by block number)

See Attached List.

20. ABSTRACT (Continue on reverse side if necessary and identify by block number)

This is a compilation of brief accounts of the Laboratory's significant work during Fiscal Year 1981 that can be reported on an unclassified level. The following areas are covered: radar surveillance and tracking systems; weapon control systems; battle group control systems; weapons technology; space science and technology; ocean science and technology; computer technology applications; biomedical science and engineering; fundamental research; and energy, environment, and urban technology.

DD FORM 1 JAN 73 1473

Unclassified

SECURITY CLASSIFICATION OF THIS PAGE

Battle Group AAW Display Group
Battle Group AAW Display System
Battle Group AAW Effectiveness
Battle Group AAW Simulation
Battle Group Gridlock System
Combustor Insulation Modeling
Computer Data Transfer
Corneal Structure
Data Maintenance Software
Data Set Access Control
Disturbance Compensation System
Earthquakes, Eastern U.S.
ECM Simulator
Electromagnetic Wave Scattering
Electron Spin Resonance
Filing System for the Blind
Finite-Length Cylinders
Geologic Faults, Eastern U.S.
GEOSAT Oceanographic Data
Geothermal/Ocean-Thermal Energy Conversion
GPSPAC Navigation Set
GRAVSAT System
Hazardous Materials Emergency Response Guidebook
Heated Anemometry
Hospital Information System
Hyperalgesia
Image Processing Laboratory
Inertial Reference System
Laminar Separation
Local Computer Network
Membrane Transport
Molecule-Surface Collisions
Motion-Compensated Launch/Recovery Crane
Navy Large-Scale Computer
NOVA-1 Satellite
Ocean Profiling
Ocean Thermal Energy Conversion (OTEC)
Organic Metals
Paravane, Surface-Controlled
Pattern-Recognition Algorithm
Power-Plant Siting
Probaility of Missile Crashing
Ramjet Combustor
Scramjet Combustor
Second, Definiton of
Silicon Solar Cells, Polycrystalline
Sloshing Frequency Bounds
Space Shuttle Data Relay Links
Spin-Orbit Coupling
Strategic Communciations Simulator
Submarine Hull Vibration
Supersonic Combustors
Surveillance Data
Traffic Studies
Wave Propagation

JHU/APL DST-9
FISCAL YEAR 1981

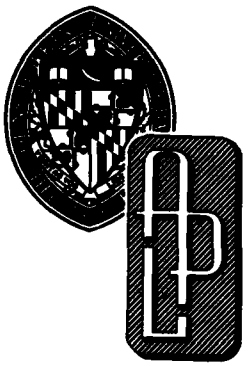

APPLIED PHYSICS LABORATORY

DEVELOPMENTS IN SCIENCE AND TECHNOLOGY

Approved for public release; distribution unlimited.

THE JOHNS HOPKINS UNIVERSITY • APPLIED PHYSICS LABORATORY
Johns Hopkins Road, Laurel, Maryland 20707
Operating under Contract N00024-83-C-5301 with the Department of the Navy

FOREWORD

The Applied Physics Laboratory (APL), a division of The Johns Hopkins University, is located in Howard County, Maryland, midway between Baltimore and Washington. Its work is carried out under contractual agreements between the University and the federal, state, and local governments. APL employs a staff of more than 2500 including 1400 professional scientists and engineers, of whom more than half have advanced degrees. Their ideas are implemented and extended through several field activities and a network of associate contractors and collaborators from coast to coast.

The primary mission of APL is to enhance national security and welfare by applying advanced science and technology to the solution of problems important to national objectives. The Laboratory conducts programs in fundamental and applied research, exploratory and advanced development, component engineering, systems engineering and integration, and test and evaluation of operational systems. Approximately 85% of the Laboratory's effort is for the Department of Defense (76% for the Navy and 9% for other DoD agencies). The remaining 15% is devoted to nondefense areas, including space research.

The current programs at APL cover a wide range of activities. Many are broad in scope, long term, or classified and therefore not reportable herein. The articles for this document are solicited annually from the whole Laboratory. Respondents are individuals or small groups who have been personally involved in particular efforts and are motivated to report to a wider audience than they usually communicate with. For these reasons, this publication does not necessarily represent all the most important accomplishments of APL during fiscal year 1981 (1 October 1980 through 30 September 1981). Nevertheless, the selected articles are typical examples of the type of R&D conducted.

APL was organized in 1942 under the auspices of the Office of Scientific Research and Development to develop a proximity (VT) fuze for antiaircraft defense; that was the principal effort during World War II. The era of emerging guided-missile technology extended from about 1944 to 1956. During that time, APL concentrated on providing better air defense for the Fleet by developing a family of shipborne surface-to-air missiles. The Navy-sponsored "Bumblebee" program pioneered many basic guided-missile technologies later used in other air, surface, and submarine missile programs.

The era of Fleet tactical systems engineering began in 1956 with the commissioning of the first guided-missile cruiser. The experience gained during that period has found application in many systems of interest to the Navy in various warfare areas and to other branches of the government. Significant activities are proceeding in areas of special APL competence, including advanced radar techniques, missile propulsion, missile guidance, countermeasures, and combat systems integration.

Among these programs, the Aegis Shipbuilding Project is of major importance. USS *Ticonderoga* (CG-47), to be commissioned in 1983, is the first ship in a new class of multimission guided missile cruisers that will carry the Aegis surface-to-air weapon system. The Laboratory is Technical Advisor to the Navy in the design and development of the Aegis system. APL now has the broader challenge of integrating this system into the operations of the Battle Groups. This effort, for which APL is Technical Direction Agent, includes the design and development of the Battle Group Anti-Air Warfare Coordination System exploiting the operation of Aegis cruisers with other ships and aircraft of the Battle Group. Other areas of tactical systems support involve aviation countermeasures as well as the improved effectiveness of Tomahawk, and Harpoon cruise missiles. APL has a major role in the conceptualization of future command, control and communications (C^3) systems to facilitate the operation of Naval forces. Both strategic and tactical aspects of the C^3 process are being examined. An important increasing effort at APL involves assessing the integrated performance of all the above systems.

The Laboratory continues to provide technical evaluation of the operational Fleet Ballistic Missile (FBM) System. Quantitative test and evaluation procedures are applied to every newly commissioned ballistic missile submarine. Similarly, APL currently provides precise evaluation of the Army's Pershing missile programs. Significant programs are also under way for Naval strategic communications and tactical targeting. Since 1970, APL has had the responsibility for planning and conducting a significant technical program to ensure the security of the FBM submarine fleet against possible technological or tactical countermeasures. The approach is to quantify all physical and tactical means that might be developed to detect, identify, and track our submarines and to propose and evaluate suitable countermeasures and tactics.

APL has a significant space program. It started with the Navy Navigation Satellite System, originally known as Transit, one of the most important accomplishments of APL since the wartime proximity fuze and the surface-to-air missile program. APL invented the concept, designed and built the initial satellite constellation, and set up and operated a worldwide satellite tracking network. The APL Space Program has greatly expanded and is now applied to the design and construction of a broad range of scientific satellites and spaceborne scientific experiments for NASA and the DoD.

With the encouragement of the Department of Defense, APL is applying its talent and the experience developed in DoD programs to a number of government-sponsored civil programs. Some examples of the areas to which attention has been devoted in recent years are biomedical research and engineering; transportation; fire research; reduction of pollution of the biosphere; ocean thermal, geothermal, and flywheel energy systems; air traffic control, leak detection in natural-gas distribution lines; and advanced education.

The development of computer applications at APL is so interwoven with all of the Laboratory's technical, systems, and administrative functions that progress in that area is difficult to report as separate accomplishments. However, by its extensive and intensive use of integrated circuits and microprocessor logic in satellites, in radar and other naval systems, and in biomedical engineering and other civil areas, APL has become a recognized leader in the area of computer technology. Furthermore, it continues to pioneer in innovative applications of computers of all sizes to problems of national importance. This trend is underscored throughout the document by the frequent references to computing as an integral part of most of the accomplishments reported herein.

To support its R&D activites through knowledge and experience in advanced research, the Laboratory performs basic research in biological, chemical, mathematical, and physical sciences related to its various missions. Through unique applications of system engineering, science, and technology to the needs of society, APL has enhanced the University's tradition of excellence while gaining worldwide recognition of its own.

CONTENTS

FLEET SURFACE AND AIR SYSTEMS

1. RADAR SURVEILLANCE AND TRACKING SYSTEMS

2. WEAPON CONTROL SYSTEMS

3. BATTLE GROUP CONTROL SYSTEMS

4. WEAPONS TECHNOLOGY

SPACE SCIENCE AND TECHNOLOGY

STRATEGIC SYSTEMS AND TECHNOLOGY

OCEAN SCIENCE AND TECHNOLOGY

COMPUTER TECHNOLOGY APPLICATIONS

BIOMEDICAL SCIENCE AND ENGINEERING

FUNDAMENTAL RESEARCH

ENERGY, ENVIRONMENT, AND URBAN TECHNOLOGY

FLEET SURFACE AND AIR SYSTEMS

1. RADAR SURVEILLANCE AND TRACKING SYSTEMS

INTRODUCTION

APL's involvement in surveillance and tracking systems covers a wide spectrum of programs. However, the work described in this section is directed at improving the present and future capabilities of Navy combatant radars used in anti-air warfare (AAW). These radars perform the functions of maintaining surveillance of the air space surrounding the ship and those in company and of tracking engaged targets in support of the fire-control process. Functionally, surveillance includes detecting aircraft and missiles and tracking them for the purpose of developing and displaying a complete and accurate picture of air activity. The fire-control tracking function differs from surveillance with respect to the requisite precision and accuracy of target position and rate measurements. In general, tracking radars considered in this section are used to control Standard Missile engagements.

Historically, the first surveillance radars used a beam shape that was relatively narrow in the azimuth plane but fan shaped in elevation in order to cover all target altitudes of interest. Such radars became known as "2D" because they could measure the target's range and azimuth. Azimuth was determined from the mechanical position of the antenna as it rotated. The radar signals were presented to the operator in a range-azimuth format from which he could develop a plot of target-position histories. In order to engage a target, a fire-control tracker had to be assigned. Because of the unknown elevation of the target, the differences in azimuth resolution, and the imprecise range and range rate data, the acquisition of the designated track by the fire-control radar entailed considerable local search. The net result was a relatively long reaction time as measured from first observation of the target by the 2D operator until weapon launch. There could be only one engagement per tracker because the mechanical pointing of the tracker antenna axis was used both to contol tracking and to update the fire-control solution.

The next major innovation was the development of the "3D" air search radar, which used a beam that was narrow in both azimuth and elevation. While the beam scan in azimuth was still produced by a mechanical rotation of the antenna, scan in the elevation plane evolved rapidly from mechanical to electronic means. Such a radar could measure target elevation in addition to range and azimuth. The 3D measurement concept, combined with the higher angular resolution afforded by the trend toward higher operating frequencies for surveillance radars, significantly reduced the local search volume during fire-control tracker acquisition. Although this shortened the reaction time somewhat, the manual track plotting and designation process still took relatively long.

As the speeds of attacking vehicles increased and the target characteristics shifted from those of aircraft to cruise missiles, reaction time became a dominant consideration in weapon system design. APL took the lead in a two-pronged attack to reduce reaction time, one addressing existing systems and the other new designs.

For the existing systems based on rotating radars, the approach was to automate the track-plotting process, to instrument the radars to provide full inherent measurement accuracy to the automated process, and to provide electrical transfer of track designation data to the fire-control radar. Before those things could be done, significant work in automatic threshold control was necessary to emulate the operator's ability to separate aircraft returns from background clutter and jamming. The result of that phase of the effort, AN/SYS-1, has been evaluated operationally in a shipboard installation and has demonstrated the expected improvement in reaction time. However, reaction time was still a few tens of seconds.

It was soon recognized that the best a conventional system (i.e., a rotating surveillance radar designating to a dedicated fire-control tracker) could achieve in terms of reaction time and rate of engagement would not be adequate against future threats requiring a reaction time of less than 10 seconds for successful defense. It was apparent that a weapon system capable of completely automatic operation from detection through evaluation of the result of the engagement was needed. Further, neither the track initiation and evaluation delays inherent in the rotation-rate limitations of conventional surveillance radars nor the surveillance-to-track handover delays could be tolerated. Event-by-event beam placement control (made possible by the phased-array antenna) combined with advanced signal-processing features and modern computer technology were required to achieve the necessary reaction time. The multifunction phased-array radar merged the surveillance and fire-control tracking functions so that track information of sufficient quality for threat evaluation and engagement support was available less than a second after initial target detection. The same features that led to fast, automatic reaction also resulted in the capability to track a large number of targets with accurate fire control, thereby increasing the number of engagements per unit time that such a system could prosecute significantly compared with conventional, dedicated tracking radar systems. In the mid 1960's, APL began the design of an advanced development radar to demonstrate these principles. Known as AMFAR, that radar was operational in 1968. The demonstrated principles formed the basis for the Aegis Weapon System. The first Aegis-equipped ship, USS *Ticonderoga* (CG-47), is scheduled to be operational in early 1983.

The two papers in this section address efforts in the continuing evolution of conventional, rotating, surveillance-dedicated tracker systems. One describes recent work in the interception of radar, electronic support measures, identification friend or foe, and infrared search and track systems. Although associated with conventionally configured combat systems, some of the techniques developed may be extendable to the newer systems based on phased arrays. The other paper describes the development and use of a computer-based simulation and response evaluation system to aid the development of the AN/SYS-2 computer programs.

Efforts in surveillance and tracking, now under way, include the Operational Evaluation of the Terrier New Threat Upgrade, which is beginning aboard USS *Mahan*. A study of the Phase II upgrade for the Mk 92 system and an examination of C-band and X-band alternatives for future Frigate class ships is being conducted. Critical Design Reviews are in progress for the Aegis radar upgrade now in development, including tests for advanced high-power waveguide and transmitter modulators.

AUTOMATIC INTEGRATION OF DATA FROM DISSIMILAR SENSORS

W. I. Citrin, R. W. Proue, and J. W. Thomas

New and sophisticated airborne threats that are supported by various surveillance countermeasures have placed new demands on the sensors used to detect, track, identify, and support the engagement of those threats by U.S. Navy surface combatants. Automatically integrating data from the various shipboard sensors helps meet these new demands by providing information that is more accurate, more complete, and more timely than is possible with manual methods. APL has pioneered in developing systems that automatically integrate data from multiple surveillance radars. This technology is being extended to integrate data from other sensor combinations including identification friend or foe radar, electronic support measures, and infrared search and track systems.

BACKGROUND

The increasing sophistication of threats to the U.S. Navy surface fleet has resulted in new demands on the sensors and weapon systems used to detect, track, identify, and engage those threats. Enemy passive detection techniques and antiradiation missiles (ARM) that home on radio frequency (RF) sources have made it expedient to limit emissions from radiating sensors. A combination of active and passive sensors can permit continuous surveillance of the environment while reducing enemy opportunities to exploit own-ship emissions. The successful engagement of threats requires that data from each sensor be correlated to perform detection and identification before the appropriate countermeasures can be selected and supported. Finally, short threat detection ranges and high threat speeds require short reaction times that are difficult to attain with manual methods. In reponse to these requirements, increased emphasis is being placed on automating sensor management and automating the integration and use of sensor data.

Sensor systems have been designed to detect specific threat characteristics and to support specific countermeasures. As a result, each sensor has particular advantages and disadvantages. Radars can provide accurate position and velocity information on targets, but they may be degraded by clutter and electronic countermeasures and are convenient targets for ARM threats. Identification friend or foe (IFF) sensors can identify cooperative friendly targets as well as provide their position and velocity. Although clutter does not degrade IFF sensors, they too are susceptible to jamming and ARM threats. In addition, the enemy can passively locate units that are responding to IFF interrogations. Electronic support measures (ESM) can passively detect and identify emitting targets and determine their bearing but cannot provide range information. Infrared (IR) sensors can passively detect targets that have a sufficient IR signature. If the data from these different sensors are automatically integrated, the information needed to assess and engage a target is quickly available. Sensor operation may be managed so that the sensors complement one another in obtaining information while limiting enemy opportunities to counter them.

All of these motivating factors have pointed to the desirability of automatically integrating both similar and dissimilar shipboard sensors.

DISCUSSION

To integrate the data from any two sensors, the data from one are compared with the data from the other to determine which correspond to the same target and which to different targets. The decision process is called correlation.

The different sensors may provide different types of data (one may provide target range but not identification, the other may provide target identification but not range) with various accuracies (one may provide coarse bearing and the other very accurate bearing). A two-hypothesis log-likelihood ratio that uses selected sensor data as arguments can be used to combine the various data types and associated accuracies to obtain functions that are measures of the likelihood that the data correspond to the same or different targets. These functions are called discriminants. Having selected the parameter set from the available sensor data, the discriminant functions are obtained by forming the log likelihood ratio (also referred to as correlation likelihood) using the following expression:

$$LL(P_A, P_B) = \log_a \frac{P[P_A, P_B|H_0]}{P[P_A, P_B|H_1]}$$

where

$LL(P_A, P_B)$ = log likelihood ratio for the parameter sets P_A and P_B,

$P[P_A, P_B|H_i]$ = conditional probability of observing the parameter sets P_A and P_B, given that hypothesis H_i is true,

H_0 = hypothesis that the sensor A and sensor B tracks correspond to the same target,

H_1 = hypothesis that the sensor A and sensor B tracks correspond to different targets,

$P_A = [P_{A1}, P_{A2}, \ldots P_{AN}]$ = set of parameters obtained from the sensor A track file, and

$P_B = [P_{B1}, P_{B2}, \ldots P_{BN}]$ = set of parameters obtained from the sensor B track file.

If the parameters $[P_{Ai}, P_{Bi}]$ are independent of the parameters $[P_{Aj}, P_{Bj}]$ for all $i \neq j$, then the ratio may be rewritten as

$$LL(P_A, P_B) = \sum_{i=1}^{N} \log_a \frac{P[P_{Ai}, P_{Bi}|H_0]}{P[P_{Ai}, P_{Bi}|H_1]}$$

$$= \sum_{i=1}^{N} LL(P_{Ai}, P_{Bi}) \ .$$

Thus the form of a discriminant may be obtained separately for each pair of parameters $[P_{Ai}, P_{Bi}]$ from $LL(P_{Ai}, P_{Bi})$. The discriminants are then summed to obtain the correlation likelihood.

Automatic Integration of Radar and ESM Sensor Data

Using the above approach, a real-time system that accepts actual radar and ESM sensor data, forms tracks from these data, performs radar and ESM track correlation processing, and designates threats to a simulated RAM Guided Missile Weapon System was designed and tested at APL.[1] This system and the testing were described in a previous *Accomplishments* article.[2]

The testing described in Ref. 2 revealed some miscorrelations, most of which occurred when one target track crossed that of another or when targets were closely spaced in bearing. Since that time, several additional correlation discriminants have been tested by means of a computer simulation of the radar-ESM track correlation algorithm. The input to the simulation, consisting of tracked radar and ESM target reports versus time, is created by a scenario generator and tracking program. The output of the simulation, radar and ESM track correlation status versus time, is analyzed by a data reduction program. Figure 1 shows the key elements in the simulation. As a result of these tests, the likelihood calculations have been modified and extended, and improvements have been made to the algorithm, some of which are outlined briefly below.

The previous correlation algorithm used discriminants based on the differences between radar and ESM bearing, identification, category, and heading, which can be found in or inferred from the radar and ESM track file data. The new discriminants substituted bearing history for bearing difference and also used range, height, and speed. Bearing history uses current and past bearing information obtained from the radar and ESM track file data. Range and speed are determined directly from radar measurements and can be found in the radar track file. Height can be determined from radar measurements if a three-dimensional (3D) radar is used. These parameters can also be inferred from emitter characteristics found in the ESM track file data. In addition to these new discriminants, association lists of correlation candidates are now formed; they are composed of radar tracks that have remained within a specified bearing window about an ESM track throughout their history. The association lists offer the advantage of a very-long-term bearing history discriminant without the attendant problem of storing bearing samples. They also eliminate the need for the periodic searches for correlation candidates that were required by the previous algorithm.

The performance of the algorithm was measurably improved by the additional discriminants, especially bearing history. Crossing targets no longer cause miscorrelations, and radial tracks that are close together in bearing but do not cross are correctly correlated a

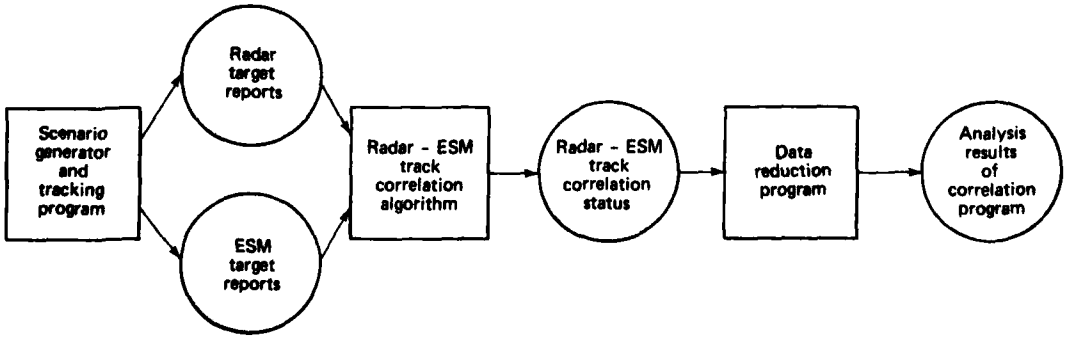

Fig. 1 Radar-ESM correlation simulation program.

higher percentage of the time than with the previous algorithm.

The log likelihood approach to correlation permits each individual independent discriminant to be summed with the others to form an overall correlation likelihood. Consequently, it lends itself to the easy inclusion of new discriminants, even those that may not be formed from sensor-related parameters. This is done simply by adding the new discriminant, properly weighted, to the sum of the discriminants included previously. As an example, a "hysteresis" term, based on the previous correlation status for a radar-ESM track pair, was added to give extra weight to the pairs that were correlated in the past. This tended to stabilize correlations and prevent them from switching because of noise. In instances where it was desirable to stabilize certain correlations, they were rendered permanent or "frozen" by adding a likelihood that outweighed all the other likelihoods combined. It was possible to add these likelihoods with minimal changes to the structure of the algorithm.

Because the correlation likelihoods are measures of the probability that the radar and ESM tracks represent the same target, the modified algorithm uses the likelihood sums to establish an ambiguity criterion for correlated track pairs. Track correlations with a likelihood greater, by a predetermined threshold, than the likelihood of any other pair involving either the radar or ESM tracks are now considered to be unambiguous correlations. Those that are not better by at least the threshold value are considered to be ambiguous with other potential pairings. This information may be useful to an operator or processing function assessing the quality of the track correlation data in cases where data must be used to make further engagement decisions.

Integration of Radar and IFF Sensors

As part of an experimental effort at APL, the same likelihood approach to correlation was applied to the development of a method to automatically integrate IFF and radar sensor data in the AN/SYS-( ) Integrated Automatic Detection and Tracking (IADT) System. The integration design goals included improvements in shipboard identification, air traffic control, and Combat Air Patrol support functions.

An IFF sensor operates by transmitting a coded RF pulse train to which a cooperating airborne or surface unit automatically responds with a different coded pulse train. The pulse train transmitted by the IFF is referred to as an interrogation, and the reply transmission that it elicits from unit transponders is termed the interrogation response. The interrogation response is received and processed by the IFF sensor to provide target reports consisting of range, bearing, and code data, including altitude.

The SYS-1 IADT performs tracking for surveillance radars by forming and updating tracks in a single, unduplicated track file with target reports (contacts) from each radar. SYS-( ) refers to a generic form of SYS-1 that has been modified to accept IFF sensor data. Each radar video processor transforms the returned radar raw video into digital centroid reports, analogous to the IFF target reports formed from IFF response data. The IFF sensor and the SYS-( ) are integrated by performing the correlation process between the IFF target report data and the SYS-( ) radar track file data, using the log likelihood approach. Range, bearing, IFF-derived target altitude, 3D radar elevation, and IFF code data are used to evaluate discriminants.

As a first step toward demonstrating the feasibility of automatic IFF and radar integration, data from an IFF set and from two different radars were collected simultaneously at the Naval Tactical Data System Development and Evaluation Site, Mare Island, Calif. The IFF set was an AIMS Mk 12 with an experimental AN/UYK-20 computer-based beacon video processor (BVP). The BVP processes IFF data and outputs IFF target reports. The two radars were an AN/SPS-52B 3D air search radar and an AN/SPS-48C 3D air search radar. IFF/BVP and radar target reports for targets of opportunity were the primary data collected and evaluated. Figure 2 illustrates the data collection and processing schemes. Two radar digital data collectors developed by APL to interface with the SPS-52B and SPS-48C radars were used to collect digitized radar hits. The UYK-20 BVP computer program was modified to record digital IFF/BVP target reports. At APL, software processing was performed to centroid the recorded radar hits and to produce magnetic tapes of radar reports in a format accepted by the SYS-1 IADT software. The recorded IFF/BVP target report data were formatted identically to the radar reports, but IFF/BVP report range and bearing were used instead of radar range and bearing. An elevation angle derived from IFF-encoded altitude was used in place of the 3D radar elevation angle. Each target report tape could be played through the SYS-1 separately. Additional processing then merged the radar and IFF/BVP reports onto a single tape. After these modified target report tapes were used to drive the SYS-1 IADT program, existing data extraction and reduction software was used to analyze system performance.

The experimental results were encouraging. When the IFF/BVP report data were used separately, SYS-1 initiated and maintained tracks from the IFF/BVP-derived range, bearing, and elevation data. This indicated not only that IFF/BVP range and bearing accuracies are adequate to support automatic track initiation and maintenance but that a discriminant based on elevation derived from IFF code data is useful. When the merged tape containing IFF/BVP and radar reports

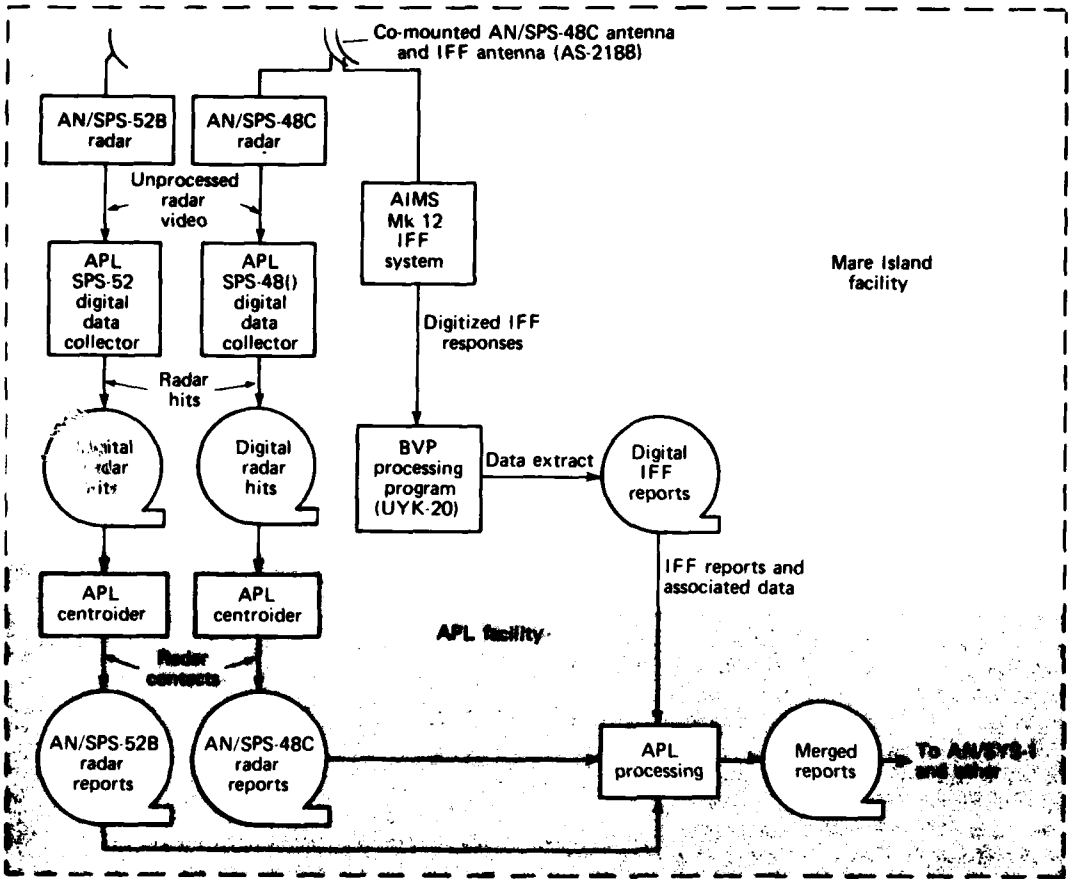

Fig. 2 Configuration for data collection and processing to demonstrate radar-IFF integration via AN/SYS-1.

was used, SYS-1 initiated and maintained integrated tracks that were updated asynchronously by both IFF/BVP and radar reports. The experiment was performed with no modifications to the SYS-1 IADT computer program.

SUMMARY

On the basis of the above two projects, significant advances have been made in the areas of sensor data integration. The log likelihood approach to sensor data correlation is appropriate for both similar and dissimilar sensor data. A future application involves the addition of an infrared search and track (IRST) set to the suite of existing shipboard sensors. In that case, the correlation may be performed between the IRST sensor data and a data base that has been formed from the integration of other multiple sensor data. The log likelihood approach and other previous correlation data processing techniques will be used to develop a similar integration and data correlation approach for the IRST sensor.

This work was supported by NAVSEASYSCOM, SEA-62X and SEA-62Z4.

WRAP-AROUND SIMULATION PROGRAM FOR AN/SYS-2 INTEGRATED AUTOMATIC DETECTION AND TRACKING SYSTEM

A. F. Krummenoehl, N. A. Tothill, and C. A. Wright

The Wrap-Around Simulation Program is a real-time computer program that simulates the radar systems, the tactical data system, and the weapon direction system that communicate with the AN/SYS-2 Integrated Automatic Detection and Tracking System. The simulation has supported the development and formal testing of the SYS-2 computer program and has eliminated the use of controlled aircraft and actual radars and tactical data systems during a substantial portion of program development and testing.

BACKGROUND

The AN/SYS-2 Integrated Automatic Detection and Tracking (IADT) System incorporates as a principal component an embedded computer program that processes reports from both an AN/SPS-48E three-dimensional search radar and an AN/SPS-49(V)5 two-dimensional long-range search radar. It sends control and signal processing orders to the radars and provides tracking data to the Naval Tactical Data System (NTDS) and the Mk 13 Mod 8 Weapon Direction System (WDS). Figure 1 shows the integrated combat system of which SYS-2 is a part. The objective of SYS-2 is to provide integrated automatic detection and tracking by producing an unduplicated track file with an acceptably low rate of false track generation. Navy Technical Evaluations (TECHEVAL's) and Operational Evaluations (OPEVAL's) are conducted in a shipboard environment, with interfaces between SYS-2 and the radars, the tactical data system, and the weapon direction system. The services of controlled aircraft are provided. However, prior to the TECHEVAL and OPEVAL and during program development, there is a need to exercise and test the SYS-2 program to the fullest extent possible and as economically as possible. A test bed that represents the actual physical environment and produces the actual system interface signals is required. To this end, the AN/SYS-2 Wrap-Around Simulation Program (WASP) has been developed.

The design of the SYS-2 WASP and its development guidelines were based upon those of the AN/SYS-1 WASP, which was used to support testing of the SYS-1 IADT computer program. The equipment for both WASP's was identical to that of the corresponding programs. An AN/UYK-20 Standard Navy Minicomputer, an AN/UYA-4(V) Display Console, and other standard peripherals ensured equipment availability, familiarity to the users, and identical intercomputer interfaces. The WASP software architecture followed a form similar to that of the SYS programs. Use of a modular design, a similar executive procedure, the same programming language, and standardized documentation ensured that WASP procedures could be readily understood and used by both SYS-2 and WASP development personnel. Finally (and unique to simulation support software), the WASP program was produced as Government Furnished Equipment to ensure objectivity in defining WASP requirements, to provide a third-party cross-check in interpreting interface specifications, and to ensure resource availability. The simulation was subjected to comprehensive validation tests, and all processing was completely verified. As a result, it is reliable, accurately represents the physical environment, and is relied upon to support formal validation of the SYS-2 computer programs prior to their shipboard installation.

DISCUSSION

Description

WASP resides in a single UYK-20 Standard Navy Minicomputer (with full 64K memory capacity and MATHPAC). Five interfaces with the SYS-2 computers

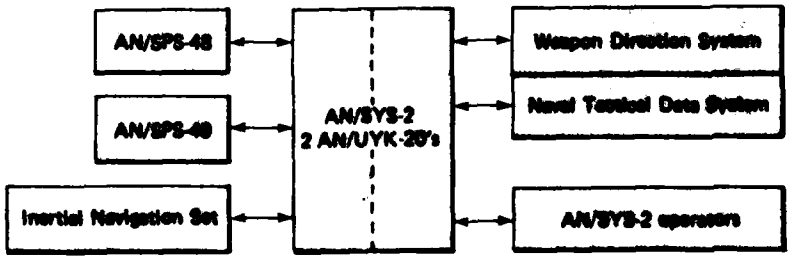

Fig. 1 The integrated combat system.

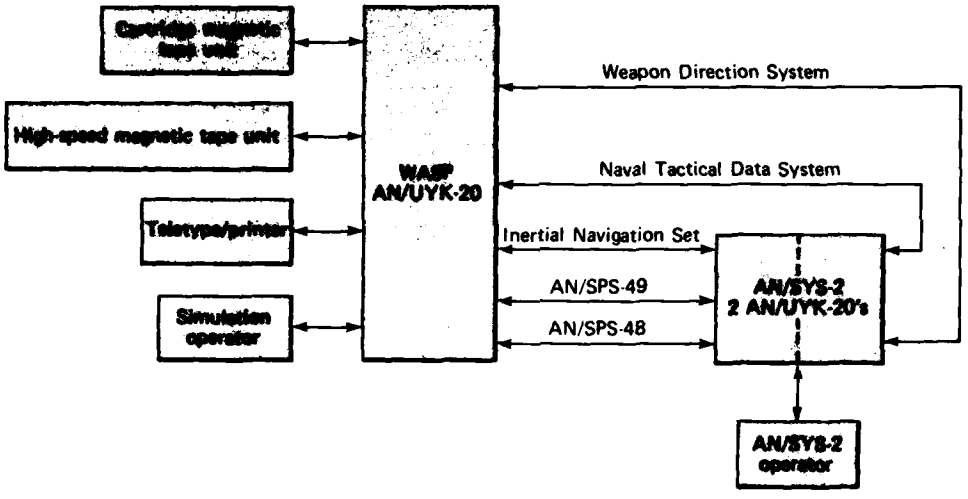

Fig. 2 Equipment configuration for WASP and AN/SYS-2.

simulate the SPS-48E 3D search radar, the SPS-49(V)5 2D search radar, the NTDS, the WDS, and the Inertial Navigation Set, respectively. WASP also interfaces with a UYA-4(V) display console, a Teletype/printer, a cartridge magnetic tape unit, and a high-speed magnetic tape unit. The cartridge magnetic tape unit provides program loading and storage/retrieval for prescripted scenario data. The high-speed magnetic tape unit allows the input of prerecorded live radar data. The WASP UYA-4 display console (or optionally the Teletype/printer) interface provides for operator control of the simulation. Figure 2 shows the WASP equipment configuration.

WASP operates in real time to provide simulated interfaces with SYS-2. A WASP operator runs the simulation and controls the simulated environment. The radar simulation portion of WASP incorporates two alternative methods for radar data generation. The first uses a radar model that is driven by scenario prescriptions contained in the computer memory. The prescriptions, generated by the operator, can be saved and retrieved via the cartridge magnetic tape unit. The second method uses the high-speed magnetic tape unit to play back actual radar buffers recorded from the SYS-2 computers during live operation. The operator starts the simulation in either mode, and thereafter the radar simulation operates unattended.

The NTDS and WDS simulations provided by WASP operate independently of the radar simulations. Similar in control to the actual systems, this portion of WASP provides a means of replicating all the message traffic between SYS-2 and the actual systems. The operator displays show the message traffic, the quality of data received from SYS-2, the engagement and designation states of simulated NTDS/WDS tracks, and SYS to NTDS/WDS tracking accuracy and timing. The target data generated by the radar simulation can be compared with the track data sent from SYS-2 to the NTDS.

The simulation of the Inertial Navigation Set interface is driven by scenario prescriptions.

Design

The major design features of WASP include its modular structure, its ability to operate using simple, operator-controlled parameters, and its use of complex, high-fidelity equations.

The performance functions of WASP are divided into separate, nearly independent entities called modules. The modules are coded in the computer's symbolic language and are maintained separately. The coded modules are combined to form a program that is loaded and executed in the computer. During WASP operation, the modules communicate through a master executive module, which maintains status information on all available modules and calls those included in the current program. Although by design the program is intended to support all SYS-2 testing needs, the modular design provides flexibility to remove, change, or add modules readily. In this way, the operational features of WASP are a product of the individual modules selected, and a unique configuration can be generated to support unusual test requirements or to accommodate equipment changes.

Use

WASP was used during all phases of the SYS-2 computer program development. The major development phases included (or will include, in the case of the at-sea test scheduled for 1982) module integration, program validation, land-based testing, and at-sea operational evaluation. Activities during each phase rely entirely or in part on WASP.

Integration testing was performed at Norden Systems, Santa Ana, Calif., the SYS-2 program development contractor, starting in early 1980. During integration testing of the software, WASP was the sole source of stimuli for exercising the SYS-2 computer program. Testing activities ranged from verifying individual modules and interfaces to verifying SYS-2 system performance. Initially, WASP performed its most basic function in driving the SYS-2 interface modules in real time. Even before the modules could be integrated to form the nucleus of the SYS-2 program, each was exercised using its counterpart in WASP to monitor control signals and data transmission. Each module benefited from the visibility provided by WASP as problems in timing and data transfer were corrected. As a result of this testing, the interfaces were operational well in advance of actual hardware availability, and the transition from simulated to real interfaces was smooth. As integration progressed, WASP provided an increasingly realistic test bed environment for exercising particular aspects of SYS-2 performance. For example, track acquisition and track promotion were tested using carefully designed scenarios with relatively simple target trajectories.

Integration testing merged with SYS-2 program validation testing at APL early in 1981. Validation testing concentrated on system level performance of the computer program. Again, WASP provided the test bed environment. Much of the integration testing was repeated in validation testing, but more emphasis was placed on total system response and use of the complex WASP simulation capabilities. For example, scenarios were designed with more targets, including complicated trajectories, and tests were run with all interfaces operating simultaneously. The ability to play back prerecorded live radar data provided the repeatable radar inputs needed to validate false-track performance.

WASP support of integration activities of the CG/SM-2 New Threat Upgrade Combat System began in May of 1981 at the APL land-based test site. WASP was used as a substitute for the radar portion of the surveillance subsystem to train Navy personnel and to simulate tactical situations for testing SYS-2 and the real NTDS. It was used frequently for fault isolation tests when radar and SYS-2 processing appeared to be in conflict. Computer programs originally developed to test WASP and to simulate the radar interfaces were employed as substitutes for SYS-2 to support interface checkout of both SYS-2 and the radar programs. Changes in the latter were reflected in corresponding WASP radar simulation changes.

APL's activities at the land-based test site have been concluded, and preparations are under way for an at-sea OPEVAL scheduled for early 1982. In the shipboard (USS *Mahan*) environment, all the WASP capabilities may be used, although the radar simulations will be foremost. Again, Navy personnel will be trained to operate the SYS-2 program by means of WASP simulations. Real-life tactical situations that develop during formal OPEVAL testing will be recorded by the SYS-2 program data extract for instant replay via WASP. Use of these WASP capabilities during the final phase of program development attests to its success as a versatile test tool for the SYS-2 embedded computer program.

This work was supported by NAVSEASYSCOM, SEA-62X321.

2. WEAPON CONTROL SYSTEMS

INTRODUCTION

As an outgrowth of the program to develop the proximity (VT) fuze in World War II, APL became actively involved in the improvement of gun directors and, by the end of the war, was engaged in the application of new technology to the problem of directing antiaircraft weapons. During the initial development of the antiaircraft guided missile and its early introduction for service use, the APL staff worked with the Navy's equipment contractors to acquaint them with the characteristics of these new weapons. The role of the Laboratory in weapon control necessarily expanded with the assumption of responsibility for technical direction of the Navy's AAW guided missile systems in the late 1950's.

The challenge to the Fleet posed by manned supersonic bombers attacking en masse under the cover of electronic countermeasures required a radical departure from the relatively primitive, human-intensive control procedures that grew out of World War II.

Working first with analog and then digital electronic computational techniques, the Navy has produced tactical data and weapon control systems that relieve weapons personnel from much of the routine bookkeeping associated with a fighting ship. APL made important contributions in this evolution, particularly in the area of threat evaluation and weapon assignment. In addition to the characteristic drive to discover and apply the basic principles underlying a problem, the Laboratory brought to the Navy weapon control community an understanding of the potential capabilities of the then-emerging world of electronic computation and automation.

APL has contributed to defining the basic structure of shipboard combat systems and to allocating functions consistently among the sensor, command, support, and weapon control elements of these very complex systems. Such consistency of structure has aided technical interchange among major developments in which APL has played a role, including the Aegis Weapon System, Terrier and Tartar New Threat Upgrades, and, most recently, the DDG-51 Combat System. APL initiatives supporting the development of weapon control systems have included Combat Information Center design, computer program development, management techniques, human control of automated system responses, and scheduling of weapons engagements in a complex threat environment.

Anticipating the potential threat of antishipping missiles, the Laboratory has focused its recent efforts in the area of weapon control on the definition and development of techniques that allow weapon systems to respond to a threat in minimum time while providing the requisite control capability for the several levels of tactical command. Integral to Laboratory efforts in this and other areas of weapon control is the identification of data processing and distribution approaches that enable the implementation of practical and economical designs — designs that provide requisite hardness to equipment casualty or battle damage.

The articles in this section represent some of APL's activities in the area of weapon control.

REFERENCE MODEL FOR COMBAT SYSTEM COMPUTER DATA TRANSFER

A. E. Davidoff

A multiple laboratory effort, led by APL, has resulted in the development of a communications reference model for combat system data transfer. The model serves as a descriptive mechanism to achieve a better understanding of computer data exchange within U.S. Navy surface combat systems. It also provides a way to compare technical approaches.

BACKGROUND

A modern Navy combat system is a very large equipment complex. It contains a diversity of interconnected weapons, weapons systems, sensors, communication systems, support systems, and medium- and large-scale computers. Collectively, the complex performs a variety of functions such as searching for enemy missiles, aircraft, surface ships, and submarines; consolidating many sources of sensor information for operator analysis; and performing defensive and offensive actions in concert with the overall tactical situation, established doctrines, and command decisions.

Because the successful performance of each piece of equipment often depends on data generated by another, extensive data exchange and cooperative computer interaction are essential within a combat system. Well-defined procedures and protocols must be employed for effective communications. At present, the U.S. Navy does not typically use a systematic layering of communications or a common conceptual framework (or reference model) in implementing for data exchange between combat system equipments.

A working group on data transfer (sponsored by NAVSEASYSCOM) formed a splinter group of engineers from the Naval Surface Weapons Center, the Naval Underwater Systems Center, and APL to address this issue. As the effort evolved, APL provided the technical leadership and developed a series of strawman reference models for group review and refinement, leading to one known as "Modelman." This communications reference model is currently being considered for use in the U.S. Navy's new Guided Missile Destroyer Class (DDG-51).

DISCUSSION

Modelman (Fig. 1) consists of five layers or levels of function. A seven-layer model developed by the International Standards Organization for telecommunication networks served as the baseline for its development, but changes were incorporated to address the different environment of a Navy combat system.

Modelman promotes understanding among developers through its common set of definitions and logical partitioning. It serves as:

- A foundation from which data transfer systems can be specified,
- An organizing construct to describe existing and developing new data transfer mechanisms, and
- A basis for comparing existing and future systems.

The concept of protocol layering is fundamental in applying Modelman to intercomputer and computer-peripheral communications. It imposes a discipline on the structure of the computer software so that changes in protocol and function should affect only a few layers

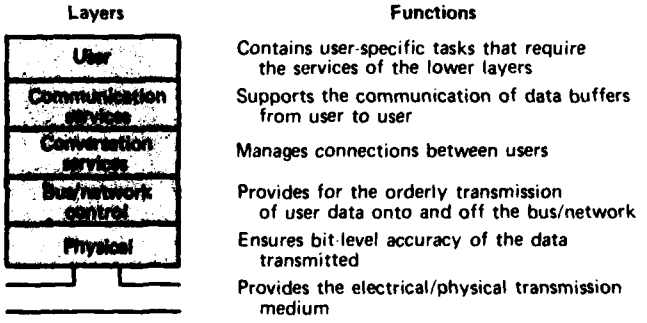

Fig. 1 Modelman reference model.

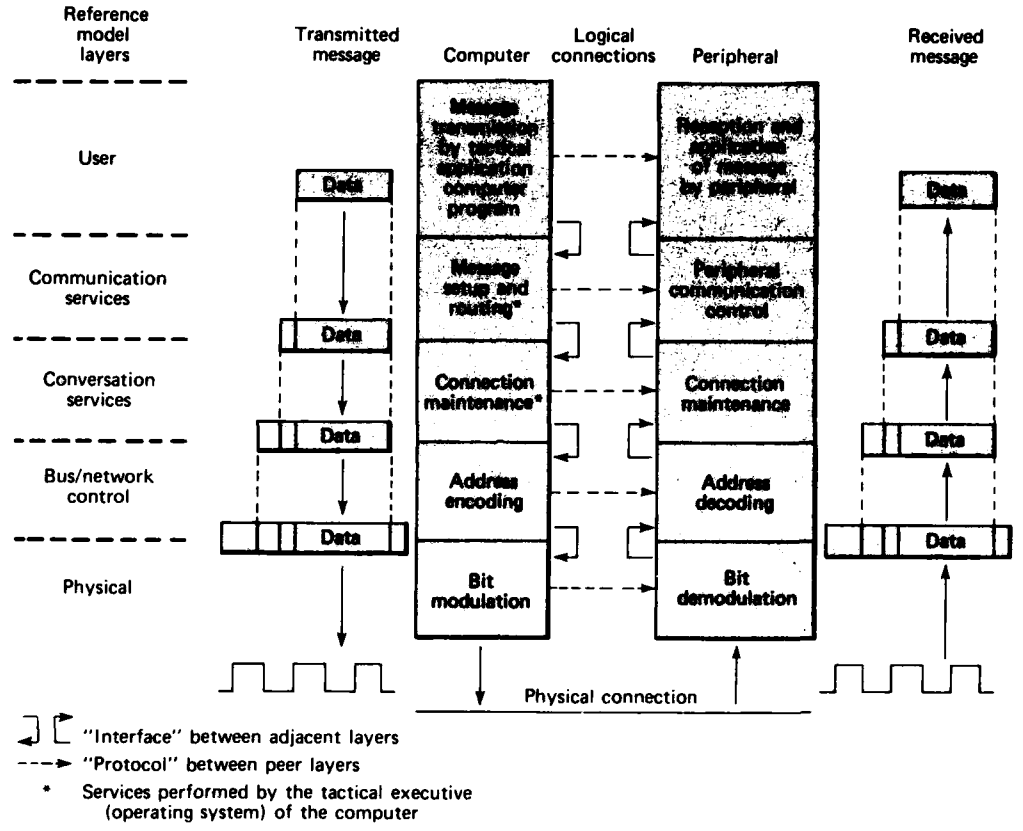

Fig. 2 Example of communication function implemented in layers.

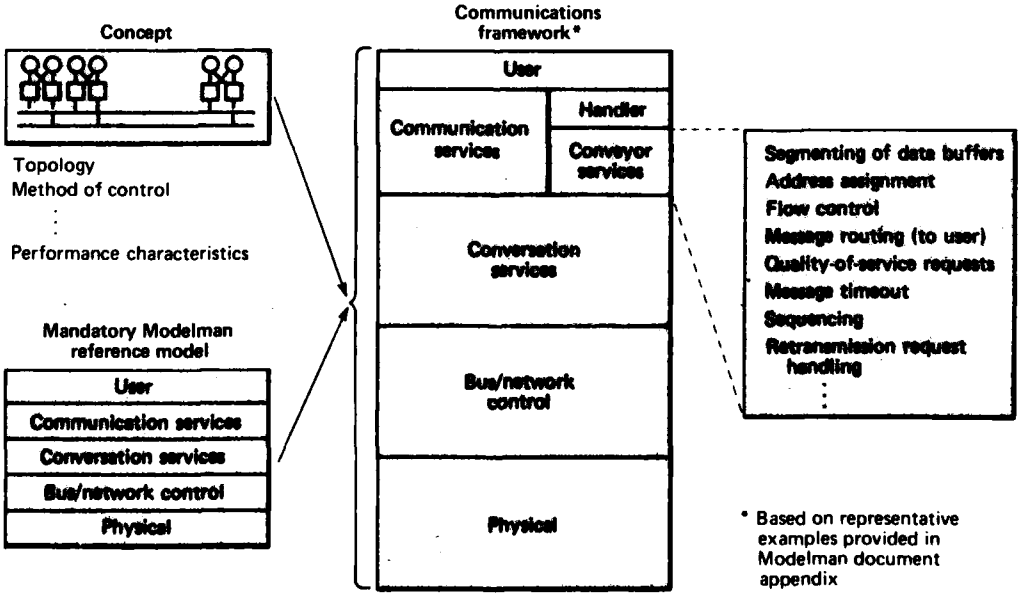

Fig. 3 Bus or network development using Modelman.

instead of the entire software. Figure 2 illustrates how the Modelman layering process sends a message from a computer to a peripheral. As seen, the process is orderly. From the computer program that initiates message transmission, data are formatted progressively at each layer to provide information required for the successful reception by the user at the peripheral. If subsequent changes are implemented, the impact should be limited. For example, a change in the addressing scheme used in the bus/network control layer should be restricted entirely to that layer and should not require expensive modifications to software in other layers.

Serving as an organizing construct and as a comparison tool, Modelman documentation gives guidance on how to describe and compare data transfer implementations. It prescribes the development of a communications framework by taking the fundamental bus or network concept (i.e., topology, method of control, performance characteristics, etc.), segmenting the desired services into the Modelman layers, and detailing the services and attributes to be found in each layer or sublayer. Figure 3 shows the development of a representative bus concept into a communications framework. Specific details of a hypothetical conveyor services sublayer are given as an example.

ACKNOWLEDGMENTS

The author is indebted to Karen Dohler, formerly of APL, who performed much of the initial Modelman work and to David Marlow, Naval Surface Weapons Center, who offered valuable insight into the data transfer problem and provided many important ideas.

REFERENCES

[1] K. M. Dohler, *Data Bus Reference Model*, JHU/APL F2F-2-430 (9 Mar 1981).
[2] A. E. Davidoff, *Communications Reference Model for Combat System Data Transfer*, JHU/APL F2F-2-472 (21 Jul 1981).

This work was supported by NAVSEASYSCOM, SEA-06D.

DEFINITION OF NEW NAVY LARGE-SCALE COMPUTER

K. R. Wander and T. P. Sleight

A collaborative effort was undertaken by the Naval Underwater Systems Center, Newport, R.I., and APL to define the Instruction Set Architecture of the new large-scale computer that is to be used in Navy tactical combat systems. This computer, the AN/UYK-43, is expected to be in service for the next 25 years; hence, considerations for future expanded memory capacity and enhanced throughput as well as provisions for expansion to facilitate new developments such as Ada (the new DoD high-order language) are inherent in the design.

BACKGROUND

The genealogy of the Navy's standard tactical computers (Fig. 1) began with the AN/USQ-20 in the late 1950's and has evolved in an architectural sense into two fundamentally different paths. Thus, the original architecture based on 30 bits has been functionally replaced with the large-mainframe, 32-bit AN/UYK-7 and the small minicomputer, the 16-bit AN/UYK-20. Under development now are technology updates that retain, from a software point of view, the architecture of the UYK-7 and the UYK-20. This approach has been used in order to minimize the software costs associated with introducing new computer hardware. Compatibility is obtained by reimplementing the predecessors' Instruction Set Architecture (ISA).

DISCUSSION

APL's work has concentrated on the new large-scale standard computer, the UYK-43. The need for this type of computer is a direct outgrowth of the 1975 Navy

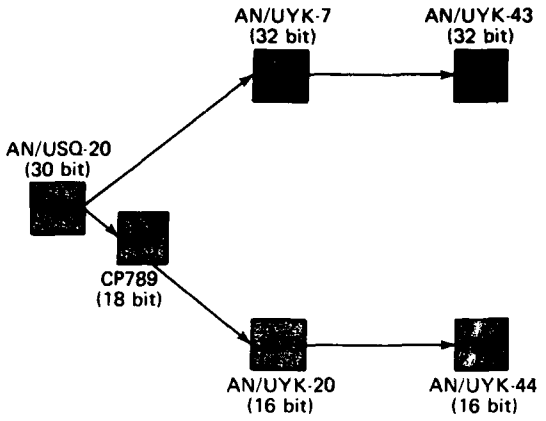

Fig. 1 Genealogy of Navy standard computer.

Embedded Computer Working Group (sponsored by the Assistant Secretary of the Navy for Research, Engineering, and Systems) on which APL served a key technical role.[1] During the development of the UYK-43, the following objectives are being stressed:

1. Software transportability (UYK-7 to UYK-43),
2. Hardware maintainability,
3. Hardware availability, and
4. Hardware technology insertion.

Because the Navy recognized the need for a replacement computer for the UYK-7, it convened a Design Review Group, under the direction of PMS-408 and made up of various Navy laboratories and APL, to develop a specification for the UYK-43. Each organization was responsible for various aspects of the computer. APL and the Naval Underwater Systems Center (NUSC) collaborated in the definition of the ISA, which is the primary subject of this article. In order to provide some perspective on the hardware capabilities, the two UYK-43 enclosures are compared in Table 1 with that of the UYK-7.

Because there is a significant investment in software for the UYK-7, transportability was one of the primary concerns in the definition of the ISA. It became encumbent upon the Navy to ensure, on one hand, that the ISA of the UYK-7 was preserved to the highest degree possible but, on the other hand, not to restrict the ISA of the UYK-43 to that of the UYK-7. Upon canvassing the UYK-7 user community, it was found that the users wanted built-in debugging features, performance monitoring, transcendental functions, stack operations, and the ability to directly access data located beyond the physical limitations of the UYK-43 enclosure.

To illustrate how software transportability was considered during this effort, all the current UYK-7 central processor unit (CPU) instructions (with one exception) and all the input/output controller (IOC) instructions (Table 2) were maintained. Furthermore, although it was not initially in the specifications, a concerted effort among IBM and Univac (the two contractors) and NUSC and APL defined a UYK-7 compatibility mode that will allow many existing UYK-7 programs to run without modification in the UYK-43. This will provide an extremely low-risk approach for program managers to change from an existing UYK-7 to a UYK-43 (UYK-7 mode) and thence, when software is developed, to the UYK-43 (expanded ISA).

The ISA of the UYK-43 has now been completely defined. The common portion of the ISA was defined by Ref. 2. IBM and Univac have provided their unique instructions to the Navy as Engineering Change Proposals in order to implement fault-tolerant features and reconfiguration software.

Hardware maintainability, availability, and technology insertion are also extremely important. As a member of the Navy-sponsored Design Review Team, APL has contributed to their definition in the development of the UYK-43.

Hardware Maintainability

Ninety-eight percent of all failures can be isolated to three or fewer line replaceable units. Single-button action is all that is necessary to initialize isolation diagnostic programs that will give an indication on the maintenance panel of the failed units. Once a failure is indicated, the unit can be replaced, and a subsequent single-button action will verify the fault correction.

Hardware Availability

The maximum size enclosure in the UYK-43 family is called the "B enclosure." Greater availability can be provided in the B enclosure by having redundant functional modules: CPU, memory, IOC, and power supply. With redundant modules, a failed unit can be isolated and on-line repairs made without complete power shutdown.

Hardware Technology Insertion

Provision has been made in the UYK-43 for other ISA's to be implemented, such as those of the AN/UYK-44, Ada, etc.. The present 5 to 10 million bytes of memory (per enclosure) can be increased without redesign as chip densities of semiconductor memory modules increase.

Table 1

COMPARISON OF AN/UYK-7 AND AN/UYK-43 HARDWARE

	AN/UYK-7	AN/UYK-43 (enclosure A)	AN/UYK-43 (enclosure B)
Throughput (minimum) (thousands of operations per second)	500	2000	4000
Memory capacity* (million bytes)	0.384	5.0	10.0
Central processors	1	1	2
Input/output controllers (megabits/s)	32	100	200
Input/output channels	116	24	64
Memory addressability (bytes)	1 million	16 billion	16 billion
Mean time between failures (minimum)(hours)	2500	6000	18,000
Cooling	Air	Air/water	Air/water
Dimensions (W × H × D, in.)	20 × 41 × 22	20 × 41 × 22	20 × 72 × 22
Power consumption (W)	2500	2500	5500

*Core memory only in AN/UYK-7; semiconductor and core available in AN/UYK-43.

Table 2

COMPARISON OF AN/UYK-7 AND AN/UYK-43 INSTRUCTION SETS

Instruction Sets	AN/UYK-7	AN/UYK-43	
		Compatibility Mode	Superset Mode
CPU			
Arithmetic	yes	same	same
Transfer	yes	same	same
Interrupts	yes	same	new
Mathpac	none	same	new
Stack	none	same	new
Addressing	18 bit	same*	32 bit
IOC			
Channels	16	same	32
Arithmetic	none	same	new

*The AN/UYK-7 compatibility mode provides full 32 bit address ability using relocation registers.

CONCLUSIONS

Because of the effort of APL and NUSC, the primary design objectives of providing the ability to capture UYK-7 applications software have been met through the completed ISA definition. It was necessary to ensure that the software would be compatible with both the completed ISA and the hardware being proposed by two independent competing vendors. Macro extensions that allow the Navy community to produce UYK-43 software code have been transmitted to the Navy.[3-5] In 1983, Engineering Development Models will be delivered to the Navy.

APL is one of four test sites for Engineering Development Model evaluation. Each vendor will deliver a B enclosure in March 1983, and tests will be conducted to demonstrate the UYK-43's software transportability as it relates to tactical operational software.

REFERENCES

[1] *Final Report of the Navy Embedded Computer Review Panel*, prepared for the Secretary of the Navy, Office of the Assistant Secretary for Research, Engineering, and Systems (Oct 1978).

[2] *AN/UYK-7 Instruction Set Architecture (ISA) Extensions*, Appendix H to *AN/UYK(XN-1) Computer Set Functional and Performance Requirements for Full Scale Engineering Development (1 Aug 1981)*.

[3] K. Wander, *AN/UYK-43 Assembler, Modified*, JHU/APL F2F-0-590 (17 Sep 1981).

[4] K. Wander, *Contractor Specific Instruction Macros for the AN/UYK-43 Assembler*, JHU/APL F2F-0-622 (25 Nov 1981).

[5] JHU/APL Lett. TL-81-496 "Modified AN/UYK-43 Assembler and Associated Documentation" (16 Oct 1981).

This work was supported by NAVSEASYSCOM, PMS-408.

RAM COMBAT SYSTEM SIMULATION

B. A. Bredland, R. W. Proue, C. L. Roe, and J. W. Thomas

A milestone in the RAM Combat System development program is the prediction of the performance capability of that system to engage threats in a realistic environment. To obtain these estimates, test data must be augmented with simulation data because current and future missile threats have characteristics that cannot be reproduced in testing with aircraft and drone targets. APL has developed a simulation of the RAM Combat System that will be used in conjunction with actual test data to develop estimates of effectiveness.

BACKGROUND

The EX-31 RAM Guided Missile Weapon System (GMWS) is a lightweight, fast-reaction system designed to engage and destroy incoming antiship capable missiles that employ active radar guidance. The system includes a 5-in.-diameter missile that uses a dual-mode (RF-IR) passive guidance system.

The RAM Combat System that will be tested at the White Sands Missile Range RAM Land Based Test Site consists of a Mk 23 Target Acquisition System (TAS), an AN/SLQ-32 Electronic Countermeasures Set that includes an Electronic Support Measures (ESM) system, the EX-31 RAM GMWS, and the missile round (Fig. 1a). The TAS computer performs combat direction system and weapon direction system functions.

For an optimal engagement, both radar and ESM track data are required when designating targets to the RAM GMWS. The radar provides target position and rate data that are used to determine the time and direction of the missile launch. The ESM system provides threat seeker RF emission data that are used to program the RAM RF guidance. The engagement sequence begins with the detection of the threat by the radar and the ESM sensors. The radar provides untracked target reports to the TAS computer, while the ESM system provides target tracks. The TAS computer tracks the radar reports, correlates the radar and ESM tracks, uses the correlated track pairs to perform weapon engagement processing, and designates threats to the EX-31 GMWS, which completes the launch.

Currently, the EX-31 RAM GMWS is in full-scale engineering development. Testing at the RAM Land Based Test Site will begin in early 1982 and will use operational jet aircraft, unmanned drones, and stationary emitters as targets. However, the jet aircraft and unmanned drones cannot be used to duplicate the high speeds, low radar cross sections, and low-altitude and high-diving trajectories that characterize real threats. Therefore, to augment the test results, a RAM Combat System simulation will be used to estimate RAM Weapon System performance against the expected threats. At the same time, the simulation will be used to evaluate various processing algorithms and system parameters.

DISCUSSION

The RAM Combat System simulation is a Fortran computer program (Fig. 1b) that resides in the VAX 11/780 computer in the APL Embedded Computer System Engineering Laboratory. The following elements of the RAM Combat System are simulated to varying extents by the program: the Mk 23 TAS radar, the SLQ-32 ESM system, the TAS computer processing (including radar tracking, radar-ESM track correlation, and weapon engagement processing), and the EX-31 RAM launcher. The RAM missile round is simulated by another program (see "RAM Hybrid Homing Simulation," by A. T. Galvin and M. D. Foust, elsewhere in this volume). Inputs to the simulation are provided by a scenario generator, which is part of the simulation program. The output of the simulation consists of missile launch data that will be input to the simulation of the RAM missile to complete the effectiveness estimates. The scenario generator and the combat system element models in the simulator are described below.

The scenario generator model determines target position and emitter power received at the ESM system as a function of time. It uses the TAS radar and the SLQ-32 ESM system detection characteristics, sea state, and target characteristics (including trajectory of the target, radar cross section, and emitter power and frequency) to calculate the range at which a track of the target will be established by each sensor. Once the initial ranges have been determined, the true target position and the ESM system received emitter power are calculated for the remainder of the trajectory.

The TAS radar tracker model takes the positions and times determined by the scenario generator for each target in a scenario, adds measurement noise to the positions, and tracks the noisy target positions. The measurement noise simulates the measurement noise characteristics of the radar. The tracker model assumes perfect association and resolution of contacts (position reports) with tracks but does allow for missed scans. A Gaussian noise model is used to simulate the radar track measurement noise for range and bearing. The standard deviations of the Gaussian noise distributions are taken to be the TAS radar measurement accuracies. Missed scans are introduced by setting the radar probability of detection to less than 1, in which case the missed scans

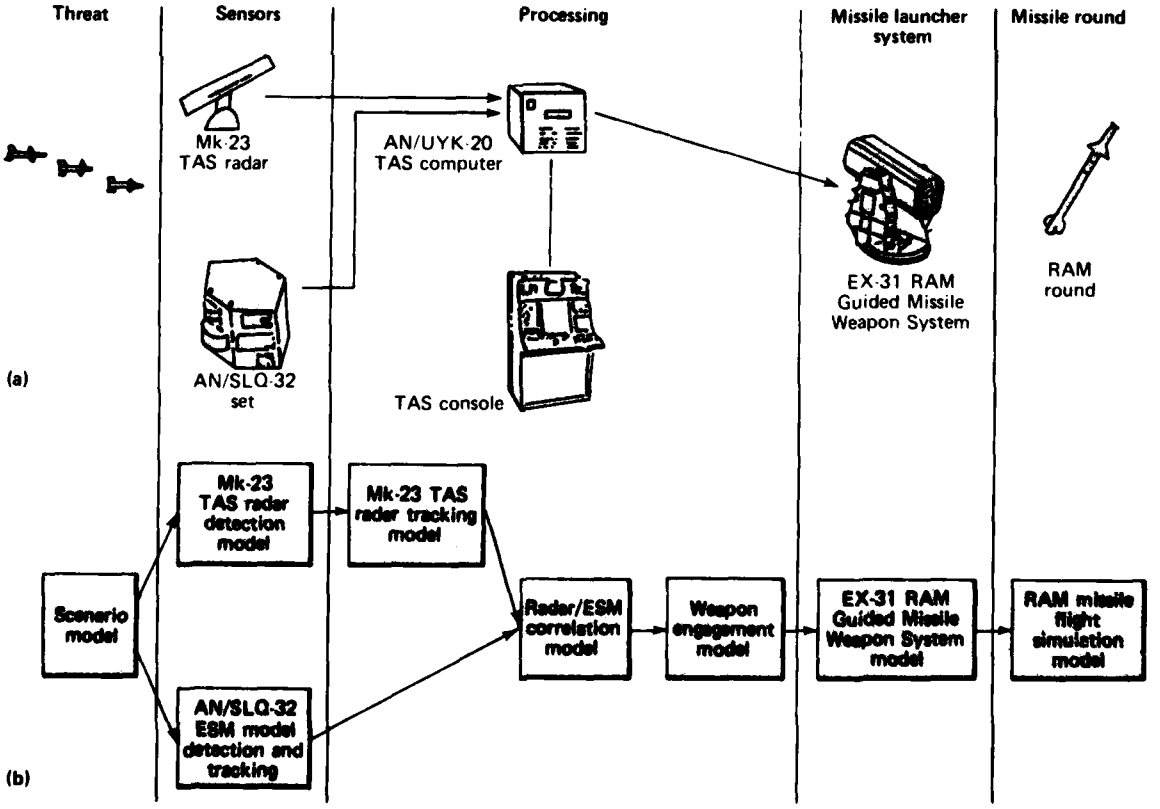

Fig. 1 Simulation of RAM Combat System.

are determined by draw from a uniform 0-1 random number generator. Tracks incurring missed scans are coasted for those scans.

The track initiation and identification logic is patterned after the TAS logic, with the final track identification (friend, unknown, hostile, or hostile missile) declared to be the one that was input to the model. The track category (air, surface, subsurface, and land) is also declared to be the one that was input. When a track is no longer seen by the radar, it is coasted for eight scans before it is dropped. The output from this model includes the target tracked position and position rates versus update time and other radar-tracker-related target parameters such as identification and category.

The SLQ-32 ESM model modifies the output of the scenario generator before sending the output to the correlation and weapon engagement models. Target bearing is the only position parameter it uses. Gaussian random noise with a standard deviation equal to the SLQ-32 bearing measurement accuracy is added to the target true bearing at 1-s intervals. The noise is limited to two ESM bearing reporting sectors, each being 2.8° in extent. The noisy bearing is then quantized to the center of the ESM bearing sector in which it falls. If this bearing is different from the one previously reported, the model updates the ESM track bearing. Thus, the ESM track updates are random in time whenever the bearing changes by one or more sectors. The output of this model is ESM track update reports for all ESM targets, ordered by update times.

The radar-ESM track correlation algorithm model is patterned after an algorithm previously developed. Radar and ESM tracks are matched by first comparing common track parameters in gate tests to filter out track pairs with inconsistent parameters. For the remaining pairs, association lists comprising radar tracks ordered by correlation quality are formed for each ESM track. This quality is a functional value that measures how closely the radar and ESM tracks correspond. Using the correlation quality, the radar and ESM tracks that are resolved to be best matches are declared to be correlated. The correlation status of each track is reviewed periodically to determine if it should be retained or changed. Within the model, the various subfunctions, gate tests, and parameters were taken from the TAS track correlation algorithm. The output of the correlation algorithm model is radar and ESM track correlation status versus time.

The weapon engagement function (WEF) model, patterned after an algorithm developed previously, simulates the TAS threat evaluation weapon assignment and engagement monitoring processing. The WEF tasks are performed in parallel with the correlation processing tasks within the simulation. The WEF tasks monitor the radar and ESM track files to evaluate each threat, designate threats to the weapon system at the appropriate times, and monitor the ensuing engagement. Breakpoints within the simulation computer program extract threat prioritization, designation, launch, and engagement data versus time. Weapon system status data are also extracted periodically.

The EX-31 GMWS model consists only of the time delays that occur within the RAM Weapon System from designation to launch. The simulated time delays are for RAM Launcher Control and Interface Unit processing, for launcher slew to the target bearing, for Launcher Switching and Multiplex Unit synchronization, and for missile round warmup, activation, and arming.

SUMMARY

When the simulation has been verified, it will be used to evaluate RAM Combat System effectiveness. The simulation verification will consist of comparing simulation results with test results for a selected set of scenarios to ensure that critical event times and data accuracies are consistent. The verified simulation will then be used to obtain effectiveness estimates for a larger set of selected scenarios that are representative of anticipated threat situations.

This work was supported by NAVSEASYSCOM, SEA-62Z4.

3. BATTLE GROUP CONTROL SYSTEMS

INTRODUCTION

The work described in this section is directed toward the Navy's Battle Group anti-air warfare (BGAAW).

Historically, development efforts to improve Battle Group control capabilities have been based primarily on improvements to individual ships and aircraft and have provided increasingly more effective missiles and radar. However, they have not changed the relative unbalanced relationship of offensive to defensive. Longer range weapons, flying at higher speeds and altitudes and launched in the presence of sophisticated penetration aids from a variety of *weapons carriers above, below, and on the sea,* necessitate control systems that fully exploit individual ship and aircraft weapon capabilities and that provide a Battle Group capability greater than the sum of individual ships and aircraft. APL has an expanding role in the formulation of concepts to achieve this synergism, in the development of models to validate the concepts, and in the introduction to the Fleet of advanced systems to meet the demands of the increasingly complex AAW environment.

Significant efforts are involved in providing a coherent air picture and computerized decision aids to the decision-maker, a continuous automatic gridlock system, and jam-resistant high-capacity data links.

Recognition of the importance of Battle Group AAW coordination and concepts for improved control processes evolved at APL in the early 1970's. Achievable gains were documented in studies by APL and others in the mid 1970's, particularly as they related to coordination of the Battle Group and use of Aegis combat system data. Proposals were made to the Navy; in June 1975 and again in March 1978 the Defense System Acquisition Review Council directed that Aegis be used to improve Task Force Anti-Air Warfare Coordination (TFAAWC). There was a subsequent name change to BGAAWC, but the basic direction remained the same — to exploit the capabilities of Aegis in concert with other ships and aircraft of the Battle Group so as to increase the total AAW defense effectiveness.

Activities in 1981 have concentrated on Battle Group AAW display upgrades to the Aegis combat system and on supporting analytic studies in gridlock and data exchange requirements. Planned upgrades to *Ticonderoga* and future Aegis ships, along with gridlock and improved data exchange, are on course.

The following articles report on various activities that support BGAAWC development.

DESIGN OF BATTLE GROUP AAW DISPLAY GROUP

E. C. Prettyman, D. P. Serpico, and F. J. Willey

The systems that provide direct support to the Commander of a Naval Battle Group are a major factor in the coordination of weapons actions among the ships and aircraft comprising the group. Within the area of anti-air warfare (AAW), APL has been developing the Battle Group AAW Display Group (BADG) to support the AAW Commander. Articles in previous years have reported the background analysis of AAW command activity and overall requirements for the coordination of AAW throughout the Battle Group. Work this year has applied those analyses to the development of BADG. The BADG system provides information processing and summary displays to aid in the command process. It provides the basis from which control may be exercised over AAW systems of the Battle Group.

BACKGROUND

The Battle Group AAW Coordination (BGAAWC) Program is devoted to the exploitation of existing and planned Fleet AAW systems to coordinate AAW in a Battle Group. The officer assigned as Battle Group AAW Commander has an urgent need for timely and accurate tactical information, for reference to the status and capabilities of all units under his command, and for a way to convey his decisions rapidly and reliably to the units that must respond. The inherent capabilities provided by Aegis ships have been made the basis for the development of a command support system that is one of the main elements of the BGAAWC Program.

Ticonderoga (CG-47) class ships have been selected as the host ships to support the AAW Commander because of the availability of the precision data from the Aegis AN/SPY-1A radar, the versatile automated weapons control, and the extensive display capabilities that far exceed the capabilities of other systems in the Navy.

DISCUSSION

A top-level functional requirements document has been generated to define the elements needed to coordinate AAW and to establish formal bounds and development objectives to guide system engineering. The document is derived from an extensive study of AAW command requirements to define the system problem and to establish the "traceability" between the official Navy definition of AAW coordination and BGAAWC system development. The BGAAWC system is organized into five major AAW functions: command, surveillance, weapons control, engagement, and communications. The BGAAWC system can be thought of as the aggregate of the elements needed to provide Battle Group AAW coordination. BADG is the element that supports the AAW Commander.

BADG is comprised of display and support equipment furnished to the AAW Commander and his immediate support staff to provide decision-making assistance, an information source, and an interface with the forces he commands (Fig. 1). BADG system design has been extended to incorporate similar support for two levels of command, the ship's Commanding Officer and an Embarked Commander allocated duty as AAW Commander. Personnel will make use of a command console to communicate decisions to subordinate personnel and automatic systems. Large-screen displays allow group viewing and facilitate comprehension. The following guidelines have been established for BADG development:

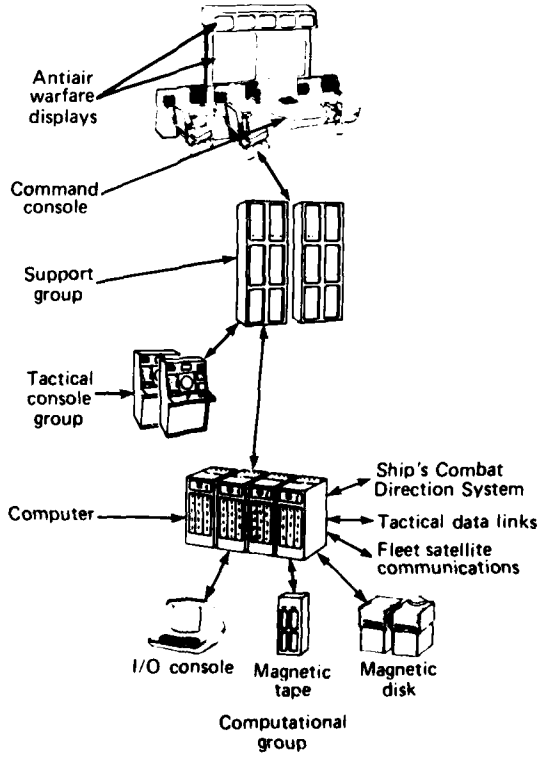

Fig. 1 The Battle Group AAW Display Group.

1. BADG will provide for the collocation of command principals. It provides battle stations for the ship's Commanding Officer and Tactical Action Officer (for the ship command function) and for the Embarked Commander and supporting staff watch officers (for the AAW coordination function).
2. All information essential to decision making will be available to the staff.
3. Large-screen displays will allow group viewing and increase comprehension.
4. Displays will be tailored to command requirements (the traceability of displayed information to specific decisions and to specific responsibilities will be emphasized).
5. Display symbology will be representative of the detail level of the information displayed.
6. An immediate and direct means of transmitting decisions will be provided for by a command console.

BADG consists of two command display groups, a tactical console group, support equipment, and computational equipment. A command display group consists of two large-screen projection displays, five automated status boards, a dual-position command console, and an assistant's console — all elements of the AN/UYQ-21 standard display equipment. The support group consists of unmanned signal data processing and graphics generation equipment. The computational equipment consists of a computer, a mass memory device, and peripherals.

The Commanding Officer and Embarked Commander display groups are adjacent to each other — allowing for cross-viewing of displays and discussion among command principals. In each group, five 17-in.-diagonal cathode ray tubes (called automated status boards) are arranged across the top of two large-screen projection displays, each 42 inches on a side. The command console[6] provides cathode ray tube readout units in each wing section and in the center unit. Control resides in the wing sections of the command console and in the assistant's console adjacent to the command console. Standard UYQ-21 console control components include action panels, a communication panel, a track ball assembly, and a keyboard.

The following is an overview of the AAW command staff positions and responsibilities.

AAW Commander — responsible for the destruction or neutralization of enemy aircraft and airborne weapons, whether launched from air, surface, subsurface, or land platforms, including all of the measures employed in achieving air superiority through the use of weapon systems.

Staff Tactical Action Officer — directs and monitors overall AAW operation in accordance with the AAW Commander's orders; communicates on the task force/task group command net with the Composite Warfare Coordinator, other warfare area commanders, and asset coordinators.

Force Engagement Coordinator — ensures engagement of air threats; ensures identification and safety of friendly air units; reports status of AAW units; and controls the AAW control net or AAW control and reporting net, if used.

Force Information Coordinator — correlates external data reports with Battle Group data; identifies forces, raids, and other air traffic; monitors AAW plots and status boards for accuracy and timeliness; coordinates air tracking and track reporting; and controls the AAW reporting net, when these tasks are not being performed by the ship's Tactical Information Coordinator.

Force Display Assistant — assists the Staff Tactical Action Officer in large-screen and automated status board setup and enters data for displays.

Information Structure

The prime objective of BADG is to aid the AAW Commander in understanding the air situation and maintaining tactical control of his assigned forces. The Commander must be kept abreast of the status of these forces, be aware of their performance capability, keep track of enemy performance capability and status, be aware of the environment, and understand the interplay of the foregoing. The amount of information that he must have may be staggering. If BADG accomplishes little else, it must manage this information by providing a structure that allows effective access and appropriate visual aids for a rapid understanding of the information and situation. The temptation to "display everything" must be avoided; displays need to be tailored to specific decision requirements. Top-level summary information must be emphasized, while detailed information must be readily available upon request.

With this in mind, a structure has been introduced into the display and information organization. Figure 2 shows the structure for large-screen and automated status board display formats. At the summary level, only top-level information (or items requiring immediate attention) is provided, for example, summaries of force status and of a particular warfare area. The next level of selectable displays is more detailed in nature; for example, each element of the AAW battle has a dedicated format, or the status of a specific unit in the force or of a specific enemy activity is provided. Additional levels of amplification are selec-

table to support detailed decision functions such as performance overlays and specific decision aids or readouts pertaining to individual systems or enemy units.

The selection of what information appears at which display window is at the option of the Commander. A typical display (Fig. 3) might show an AAW summary on one large screen and "outer battle" information on the other. Status boards would be complementary to the large-screen displays. Command console center unit displays may be more specific, focusing on some aspect of the outer battle, for example, the "Aircraft Commitment Guide" and the "Weapons Allocation Guide" formats.

Summary	
Elements of AAW battle	Outer battle Inner battle Point defense Disposition of own forces Disposition of enemy forces
AAW system configuration	Performance overlays Detection characteristics Weapon characteristics Operating doctrine
Specific decision aids	Aircraft commitment guide Station location planning Intercept zones Attack geometry Remote designation Kill evaluation Engagement planning Surface maneuvering Estimated time of arrival of units

Fig. 2 Structure for display of AAW information.

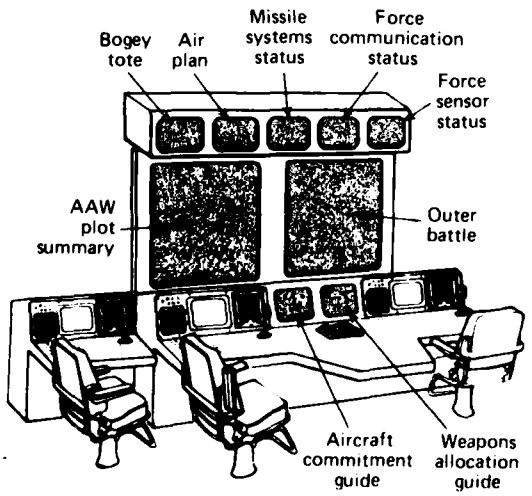

Fig. 3 Typical BADG display configuration.

Functional Description

Information access, display, and control of BADG are accomplished largely through interaction of the BADG operators with computer programs. The BADG computer program has been partitioned into four functional areas: Data Management, Display and Evaluation, Tactical Control, and Support Control.

Data Management. The BADG computer accepts tactical data from Battle Group units via the host unit's (i.e., CG-47) Combat Direction System (CDS). It also accepts data from Battle Group and remote sources via voice and Teletype communication, although these data are entered manually into the BADG computer data files. The BADG computer processes aid in the interpretation of these data by recognizing and declaring track groupings, maintaining track history, and enhancing displays. The processes provide for computer-to-computer communication with the host ship's CDS and with participating ships and aircraft. They also support communication with higher authority and with other warfare areas within the Battle Group. The result is a flexible, accessible ensemble of all available information regarding the Battle Group's AAW operation and the means to distribute selected portions of that information to other systems.

Display and Evaluation. The BADG displays are required to present a comprehensive, clear, and timely picture of the AAW tactical situation, including summaries of the strategic situation and of other warfare areas. The display controls allow the level of detail to be selected, provide multiple simultaneous viewing of display formats, and are readily adaptable to current mission needs.

Modern combat involves environments with heavy concentrations of targets, weapons, and ships. The complexity of the tactical situation can render operators ineffective to the point of helplessness. BADG consequently is required to simplify the role of the operators and Commanders by integrating and abstracting the tactical environment to clarify the situation. The displays are built from the information base described in the Data Management Functional Area. Primary inputs for display include (a) the air-track picture, derived from AN/SPY-1A tracking and supplemented by other sensor and data link reports; (b) the situation picture, with data from both manual inputs and automated sources; and (c) the Battle Group's AAW configuration picture, constructed from AAW doctrine entries and from status reports of participating AAW units.

The final result of the Display and Evaluation Functional Area is a tactical data summary that allows the operational personnel to pursue their mission without being swamped by detail while still retaining the availability of detail for perusual when desired.

Tactical Control. BADG assists the AAW Commander and his staff in controlling air surveillance, AAW weapons control, and AAW engagement. It supports the formulation and promulgation of AAW operating doctrine for the Battle Group. Its capabilities permit both centralized and decentralized operations and provide automated support of the centralized modes of operation.

The AAW Commander and his staff can control operations through reconfiguration of dispositions and readiness status, modification of doctrinal rules, and direction or negation of AAW unit actions. BADG personnel generally effect AAW engagements by promulgating operational and weapons doctrine, but retain the capability for several optional levels of centralized engagement control.

In support of the AAW weapons control objectives, controls are provided for the management of radars and track reporting, radar and illuminator frequency allocations, and data link operations. Conflicts in radar coverage and track reporting are monitored, and recommendations are made when indicated for the reconfiguration of radar and ESM operations.

Support Control. This area is allocated BADG requirements that are not directly a part of the tactical operation but that support the system initiation and configuration and provide general capabilities supportive of the tactical functions, such as data extraction and test-target generation.

BADG Implementation

The initial BADG implementation is targeted for *Ticonderoga* (CG-47) class ships to exploit the SPY-1A track data sets and other capabilities of the Aegis Combat System. The Aegis design includes an Aegis Display System (ADS) that can be extended to incorporate BADG. The ADS supports both the Embarked Command and the Aegis ship's Commanding Officer, either of whom may be assigned Battle Group AAW command duty. The initial ADS design for *Ticonderoga* includes essential elements of the BADG equipment, display support, and functional support of ship command. Its development has been the responsibility of the RCA Corp., the Aegis Prime Contractor. Planned upgrades of this system will incorporate additional BADG capabilities as the requirements are validated and approved.

Consideration has been given to using selected Terrier/Tartar cruisers as control units in a parallel effort to act as AAW control units in non-Aegis Battle Groups. Subsequent BADG implementation may extend AAW Command support to other ship classes and thus accommodate situations where Aegis ships are not available.

SUMMARY

Requirements for BADG, as summarized above, have been stated in a Design and Operations Concept Document and a System Development Specification. The preparation of detailed computer program performance and design specifications has begun. Future work includes completing the APL model for requirements validation and integrating the system requirements into the *Ticonderoga* class combat system.

This work was supported by NAVSEASYSCOM, PMS-400.

BATTLE GROUP GRIDLOCK ANALYSIS

J. T. Miller

Significant efforts have been made to develop a continuous automatic gridlock system to solve a long-standing Fleet problem involving the exchange of track data among ships of a Battle Group. In support of the development of this capability, experiments using radars at APL and at the Naval Research Laboratory graphically demonstrated one step in the development of the ability to align Battle Group radar data bases with a precision comparable to the accuracies of the radars used.

BACKGROUND

Gridlock is a process for aligning the coordinate frames used by individual Naval units to report on targets detected and/or engaged during normal combat operations. Because of various systematic errors in the units' navigational position estimates, radar calibration and alignment, and data manipulation systems, the coordinate frames do not normally align to the degree necessary to support Battle Group Anti-Air Warfare (AAW) Coordination. Gridlock corrects these misalignments by correlating own-ship tracks and remote tracks that represent the same physical object (i.e., mutual tracks) and then uses the differences in the observed positions of the tracks to compute corrections to the coordinate transforms employed in transferring data between units.

The Battle Group Gridlock Analysis effort is directed toward assessing the nature of the misalignments actually realized by operational units and developing improvements to the current Naval Tactical Data System (NTDS) gridlock processing to achieve more precise alignment of the Battle Group's track data bases. Such improvements support the development of more comprehensive and coherent surveillance pictures that are the basis for allocating and controlling the Battle Group's weapon assets. The improvements become more imperative with the introduction of automatic surveillance systems, such as Aegis AN/SPY-1, AN/SPS-48C Automatic Detection and Tracking, and the New Threat Upgrade AN/SPS-4E with AN/SYS-2, which develop large comprehensive track data bases of the air situation. These data bases could easily saturate any force-level data handling/manipulating system, particularly if redundant detections are improperly handled as separate targets, as is likely to occur in high-density raids if the unit coordinate frames are not adequately aligned.

DISCUSSION

The three aspects of the Battle Group Gridlock Analysis are being pursued more or less simultaneously.

Assessment

To develop a system that can correct misalignments in tactical air pictures of individual combat units, it is necessary to assess the nature of the misalignments actually encountered by operational units by obtaining simultaneous track data from two or more operational radar suites, extracting the mutual track data, and observing the differences in parameters for tracks held in common by the two sites.

The data can be collected in several ways. For example, during the late summer of 1979, two Digital Data Collector tape recorders were placed at two AN/SPS-39 radar facilities, one at APL and one at the Naval Research Laboratory (NRL). The machines simultaneously recorded the detections made by both radars during a half-hour period. The tapes were processed at APL as outlined in Fig. 1.

The recordings of radar hit data were processed off line to develop simultaneous track data bases for the two sites. The track files were then collated and correlated to provide a simultaneous track picture as seen by both sites. Subsequent evaluations of these data indicated that, despite the exact knowledge of the position of each radar and the high level of technical support at both facilities for maintaining them, the reported positions of the mutual tracks differed significantly (almost 3 nmi average). Part of this error was eventually attributed to north pointing errors of the sites and part was due to the presence of bearing-dependent errors in the reported track positions, as is illustrated in Fig. 2. This figure shows the actual observed azimuth difference between NRL tracks translated to APL and the corresponding APL tracks, as a function of the azimuth of the APL tracks. These types of bearing-dependent biases are not accommodated by current NTDS algorithms and are an area for potential improvement of the NTDS design. The cause of these errors is unknown but is believed to be the result of radar synchronizer errors.

While the NRL/APL data provided valuable experience and insight as to the nature of biases in SPS-39 radars, actual data from shipboard radars at sea, particularly SPS-48C radars, were essential for the assess-

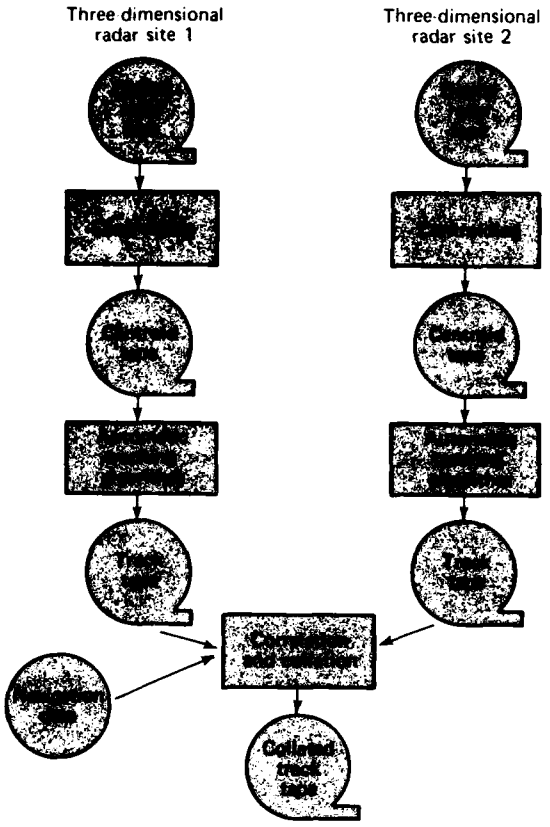

Fig. 1 Gridlock data-reduction chain.

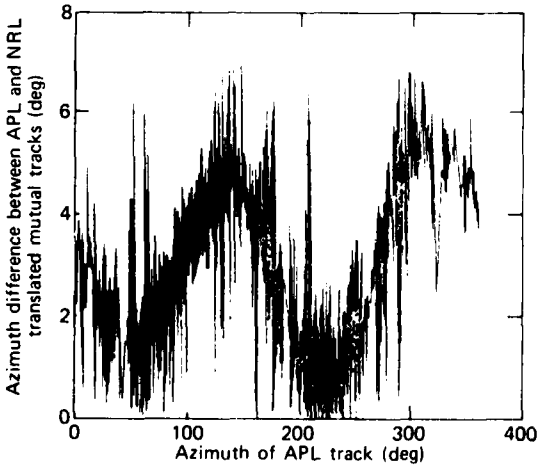

Fig. 2 Azimuth errors observed when NRL and APL data bases are compared in the APL coordinate frame.

ment of operational-system biases. Two subsequent attempts to repeat the Digital Data Collector recording aboard ship were incomplete because of equipment failures. As a result, an alternative approach was developed that uses less equipment. It uses the standard NTDS Link Buffer Extract routines to record Link 11 message traffic (particularly the Link track reports) normally exchanged by NTDS units. To overcome potential problems with the suppression of mutual tracks normally performed by NTDS to prevent Link saturation in an operational environment, the Data Link Reference Point of one unit was offset relative to a second unit. When the Link buffers are examined for the two units, the complete data bases of both units are found if no other units are on the Link.

Such a data collection was performed on 28 August 1981, using an E2C and the Aegis Combat Systems Evaluation and Development Site at Moorestown, N. J. and more recently aboard USS *Eisenhower* (CVN-69) and USS *R. K. Turner* (CG-20). Both of these data bases are being further evaluated for gridlocking at this time.

Bias Estimation Algorithms

Given the observations derived from the assessment of actual data, the next step is to develop analytical models that describe the differences in the observed mutual tracks. Such models provide intuitive explanations for the root sources of the biases in the system, indicate possible interrelationships, and guide the development of computer program routines for correcting the biases.

The full gridlock process involves three major algorithms: a correlation algorithm to identify mutual tracks, a bias estimation algorithm to estimate corrections (called pads) needed to align the data bases, and a bias pad application routine that actually realigns data transmitted and received between units. The design of each algorithm depends on the bias models developed from the data assessments.

For example, the correlation algorithm identifies mutual tracks based on the proximity of local and remote tracks. A remote track close to a local track going in the same direction with the same speed and height probably indicates a mutual track pair. Such judgments may be corrupted in the presence of coordinate frame misalignments, making true mutual tracks appear widely separated. Simultaneously, the misalignments may cause true nonmutual tracks to appear closely correlated and therefore judged as mutual tracks by the correlation routine. For gridlock processing, the correlation must be resistant to such miscorrelations. If the units are aligned relatively well initially, techniques can be devised to maintain valid correlation judgments on

mutual tracks by coupling the correlation routine with the bias estimation routine. More robust but computationally more complex approaches are also possible for situations when the initial alignment is poor. If it is too poor, however, manual correlation by operators is the last resort.

Bias estimation algorithms need to know what biases to estimate (and the correction algorithms need to know what corrections to make). Therefore, these designs rely on the bias models to guide in the selection of the biases to estimate and the selection of other features such as maneuver adaptions.

Even with the assessments and the models, it is possible to overlook biases in the data because the effects of some biases may mask the effects of others. It is often necessary to develop algorithms based on theoretical considerations, exercise them with actual data, and assess the results. This is done by evaluating various measures of effectiveness for the algorithms and selecting the techniques that appear most effective with actual data. Such evaluations can also be used to compare the relative performance of various estimation techniques (Fig. 3).

For example, in order to quantify the differences in alignment quality achieved using various gridlocking techniques, the average distance in nautical miles between NRL radar tracks (translated to APL) and the corresponding APL radar tracks was evaluated for each scan. Figure 3a illustrates this distance for navigational alignment only, i.e., the known geodetic position of both sites that was used to align the two data sets. No other alignment correction was applied. Figure 3b illustrates the quality that can be achieved with a properly redesigned NTDS algorithm that corrects for constant translational and rotational biases. Figure 3c illustrates the quality achieved when an algorithm accommodates the bearing-dependent biases as well as translational and rotational biases. In fact, this value was found to be comparable to an estimate of the combined measurement noise for the SPS-39 radars used. Thus, it represents essentially the statistical limit that could be achieved with these data. Fluctuations in the curves are a consequence of measurement errors in the radars and of variations in the spatial distributions of the observed tracks.

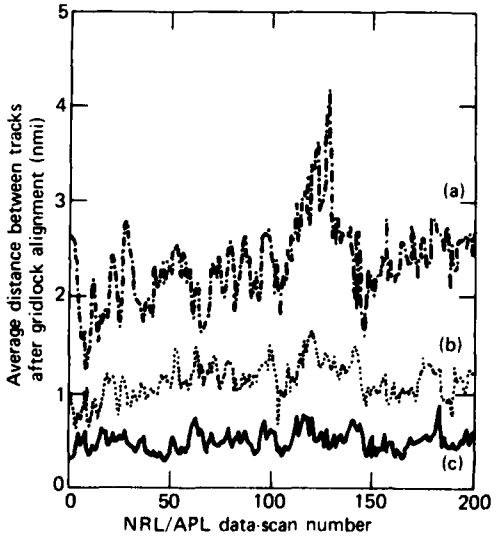

Fig. 3 Comparison of three alignment techniques.

A point should be made on the observation that alignment based on precise navigational data is the poorest of the three. This is a consequence of the fact that improving navigation alone cannot overcome radar misalignments (as was done to provide the alignment using the last two techniques in Fig. 3). Thus, to achieve precise alignment of the track data bases used by tactical units, the gridlock function must compensate for both navigational misalignment and sensor biases.

Bias correction algorithms are relatively easy to define because they are strongly related to the corresponding bias estimation routines. Defining the estimation algorithms essentially defines the correction algorithm.

At APL, complete software systems have been developed to aid in the rapid development and assessment of algorithms for aligning multisite data. The systems have been used to perform all the functions described.

Design Support

Design considerations of operationally useful systems pivot on ensuring the availability of appropriate track data bases for bias estimation and on providing computational assets to ensure that the desired function can be performed. As a result, this effort involves detailed functional studies of the actual processing and data flow of operational units and of the limitations of the hardware on the units. For example, on most operational units today NTDS has very limited ability to perform additional computational functions. In particular, the processing limitations for most operational systems are so severe as to necessitate the performance of desired gridlock functions in a separate computer (such as a UYK-20 minicomputer).

This leads to considerations of where an additional computer could be placed to supply the needed data and yet not require a major revision of the NTDS structure. In particular, once the corrections are computed, how are they made available to NTDS? Because NTDS computers currently have no spare in-

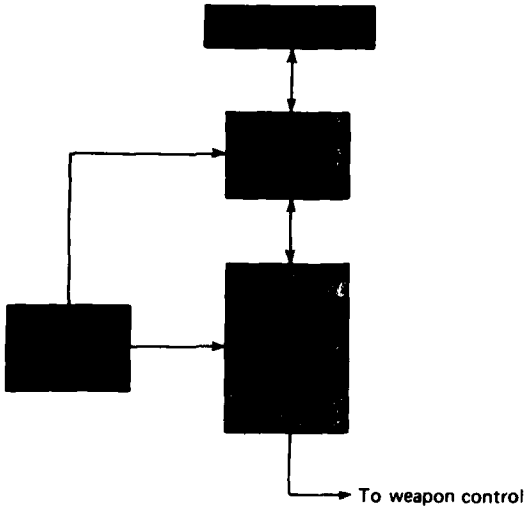

Fig. 4 Concept of gridlock system.

put/output (I/O) ports for communicating with new equipments, the new design must use one of the existing I/O ports in a new way. As the coordinate frame alignment only needs to be applied during Link data exchanges, the I/O port to the Link terminal is the most logical candidate.

Because the link reporting responsibility suppresses mutual tracks, a separate interface to the unit's tracking computer would ensure a complete copy of own-ship tracks for the correlation and alignment process. A design (Fig. 4) that would perform all the functions necessary to align track data communicated between units over the data link as the track data flow between NTDS and the Link terminal, without the modification of either system, is currently being implemented for demonstration aboard ship at sea.

This work was supported by NAVSEASYSCOM, PMS-400.

BATTLE GROUP AAW DISPLAY SYSTEM

F. R. Skolnick

The Battle Group Anti-Air-Warfare Display System is a multicolor graphical display of the area of protection and depth of fire provided by a single ship or Battle Group in defense of an aircraft carrier (CV). A demonstration model is operational on the RAMTEK 9400 graphics system operating on the AN/UYK-7 computer, displaying data on a color monitor.

BACKGROUND

The traditional representation of missile or system intercept coverage has been in the form of intercept contours against constant-speed, constant-altitude targets, as illustrated in Fig. 1. When consideration is given to the vertical profile of the target, particularly for the newer air-launched antiship cruise missiles (ASCM's), the contour represents a horizontal projection of the intercept capability. Recently the effects of the spacing between the firing ship and the targeted point (nominally the CV in a Battle Group situation) have been taken into consideration. The area defense coverage is particularly sensitive to the attack geometry of diving high-performance targets. This information would be quite valuable in determining the disposition of a Battle Group and also in evaluating the impact of specific dispositions. These considerations led to the investigation of a display system for on-board application. Coincidently, color graphics appeared to be an ideal tool to illustrate both area and level of coverage provided by the surface-to-air missile (SAM) ships in a Battle Group.

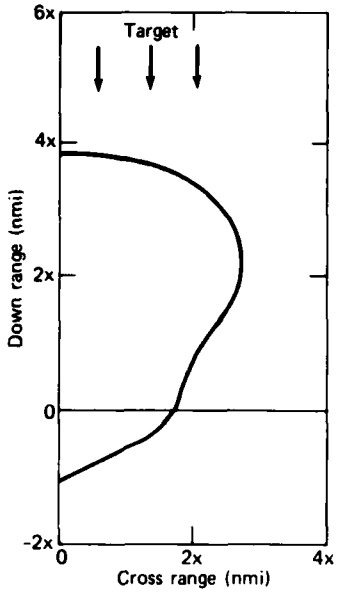

Fig. 1 Intercept contour.

DISCUSSION

The concept for the development of the Battle Group Anti-Air-Warfare Display System (BGAAWDS) includes the computation of contours as a function of target, spacing, and weapon system and the ability to select and display coverage associated with a defined disposition. The first phase of system development was to attack the last part of the problem, that is, the display. A demonstration model was developed that can display up to four systems. It has been used to demonstrate the feasibility of the concept and to evaluate various techniques concerning the use of color.

The current system has the following capabilities:

1. Contour display of the area of protection referenced to the CV,
2. Composite contour for up to four SAM ships in the Battle Group,
3. Plots of depth of fire versus threat direction,
4. Composite depth of fire for the Battle Group,
5. Overlay comparison of any contours stored in the library, and
6. Selectable orientation of the firing ship.

Figure 2 shows a single-system contour and depth-of-fire chart. They appear on the display in green. The gray area of the contour on the left represents the system's intercept capability against targets inbound to the CV, which is located at the origin. In this example, the firing ship is located x nmi north of the CV. The depth-of-fire chart, in polar coordinates, indicates that the system can achieve a depth of fire of three against targets approaching within about 45° of north. The capability against all other targets is a depth of fire of two.

Once the basic contours have been stored in the system library, the display can be used either to perform a parametric comparison of two systems or to build up a composite picture of the Battle Group coverage. Parameters that could be investigated include ship spacing, target capability, reaction time, detection capability, and missile capability. The effect of ship spacing is illustrated in Fig. 3. The light-tint zone (yellow on the display) represents the area associated only with the 2x nmi spacing; the dark-tint zone (blue on the display) represents the area where both systems have coverage; the medium-tint zone (green on the display) represents the area of coverage unique to the x nmi spacing. Thus, one can observe the area of earlier intercept that was gained by moving out to 2x nmi and the amount of close-in and rear protection that was lost. The depth-of-fire chart reveals that the potential number of engagements against targets from various directions does not improve for any targets when the ship is moved out to 2x nmi and is worse for most target attack directions.

Because there is no capability to intercept the illustrated high-performance target once it has passed the firing ship, placement of the firing ship farther from the defended point has the effect of shifting the engagement zone but not increasing its size. Against a slow target, there typically would be an improvement in depth of fire about the 0° axis when the firing ship is placed farther from the CV.

Figure 4 is an example of a three-ship Battle Group. There is one ship at 2x nmi at 0°, a second at x nmi at 135°, and a third at x nmi at 225°. The light-tint zone represents the area of single-ship coverage by any of the three ships. The medium-tint zone indicates the areas in which two ships have overlapping coverage. The dark-tint zone represents the coverage area for all three ships. This display format can be used to obtain a qualitative measure of the area of individual or mutual system coverage as a function of ship disposition in a Battle Group. A composite depth-of-fire chart can be obtained for the same ship disposition by overlaying the individual depth-of-fire charts.

Depth of fire is the first level of a quantitative measure of coverage for a Battle Group. One aspect of the continuing system development is to investigate deterministic measures of effectiveness that will take into account system capacity and mutual coverage.

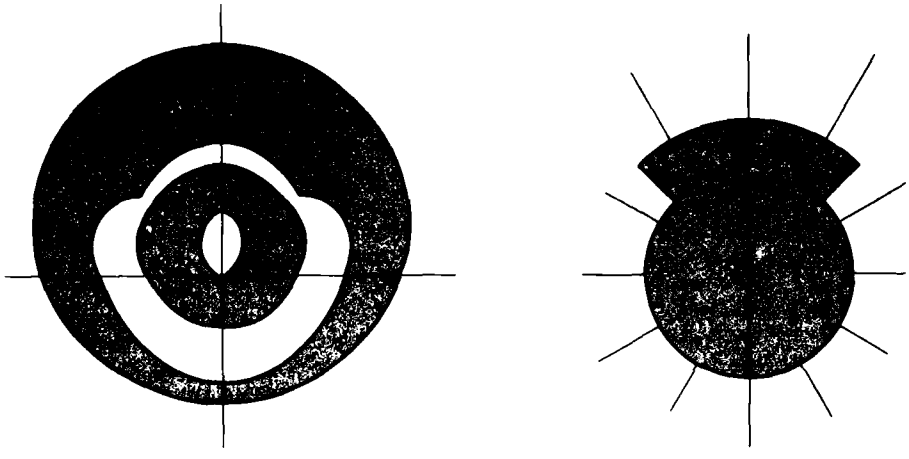

Fig. 2 Single-system contour and depth-of-fire chart.

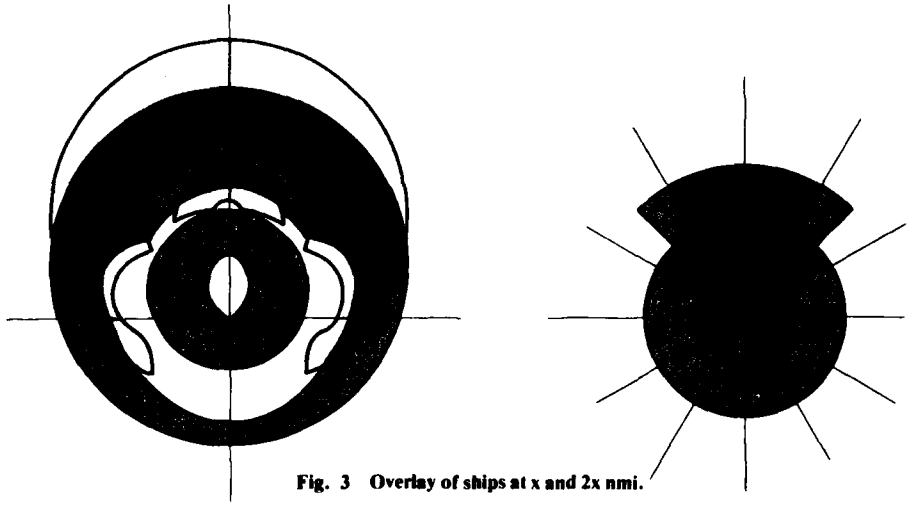

Fig. 3 Overlay of ships at x and 2x nmi.

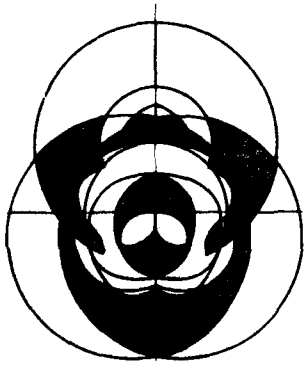

Fig. 4 Battle Group composite contour for three ships.

The demonstration model has achieved its goal of showing the potential for color graphic presentations of area defense coverage contours. The monitor is currently located in the APL Combat Systems Evaluation Laboratory, and a demonstration of BGAAWDS has been given to a number of visiting military personnel.

This work was supported by NAVSEASYSCOM, PMS-400.

REAL-TIME SIMULATION ARCHITECTURE FOR BATTLE GROUP AAW

C. E. Crooke, J. G. Frink, A. H. Mattheiss, and J. M. Pierce

A Battle Group Anti-Air-Warfare (AAW) Coordination Display Group (BADG) under development at APL will require extensive environmental simulation to support test and evaluation. As the BADG development progresses, a widening of scope and an increase in fidelity level will be required of the simulation. A system architecture developed for the BADG environmental simulation has been designed to survive the changing requirements expected during the life of the project.

BACKGROUND

The basic concept selected for the real-time simulation is one of independent simulation functions contained in microprocessors and communicating by means of messages. These messages are sent to all other simulation functions in the system (i.e., other simulation functions resident in the same or other microprocessors). Each function receives only those messages it has previously selected as germane to its task. This concept is called "message broadcast with receiver selection." An illustration of the concept is the paging system in a public building. Everyone hears the page but only those interested in the message listen to it.

The broadcast architecture is implemented in both hardware and software. The functional elements of the software, broadcast elements, are mapped into a network of computers called computing elements. The broadcast elements communicate via messages, and the computing elements transfer the messages via a broadcast data bus.

The concept of an extensible, multiple-computer architecture has already been demonstrated in a series of prototype systems at APL.

DISCUSSION

An architecture was needed that not only could meet current simulation requirements but also could be easily extended or modified to incorporate new or modified functions. Such an architecture has been developed and implemented in both hardware and software. This functional extensibility is important in any system design but is critical for the simulation being developed for BADG.

The development of this architecture involved work in three parallel but mutually supporting areas: simulation software, executive software, and bus-related hardware. The process of broadcasting messages ties together all three areas.

Simulation Software

A guiding principal in the design of the simulation software is to make simulation elements correspond as closely as feasible to Battle Group equipments, groups of equipments, or combat units. A sensor is installed or removed from a simulated ship by loading or unloading one of the functions in a computing element. A missile is launched or destroyed in the same way. Because simulation functions communicate only by broadcast messages, they can be added or deleted without affecting the integrity of the simulation as a whole.

This concept is illustrated in Fig. 1, where simulation functions are represented as vertical lines and messages as circles. The idea is that each function is a transition in a left to right flow of information. A transition is activated by the receipt of a message and may, in turn, activate one or more other transitions by broad-

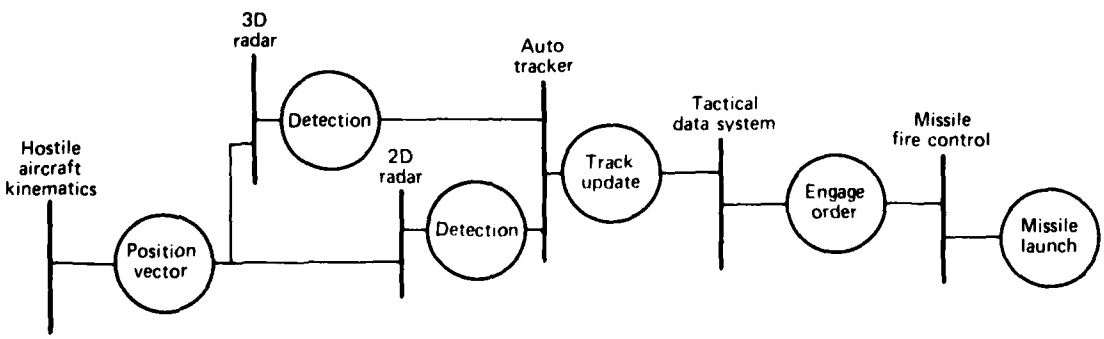

Fig. 1 Successive triggering of simulation functions by message.

casting a message. Two radars are shown in the figure. One could be removed without affecting the flow of information from the hostile aircraft to the tracker.

Combat environment simulation programs generally include a central file where information on all units of the scenario is maintained. A consequence of this design is that, whenever a unit is no longer involved in the scenario, it must be purged from the file along with all pending events associated with it. A cleaner design has emerged from the notion of broadcast elements because each unit maintains its own kinematics parameters and associated events. Thus, when a unit is deleted from the exercise, all its ties with the rest of the simulation automatically disappear.

Executive Software

Within each computing element there is an independent executive program that provides services typical of an executive in a traditional system. Included are control over which hosted tasks are executing at any given time, the dynamic allocation and deallocation of memory, and the ability to define and start new tasks. The executive can also be thought of as having the function of making the physical environment transparent to the executive's hosted tasks. Stated another way, a simulation task does not have to know which computing element it is in or which computing element any other simulation task is in.

The executive provides additional services that are specialized to the concept of distributed processing. The main services in this category are those that allow a hosted task to send and receive messages and to register for the messages it wishes to receive.

Bus-Related Hardware

The bus-related hardware is responsible for providing the communications between computing elements. It is the key element of the architecture because it forces a broadcast mode of communication between computing elements.

The anticipated scope of the simulation software imposes severe constraints on the design of the hardware. The design goal is to support up to 256 computers

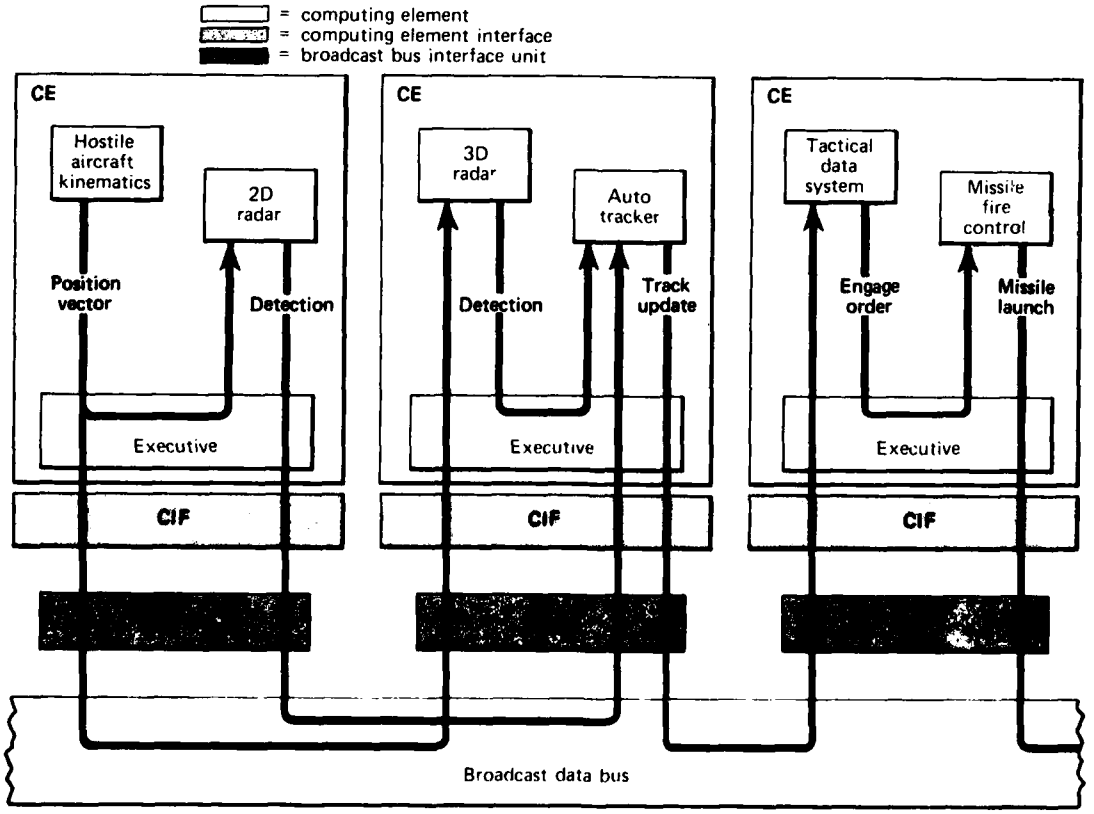

Fig. 2 Example application of broadcast architecture in hardware and software.

at a bandwidth of 16 million bits per second with a maximum intermessage gap time of 16 μs.

In order to achieve these goals, a design was conceived that includes an intelligent bus interface associated with each computing element. Each bus interface will have two separate units, a computing element interface (CIF) and a broadcast bus interface unit (BBIU). An immediate advantage of this partition is that if a computing element processor is replaced with one from a different manufacturer, needed interface changes are confined to the CIF. The same simulation functions that were used in Fig. 1 to illustrate the flow of data are shown in Fig. 2 mapped into three computing elements. Also shown is the role of the interface units in the distribution of messages.

The use of an intelligent interface with direct memory access has a number of advantages. The computing element processor is relieved of the chore of providing routine control over the interface. The bus bandwidth is conserved by not involving the computing element in intermessage operations; therefore, the average message rate across the bus is increased. The interface can perform limited self-testing. If a malfunction is discovered, the interface is automatically isolated, logically, from the broadcast bus.

To achieve a low data error rate, only differential signals are used on the bus. The hardware also supports limited error detection and retransmission transparent to the computing element processor.

Broadcasting Messages

How messages are delivered is central to this architecture. As shown in Fig. 2, both the executive software and the bus interface hardware are involved. The concept is one of broadcast messages with receiver selection. Each simulation task registers with its executive for the messages it wants to receive. The executive summarizes this information for all tasks in its computing element. The summary is programmed into the BBIU as a receive filter. Furthermore, each executive is given the receive filter summary for all other computing elements.

When a simulation task requests its executive to send a message, the executive checks for both local and remote delivery. If any tasks in its own computing element have registered to receive the message, the message is queued for delivery to those tasks. If the executive determines from the filters provided by other computing elements that they host tasks that have registered to receive this message, it will request the interface to transmit the message. The interface will request the use of the bus and, after it becomes bus master, will move the message from the computing element's memory out onto the bus.

When not transmitting, all computing element interfaces are prepared to receive messages. When a BBIU recognizes a message on the bus that it has been programmed to receive, it reads the message into its computing element and informs the executive. The executive then queues the message for delivery to tasks that have registered to receive it. Later, when those tasks are executing, they can call their executive to receive the next available queued message.

SUMMARY

A functionally extensible system architecture with a broadcast mode data bus and receiver selection of content-tagged messages has been developed. The architecture is particularly well suited to a combat environment simulation in which the requirements are expected to expand significantly during the BADG development.

This work was supported by NAVSEASYSCOM, PMS-40[illegible].

NAVAL AAW ANALYSIS PROCEDURES

B. Bundsen, J. R. Earhart, and J. Wang

Analysis procedures to estimate the effectiveness of a Battle Group's area and point defenses in an anti-air-warfare (AAW) environment are programmed on a Hewlett Packard HP-85 desk-top computer. While providing rapid answers to AAW questions, the programmed procedures are precise enough to account for major tactical factors, jamming environments, Battle Group and threat geometry, and system parameters.

BACKGROUND

During the past year, a series of mathematical procedures has been developed for the Chief of Naval Operations (OP-96) to estimate rapidly the AAW effectiveness of a Battle Group's area and point defense.[1] The analysis procedures are organized into two categories coinciding with the area and point defense zones of an AAW battle and are programmed for use on the HP-85 desk-top computer.

The area defense zone considers surface to air missiles (SAM's) acting against anti-ship cruise missiles (ASCM's) launched from various platforms. The outer extent of the area defense zone is the maximum range at which ASCM's are detected; the inner extent is the minimum intercept range of the SAM's. In area defense, surface radars detect incoming threat targets and assign SAM batteries to fire in defense of the Battle Group.

The area defense procedures consist of four program modules, RADET, DETINT, DEPTH, and AREA, which calculate the radar detection range in jamming, maximum intercept range of the SAM's, depth of fire of SAM batteries, and combined performance of all SAM batteries against the postulated attack, respectively.

The point defenses engage the ASCM penetrators of the area defense and determine the penetrators reaching each ship in the Battle Group. The single program module in the point defense zone is named POINT.

DISCUSSION

Area Defense Zone

The four program modules are employed in the area defense zone. Figure 1 shows the geometry of the threatened ship or high value unit (HVU), the escorting AAW ship, the target profile at various instants of time, and the jammer position used in the modules described below.

RADET determines the maximum range at which a radar can detect an ASCM target in a jamming environment. The target flies a trajectory that consists of cruise and dive segments with the dive segment terminating on the HVU. The procedure allows the radar to be located on the HVU (self-defense case) or on an accompanying escort ship at some distance from the HVU.

DETINT determines the maximum intercept range of an escort ship against the ASCM target. The

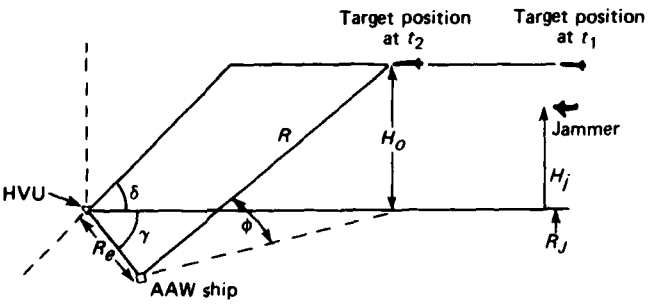

HVU	= high value unit	t_1, t_2	= instants of time
R	= slant range to target at one instant of time	δ	= dive angle of target
R_j	= ground range to jammer	ϕ	= elevation angle of radar to target
H_o	= height of target	R_e	= distance from HVU to AAW (escort) ship
H_j	= height of jammer	γ	= angle of AAW (escort) ship to threat axis

Fig. 1 AAW geometry.

intercept range takes accunt of the location of the escort relative to the attack profile, the speeds of the SAM and the ASCM, the time delay from detection to launch, and the radar detection range determined from RADET.

DEPTH determines the number of missile launch opportunities against any particular attacker using a shoot-look-shoot SAM launch doctrine. The number of missile launch opportunities is a function of the location of the escort ship relative to the attack profile, the speeds of the SAM and the ASCM, the time delay for kill assessment, and the intercept range determined from DETINT. In addition to depth of fire, the program module calculates the engagement kill probability, the mean number of missiles and salvos launched, and the illuminator and launcher tie-up times of the escort ship.

AREA estimates the area defense effectiveness of a Battle Group by determining the probability of engaging the Poisson-distributed targets entering the area defense zone. The measure of the area defense effectiveness is the number of penetrators (ASCM's) that are expected to enter the point defense zone from the area defense zone. The engagement probability of the Battle Group against the targets is a function of target arrival rate, illuminator engagement rate, and the number of illuminators available.

Point Defense Zone

The single programmed module POINT is employed in the point defense zone. It estimates the point defense effectiveness of a Battle Group by determining the probability of engaging each of the Poisson-distributed targets by each point defense system. Using this probability of engagement and the basic parameters of the defensive system, the expected number of penetrators and the number of hits on each ship are calculated.

Program and Module Features

The computer program modules for these analysis procedures are interactive, allowing the user to input the parameters that the computer requests. Figure 2 illustrates the sequence of program modules that is used in the complete area and point defense analysis of high altitude targets. An additional feature of the programs is that each can be used separately merely by defining the appropriate inputs of the program.

The mobility of the HP-85 desk-top computer allows these analysis procedures to be applied in any convenient location. The graphic display gives the user immediate assessment of the Battle Group's performance. In addition, the hard-copy output from the printer enables the user to retain a useful and complete record of each computation. In conclusion, the described procedures coupled with the HP-85 desk-top computer provide rapid answers to AAW questions. At the same time, the procedures are precise enough to account for tactical factors, jamming environments, Battle Group and threat geometry, and system parameters.

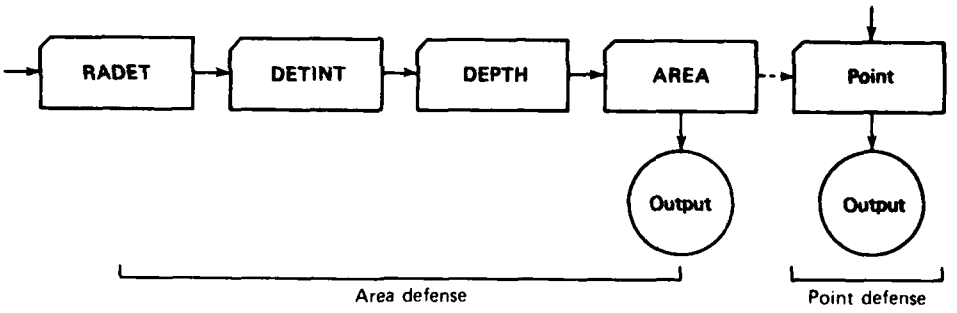

Fig. 2 Sequence of program modules for point defense analysis.

ACKNOWLEDGMENT

The concept of analytically estimating the zonal AAW performance of a Battle Group was originated by Dr. Charles F. Meyer, Senior Fellow. His critical reviews and suggestions are acknowledged by the authors.

REFERENCE

[1] J. Wang, B. Bundsen, and J. R. Earhart, *Naval AAW Analysis Procedures User Guide*, JHU/APL CA-81-002 (Sep 1981).

This work was supported by the Chief of Naval Operations, OP 96.

4. WEAPONS TECHNOLOGY

INTRODUCTION

Since World War II, APL has been actively involved in the development of the Navy's surface- and subsurface-launched missiles. The effort included the development of the Talos, Terrier, and Tartar missiles, the evolution of Standard Missile, the flight development of Long-Range Typhon, and the test and evaluation of Polaris, Poseidon, and Trident. Supporting these efforts have been exploratory and advanced development programs in all aspects of weapons technology, including the design, fabrication, and testing of guidance system components, propulsion systems, and aerodynamic models. The objectives of these weapons technology efforts are to advance the state of the art and to contribute to the timely evolution of operational systems.

Although APL's involvement in weaponry began with the proximity fuze and progressed primarily into anti-air warfare systems, since the late 1960's APL has been strongly involved in offensive missilery, specifically in the Harpoon and Tomahawk tactical and strategic cruise missile developments. Much of the Harpoon guidance system feasibility demonstration was undertaken by APL, and the early analysis of the terrain contour matching (TERCOM) scheme used by Tomahawk was also performed at APL.

With the introduction of the Soviet Backfire bomber, the air threat to the surface Navy has intensified. In addition to the high performance of the Backfire, its antiship weapons and electronic countermeasures capability represent significant challenges to weapons systems development. APL effort has been devoted recently to the development of a concept for new long-range SAM's to supplement fighter aircraft in the outer air battle. New approaches to missile guidance that allow handover to third-party control will be required. APL has been developing guidance concepts and performing simulations and experiments in order to validate approaches that minimize targeting requirements in the outer air battle while maintaining performance in a severe ECM environment. The physical and functional integration of the resulting multimode guidance systems is a major area of effort.

Future long-range SAM's will require hypersonic speed capability in order to be effective against the intensified threat to the surface Navy. APL is pursuing analytical and experimental efforts to provide a firm technological base for ramjet-powered-missile concepts. Activities include tests to extend the database on inlet and combustor configurations and the development of prototype systems and hypersonic airbreathing engines. The use of higher-impulse rockets and the hypersonic speeds under consideration for ramjets have resulted in a more severe flight environment for the missile, requiring an assessment of the structural and mechanical limitations of airframes and radomes.

Stresses on the area and point defense zone SAM's continue to increase with the Soviet introduction and evolution of supersonic antiship missiles. APL continues to support the improvement of existing point and area defense

weapons through the development of the RAM Missile and Standard Missile-2 Block II. These systems will significantly upgrade the kinematic and homing performance of existing weapons.

The articles in this section are examples of recent APL accomplishments in the broad areas of guidance technology and aeronautical technology.

PATTERN RECOGNITION ALGORITHM FOR TARGET DISCRIMINATION

P. G. Barnett and G. E. Mitzel

One of the major difficulties with antiship missile targeting is to distinguish a target ship from among other ships in its vicinity. A pattern recognition algorithm has been developed that enables a missile to pick out its target in the midst of other ships on the basis of the (nearly simultaneously) observed positions of all the ships.

BACKGROUND

The potential performance of a long-range, high-speed, surface-to-air missile is being studied by APL for use primarily against standoff air jammers. However, its characteristics suggest a possible use against long-range surface threats. A typical situation is presented in Fig. 1; in Fig. 1a, five ships are observed to be in the positions shown, and the target ship is located. Figure 1b shows the picture as observed by the missile when it comes within range. The problem is to identify the target ship by using only the relative positions of all five ships. This approach is distinct from those in which the missile attacks the first object acquired after reducing the search area (which reduces the probability of acquiring the true target). It differs also from approaches that require confirming emissions from the target or a match of a radar image with a prestored silhouette.

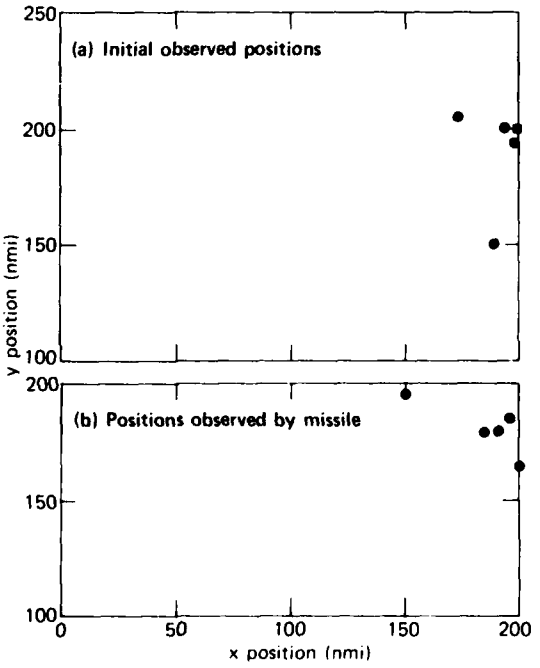

Fig. 1 Target discrimination problem. Given the picture in (a) with the target identified (square), the missile must pick the target out of the picture in (b).

There are several complicating factors: (a) the observations may be (probably will be) inaccurate, (b) the ships will have moved between the initial set of observations and the missile's observations, and (c) the ships observed initially may not be the same ones observed by the missile. The algorithm automatically accounts for the first two complications (indeed, without them there would be no problem). The basic algorithm assumes that the missile and the initial sensor observe the same ships; a refinement treats the case where the number of ships observed is different.

DISCUSSION

The basic target discrimination problem posed above can be restated as follows: given an initial observation of N ships and a subsequent observation (by a missile) of the same N ships, how can the two sets of observed positions be matched so that two corresponding observations are associated with the same ship? If the initial set is ordered in some (arbitrary) way, the missile needs to order its observations so as to best match the original set. The key is the word "best." The pattern recognition algorithm that has been developed is simply a quantification of best. It is assumed that at the time of the missile's observations, the ships' observed positions have some joint probability distribution that is affected by sensor accuracies and the ships' motions. According to the algorithm, the missile should try all possible orderings of its N observed positions (a total of $N!$ orderings) in the joint probability density function (pdf). The ordering that gives the largest value of the pdf should be chosen as the correct one (i.e., the one that corresponds to the ordering of the initial observations). In particular, this process determines the current observed position of the target ship.[1]

The algorithm depends to a large extent on the joint pdf that is assumed. The ships' observed positions may have a jointly Gaussian distribution with pdf

$$p_X(x) = \frac{1}{(2\pi)^N \sqrt{\det(\Sigma)}} \exp\left[-\tfrac{1}{2}(x - M)^T \Sigma^{-1}(x - M)\right],$$

weapons through the development of the RAM Missile and Standard Missile-2 Block II. These systems will significantly upgrade the kinematic and homing performance of existing weapons.

The articles in this section are examples of recent APL accomplishments in the broad areas of guidance technology and aeronautical technology.

where M is a $2N \times 1$ vector containing the two-dimensional mean positions of the N ships, Σ is the $2N \times 2N$ covariance matrix, and x is a $2N \times 1$ vector.[2] The mean positions would, in general, be the same as the initial observed positions. The covariance matrix takes into account the errors in the observations, the time since the initial observations, the ships' speeds, and the correlation in the ships' motions.

Given the pattern recognition algorithm as described, the natural question is: how well does it work? In other words, given a set of positions observed by the missile, what is the probability that it will pick out the target ship correctly? (If it were to guess blindly, the probability would be $1/N$.) Only for the simplest cases is it possible to answer this question analytically; usually Monte Carlo techniques must be used.[1,3] As a test case to validate the Monte Carlo technique, Fig. 2 shows the probability of target recognition (p_{TR}) plotted against the mean separation of two ships with equal variances and no correlation. The smooth curve is the theoretical result; the Monte Carlo results are superimposed along with their 90% confidence intervals.

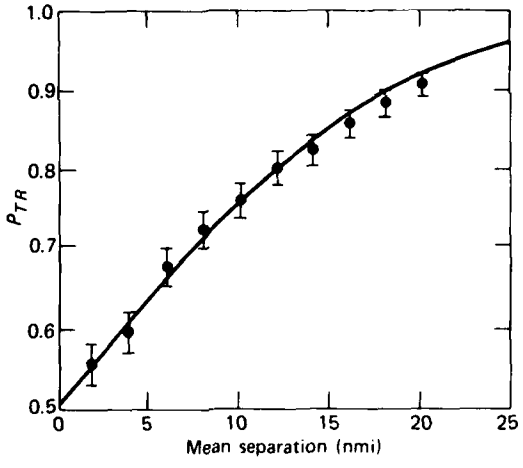

Fig. 2 Probability of target recognition versus mean ship separation. The curve gives the theoretical values; the points give the results of the Monte Carlo runs with 90% confidence intervals overlaid.

Extensive Monte Carlo runs have been made based on the mean positions shown in Fig. 1a with various amounts of correlation and errors in the observed positions. Figure 3 shows the probability of target recognition versus error (σ) in the case where the five ships have equal variances (σ^2) and no correlation. Note that blind guessing would give a probability of 0.2. It has been found that higher correlation between ships greatly increases the probability of target recognition, which is intuitively satisfying.

In addition to the basic algorithm, a refinement was studied that allows for different numbers of ships in the initial set of observations and the missile's set of observations.[4] Instead of simply permuting the observed positions, the missile must check the permutations of all combinations of the smaller number (N_{min}) chosen out of the larger number (N_{max}). This situation may arise from observation error or from ships moving in and out of range. However, even when $N_{min} = N_{max}$, it may be desirable intentionally to take combinations of some number less than N_{max}; with a large number of ships, the number of permutations checked with the basic algorithm is enormous (1,307,674,368,000 for 15 ships), and checking the combinations of smaller numbers of ships greatly reduces the number of computations. As it turns out, the probability of target recognition is not reduced very much as long as N_{min} is not less than the number of ships close to the target.

Finally, it has already been pointed out that the algorithm is dependent on the assumed joint probability distribution. In addition to a Gaussian distribution, a modified Washburn distribution[5] and a generalized Ricean distribution[6] have been investigated. They can be used in the algorithm itself, or they can be used to test how the algorithm with a Gaussian pdf performs given positions that are non-Gaussian.[7] The results are inconclusive so far but seem to indicate that performance is not drastically reduced when the positions come from a distribution different from that assumed by the algorithm.

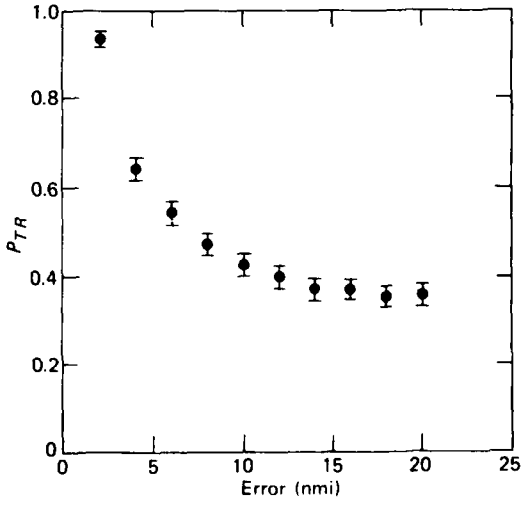

Fig. 3 Probability of target recognition versus error. The points give the Monte Carlo results with 90% confidence intervals overlaid.

REFERENCES

[1] G. F. Mitzel, *Presentation of Preliminary Results on Use of Pattern Recognition for Positional Discrimination of Surface Targets*, JHU/APL F4A-80-039 (Feb 1980).

[2] G. E. Mitzel, *Probabilistic Representation of Ship Positions Using Jointly Gaussian Random Variables*, JHU/APL F4A-80-016 (Jan 1980).
[3] G. E. Mitzel, *Analytical and Monte Carlo Results on the Performance of a Positional Discrimination Pattern Recognition Algorithm*, JHU/APL F4A-80-074 (Apr 1980).
[4] P. G. Barnett, *Monte Carlo Results on a Modification of the Mitzel Pattern Recognition Algorithm for Positional Discrimination of Surface Targets*, JHU/APL F4A-80-157 (Aug 1980).
[5] A. Washburn, "The Propability Density of a Moving Particle," *Oper. Res.* 17, 861-871 (Sep-Oct 1969).
[6] B. O. Koopman, "The Theory of Search: I. Kinematic Bases," *Oper. Res.* 4, 324-346 (Jun 1956).
[7] P. G. Barnett, *Rican and Washburn Distributions and Applications to the Mitzel Positional Discrimination Pattern Recognition Algorithm*, JHU/APL F4A-80-215 (Nov 1980).

This work was supported by NAVSEASYSCOM, SEA-62R1.

MULTIMODE GUIDANCE LOW-FREQUENCY ECM SIMULATOR

H. M. Kaye and J. M. Van Parys

A computer-controlled electronic countermeasures (ECM) simulator has been developed that can emulate up to six independent jammers in frequency bands B through F (250 MHz to 4 GHz). The six RF sources can be modulated independently by four different modulation sources under computer control. Frequency modulation of the RF carrier can be combined with linear amplitude modulation, biphase modulation, and pulse modulation to produce an exceptionally wide variety of ECM waveforms for anechoic chamber testing of wideband home-on-jam missile seeker systems.

BACKGROUND

The Multimode Guidance Project, which is part of the Army/Navy Area Defense SAM Technology Prototyping Program, was established to conduct a feasibility demonstration of multimode guidance concepts. To evaluate the countermeasures performance of contractor-produced prototype missile guidance systems, APL is developing a family of computer-controlled ECM simulators that can simulate wideband multiple-jammer environments.

This article describes the computer-controlled low frequency ECM simulator that can simulate up to six independent surveillance frequency jammers in order to evaluate the home-on-jam modes of guidance during anechoic chamber testing. The system provides a unique capability in that the test operator can program complex ECM test scenarios with either fixed or time-varying parameters. Its flexibility and repeatability make this simulator an extremely powerful and versatile piece of laboratory equipment.

DISCUSSION

The simulator has the following principal features:

1. Full software control of the output of the ECM simulator;
2. Multiple frequency band coverage with multiple sources in each band;
3. Independently produced modulation formats combined as required;
4. Simultaneous amplitude, frequency, pulse, and biphase modulations of each RF source;
5. Formation of arbitrary waveforms;
6. Coordination of RF channel outputs; and
7. Control via standard IEEE-488 data bus.

Hardware Description

Figure 1 shows the simulator. There are six fully independent RF channels: three cover 250 MHz to 1 GHz and the other three, 1 to 4 GHz. Major system control components are indicated in Fig. 2, together with functional details of one of the RF channels. Each RF channel contains two voltage-controlled oscillator (VCO) modules that permit frequency coverage of two octaves.

The VCO center frequency and the modulation format of each RF output are set under program control. Four modulators in each channel (FM, AM, biphase, and pulse) may be used separately or combined to produce a wide variety of ECM techniques.

The system is controlled by a Hewlett Packard (HP) model 9825S computer over an IEEE-488 standard bus interface.

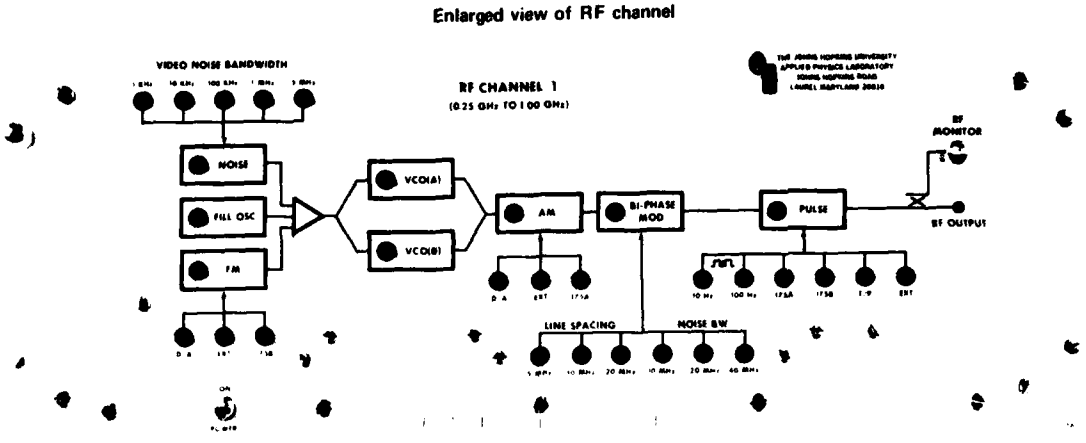

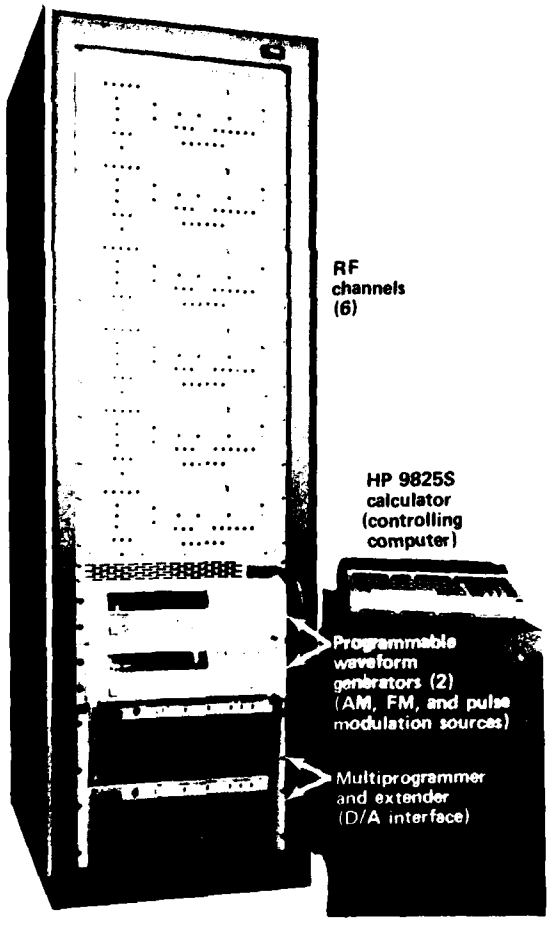

Fig. 1 MMG low-frequency ECM simulator.

An HP model 6942/6943 multiprogrammer/extender acts as a control interface between the computer and the six RF channels. Digital output cards are used for frequency tuning and channel control functions. Digital-to-analog (D/A) converter cards provide AM and FM modulation sources, and a pulse generator card provides a pulse modulation source. The multiprogrammer also acts as a control interface for the level set attenuator driver and for the AM and FM switch matrices.

Two arbitrary waveform generators (Wavetek model 175) provide additional sources of AM, FM, and pulse modulation. These generators can be programmed to generate sine, square, triangle, and ramp waveforms as well as any arbitrary waveform that can be specified by amplitude as a function of time. The Wavetek outputs are connected to the appropriate RF channels by the AM and FM switch matrices.

The major system output parameters are listed in Table I.

Software Description

The multimode guidance ECM simulator's software control is organized in three levels: the user's program, the subroutine blocks, and the data.

The user's program, which determines the test format, is written for each desired test, drawing on standard subroutines and data as required. It can be constructed to allow a wide range of operator inputs, including a detailed menu of test parameters.

Subroutine blocks allow the simulator to achieve the desired outputs as specified in the user's program. In accordance with instructions from the user's program, subroutine blocks select the required RF channels, frequencies, modulation sources, filters, and attenuator settings. In performing these and other tasks, the blocks use tables, lists, and values stored as program data, send data to the multiprogrammer or

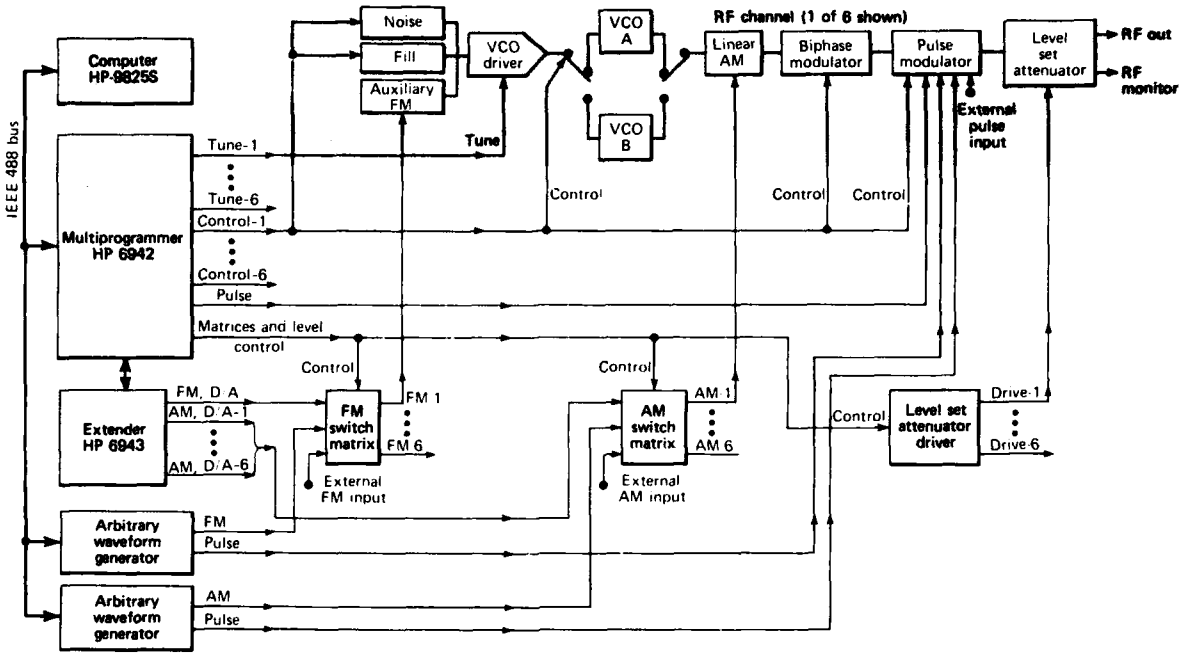

Fig. 2 Block diagram of MMG low-frequency ECM simulator.

Table 1
MAJOR SYSTEM PARAMETERS

Parameter	Specification
Frequency coverage	250 MHz to 4 GHz
Modulation	4 independent types
FM by noise	Gaussian or non-Gaussian noise Video bandwidths: 5 or 1 MHz, 100, 10, or 1 kHz
FM by fill	FM by 100 kHz triangular waveform
Auxiliary FM	3 sources including external input Bandwidth: DC to 5 MHz
AM	Linear AM of RF output 3 sources including external input Dynamic range: 55 dB Bandwidth: DC to 50 kHz
Biphase modulation	Comb spectra: 5, 10, or 20 MHz Pseudorandom noise bandwidth: 10, 20, or 40 MHz
Pulse modulation	6 sources Maximum PRF: 500 kHz
RF output bandwidth	± 1 MHz to ± 40% of VCO octave band
RF output power	+ 20 dBm (250 MHz to 1 GHz) + 16 dBm (1 to 4 GHz)
Level set attenuation	81 dB attenuation, 1 dB steps

function generators, and return status information to the user. Examples of tasks performed by the subroutine blocks are listed in Table 2.

Table 2
EXAMPLES OF SUBROUTINE TASKS

Type of Task	Examples
Setting parameters	Center frequency Noise spot width Pulse modulation Biphase modulation FM and AM modulation Output power level Arbitrary waveform generators
Running programs	Frequency sweep AM from D/A card Synchronous hopping noise spots
Other	Initialize simulator Shut down simulator Prompt operator

Several types of data are used by the subroutine blocks. For example, RF channel calibration data allow subroutine blocks to tune a VCO or set a specified bandwidth. Other data, in the form of tables, can provide predetermined values (default values) to serve as test parameters in lieu of operator inputs or can serve as a previously prepared data sequence for a test.

ACKNOWLEDGMENTS

The authors wish to thank M. E. Antonicelli, J. H. Braun, J. B. Glover, D. W. Kunaniec, and M. M. Soukup for their technical assistance during the development of this system.

This work was supported by NAVSEASYSCOM, SUA-62R55

ESTIMATING THE PROBABILITY OF CRASHING FOR A TERRAIN-FOLLOWING MISSILE

E. P. Cunningham

The probability of crashing, P_c, is an important measure by which a mission planner assesses, in advance, the chances of success of a terrain-following missile. The altitude clearance command is programmed accordingly. Monte Carlo methods are unreliable for estimating small values of P_c over a typical mission length, and an extensive simulation would be needed to improve the reliability. An analytic method for estimating P_c has been derived that uses an analytical expression for the mean frequency of crashing, in conjunction with the statistics of missile altitude error and error rate obtained from a simulated terrain-following flight over a much shorter stretch of terrain than is needed for Monte Carlo runs. The method is applicable to both Gaussian and non-Gaussian error statistics and provides data on small P_c values for typical mission lengths. Obtaining this information by Monte Carlo techniques would be much more expensive.

INTRODUCTION

A low-flying missile in a terrain-following mode typically uses a radar altimeter to sense its clearance altitude above the ground because a forward-looking radar would increase its chances of being detected. One of the main tasks confronting the mission planner is to set, in advance, the clearance command inputs to the missile altitude control system. Those settings will depend on the nature of the terrain being overflown; they should be as low as possible to avoid detection and yet not be so low that the missile crashes. The task is complicated by the fact that, because of lateral navigational errors, the exact terrain to be overflown is not known in advance, even if relatively error-free maps of the mission route are available.

An important criterion that enables the planner to assess the missile's projected performance and to program reasonable clearance commands is P_c, the probability of crashing (or "clobber") over a certain range or flight time. Many terrain-following studies rely on Monte Carlo simulation to estimate P_c over various types of terrain. Those methods are unreliable for estimating small P_c values for a mission of reasonable length.[1]

In contrast to Monte Carlo methods that count the numbers of observed crashes, an analytic method for deriving P_c was developed.[2] For brevity in this paper, the technique is called the "analytic method" although, strictly speaking, it is semianalytic in that it uses an analytical expression for the mean frequency of crashing, λ, in conjunction with the statistics of missile altitude error and error rate obtained from a simulated terrain-following flight over a stretch of terrain that is much shorter than that needed for Monte Carlo runs. An expression for P_c is given in Ref. 2 for the special case where the underlying altitude error process is Gaussian. In many cases in practice, however, unsymmetrical climb and dive limits and other nonlinearities in the altitude control system cause the clearance error distribution to be skewed so that the Gaussian assumption is no longer valid.

In Ref. 3, summarized here, the method of Ref. 2 is extended to the situation of non-Gaussian error statistics, and analytical expressions for P_c are given for various assumptions on the relationship between the error and error rate processes. The use of these expressions to estimate P_c for both Gaussian and non-Gaussian statistics is indicated. Confidence limits for the true values based on the estimate are derived for the Gaussian case. Confidence limits are also obtained for the Monte Carlo estimate based on a Poisson distribution of crash events, to complement the confidence limits for Monte Carlo estimates based on independent trials.[1]

Finally, P_c estimates obtained from Monte Carlo simulation and by the analytic method outlined here are compared. Results indicate reasonable agreement between the two methods at clearance commands that give large values of P_c. However, while the analytic method gives estimates of small P_c values that vary smoothly with increasing clearance command, the Monte Carlo method provides little information in this situation. Furthermore, the results are provided from much shorter simulations than are required for the Monte Carlo approach, resulting in considerable savings in computer time.

DISCUSSION

Analytical Expressions for Mean Frequency of Crashing

The missile, flying at constant speed, is assumed to be controlled to a certain clearance altitude, h_0, as indicated in Fig. 1. Because of navigational errors, it is not known precisely in advance which particular stretch of terrain will be overflown. Hence, the terrain input, $h_I(t)$, may be considered as a realization of a random process, $H_I(t)$, and the resulting altitude error, $E(t)$, is also a random process with realization $e(t)$ as shown in Fig. 2a.

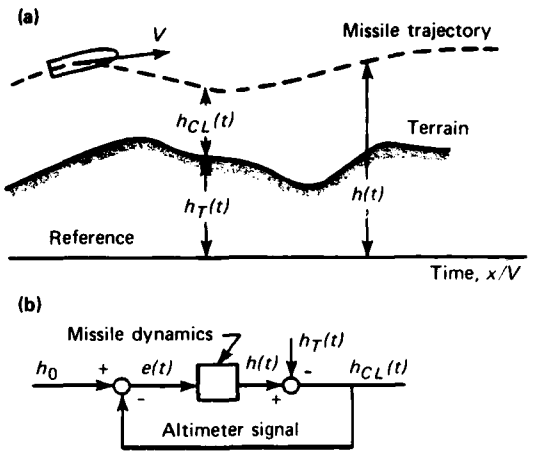

Fig. 1 Terrain following.

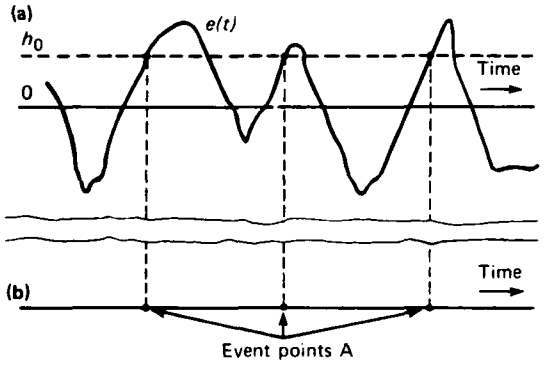

Fig. 2 Crossing of arbitrary level by altitude error signal.

The missile hits the ground when $e(t)$ crosses the h_0 line with $e'(t) > 0$. Each such crossing is considered to be an event A as depicted in Fig. 2b. If the mean frequency, λ, of such events is known, then, assuming a Poisson distribution of event points,[2] the probability of crashing may be computed:

$$P_c = 1 - \exp(-\lambda T) , \qquad (1)$$

where T is the flight time or range.

Under the assumption that $E(t)$ is stationary, classic "zero crossing" theory[4,5] gives the mean frequency as

$$\lambda(h_0) = \int_0^\infty e' f_{E,E'}(h_0, e')\, de' , \qquad (2)$$

where $f_{E,E'}$ is the joint probability density function of altitude error, e, and error rate, e'.

Equation 2 is the most general expression for λ under the stationarity assumption. Under various assumptions, several different expressions can be derived from Eq. 2 for λ (see Ref. 3). For example,

$$\lambda(h_0) = \frac{1}{2} f_{CL}(0)\, \langle |H'_{CL}(t)| \rangle , \qquad (3)$$

where f_{CL} is the probability density of clearance above ground and $\langle |H'_{CL}(t)| \rangle$ is the mean of the absolute value of clearance rate.

The appropriate expression for λ can be inserted in Eq. 1 to obtain P_c. Of course, in general, the exact probability distributions will not be known. An estimate of λ can be obtained from the statistics resulting from the simulation of a terrain-following flight over a single terrain strip as described in the following section. Which expression for λ is appropriate can be determined by inspecting the histograms for error and error rate (or clearance and clearance rate).

Estimating P_c from Curtailed Clearance Statistics

As noted above, Eq. 2 is the most general expression for λ, assuming stationarity. Fortunately however, tests for independence carried out on samples of e and e' taken simultaneously from the simulation indicated that, in general, $E(t)$ and $E'(t)$ may be considered to be independent at the same time t. Furthermore, it was noted that frequently the error or clearance histogram was skewed considerably because of the unsymmetrical nonlinearities in the altitude control loop whereas the error rate was symmetrical with approximately zero mean. In such cases, it is appropriate to use Eq. 3 for λ. The procedure for obtaining λ is as follows:

1. Simulate a missile flight over a suitable terrain sample with constant clearance command, h_0.
2. From the simulation, measure $e(t)$ and $e'(t)$ or $h_{CL}(t)$ and $h'_{CL}(t)$.

An estimate of the mean of the absolute value of clearance rate required in Eq. 3 may be obtained from the clearance rate samples without difficulty. Estimating $f_{CL}(0)$ from the clearance rate samples requires that the latter be fitted with a probability density function.

N. L. Johnson[6] outlined a method for fitting a probability density function to experimental data. The method uses the first four moments of the data as constraints. The method was coded for use in A Programming Language by J. N. Bramhall.[7] The clearance data from each simulated flight were stored on disk for use with this program. The program computed the parameters of the distribution fit and the value of the function at zero, as required for the λ estimate.

With the values of $f_{\dot{C}L}(0)$ so obtained, the estimate of λ is computed according to Eq. 3. The P_c estimate for any desirable time of flight or distance can be computed from Eq. 1; of course, this value is for the h_0 value selected for the simulated flight.

The actual choice of h_0 for the simulated run has little effect on the clearance statistics upon which the probability of crashing is based. For example, if one run is made at $h_0 = h_1$ and a second run over the same strip at $h_0 = h_2$, the mean clearance will change by an amount $(h_2 - h_1)$, but the standard deviation of clearance, σ_{CL}, and the mean of the absolute value of clearance rate, $\langle |\dot{h}_{CL}(t)| \rangle$, will be relatively unchanged except for some minor effects arising from the change in air density if the difference between h_1 and h_2 is large. The histogram of clearance values will have the same shape but will be translated by the change in mean value. This relative invariance in clearance statistics for different values of h_0 over a given terrain strip permits the required clearance command to be determined for a desired P_c. The problem of estimating P_c is simplified considerably if the error and error rate statistics are approximately Gaussian.[2]

Monte Carlo Estimate of P_c

The problem of estimating P_c from a Monte Carlo simulation is treated in Refs. 1 and 3. Briefly, it involves simulating a terrain-following flight at a fixed h_0 over a long stretch of terrain, T_{mc}, and counting the crashes, n_c, that occur. Then an estimate of λ is given by

$$\hat{\lambda}(h_0) = n_c(h_0)/T_{mc} \ , \qquad (4)$$

and the P_c estimate for an arbitrary flight time or range T by

$$\hat{P}_c(h_0, T) = 1 - \exp[-\hat{\lambda}(h_0)T] \ . \qquad (5)$$

Experimental Results

To compare the Monte Carlo and analytic methods for estimating P_c, a three-degree-of-freedom digital simulation was made of a missile in the terrain-following mode. The terrain input was synthesized using a first-order autoregressive (AR) or Markov process in order to provide relatively homogeneous terrain data for the comparison. The AR process was selected to approximate actual terrain data in its correlation and frequency characteristics. The problem of terrain classification is treated in Ref. 8. A constant value for h_0 was selected and the missile was flown over a typical length of terrain. The number of crashes in T_{mc} for the selected h_0 value was noted. The simulation also contained logic to count the number of crashes that would have occurred if h_0 were raised or lowered by specified increments. The resultant P_c estimate was computed by combining Eqs. 4 and 5 with $T = T_{mc}$, obtaining

$$\hat{P}_c = 1 - \exp(-n_c) \ . \qquad (6)$$

A comparison of results obtained from the analytic method and the Monte Carlo runs is shown in Fig. 3. A plot of n_c versus h_0^2 (Fig. 4) indicates a relationship that is approximately exponential.

CONCLUSIONS

1. The analytic technique presented here offers a practical way to estimate P_c with much less simulation than is required for a Monte Carlo estimate.

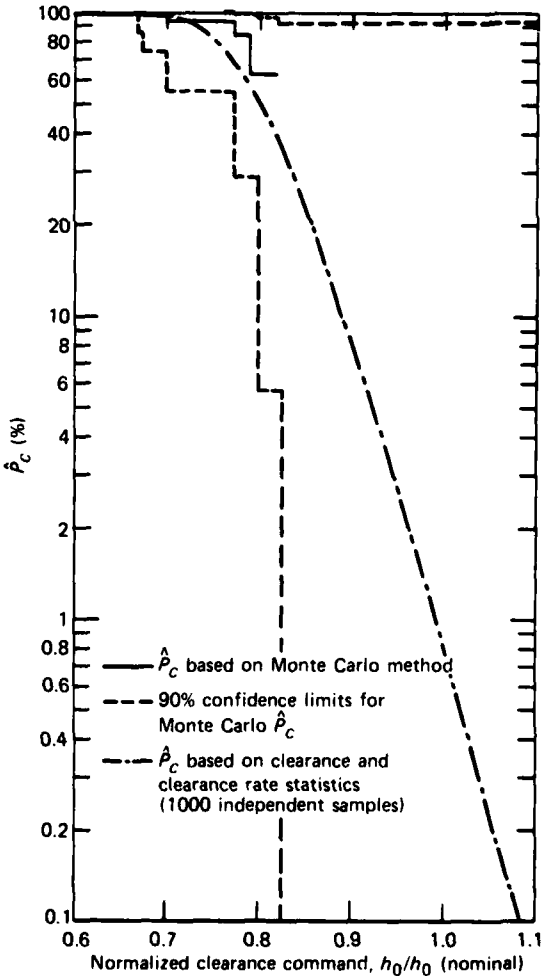

Fig. 3 Comparison of P_c estimates with clearance command, over a Monte Carlo length $T = T_{mc}$.

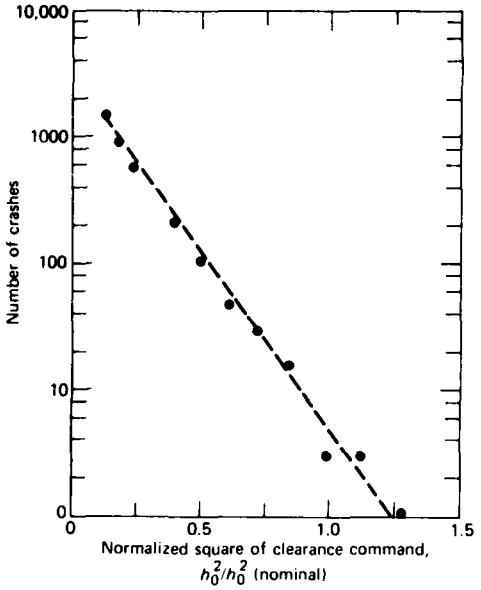

Fig. 4 Number of crashes versus square of clearance command, from Monte Carlo simulation.

2. When results for the two approaches overlap, the Monte Carlo method tends to validate the analytic method.
3. Confidence intervals for P_c are readily obtainable for the estimate provided by the analytic method with Gaussian statistics and also for the Monte Carlo estimate. However, determining the confidence interval for P_c based on non-Gaussian statistics requires further research.
4. Although the method described was developed specifically for the case of a terrain-following missile with a downward-looking radar, it also seems applicable to the similar problem of estimating P_c for a terrain-following missile or aircraft with a forward-looking radar.

REFERENCES

[1] E. P. Cunningham, "Probability of Crashing from Monte Carlo Simulation," *J. Spacecr. Rockets* **16**, 348-350 (Sep-Oct 1979).
[2] E. P. Cunningham, "Probability of Crashing for a Terrain-Following Missile," *J. Spacecr. Rockets* **11**, 257-260 (Apr 1974).
[3] E. P. Cunningham, "Estimating the Probability of Crashing for a Terrain-Following Missile," *J. Guidance Control* **5**, No. 1, 86-91 (Jan-Feb 1982).
[4] A. Papoulis, *Probability, Random Variables and Stochastic Processes*, McGraw-Hill, New York, Chap. 14 (1965).
[5] P. Beckman, *Probability in Communication Engineering*, Harcourt, Brace and World, New York, Chap. 6 (1967).
[6] N. L. Johnson, "Systems of Frequency Curves Generated by Methods of Translation," *Biometrika* **36**, 146-176 (1946).
[7] J. N. Bramhall, *Performance of the API Function JHUFIT in Identifying and Fitting the Parameters of the Probability Distribution in the Johnsonian System*, JHU/APL BCP-685 (7 Dec 1978).
[8] E. P. Cunningham, "Single Parameter Terrain Classification for Terrain-Following," *J. Aircr.* **17**, 909-914 (Dec 1980).

This work was supported by the Joint Cruise Missile Project Office.

TRACKING SEEKER SIMULATOR

J. J. Lorditch

A Tracking Seeker Simulator has been successfully developed at APL. When installed in an AN/BQM-34 drone aircraft, it simulates an active-homing, antiship missile. The development was undertaken because the Navy target inventory did not include a realistic simulation of an active antiship missile for use in the RAM missile flight test program. The Tracking Seeker Simulator has been successfully test flown, both in the BQM-34 drone and in a pod installation mounted below the wing of a T-33 aircraft.

BACKGROUND

Active antiship missiles use on-board radar systems to illuminate the target ship and derive homing information from energy reflected from the ship. A characteristic of the active antiship missile is that it points the main beam of its transmitting antenna toward the ship. The RAM missile homes on the active radar radiation of the antiship missile. An active cruise missile or a realistic simulation of a cruise missile is required to conduct RAM missile flight tests. Active cruise missiles are complex, expensive, and lack the versatility required of targets for flight tests. A satisfactory solution is a simulation of an active antiship missile obtained by installing an emitter that is carried on a recoverable target drone such as the BQM-34.

DISCUSSION

The Tracking Seeker Simulator, when installed in a BQM-34 drone, simulates an active-homing, antiship cruise missile. The drone is radio controlled from a ground station and is flown inbound toward the RAM missile launch site. The simulator is configured to point its antenna's main beam toward the RAM launch site. Pointing is achieved by providing a ground-based CW beacon at the launch site, which is tracked by a tracking CW receiver with a steerable antenna in the drone. The drone antenna operates in dual mode (transmit/receive). The receiver produces information for keeping the antenna main beam centered on the beacon while a high-powered pulse transmitter, using the same antenna, simulates the radiation of an active-homing seeker radar. Small deviations in the drone trajectory are canceled by steering the simulator antenna. The system is designed to provide reliable operation with minimum routine maintenance.

Figure 1 is a simplified block diagram of the Tracking Seeker Simulator. The signal from the ground-based beacon is received by the four-port monopulse antenna. The four signals are processed by the monopulse comparator to produce sum, azimuth, and elevation channel signals, which are routed to the receiver through a diplexer and two bandpass filters. The transmitter frequency is sufficiently removed from the beacon frequency to allow the diplexer and filters to provide adequate isolation for the receiver.

The Tracking Seeker Simulator is located in the nose of the BQM-34 drone (Fig. 2). A hemispherical radome is provided in place of the standard BQM-34 nose cone. The simulator is controlled by means of the BQM-34 radio frequency command link. Separate input commands are: STANDBY, TRANSMITTER ON, CAGE, and UNCAGE. The system is automatically placed in the standby condition when the drone's +28 V DC special-devices bus is energized. A special prelaunch signal places the antenna in the cage mode during launch, fixing the antenna pointing angle relative to the aircraft. In pretracking operation, the system is in the caged position and is transmitting. When the beacon signal is strong enough to provide reliable system track, the drone controller receives an indication that the beacon signal is present and gives an UNCAGE command, placing the system in track. The simulator has a pull-in capability of $\pm 5°$ initial pointing error.

The CW beacon, located at the missile launch site, transmits a 10 W CW signal downrange. The beacon antenna provides azimuth and elevation beamwidths of 26° (3 dB points), which allow for drone trajectory errors in altitude and cross range.

The Tracking Seeker Simulator is composed of a transmitter, antenna assembly, receiver, radome, and beacon. Each major subsystem is described below.

Transmitter

The AN/DPT-1 transmitter is a pulse-modulated magnetron with the following characteristics:

Frequency	J band, mechanically tunable prior to flight
Peak power:	75 to 100 kW
Pulse width:	0.4 and 0.8 μs (fixed selectable)
PRF:	200 to 2000 Hz, mechanically tunable prior to flight
Weight:	45 lb

The drone controller remotely commands the unit to radiate. The transmitter is operable over the complete flight profile of the drone and does not require the aid of refrigerated air.

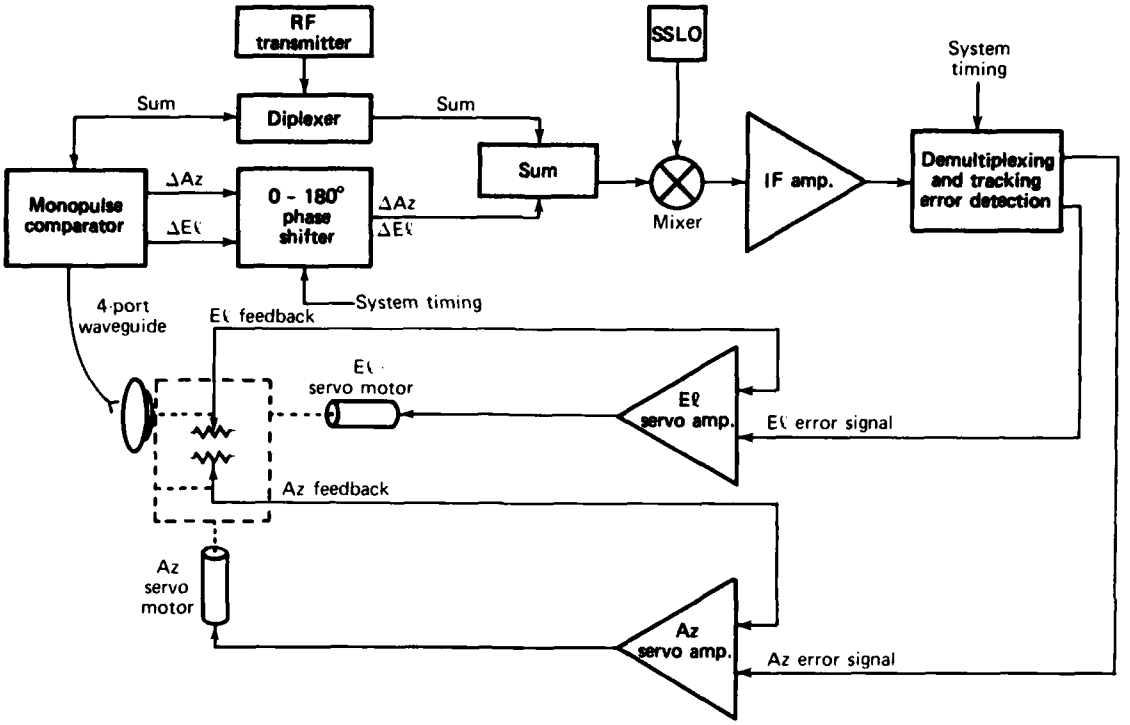

Fig. 1 Simplified block diagram of the Tracking Seeker Simulator.

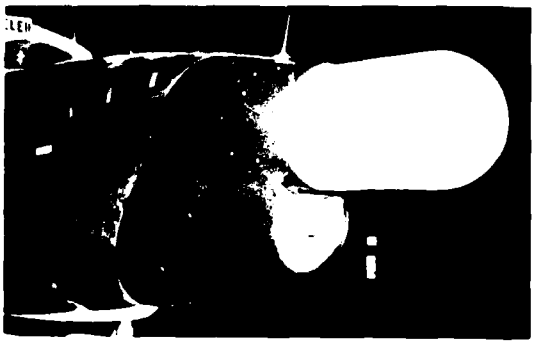

Fig. 2 The AN/BQM-34 drone.

Antenna Assembly

The simulator has a fixed-feed, moving-dish antenna. This design was selected so that rotary joints would not be needed. The antenna is mounted on a two-bar linkage-and-gimbal assembly obtained from a production Standard Missile Program. The assembly (including antenna, gimbal, and servos) has three modes of operation: cage, track, and memory. In the cage mode, the antenna position is fixed with respect to the aircraft. In the track mode, the antenna beam position is controlled from the error signals developed by the receiver. Switching between the cage and track modes is controlled by the flight controller. The memory mode is entered automatically from the track mode whenever the received signal is too weak to provide a reliable error signal.

Receiver

The receiver uses the conical-scan-on-receive technique. The four antenna beam positions (up, down, right, and left) are sequentially sampled to provide the up-down (elevation) and right-left (azimuth) error signals to the antenna assembly. Automatic gain control provides a constant-error scale factor independent of signal strength. The receiver produces three signals: beacon signal present, azimuth error, and elevation error. The latter two signals are DC voltages having amplitudes proportional to the antenna pointing error and polarities that indicate the direction of the error.

The receiver consists of microwave bandpass filters, azimuth and elevation commutators, a solid-state local oscillator, a mixer, a 60 MHz IF amplifier, an azimuth and elevation angle decoder, and a signal processor.

Radome

The radome, designed to replace the standard BQM-34 nose cone, is constructed of polyester/resin laminate and is a 15-in.-diameter hemisphere connected

to a 14-in.-long cylinder for smooth fairing into the airframe. In order to provide watertight integrity for water recovery of the drone, a gasket and backup ring are used to mount the radome to the waterproof bulkhead of the nose cowling. Insertion loss through the radome is less than 1 dB over both the transmit and receive frequency bands.

Beacon

The ground-based beacon is a single assembly and its antenna is an integral part of the unit. It transmits a 10 W CW signal downrange toward the incoming target drone. The transmitter frequency is crystal controlled. The beacon antenna is a horizontally polarized, standard gain (20 dB) horn.

This work was supported by NAVSEASYSCOM, SEA-62Z4.

SIMULATION OF AERODYNAMIC HEATING USING A SOLAR FURNACE

R. K. Frazer and L. B. Weckesser

An analysis of the Block II improvement to the Navy's Standard Missile showed that unacceptable radar performance might result when the radome is aerodynamically heated to flight temperatures by advanced propulsion systems. A technique was conceived to compensate for the heating effects, and an environmental test was carried out to validate the concept. A facility for accurately measuring boresight errors in radomes heated to flight conditions (temperatures up to 2000°F) was constructed at the Department of Energy's solar furnace in Albuquerque, N. Mex., and was used to validate the new radome design. No such capability had previously existed.

BACKGROUND

The nosetip of a supersonic tactical missile is usually a streamlined aerodynamic covering for the missile radar seeker. As such, the structure must be as transparent as possible to the radar signals used by the missile's homing device. The radome of the Navy's Standard Missile (SM) is made of a glass ceramic material. To the missile seeker antenna, the radome is an imperfect lens that introduces errors in the true line of sight to the target. These aberrations depend on the look angle (measured from the missile centerline) and are called boresight errors (BSE). By means of careful manufacturing techniques and radar pattern measurements in an anechoic chamber, the radome wall thickness contour can be controlled so that BSE's are acceptably small. However, at expected flight temperatures, the dielectric properties of the Pyroceram change. Consequently, the radome may appear too thick for acceptable transmission, and boresight errors exceed the seeker requirements. To compensate for this effect, APL and the SM-2 prime contractor, General Dynamics/Pomona Division, proposed to manufacture the new SM-2 radomes slightly thinner than optimal at room temperature so that the radomes could "expand" to the proper condition at flight temperature. The radar frequency used during acceptance testing is adjusted upward to compensate for the thinner walls at room temperature.

An experimental program was conceived in 1977[1] to provide BSE measurements with an accuracy of ±0.1 mrad on radomes at flight temperatures. The experimental program evolved into six phases, the last of which was completed in April 1981. The present discussion will focus on the phase of the effort that validated the use of the Central Receiver Test Facility

(CRTF) solar furnace (operated by the Sandia National Laboratories in Albuquerque) as the site for accurate BSE measurements of heated SM-2 radomes.

DISCUSSION

The prime consideration for the selection of the facility was to be able to heat the full-size SM-2 radome to flight temperatures with realistic longitudinal temperature distributions while taking accurate BSE measurements. The BSE measurement process requires many separate tests, and the facility would have to reheat the radome many times to the same temperature. Rocket-sled or wind-tunnel facilities could provide faithful reproductions of the aerodynamic heating, but simultaneous BSE measurements would not be possible, and the rapid turnaround requirement would not be easily met. Quartz heat lamps installed in an existing BSE range were considered, but the amount of electrical energy required would be very large and a duplication of the aerodynamic heat flux in the nose region of the radome would not be possible. Some consideration was given to using laser heating, but no laser facility has a large enough test volume.

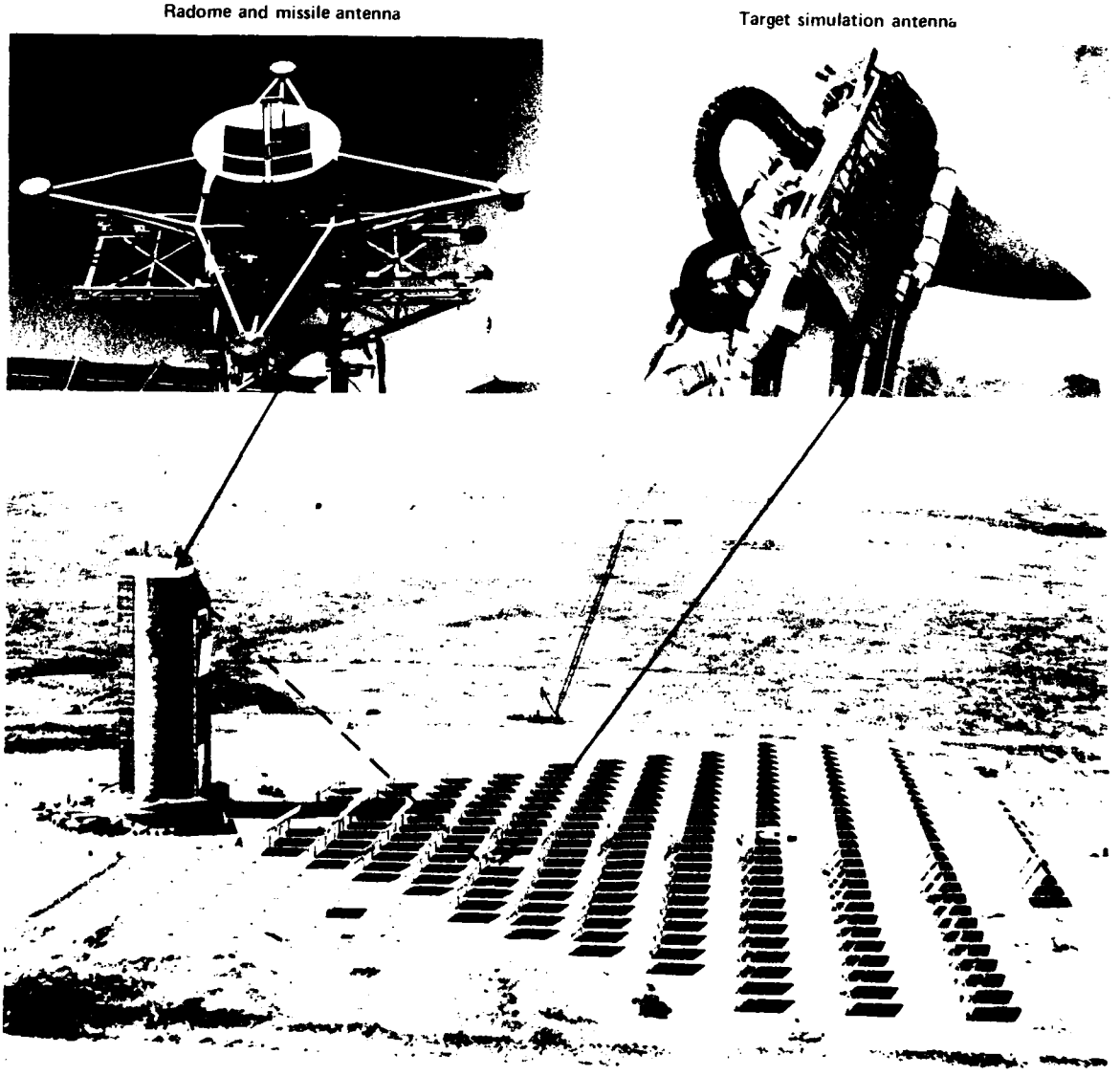

Fig. 1 Arrangement for testing heated radomes at CRTF.

The use of concentrated solar energy to heat radome structures was first suggested by Walton et al. in 1972[2] and carried out by Bassett and Langley in 1974.[3] The attraction of a solar furnace lies in its ability to provide a clean, controllable heat flux in a low-interference RF environment. A survey of the solar furnaces at White Sands, Georgia Tech, Odeillo (France), and Sandia resulted in the selection of the Sandia site. The CRTF at Sandia appeared to provide the most favorable geometry for clean BSE measurements, selectable heat flux histories, and data acquisition and reduction. The facility is shown in Fig. 1, where the radome is mounted atop the 200 ft tower and pointed down toward the center of the heliostat field. In this position, every portion of the radome has a view of some portion of the heliostat field.

To verify that the solar heat flux would approximate the SM aerodynamic heating condition, direct measurements were also made at CRTF. A tree structure was built to hold eleven Gardon gauge calorimeters in orientations that represented selected stations on the radome surface. Three of the eleven calorimeters were located at the base of the tree and faced normal to the solar beam. These units helped to measure the circumferential distribution of heat flux as well as the overall heat flux level that supporting structures would have to endure during subsequent testing. The results of this survey (Fig. 2) were achieved with the heliostats' aim point and the calorimeter tree's axis orientation held constant. Figure 2 shows how the heat flux varied with axial location under steady-state conditions. There were two configurations: one had approximately 130 heliostats and presented a high heat flux environment while the other produced a lower heat flux environment with approximately 40 heliostats. There are 222 heliostats in the whole CRTF field. The high-level fluxes approximated the time-averaged heating experienced by the radome during the boost and climbout phase of SM flight while the low-level fluxes approximated the heating experienced during high-altitude cruise.

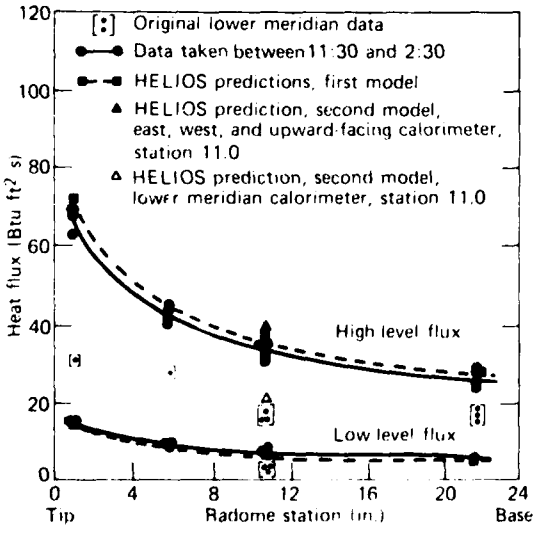

Fig. 2 Comparison of heat flux measurements made from calorimeter tree with theory.

At least eight heat flux measurements are represented at each station in Fig. 2. The data were taken within 1½ hours of solar noon while the sun's intensity remained high and constant. The overriding characteristic of the data in Fig. 2 is that the heat fluxes produced by CRTF are repeatable.

CRTF analysts predicted theoretically the heat fluxes expected at the radome's surface using the HELIOS computer code. These predictions are also plotted in Fig. 2. The correlation is quite good except for the points noted as "lower meridian". Repeated measurements of the heat fluxes along the downward facing meridian of the calorimeter tree were all below the east, west, and upward facing meridian data, which lie along the curves as expected. A detailed investigation of this anomaly revealed that the heliostats viewing the lower side of the radome contour were incorrectly modeled in the HELIOS calculations. The error was corrected and the HELIOS code was rerun for radome station 11 only; the resultant predictions more nearly matched the measurements (cf, Fig. 2).

The heat flux distributions shown in Fig. 2 were used to calculate the expected radome temperatures, and it was concluded that CRTF could produce flight-like radome temperatures. The desired uniform circumferential temperature was achieved by rolling the radome about its longitudinal axis during the heating cycle. Work then proceeded toward building a suitable boresight error range at CRTF (see Ref. 4 for details).

To develop the heating process, a calibration radome was mounted on the test tower and several experiments were conducted. The radome was specially manufactured with a 0.10 in. wall thickness and instrumented with 36 thermocouples on its inner surface. Combinations of heliostats were tried in order to provide the desired radome temperatures. The HELIOS computer model was used extensively as a guide during this process. The results of the calibration are summarized in Fig. 3, where the temperature distributions expected during SM-2 Block II flights are plotted along with those achieved at CRTF for three conditions of interest. The small differences between desired and achieved temperatures demonstrated the acceptability of CRTF as a facility for testing heated radomes.

In subsequent testing phases, extensive BSE data were taken at radome temperatures covering present and planned SM-2 performance capabilities. The Block

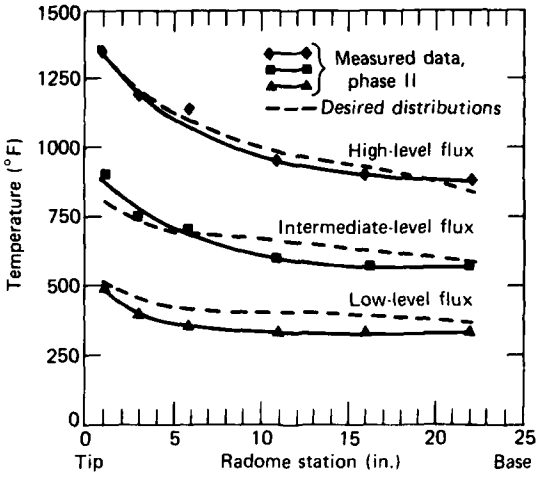

Fig. 3 Required and achieved temperature distributions for solar-heated SM-2 radomes.

II radome, manufactured slightly thinner than previous models and tuned appropriately, was shown to perform acceptably at the Block II temperature levels; production radomes will be manufactured using this new technique. References 4 through 6 describe the radome test effort.

REFERENCES

[1] L. B. Weckesser, *Proposed Program for FY '78 SM-2 (ER1) "Blue Book" — Aeroheating Effects on Boresight Error Slope*, JHU/APL EAM-5528 (16 Mar 1977).

[2] J. D. Walton, Jr., "High Temperature Evaluation of Radomes and Radome Materials Using the French Solar Furnace," *Proc. 11th Symposium on E-M Windows*, Georgia Institute of Technology, Atlanta (2-4 Aug 1972).

[3] H. L. Bassett and J. B. Langley III, "High Temperature Radome Effects on Antenna Radiation Patterns," *Proc. 12th Symposium on E-M Windows*, Georgia Institute of Technology, Atlanta (12-14 Jun 1974).

[4] L. B. Weckesser et al., *Aerodynamic Heating Effects on the SM-2 Block II Radome — Test Report*, JHU/APL FS-80-146 (Oct 1980).

[5] L. B. Weckesser et al., *SM-2 Block II Improvement Program Thermal/RF Validation of the SM-2 Block II Radome*, JHU/APL FS-81-230 (Nov 1981).

[6] R. K. Frazer and J. R. Kime, *Thermal Stress Investigation for the SM-2 Block II and Block III Radomes*, JHU/APL FS-81-273 (Nov 1981).

This work was supported by NAVSEASYSCOM, PMS-400M.

THERMAL MODELING OF DC 93-104 COMBUSTOR INSULATION

L. L. Perini and L. B. Weckesser

Organo-silicon elastomeric materials show promise for use as insulators for airbreathing combustors. DC 93-104 is an attractive material of this family. A literature review revealed six different thermal models of DC 93-104, but none could be relied on to give the valid in-depth thermal response needed to evaluate the material's use in a new combustor design. A program was undertaken to gather experimental property data for the material and to formulate a valid thermal model.

BACKGROUND

DC 93-104, introduced in 1968, is the trade name of a silicone elastomer ablative material manufactured by the Dow Corning Corp. Experimental testing indicated that it was an excellent insulation for airbreathing combustors. Basically, the material is a pyrolyzing, char-forming insulation (see Fig. 1) that swells during the process of going from the virgin state to the char state. No loss of material as a result of chemical ablation is normally observed. The char is a hard black material of lower density and higher thermal conductivity than the virgin material.

Over the past decade, much exploratory research and development has been expended in attempting to use the material in a viable thermal protection system. A review of the literature disclosed six different thermal models for DC 93-104. It was concluded that (a) none of the available published models could be relied on to give a valid in-depth thermal response; (b) the amount of experimental thermal property data was meager, and more should be obtained; and (c) the effect of material swell should be considered in the modeling of DC 93-104. A new experimental and analytical effort[1] was undertaken to address the three areas described above.

DISCUSSION

Experimental Determinations

The successful development of a thermal model requires knowledge of the basic thermophysical properties of the material, such as thermal conductivity, specific heat, heats of formation, elemental composition, and kinetic decomposition data, in addition to the material's response to a heat flux. In the thermal models that had been developed, one or more properties of the material had been "tuned," i.e., the property value was adjusted to correlate with combustor test data.

In order to obtain independent estimates of the properties, samples of the virgin, pyrolysis, and char states of DC 93-104 were prepared at heat flux levels and rates appropriate to airbreathing combustors and tested at several chemical and thermophysical measurement laboratories. The agreement among the laboratories was poor for the elemental analysis and heat of combustion tests upon which estimates of heats of formation could be based. The problem was the formation of

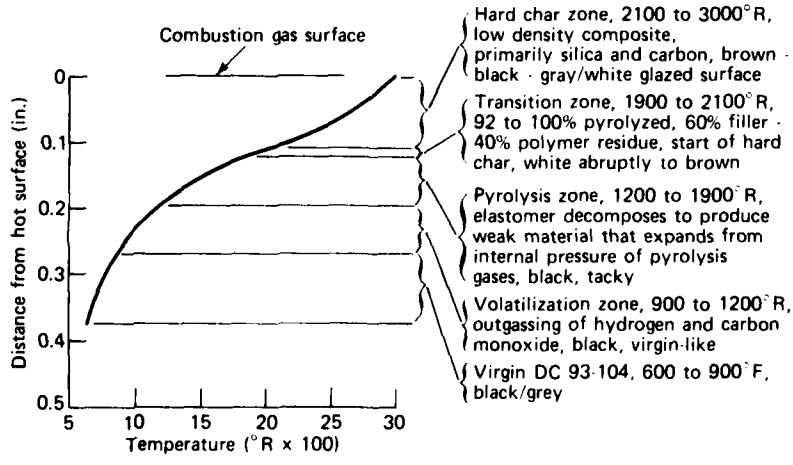

Fig. 1 Insulator temperature and composition profile.

a silica skin on the surface of the burning substance that caused the premature extinction of the flame during calorimetry tests. Additional testing to establish more reliable values for the organo-silicon compounds will require a rotating calorimetry bomb, rather than the standard static bomb, and a reagent, such as fluorine, in order to keep the silica skin from forming.

The kinetic rate constants that describe the decomposition of a charring material are derived from thermogravimetric analysis (TGA). The TGA's that had been conducted for DC 93-104 were reviewed; apparently TGA results depend on the heating rate applied to the samples. For those that were prepared at APL under a high-heat-flux condition (about 1000°R/min), only a 12% weight loss was observed, whereas at 18°R/min, the weight loss was 22%. It was concluded that kinetic rate data derived from low-heat-flux TGA's are inappropriate and that higher heating rates should be used.

Thermal conductivity and specific heat were determined for the three different phases of DC 93-104. An electron beam microscope study of the char showed that its microstructure varied according to the heat flux level under which it was prepared. Therefore, charred samples were prepared in an apparatus in which quartz heat lamps provided a controlled heat flux equivalent to that experienced in airbreathing combustors. Samples of the three phases were provided to Southern Research Inc., and thermal property measurements were performed as a function of temperature. The data provided a base from which thermal modeling of DC 93-104 could proceed.

Virgin and char samples were submitted to the E. I. duPont Co. for a differential thermal analysis (DTA). With the virgin sample, a small exotherm was observed at about 938°R, a large exotherm at about 1211°R, followed by a continuous exothermic reaction. Upon recycling, the two low-temperature exotherms were eliminated as expected; however, the succeeding exothermic reaction continued at a higher temperature and prevented measurement of the total heat of reaction. It was postulated that the heating rate of 18°R/min was too slow compared to the heating rate experienced in a combustor, so the testing was terminated. However, the data supported the conclusion that the reaction is largely exothermic. To determine quantitative values of the exotherm would require further testing.

Substantial swelling occurred as the samples charred. An experimental procedure was developed to approximately measure the swell during heating (see Fig. 2). A helium-neon laser was directed across the heated surface of the specimen onto a photodetector. As the swelling occurred, the beam was partly blocked, thereby reducing the signal from the photodetector. Thus, a measure of swelling versus time was obtained as the specimens were heated by the quartz heat lamp unit. A total swell of 29% was determined for two samples, based on pretest and posttest measurements. Both samples experienced a 12.3% weight loss.

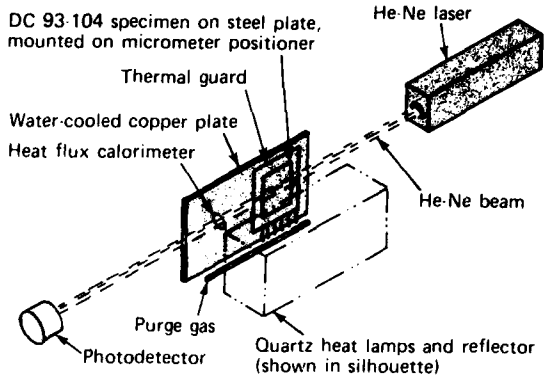

Fig. 2 DC 93-104 test arrangement.

Thermal Modeling

A thermal model of DC 93-104 was formulated using the experimental data. The Charring Material Ablation (CMA) code[2] was used as a baseline, and modifications were made as needed to obtain a satisfactory thermal analysis procedure. In addition to using the property information discussed previously, swelling was accounted for by defining an effective char thermal conductivity[3]: $K_c = K_c/(\ell_c/\ell)$, where K_c is the char conductivity and ℓ_c/ℓ is the swell length ratio, which is 1.3 according to experimental results.

Subscale test data reported by the Aerotherm Co.[4] were selected to validate the thermal model. A simplified one-component decomposition rate developed at APL was used in the model along with final char density values of 72 lb/ft^3 as suggested by Aerotherm and 80 lb/ft^3 as determined from the APL results. The resultant in-depth temperatures for the two cases are compared with the experimental data in Fig. 3. The results tend to substantiate the effect of heating rate. At the high heating rates that occur near the surface, the density would be high, while at the back face, the heating rates would be low and the density would also be low. Also to be noted in Fig. 3 is the rather poor correlation between prediction and measurement, indicating the need for further improvement in the thermal model.

Organo-silicon materials appear to be very promising for use as combustor insulations, and much effort is being devoted to developing new formulations. On the basis of the results of this experimental effort, it is clear that the proper characterization of these materials will require nonstandardized testing methods and techniques — first, to understand how the material re-

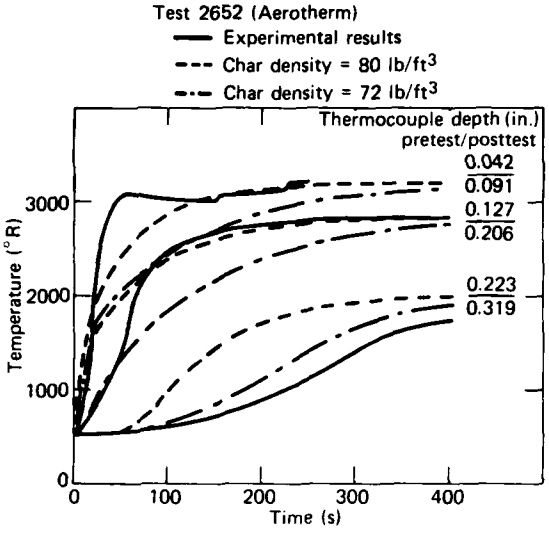

Fig. 3 Comparison of measurements with predictions using the API thermal model.

sponds to a prescribed heat flux and, second, to form a basis for developing a phenomenological model of the material's behavior.

CONCLUSIONS

This study has resulted in a set of previously unavailable experimental thermophysical properties for the virgin, char, and pyrolysis stages of DC 93-104 as a function of temperature. Experimentally based values of the heats of formation of the char and virgin state have been obtained and, in conjunction with a DTA, have been calculated for the first time. It has been ascertained that there is a relationship between heating rate and the decomposition kinetics, and an algorithm has been developed for the CMA computer code to incorporate this effect.

REFERENCES

[1] L. L. Perini and L. B. Weckesser, "Thermal Modelling of Combustion Insulation DC 93-104," presented at JANNAF 1980 Propulsion Meeting (Mar 1980).

[2] Aerotherm Co., *User's Manual, Aerotherm Charring Material Thermal Response and Ablation Program, Version 3*, I and II, UM-70-14 (Apr 1970).

[3] L. W. Hunter, "Transient Thermal Expansion of Solids During Inert Heating, Phase Change and Surface Gasification," *J. Heat Transfer* **103**, No. 3, 601-602 (1981).

[4] Marquardt Co., *Ramburner Internal Insulation Investigation, Volume I - Modelling and Computer Program*, AFP AFAPL-TR-75-109, Air Force Aero Propulsion Laboratory, Wright-Patterson Air Force Base, Ohio (Dec 1975).

This work was supported by NAVSEASYSCOM, SEA-062R.

THEORETICAL MODELING OF A SCRAMJET COMBUSTOR WITH A CENTRAL FUEL JET

J. A. Schetz and F. S. Billig

The performance of supersonic combustion ramjet (scramjet) engines is critically dependent on internal losses resulting from wall skin friction and on obtaining high combustion efficiency in very short residence times. To assist in the evaluation of experimental results, a complete, modular, calculational procedure for predicting the flowfield, including wall shear and heat transfer of a scramjet with a center fuel jet,[1] has been developed.

BACKGROUND

The analytical prediction of the flowfield in the combustion chamber of a scramjet engine is important to ensure that enough length for efficient heat release has been provided, to determine the distribution of heat transfer and skin friction, and to define the degree of nonuniformity of the flow leaving the combustor. Heat transfer predictions are important for designing engine cooling systems and structure, skin friction values are important for calculating overall system performance, and the combustor exit flow profile is needed to define the nozzle flow and exit thrust.

A modular approach to the analysis of this complex flowfield was adopted. The mixing and burning of the center jet was treated with one computer code, and a separate wall boundary layer calculation procedure was then coupled to it. This approach was suggested mainly by the substantial difference in grid resolution required in the two parts of the flow.

The main mixing and burning calculation is made with an extended version of the code from Ref. 2. The most significant extension was the incorporation of chemical reactions. The chemical system is written to include H, C, O, and N atoms with only the following species considered: O_2, N_2, H_2, CO, CO_2, H_2O, OH, O, H, N, and NO. Because of the high static pressures and temperatures, and the great simplicity thereby introduced, local diffusion-controlled chemical equilibrium was assumed to apply.

The computer code given in Ref. 3 was modified extensively to permit more efficient calculations. This resulted in reducing the cost per calculation from about 10 to 50 cents per point to about 1 cent. However, it was still necessary to introduce further simplifications to bring the computation cost to an acceptable level. Thus, the double-flame-sheet model of Ref. 4 was adapted to the present problem. Simply stated, the model considers an inner H_2 flame and an outer CO flame, and only the O_2, H_2, N_2, H_2O, CO, and CO_2 molcular species are assumed to be present. (As long as the temperature remains below about 2500 K, the model provides a good approximation to the exact equilibrium state.) Therefore, a composite model was adopted. At each axial station, a complete calculation is made using the double-flame-sheet model. The temperature profile is searched for points having a predicted temperature greater than 2500 K; for those points, a complete equilibrium calculation is made. The resulting cost has been reduced by a factor of about three to five.

The calculations have been made with the axial pressure distribution, $P(x)$, determined from the integral technique in Refs. 1 and 5 from a specified combustor wall shape. This step is very important because the system comprising the boundary layer form of the equations of motion is parabolic. Thus, the mixing code cannot calculate the upstream influence of heat release in the duct. On the other hand, the procedure of Refs. 1 and 5 was designed to provide just that important information.

For the combustor wall boundary layer calculations, the adaptation of existing codes was again sought. Several elaborate computer codes are available for the calculation of boundary layer flows under turbulent, high-speed flow conditions (e.g., Ref. 6); however, none of these codes is suitable for calculating the boundary layer on the walls of a scramjet combustor. The major shortcomings are that the chemistry generally is limited to air and not fuel-air mixtures and provisions for the entrainment of rapidly streamwise-varying, boundary-layer "edge" conditions under turbulent conditions have not been made. In the present case, this occurs because of the impingement of the edge of the jet mixing zone on the wall boundary layer. The extension to include reactive mixtures of the H-C-O-N system involves not only chemistry but significant complications in terms of the laminar physical properties such as the viscosity, Prandtl number, and Lewis number of the resulting mixtures. There are also important new questions in regard to the modeling of turbulent transport processes in these types of flow. The chemistry and physical property procedures were taken from Ref. 7.

The required modifications to the code of Ref. 6 included (a) the addition of a routine to solve the diffusion equations, (b) additions to the routine to solve the energy equation to account for energy transport as a result of diffusion and for the effect of the streamwise variation of the edge conditions on total enthalpy, (c) revision and/or replacement of routines that relate en-

thalpy to temperature and species concentration and that calculate the equation of state, and (d) the establishment of proper calling sequences for the new physical property subroutine. Numerous other minor modifications were necessary. The code of Ref. 7 was modified substantially to operate as a subroutine. The calculation procedures were streamlined and simplified to the H-C-O-N system in order to reduce the computing cost.

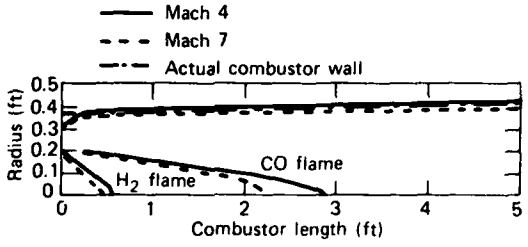

Fig. 1 Predicted duct contours and flame shapes.

DISCUSSION

The various parts of the total computational scheme have been tested by comparing them with relevant experimental data. It was shown in Ref. 5 that the one-dimensional calculation procedure accurately predicts $P(x)$ and the upstream influence of heat release in the duct. The jet mixing code can give good predictions for the cases of interest with large density variations. Finally, the boundary layer code can predict the effects of high external Mach numbers and high freestream turbulence levels.

Detailed calculations have been made for a representative engine based on inlet design D of Ref. 1. The calculated shape of the boundary corresponding to the given $P(x)$ distributions and the shape of the H_2 and CO flames for the two operating conditions are shown in Fig. 1. The CO flames are somewhat less than 3 ft long, while the H_2 flames are only abut 0.5 ft long. Thus, a 5 ft combustion chamber is sufficient to provide for complete combustion for the selected cases, assuming a diffusion controlled reaction.

Boundary layer calculations were run to an axial distance about halfway down the combustor. The variation of the skin friction coefficient along the combustor wall based on local edge conditions, C_f, is shown in Fig. 2. Calculations both with and without the influence of the higher freestream turbulence, k_e, are shown. The C_f values are rather high for this high Reynolds number flow, and they do not decay roughly as $x^{-1.5}$ as they would for a constant-pressure flow. Thus, the indirect effects of the flame on the boundary layer are significant. The dimensional wall heat-transfer rate, $\dot{q}_w$, also shown in Fig. 2, is more sensitive to the local pressure

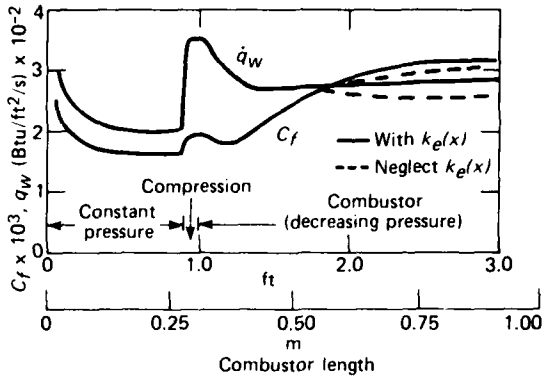

Fig. 2 Skin friction and wall heat transfer rate at Mach 7.

gradient. The sensitivity of C_f and $\dot{q}_w$ to the variations in edge properties is also quite different. These heat transfer rates are large, even though this case has lean overall conditions and the flame does not impinge on the wall.

REFERENCES

[1] F. S. Billig, P. J. Waltrup, and R. D. Stockbridge, "The Integral Rocket, Dual Combustion Ramjet: A New Propulsion Concept," *4th International Symp. on Air Breathing Engines*, Orlando, Fla., pp. 433-444 (1979).

[2] J. A. Schetz, "Turbulent Mixing of a Jet in a Coflowing Stream," *AIAA J.* **6**, 2008-2010 (Oct 1968).

[3] S. Gordon and B. McBride, *Computer Program for Calculation of Complex Equilibrium Compositions*, NASA SP-273 (1971).

[4] J. A. Schetz, "A Simplified Model for the Combustion of Multicomponent Fuels in Air," *Combust. Flame* **15**, No. 1 (Aug 1970).

[5] F. S. Billig and G. L. Dugger, "The Interaction of Shock Waves and Heat Addition in the Design of Supersonic Combustors," *Twelfth Symp. (International) on Combustion*, the Combustion Institute, Pittsburgh, pp. 1125-1134 (1969).

[6] E. C. Anderson and C. H. Lewis, *Laminar or Turbulent Boundary-Layer Flows of Perfect Gases or Reacting Gas Mixtures in Chemical Equilibrium*, NASA CR-1893 (Oct 1971).

[7] R. A. Svehla and B. J. McBride, *Fortran IV Computer Program for Calculation of Thermodynamic and Transport Properties of Complex Chemical Systems*, NASA TND-7056 (Jan 1973).

This work was supported by NAVSEASYSCOM, SEA-62R2.

IN SITU SAMPLING AND NONINTRUSIVE INSTRUMENTATION FOR SUPERSONIC COMBUSTORS

F. S. Billig, R. E. Lee, and R. Turner

The development of hypersonic ramjet engines is critically dependent on the accurate measurement of the properties of the flow in a multiphase, reacting supersonic stream. The evaluation and demonstration of several nonintrusive optical measurement techniques has shown that laser Doppler velocimetry and particle sizing interferometry are viable techniques for measuring particle velocity, size distribution, and number density in the hostile environment of a combustor test apparatus.

BACKGROUND

The development of the supersonic combustor has presented uniquely difficult challenges to the instrumentation community. Measurements not only are more difficult to make than in a subsonic combustor but they must be considerably more extensive. In addition, new combustion systems are being developed for advanced airbreathing propulsion systems having mixed combustion cycles in which very fuel-rich flows are generated in a subsonic combustion chamber and burned at supersonic speeds in a main combustion chamber. A thorough understanding of the character and properties of such flows (i.e., profiles of chemical species concentrations, temperature, and velocity) is needed.

Various remote diagnostic techniques apparently can make the desired flow measurements. Those that may prove useful include laser light transmission/absorption and scattering for particulate or soot measurements, direct spectral emission for species identification and measurements, Raman spectroscopy (spontaneous and coherent anti-Stokes Raman scattering) for species and temperature measurements, and laser Doppler velocimetry for velocity measurements. Usually, the techniques have been developed in a controlled laboratory environment for specific applications. Their extension for use in the harsh, "real-life," ramjet engine testing environment requires further performance analysis and test confirmation. The evaluation of selected techniques to characterize particulate flow in a 1500 to 3000 K gas flow is the focus of this project.

The tools used to evaluate these techniques include two computer programs that describe the laser light scattering (Mie theory) and light diffraction: a cold-flow, supersonic (Mach 3.5) jet that can be seeded with controlled particle sizes and shapes; and a small combustor that simulates the ramjet engine combustion at combustor pressures up to 4.5 atm, inlet air temperatures from 700 to 870 K, and fuel-air equivalence ratios (ER's) between 0.8 and 4.0 using JP-5 fuel.

DISCUSSION

Particulate flows strongly influence the selection of nonintrusive diagnostic techniques and also the combustion efficiency; consequently, the first flow parameter to be addressed is the number density and size distribution. If the number density and sizes are small, particles will be of little importance in the combustor performance. Conversely, large numbers and sizes of particles will affect combustor performance and may interfere with potential diagnostic methods. At the onset of this task, the combustor particulate flow characteristics of JP-5 fuel were unknown. A unique sampling probe was designed[1]; it showed that the range of particle sizes of interest extended from 0.5 to 50 μm. It was anticipated that the larger particles would occur in the first stage of combustion at high ER values and would subsequently be reduced to smaller particles in the afterburning stage.

Many optical techniques for characterizing particles in combustion flows have been reported in the literature. However, most of them were developed for atmospheric-pressure, open flames of gaseous fuels in which the particles were generally of submicron size. In contrast, the elevated pressure of a ramjet's subsonic combustor can lead to the production of large polydispersed particles, incomplete combustion, greater flow noise, and high particle velocities that could greatly affect the optical techniques.

Initially, the techniques were studied by means of computers, using laser light transmission and scattering principles and selected known values of the particle refractive index reported for other hydrocarbon fuels. It was assumed that this would produce a data spread that would encase the results for JP-5 fuel combustion particles when the refractive index is unknown. The light transmission technique studied was similar to that used by Dobbins,[2] which related particle size to the laser light intensities transmitted at two different wavelengths. The range of particle size for this technique is governed by the spread of the two wavelengths. The He-Cd and Nd-YAG lasers had wavelengths of 0.4416 and 1.064 μm, respectively. The computed results showed the upper particle size limits for these wavelengths to be about 1 μm.

The laser light scattering technique was that used by Gravatt[1]; it related the particle size to scattered light intensities measured at two small angles. Light-scattering theory showed that the scattered light intensity depends on the wavelength, scattering angle, and index of refraction. At very small forward scattering angles, the effect of refractive index is negligible, and the particle size range increases with decreasing angles and increasing wavelength. For the Nd-YAG laser and measuring angles of 8 and 4°, the upper limit of particle size was about 10 μm. Consequently, neither the light transmission technique nor the scattering technique could discriminate the anticipated 30 to 50 μm particles with the available lasers.

The third particle sizing technique analyzed was laser Doppler velocimetry. The modulating output signal could be related to all three parameters: the velocity from the frequency of modulation (Doppler frequency),[4] the particle size from the amplitude of the modulation (using the so-called particle sizing interferometry technique),[5] and the particle number density from signal counting. Figure 1 illustrates the optics configuration. The He-Ne laser beam was split into two equal parallel beams that were focused to cross at the measuring location. To permit the measurement of the very high combustor exhaust flow velocities, a beam spacing of 9 mm corresponding to a beam crossing angle of 2.06° was used. The crossing beams formed an ellipsoidal region that contained constructive and destructive light interference fringes, approximately 15 fringes spaced 17.6 μm apart. A particle moving across the region scatters light from each beam and produces a modulating signal. Typically, a particle moving at 1400 m/s will produce a pulse approximately 0.35 μs wide that is modulated at a frequency of 80 MHz.

The collected modulating light intensity, I, expressed in terms of the signal visibility, $V = (I_{max} - I_{min})/(I_{max} + I_{min})$, provides a relative measurement of the scattering particle size. (The use of this visibility term to define the particle size is known as particle sizing interferometry.) Samples of data from the laser Doppler velocimetry/particle sizing interferometry technique are shown in Table 1. In general, the results showed good agreement with computations and intrusive probe measurements, and this technique can resolve particle sizes as large as 35 μm.

Particle velocity lag is important in the analysis of laser Doppler velocimetry data. It can be used as a supplemental method to predict the particle size from velocity data. Results from this approach are shown in

Table 1

MEASURED PARTICLE SIZES IN COMBUSTOR EXHAUST FLOW

Flow Conditions			Particle Size (μm)	
Combustor Pressure		ER	Instream Probe	Particle Sizing Interferometry
(kN/m^2)	(psia)			
430	62	2.6	11-20	10-18
390	57	0.9	4-8	15-18
260	37	2.5	5-13	15-17
240	35	1.0	10-15	6-19

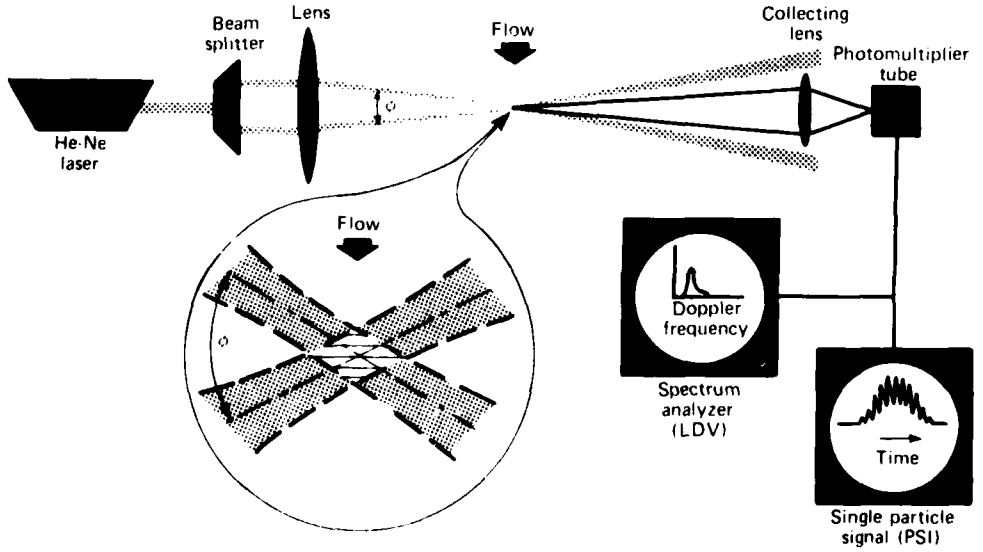

Fig. 1 Optics configuration for laser Doppler velocimetry and particle sizing interferometry.

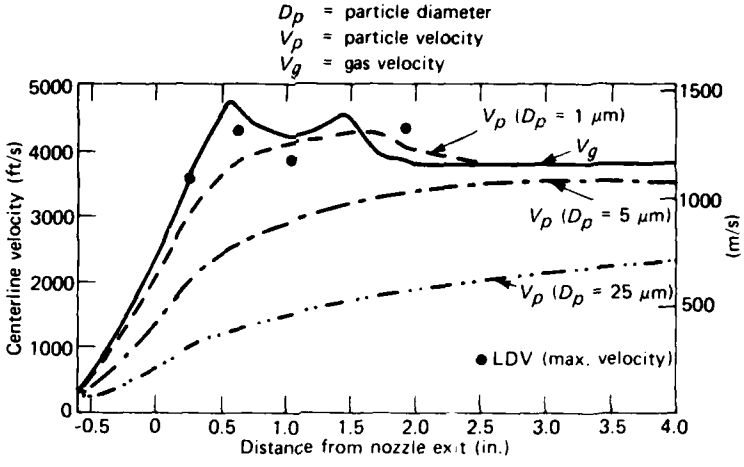

Fig. 2 Comparison of gas and particle velocities along centerline; combustor pressure, 430 kN/m^2; combustor temperature, 1590 K.

Fig. 2, where one-dimensional flow analysis and pitot-probe measurements were used to define the gas velocity distribution at the combustor exhaust, and an assumed Stokes drag was used to calculate the particle velocity distributions for comparison with the laser Doppler velocimetry measurements. A more detailed description of these results is given in Ref. 1.

REFERENCES

[1] F. S. Billig, R. E. Lee, and P. E. Waltrup, "Instrumentation for Supersonic Combustion Research," presented at 1981 JANNAF Propulsion Meeting, New Orleans (26-28 May 1981).

[2] R. Dobbins, "Remote Size Measurements of Particulate Products of Heterogeneous Combustion," *Proc. 11th International Symp. on Combustion*, pp. 921-929 (Aug 1966).

[3] C. C. Gravatt, "Real Time Measurement of the Size Distribution of Particulate Matter in Air by a Light Scattering Method," *J. Air Pollut. Control Assoc.* 23, No. 12, 1035-1038 (Dec. 1973).

[4] L. R. G. Eckert, ed., *Proc. Minnesota Symp. on Laser Anemometry*, Univ. Minnesota (22-24 Oct 1975).

[5] W. M. Farmer, "Measurement of Particle Size, Number Density and Velocity Using a Laser Interferometer," *Appl. Opt.* 11, 2603 (1972).

This work was supported by Indirectly Funded R&D and NAVSEASYSCOM, SEA 62R2.

SPACE SCIENCE AND TECHNOLOGY

INTRODUCTION

The Laboratory's involvement in space programs began in the post World War II years when Aerobee and captured V-2 rockets carried Geiger tubes, magnetometers, and optical spectrometers high above the earth's surface. The flights, which provided the first high-altitude measurements of cosmic rays, the geomagnetic field, and atmospheric constituents such as ozone, were conducted by pioneers James A. Van Allen, John J. Hopfield, and S. Fred Singer (who were then APL staff members). In 1946, a V-2 rocket carried the first camera, installed by APL, to photograph the earth from an altitude of 100 miles. From these distinguished beginnings, APL's record of accomplishments proceeds and includes the conception, design, and development of the Transit Navigation Satellite System and the SATRACK Missile Tracking System for the Navy.

The satellite activities spawned a multitude of firsts by APL, including the development of the first gravity-gradient satellite, the first color photographs of the entire earth from synchronous-altitude satellites, the first solid-state particle detectors flown on a satellite, and the first extremely accurate measurements of the geomagnetic field.

Space activities at APL have been supported by a program of basic research directed toward understanding the chemical and physical processes involved in the earth's atmosphere, ionosphere, and magnetosphere, and in interplanetary phenomena. Some significant Laboratory achievements include the first detection of solar cosmic rays with satellite-borne solid-state detectors, the design and construction of one of the longest lived and most productive scientific satellites ever launched (1963-38C), the first measurement of short-period magnetohydrodynamic waves near synchronous altitude, the discovery of heavy ions trapped in the earth's radiation belts, the experimental confirmation of large-scale field-aligned currents in the auroral regions, the demonstration of the effect of stratospheric pressure variations on the ionosphere, and the development of radio astronomy techniques for predicting geomagnetic storms that can disturb terrestrial radio transmissions. The research activities have involved international collaborations with scientists from more than a dozen academic and defense organizations.

Currently, the Laboratory's space programs may be categorized as follows: military systems, solid earth science and geodesy, remote sensing and oceanography, space science and exploration, and space systems development.

In military systems, the Laboratory supports the Navy's Strategic Systems Project Office in the Transit program, conceived at APL in 1958 and currently the nation's only fully operational worldwide navigation system. Current activity is in support of the operational system plus Nova and Stacked Oscars on Scout (SOOS). The first Nova, an improved station-seeking and station-keeping Transit satellite designed and developed by APL and fabricated at RCA, was launched in May 1981 and added to the constellation of in-service satellites in July. Two more Nova satellites are being fabricated at RCA for possible launch in 1982. SOOS is a development program to enable two Transit satellites to be launched on one Scout vehicle for in-orbit storage. The initial SOOS launch is projected for 1984.

Programs in satellite and missile tracking include the development of equipment to use navigation signals transmitted by satellites of the Department of Defense Global Positioning System (GPS). Three GPS applications are being pursued. The first is a GPS package (GPSPAC), sponsored by the Defense Mapping Agency, which will be used for position determination on low altitude host vehicles and on NASA's LANDSAT-D spacecraft. The objective of GPS/SMILS, an Air Force program, is to develop a sonobuoy missile impact location system (SMILS) using GPS satellite signals. SATRACK-II/ACES, a major ballistic missile instrumentation system for the U.S. Navy, will use GPS satellite signals to assess missile performance during the boost phase of launch.

Major activities in solid earth science and geodesy include two satellite programs, GEOSAT-A for DoD and GRAVSAT-A for NASA, and the development of precise time standards. GEOSAT-A, to be launched in early 1984, will collect satellite altimetry data over ocean areas to determine the local vertical to within seconds of arc. GRAVSAT-A will determine worldwide gravity variations to within 100 km in extent. Recent efforts have been to define the mission and spacecraft, study data processing techniques, and conduct laboratory tests and simulations of critical subsystems. NASA anticipates a 1984 start, with launch in 1987. In support of very long baseline radio interferometry, APL has had a hydrogen maser development program for the last seven years. In 1982, APL will design and fabricate three instruments with a stability of one part in 10^{15} over a 1000-second interval.

In the remote sensing and oceanography program, the laboratory is developing advanced satellite radars for NASA. The Topography Experiment for Ocean Circulation Program includes the development at APL of an altimeter with a measurement precision of 2 cm. This precision will allow the remote measurement of mesoscale oceanographic features and geostrophic currents. Other radars being developed at APL for NASA will allow the measurement of ocean wave spectra and the wide swath mapping of ocean features. The characteristics of ocean wave spectra measured with the SEASAT Synthetic Aperture Radar (SAR) are being examined to better understand the global ocean environment.

The Laboratory's efforts in space science and exploration are directed toward investigations of solar-terrestrial physics, planetary physics, and spacecraft technology. The goal of APL's program in solar terrestrial physics is to determine the principles governing the energy flow between the sun and earth. Of particular interest are charged particles and magnetic fields in interplanetary space and in the earth's magnetosphere. The NASA AMPTE (Active Magnetospheric Particle Tracer Explorers) Program will involve three spacecraft, built in the United States, West Germany, and Great Britain, to investigate how solar wind plasma enters the earth's magnetosphere. Tracer ions will be released from the West German spacecraft and monitored with the United States and British

spacecraft. The AMPTE spacecraft are scheduled for launch in 1984, and APL will also provide the central data-handling facility for scientific analysis of the data acquired by the United States spacecraft. This program is expected to continue through the 1980's.

The sun's magnetic fields and energetic particles have a profound influence on the earth and the other planets. Particle experiments built at APL and flown on the Voyager spacecraft have explored very hot plasmas near Jupiter and Saturn; there are plans to study Uranus. Particle experiments are presently under development for the International Solar Polar Mission spacecraft to be launched in orbit over the sun's poles in 1986 and for the Galileo spacecraft to be launched in 1985 to orbit Jupiter. Participation in the analysis of data acquired by these spacecraft will continue at APL into the 1990's.

The major activities in spacecraft technology are the Hopkins Ultraviolet Telescope (HUT) experiment and a Search and Rescue spacecraft. The HUT project is a collaborative effort with The Johns Hopkins University Physics Department for the spectrophotometry of faint astronomical objects at far-ultraviolet wavelengths. Fabrication of the structure and electronics has begun, and the first of four planned flights is to be on the Shuttle in February 1985.

The Laboratory has been asked by NASA to do a conceptual design of a dedicated spacecraft for search and rescue of aircraft and marine vessels. The mission plan, conceptual design, and cost estimates are to be completed in mid-1982.

In space systems development, NASA's Communications Division sponsors APL investigations of the attenuation, resulting from precipitation, of earth-satellite communications at frequencies above 10 GHz. The effort has involved multiyear rain attenuation measurements and numerical modeling. In addition, NASA Wallops Flight Center, in connection with the Department of Agriculture, has been supporting an APL program since 1979 on the radar detection and characterization of certain species of insects in flight.

SUCCESS OF THE SINGLE-AXIS DISCOS FOR THE NOVA-1 SATELLITE

The single-axis disturbance compensation system (DISCOS) was operated successfully in the Nova-1 satellite. Because of the implementation of DISCOS, Nova ephemeris update intervals as long as eight days are possible.

BACKGROUND

Since 1964, the Navy's Transit navigation satellite system has been providing precise navigational data to military and civilian users worldwide. In this system, a satellite transmits information about its orbit to a user. Using his knowledge of the orbit and the measured Doppler shift of the transmission, the user can compute his position on earth. The accuracy of the computation depends on the accuracy of the transmitted orbital elements. Variable atmospheric drag on the satellite causes its orbit to change unpredictably with time. For this reason, updated orbital elements must be transmitted to Transit satellites twice daily. To minimize this dependence on ground-based support, APL has developed for the Navy a DISCOS that cancels along-track drag forces autonomously on board the satellite.[1,2]

For navigation purposes, the along-track component of the disturbing force is the most important; it is theoretically possible to achieve acceptable orbit predictability by providing active compensation in this single direction. Thus, under the Transit Improvement Program (TIP), APL and Stanford University developed a single-axis DISCOS that was flown on TIP-II in the fall of 1975 and on TIP-III about a year later. Although the solar panels failed to deploy on both TIP satellites, enough data were obtained from TIP-III to evaluate the performance of DISCOS and to show that the disturbance compensation did not meet the specification of less than 10^{-11} g for the along-track force. A study conducted by APL found the problem to be the instability of the proof-mass suspension.[3] The single-axis DISCOS was redesigned to provide stability through eddy current damping. The redesigned system was launched in May 1981 on a Navy Navigation Satellite built by RCA, Nova-1.

DISCUSSION

The single-axis DISCOS consists of a cylindrical cavity containing a hollow cylindrical proof mass suspended about a tube that carries the proof-mass suspension current (Fig. 1). The cavity axis is oriented in the along-track direction. The proof-mass position along track is sensed optically and is fed back to control thrusters that act on the spacecraft to center the proof mass and thus compensate for along-track disturbance forces. The proof mass is centered radially by electromagnetic suspension. An alternating current in the axial tube causes eddy currents in the proof mass. The eddy currents interact with the magnetic field produced by the current in the axial tube, providing a restoring force to center the proof mass in the tube.

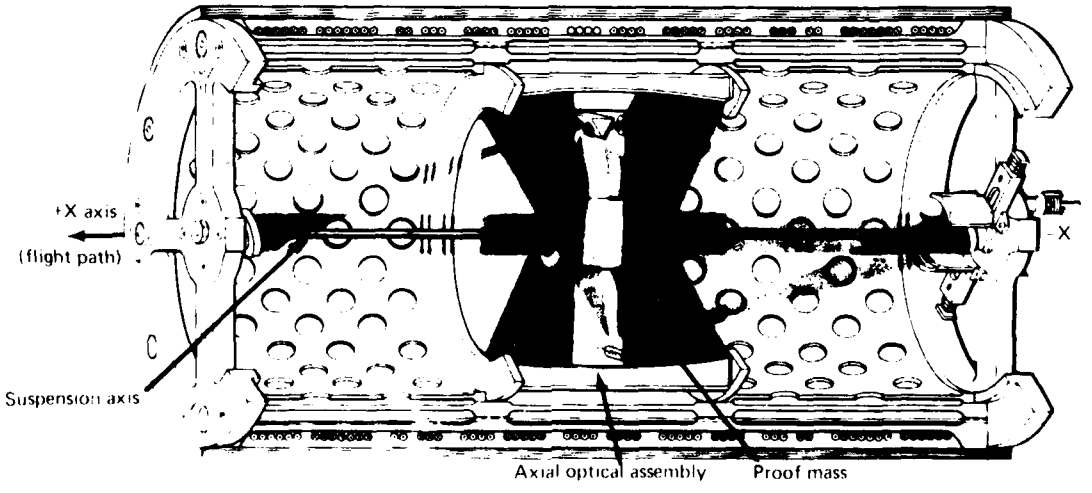

Fig. 1 The single-axis DISCOS concept.

The restoring suspension force acts like a spring, and there is very little natural damping of radial oscillation of the proof mass. On TIP-II and TIP-III, active damping was provided by a closed-loop system that optically sensed the proof-mass radial motion and appropriately modulated the amplitude of the suspension current. This scheme works well for damping radial motion but is nearly ineffective for damping orbital motions of the proof mass about the tube. Analysis of the TIP-III data showed that small nonlinearities in the optical sensor caused the orbital motions of the proof mass to diverge. Ultimately, the proof mass hit the tube, interrupting its along-track motion and severely degrading the accuracy of the drag compensation.

The solution to this problem adopted for Nova was to place a permanent magnet, consisting of a platinum-cobalt alloy wire, within the hollow tube that carries the proof-mass suspension current. The magnet was polarized normal to the axis and had a magnetization of 1 pole-cm/cm. Ideally, the field of such a magnet is axially uniform and has no component or gradient along track to disturb the proof mass in that direction. However, the radial dipole field damps all modes of proof-mass motion in the plane normal to the axis by eddy current interaction.

All real magnets, of course, have imperfections that contribute along-track forces and detract from the accuracy of drag compensation. To hold these undesirable effects to an acceptable level, the magnet wire carefully remagnetized transversely at APL. The uniformity of the transverse field was measured by rotating the wire in a lathe bed and recording the radial field sensed by a Hall-effect probe as it was moved along the length of the wire. The magnitude of the field nonuniformity was held to within 1%.

To reduce further the effect of magnet imperfections, the proof mass must have minimum magnetic susceptibility. An additional constraint on the design was imposed by the fact that sufficient eddy current suspension of the proof mass can only be achieved if the product of resistivity times density is 20 $\mu\Omega$-g/cm^2 or less. The Nova proof-mass design consists of concentric cylinders of silver and aluminum (Fig. 2). The thicknesses of the cylinders were chosen so that the diamagnetism of silver cancelled the paramagnetism of aluminum. The final configuration had an effective resistivity times density of 12.7 $\mu\Omega$-g/cm^2. Ferromagnetic impurities were kept to one part per million or less to ensure that forces resulting from contaminants would not affect performance. Raw materials and fabricated proof masses were tested with a force balance magnetometer and a Squid second-order gradiometer. Measurements of the Nova-1 proof mass demonstrated that the achieved susceptibility was less than 4% that of silver.[4]

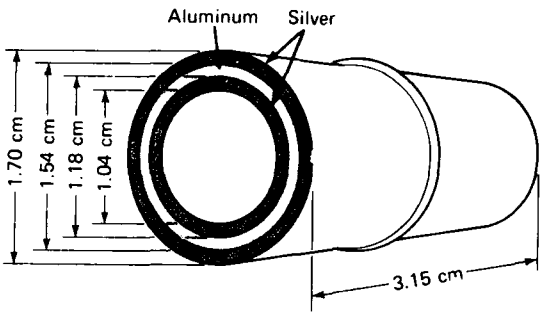

Fig. 2 The low-susceptibility proof-mass design.

After Nova-1 was launched, the satellite's orbit was circularized and three-axis attitude stabilization was achieved. DISCOS was turned on and, after initial capture, the active damping circuit was turned off. Telemetry showed that the proof mass remained centered radially and that oscillations induced by perturbations damped out within minutes, as predicted. The damping magnet was completely effective in eliminating the orbital instability of TIP-III.

In Fig. 3, the root mean square (rms) total navigation error for a fixed site is plotted against day number for the Nova-1 and the Oscar 13 Transit satellites. During that period, the Nova-1 ephemerides were updated every 24 hours while those of Oscar 13 were refreshed twice daily. The large spikes exhibited in the Oscar error are a consequence of the inability to predict variations in atmospheric density (and the resulting drag). Analysis of the performance over eight days shows that DISCOS compensates for drag and radiation pressure to 10^{-11} g; therefore, ephemeris update intervals as long as eight days are possible. The Nova-1 nodal period has been maintained at the selected value of 6540.5 s since early September with no sign of orbit decay.

With the proof-mass suspension problem solved, single-axis drag compensation has finally been demonstrated. Nova-1 has been an operational Transit navigation satellite since 31 July 1981.

ACKNOWLEDGMENT

The success of the single-axis DISCOS on the Nova-1 satellite was due to the efforts of many APL staff members as well as employees of RCA. Special mention should be made of the work of R. B. Kershner and R. E. Fischell.

This article was written by J. C. Ray, J. R. Champion, and A. C. Sadilek. A. Eisner and S. M. Yionoulis furnished the results shown in Fig. 3.

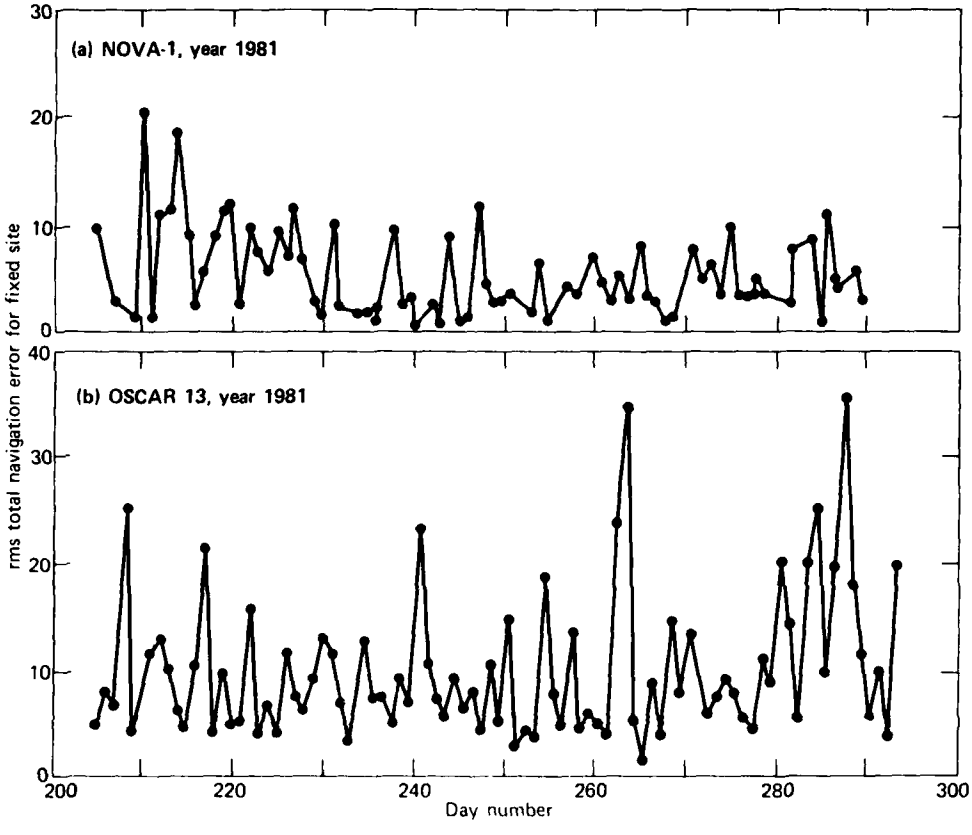

Fig. 3 Comparison of fixed-site navigation errors for Nova-1 and Oscar 13.

REFERENCES

[1] *APL Tech. Dig.* **12**, No. 2 (Apr-Jun 1973).

[2] A. C. Sadilek, "DISCOS System for the TIP-II Satellite," *Developments in Science and Technology, Fiscal Year 1975*, JHU/APL DST-3.

[3] V. L. Pisacane and G. B. Bush (APL), W. Franklin (RCA), and R. A. Quinnell, J. C. Ray, A. C. Sadilek, and S. M. Yionoulis (APL), "TIP-III DISCOS Study Group Report," JHU/APL SDO-5592 (Feb 1980).

[4] J. R. Champion, F. F. Mobley, and A. C. Sadilek, "A Low Susceptibility Proof Mass for the NOVA Satellite," *IEEE Trans. Magn.* **17**, No. 6 (Nov 1981).

This work was supported by the Strategic Systems Projects Office.

ELECTROMAGNETIC THEORY FOR FINITE-LENGTH CYLINDERS

J. F. Bird

A formal analysis was made of the electromagnetic end-effects resulting from the finite length of a cylindrical metal shell that is being magnetically levitated about an AC filament. From that analysis, we derived an effective approximation for levitational end-corrections that agrees well with measurement. Since electromagnetic theory has found it notoriously difficult to calculate any but an infinite cylinder, or to compute numerically full three-dimensional geometries, our analysis represents a needed new contribution to the theory. Its immediate practical significance is that the shell-filament system models the magnetic suspension flown in Nova spacecraft.

BACKGROUND

Earlier theoretical calculations[1] on the magnetic levitation of cylindrical metallic shells of varied constructions encircling an AC filament were accomplished by neglecting the boundary conditions at the cylinder end-planes. That neglect is acceptable for a long enough cylinder and is desirable for an extensive analysis of system parameter variations, as in Ref. 1. But one should like some quantitative measure of end-effects on the levitation, to know what is "long enough," and to correct what is not. It is recognized that it is difficult to calculate analytically any but an end-less cylindrical geometry. However, the computational solution for a full three-dimensional problem is no mean task either, and numerical success requires felicitous formulation of the interacting vector field and current distributions.[2] Therefore, we undertook to carry forward a formal analysis of the finite cylinder problem to a point where we can readily calculate end-effects on the levitation in the shell-filament system.

The immediate practical motivation for the analysis lay in application to the magnetic suspension incorporated in the disturbance compensation system (DISCOS) flown in recent APL-Navy earth satellites. Some laboratory measurements[3] of the levitation for various designs of the suspended shell differed from the calculations neglecting end-effects,[1] to greater or lesser degree. For example, the difference was under 20% for the original flight design (a thick, pure aluminum shell); but it became as much as twofold in an extreme case (a thin, aluminum alloy shell). In order to establish the reliability of the basic theory, as well as to confirm the experimental technique, it was essential to increase the calculation accuracy by including levitational end-corrections.

Reference 4 details the formal analysis of end-effects, derives therefrom effective approximation formulas, and illustrates the results by representative numerical calculations.

DISCUSSION

We consider a homogeneous metal shell with its axis parallel to the filament current axis. As seen in Ref. 1, this paraxial case is representative of the levitation force in more complex cases of inhomogeneous shells and nonparallel shell and current axes. After presenting a formal analysis of the homogeneous paraxial system, Ref. 4 eventually calculates the force constant, k_f, corresponding to small displacements from equilibrium, as a convenient index for the levitational end-effects.

The formal analysis of Ref. 4 proceeds by analyzing the differences in magnetic field distribution between the finite-length and the end-less geometries. This approach yields a new eigenvalue equation that quantizes the axial dependence of the magnetic field via a doubly infinite sequence of eigenvalues,

$$Q_{ms}\ (a,b,\delta) \qquad [m,s = 1,2,3,\ldots,\infty]\ , \qquad (1)$$

that depends on the shell radii—inner a, outer b—and its skin depth δ, but *not* on shell length. Expansion of the magnetic field corrections in the corresponding eigenfunctions leads, after some reduction, to a compact set of equations for determining the expansion coefficients. From this formulation, the levitation force is expressed solely in terms of field coefficients for the region bounded by the shell inner surface and end-planes. An approximation for these coefficients is then developed from the basic equations, yielding an analytical formula for the levitational end-corrections.

Some calculated results are shown in Table 1 for two representative cases. Both are for the standard DISCOS AC frequency (2080 Hz) and shell length (31.5 mm). Case 1 corresponds to the thick, pure aluminum shell used in the original (TIP) flight suspension. Case 2 is the thin, aluminum alloy test shell mentioned above as showing the largest (about twofold) discrepancy between experiment[3] and the end-less theory.[1] Thus, it is particularly noteworthy that in Case 2 the first approximation already yields the large correction needed to reconcile theory and experiment to within the experimental precision. In Case 1, the successive theoretical approximations very satisfactorily converge with the measurements.

Table 1

REPRESENTATIVE LEVITATION RESULTS

	Case 1 (thick)	Case 2 (thin)
Shell dimensions (mm)		
Inner radius, a	5.21	8.02
Outer radius, b	8.51	8.51
Skin depth, δ	1.885	2.74
Thickness, $b - a$	3.30	0.49
Force constant, k_f *		
End-less approximation	0.79	0.103
First end-effect approximation	0.71	0.054
Second end-effect approximation	0.676	—
Measured value	0.67	0.056

*k_f is given in units $10^{-4} I_0^2$ Newton, for sinusoidal filament current of amplitude I_0 at frequency 2080 Hz, in both cases for L = 31.5 mm. The measured values (last entry) are adapted from the square-wave current measurements of Ref. 3.

The length dependence of the levitation—the general problem motivating this investigation—may be discerned adequately from the *first-order* approximation formula we obtained for the force-constant correction,

$$\Delta k_f = Re[Y(a,b,\delta) \cdot \tan Q_{11} L/2] , \qquad (2)$$

where Re denotes real part and Y is a complicated function but, like Q in Eq. 1, is independent of shell length, L. Thus, the entire L variation resides in the (complex) tan $Q_{11}L/2$. One finds that, relative to the end-less force constant k_f^1, the length behavior is

$$\frac{\Delta k_f}{k_f^1} \approx \begin{cases} \text{const. (for } L \leq 1/\text{ Im } Q_{11} \text{)} , & (3a) \\ 1/L \text{ (for } L \geq 3/\text{ Im } Q_{11} \text{)} , & (3b) \end{cases}$$

where the L criteria are for about 10% accuracy of the behavior quoted and Im Q_{11} is the imaginary part of the lowest eigenvalue of Eq. 1.

Figure 1 illustrates the full march of the length variation from the short L (Eq. 3a) to the long L (Eq. 3b) asymptote for the two cases above. Since the Cases 1 and 2 are for shells of geometric thickness ratio $(b - a)/a$ = 0.63 and 0.06, respectively, and electromagnetic thickness ratio $(b - a)/\delta$ = 1.8 and 0.2, respectively, the corresponding curves 1 and 2 in the figure span the range of shells from thick to thin by either measure. Thus, over a wide spectrum of shell parameters, the figure fairly well represents levitational end-effects.

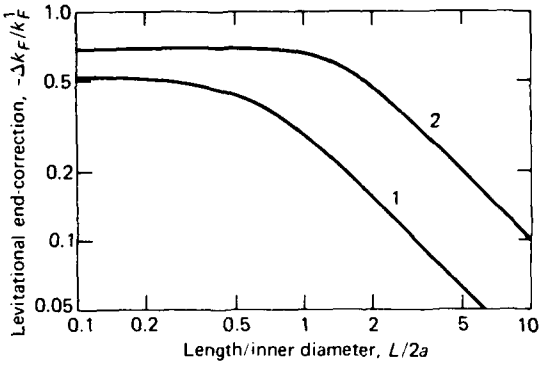

Fig. 1 *Force-constant corrections, Δk_f, relative to end-less values, k_f^1, in the first approximation (Eq. 2) are shown as functions of relative length for both thick and thin shells (curves 1 and 2, respectively, corresponding to Cases 1 and 2 in Table 1). Note the logarithmic scales.*

In any case, Ref. 4 shows that the exact levitation force always eventually approaches its end-less asymptote via a hyperbolic correction law like Eq. 3b.

REFERENCES

[1] J. F. Bird, "Theory of magnetic levitation for biaxial systems," *J. Appl. Phys.* **52**, 578-588 (Feb 1981).
[2] C. J. Carpenter, "Three-dimensional magnetic-field and eddy-current problems at power frequencies," *Proc. IEE* **124**, 1026-1033 (1977).
[3] A. C. Sadilek (private communication).
[4] J. F. Bird, "Levitational end-effects in a cylindrical magnetic suspension," *J. Appl. Phys.* **52**, 6032-6040 (Oct 1981).

This work was supported by Indirectly Funded R&D.

GPSPAC SPACEBORNE NAVIGATION SET

E. J. Hoffman

The Global Positioning System Package (GPSPAC) is the first positioning set specifically developed for use on satellites. It will provide the highly accurate, on-board, real-time, three-dimensional position, velocity, and time information about a host satellite using signals from the GPS satellites. The system, developed by APL, is now fully flight qualified and has been integrated into two spacecraft in preparation for launch in 1982.

BACKGROUND

Currently, the most widely used method of determining satellite position and orbit parameters accurately is to place an ultrastable Doppler beacon on board the host vehicle satellite and collect Doppler shift data by means of a worldwide network of ground stations. This approach has begun to entail high operational and post-processing costs, delays in delivering the data to the point of use, and political difficulties in locating the stations optimally. APL took a first step toward an autonomous, on-board navigation system with its development of the Navigation Package (NAVPAC).[1] Installed on a host vehicle, NAVPAC automatically collects Doppler data from several Navy Navigation (TRANSIT) Satellites and stores and dumps the data to the ground for post-processing. Several NAVPAC's have been launched successfully.

GPSPAC represents the ultimate step to a completely autonomous, real-time navigation set. Originally proposed in 1975, it is now fully flight qualified. By making range and range-rate measurements from the GPS satellites and performing an on-board solution, GPSPAC provides continuous position and velocity data for sensor annotation, experiment control, maneuvering, and other operations. Host vehicle position errors on the order of 10 m are expected; computer simulations and ground tracking with real GPS satellites support this estimate.

DISCUSSION

Figures 1 and 2 show the basic GPSPAC components and the flight hardware. An L-band antenna and preamplifier receive the 1575 and 1227 MHz GPS spread spectrum signals and pass them on to two independent receiver channels. The receivers acquire the ranging codes, reconstruct the suppressed carriers, make range and range-rate measurements, and recover the GPS ephemeris message. A single 16-bit microcomputer provides receiver control, data handling, and on-board orbit solution and prediction. A stable oscillator and an optional interface and mass storage unit complete the flight system. References 2 and 3 contain more detailed descriptions of the hardware and software.

Several experimental features of GPSPAC are designed to help determine the minimum system needed for operational use. For example, the two receiver channels can perform simultaneous dual-frequency ionospheric measurements or, alternatively, only a single channel can be powered and the measurements made se-

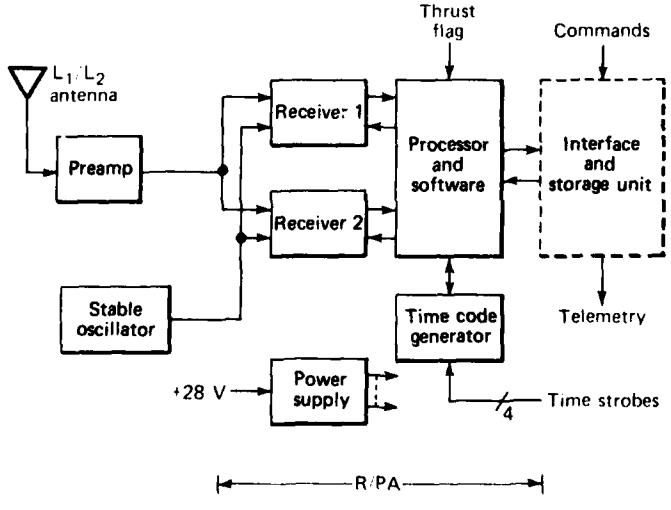

Fig. 1 Block diagram of GPSPAC.

quentially. The microcomputer is fully reprogrammable from the ground to permit "tuning" the navigation filter and testing alternative control algorithms in orbit. GPSPAC can also provide a variety of data files, including all the raw measured data that were the basis for the on-board computed position, thereby allowing more powerful post-processing software on the ground to verify GPSPAC performance.

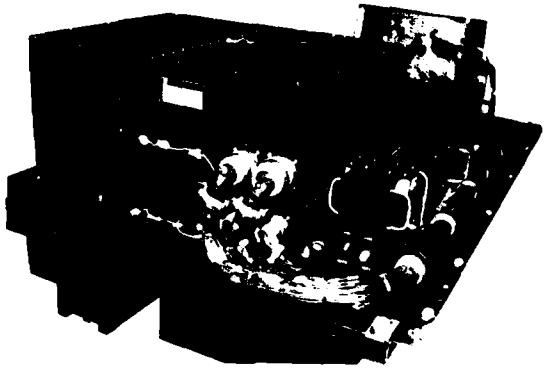

Fig. 2 GPSPAC flight hardware on host vehicle pallet.

The Receiver/Processor Assembly (R/PA), the heart of GSPAC, will be launched for the first time aboard Landsat-D in 1982. Additional R/PA's and full GPSPAC systems will be flown on other NASA and DoD satellites. Figure 3 gives typical results of computer simulations for the Landsat-D orbit. The periods of error growth in GPS Phase I reflect times when GPSPAC must propagate its solution without measurements because no GPS satellites are in view. For the fully populated Phase III constellation, GPS satellites will always be in view, measurements will always be available, and the position error will be better controlled. Figure 4 shows the results of tracking live Phase I GPS satellites with GPSPAC on the ground at APL.[4] Although APL's geometry is suboptimal and the navigation filter is not optimized for ground use, the average error of 12 m gives confidence in the flight equipment.

APL is not planning further work beyond the experimental GPSPAC, but the potential benefit of this system is so great that GPSPAC derivatives are already under development by industry for the Space Shuttle and for other NASA and DoD spacecraft.

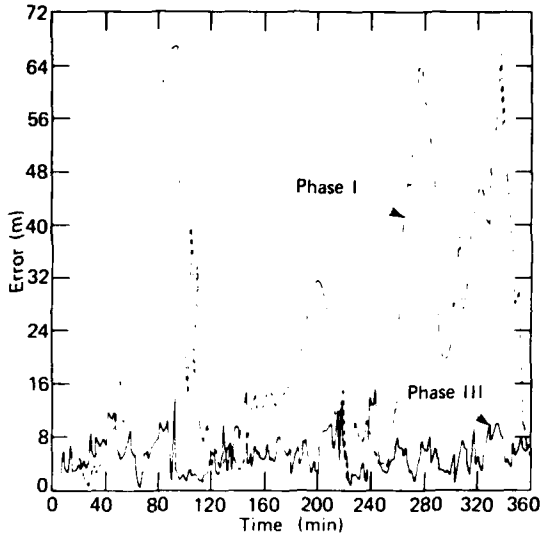

Fig. 3 Simulated true position error, Landsat-D orbit.

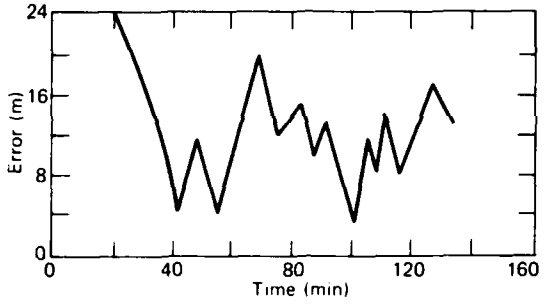

Fig. 4 True position error, live tracking tests at APL.

REFERENCES

[1] D. L. Zitterkopf, *NAVPAC — A Space-Qualified Navigation Package*, JHU/APL TG1317 (Feb 1979).

[2] E. J. Hoffman and W. P. Birmingham, "GPSPAC: A Spaceborne GPS Navigation Set," *Proc. IEEE Position Location and Navigation Symp.*, pp. 13-20 (Nov 1978).

[3] R. Thorensen et al., "NAVSTAR GPS Receiver for Satellite Applications," AGARD 31st Guidance and Control Panel Symp., London (Oct 1980).

[4] W. L. Senus and R. W. Hill, "GPS Application to Mapping, Charting and Geodesy," *J. Inst. Navig.* **28**, No. 2, 85-92 (1981).

This work was supported by the Defense Mapping Agency.

TESTS OF THE GRAVSAT RANGE-RATE MEASUREMENT SYSTEM

J. L. MacArthur and E. E. Westerfield

A system that can measure the range rate between two satellites to a precision of 1 μm/s (a micrometer equals 1.7 wavelengths of red light) has been developed, breadboarded, and tested. The system represents a major milestone in demonstrating the feasibility of a gravity satellite mission to measure the earth's gravitational field with milligal precision.

BACKGROUND

A gravity satellite (GRAVSAT) mission has been under study by the NASA/Goddard Space Flight Center and APL. It has been established that gravity anomalies can be measured with a precision of a few milligals (1 gal = 1 cm/s^2) if the range rate between two satellites in low orbits can be determined to within 1 μm/s (10^{-6} m/s). Also, it has been shown theoretically that such precise measurement of range rate can be realized with Doppler instrumentation using commercially available frequency sources with fractional frequency stabilities of less than 1 part in 10^{12} at satellite separations not exceeding 1000 km. The range must be limited to take advantage of the noise cancellation inherent in two-way Doppler systems of the type proposed. To verify the feasibility of making these measurements, an experimental program was conducted with the following objectives:

1. Select and procure the components needed to assemble and demonstrate a range-rate measurement system.
2. Perform phase and frequency stability tests on individual components (oscillators, mixers, etc.).
3. Assemble the components into a complete system (two Doppler transceivers) and evaluate closed-loop performance.

This work has been completed and the feasibility of making the desired measurements proven.

DISCUSSION

The system proposed for measuring range rate consists of a two-way continuous wave (CW) Doppler system operating in the vicinity of 90 GHz for the basic measuring channel and a parallel system operating near 50 GHz for the purpose of removing ionospheric effects. A block diagram of the system in its simplest form is shown in Fig. 1. The satellites will contain essentially identical Doppler transceivers, the only difference being that the basic reference oscillators will be slightly offset. This concept will permit simultaneous transmission and reception where the transmit frequency will serve the dual role of transmitter source and local oscillator to produce a beat with the incoming sig-

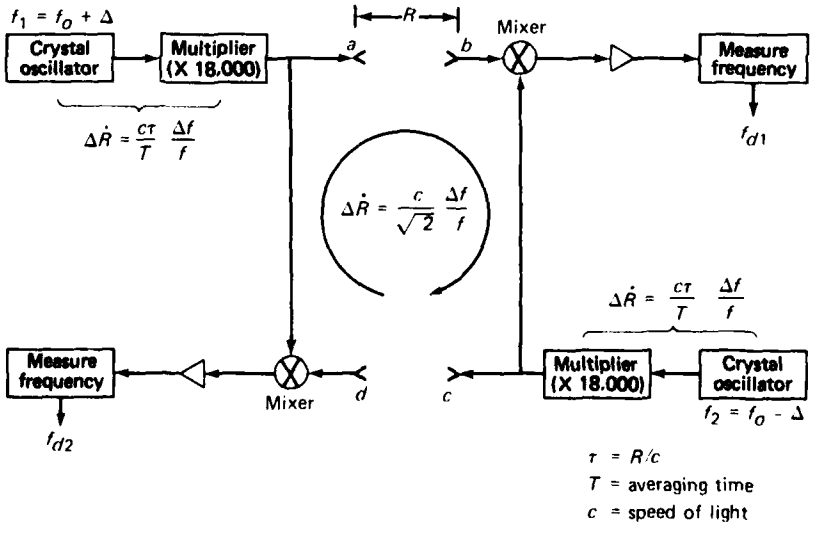

Fig. 1 The GRAVSAT range-rate system.

nal at a convenient intermediate frequency. In the absence of relative motion between the satellites, the offset frequencies, f_{d1} and f_{d2}, will be equal, on the average. With relative motion, the received frequency of either system will be altered by the factor

$$1 - \frac{\dot{R}}{c},$$

(where $\dot{R}$ is the range rate in meters per second and c is the speed of light), causing f_{d1} and f_{d2} to change in equal and opposite directions, i.e., one increasing in magnitude as the other decreases. The range rate may then be related to the net change in Doppler frequency as

$$\dot{R} = \frac{c}{2Kf_o}(f_{d1} - f_{d2}),$$

where K is the multiplication factor and f_o is the reference oscillator basic frequency, $(f_1 + f_2)/2$. If the nominal frequency of the reference oscillator is 5×10^6 Hz, operation at 90 GHz implies a multiplication factor, K, of 18,000.

Frequency measurements over a desired averaging time (typically 4 s) will be made in each system. The final determination of range rate will be made by combining the two measurements on the ground. Alternatively, phase or zero-crossing time measurements may be transmitted at a higher rate from each spacecraft for ground processing. In either case, it is this combination of identical observations made in both systems that makes possible the extremely low measurement noise. To appreciate this, consider the result of colocating the two systems and making direct waveguide connections between a and b and between c and d as shown in Fig. 1. Frequency fluctuations of the high frequency signal at a (or c) will have an equal effect on f_{d1} and f_{d2} and thus will cancel.

In the satellite-to-satellite case, the range separation will cause a time lag between the frequency variations appearing at each output in response to the frequency fluctuations of the signal at a or c. Therefore, the noise cancellation will not be complete. Nevertheless, 1 Hz away from the carrier the cancellation factor is 44 dB for a range separation of 300 km. For the averaging time under consideration, frequencies higher than this will be filtered out.

Figure 2 is a simplified block diagram of the microwave measurement assembly, i.e., the microwave system proposed for each spacecraft. Two of these subsystems were used to form the range-rate measurement system like that shown in Fig. 1. Each system was mounted on a platform located on an optical bench. One platform could be moved at a controlled rate by means of a piezoelectric device.

Figure 3 is a simplified drawing of the range-rate system motion apparatus used in these tests. Microwave assemblies were located on the right fixed platform and on the center movable platform. The left platform held a laser interferometer system that allowed the movement of the center platform to be measured accurately. Tests on the hardware demonstrated the feasibility of accurately measuring motion of significantly less than 1 μm/s.

Figure 4 shows a measured motion rate of about 1 μm/s. The platform was moved in one direction and then returned to its initial position. The solid line is the output of the microwave measurement system; the dashed line is the output of the interferometer system. The X axis is a function of time, and the sample interval is 4 s. The rate of motion varies somewhat because of the characteristics of the piezoelectric drive device, but since the interferometer accurately measures that rate, the variation does not invalidate the results.

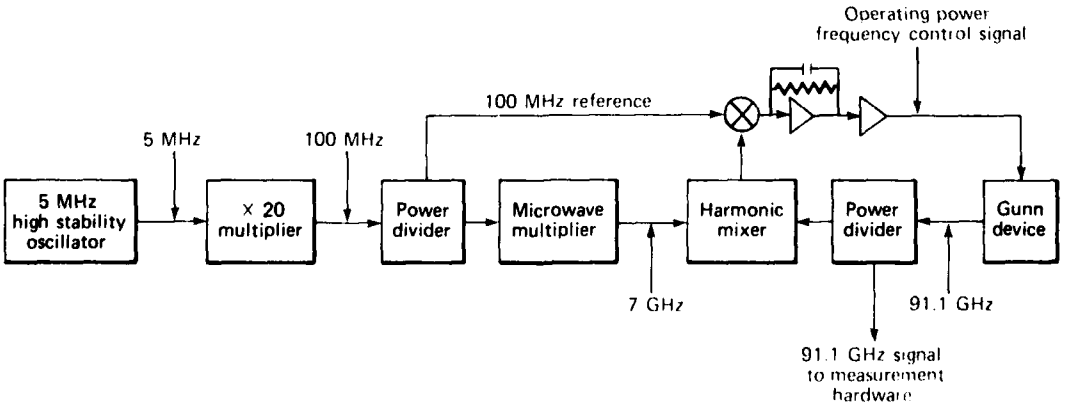

Fig. 2 Simplified diagram of the microwave measurement assembly.

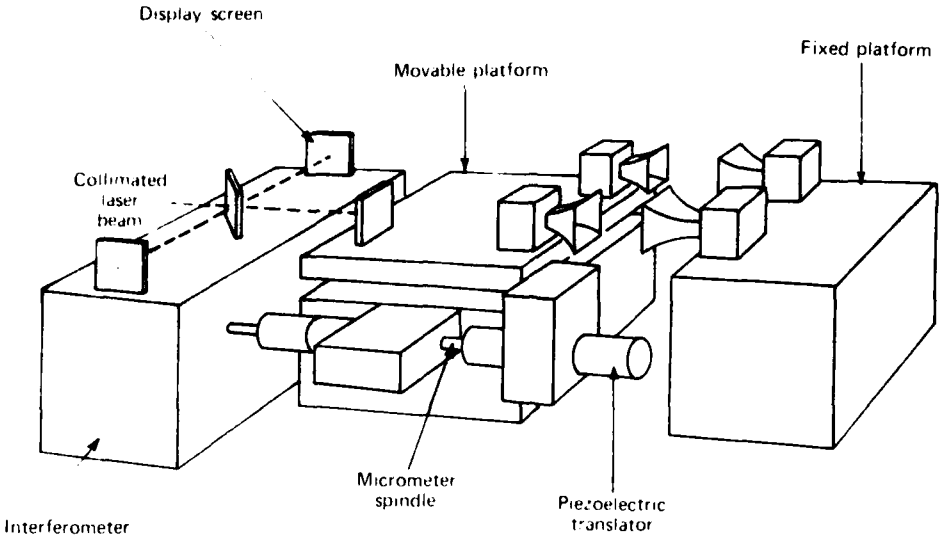

Fig. 3 The range-rate system motion apparatus.

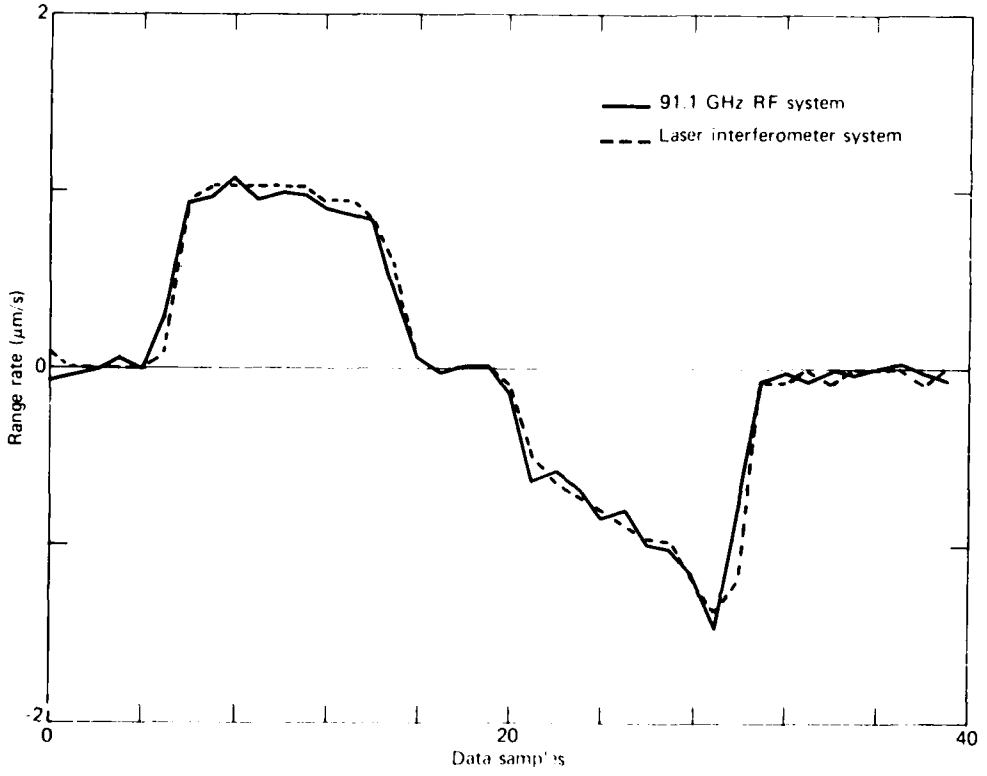

Fig. 4 Comparison of range-rate measurements.

CONCLUSIONS

These tests have shown that:

1. The stability of the basic 5 MHz reference oscillator is not measurably degraded by the multiplication to 91.1 GHz.
2. Fractional frequency deviation (Allan variance) measurements of phase-locked oscillators at 91 GHz demonstrated an instability below 10^{-12} for averaging times above 1 s.
3. Multiplier chains are in the compensated part of the two-way loop, so that a range-rate noise contribution from this source of 10^{-7} m/s is predicted for a 300 km separation and a 4 s averaging time.
4. Measurement of the mixer contribution alone has shown a time delay jitter of 0.3×10^{-15} s. The mixers are in the uncompensated part of the system for which no phase noise cancellation is realized. Accordingly, the predicted range noise for the two mixers (one in each system) is 1.6×10^{-8} m/s for a 4 s averaging time.
5. The temperature sensitivity in the mixer was 0.3° (2.5 μm at 91.1 GHz) per degree centigrade. Thus, a temperature rate of change of less than 0.4°C/s is needed, which is not a stringent requirement.

A motion measurement with a precision of 0.03 μm/s for a 4 s averaging time has been demonstrated. Consequently the work has shown that a range-rate system can be developed that exceeds the GRAVSAT requirements.

This work was supported by NASA/Goddard Space Flight Center

APL PARTICIPATION IN THE INTERNATIONAL DEFINITION OF THE SECOND

L. J. Rueger, B. W. Shaw, E. E. Mengel, and M. C. Chiu

The three cesium frequency standards in the Time and Frequency Facility at APL are now part of a global ensemble of 90 atomic clocks used for the international definition of the second. The Laboratory's participation in this activity is evidence of international recognition of its capabilities in precise time and frequency measurements.

BACKGROUND

The Time and Frequency Facility was created in 1959 to support the engineering evaluation of frequency references used in the development of geodetic satellites. Later, the facility provided a real-time service by monitoring very low frequency (VLF) radio signals. Tracking stations around the world could be warned of anomalies in the VLF signals within hours and could thus keep worldwide synchronization.

When directives issued by DoD and NASA required APL to have standards consistent with the basic United States standards, the Time and Frequency Facility began sending standard time and frequency signals to the Calibration Facility at APL; this service continues. Throughout the history of the facility, timing has been linked to clocks at the National Bureau of Standards (NBS) and the U.S. Naval Observatory (USNO) by various radio signals and by portable-clock time transfers. For a number of years, portable cesium

clocks have been carried to APL from USNO weekly to provide calibration with the USNO master clock. Data received from the Bureau International de l'Heure (BIH) were used to gauge the performance of the APL cesium standards. When sufficient confidence in the APL instruments was attained, an independent time scale was created as the APL local definition of the Universal Time Coordinated time scale, UTC (APL). The UTC (APL) is also measured relative to the USNO master clock and reported internationally by BIH.[1-3]

DISCUSSION

The APL cesium standards are compared for accumulated time relative to UTC (APL) three times each week. The information forms a data base from which the individual cesium clock times can be interpolated for the ten day points that are forwarded to BIH. Data received at BIH from APL are correlated with all other data on cesium standards from contributing laboratories by Loran-C, microwave via satellite, portable clocks, or line 10 TV. BIH uses an algorithm to weigh the influences of each clock on the total, based on prior consistent frequency-stable performance. Clocks must vary by less than 10 ns/day over successive 60 day intervals to be considered for full weight.

Figure 1 shows the BIH rates for the three cesium frequency standards identified by serial number for the three years since the reporting started. (The dotted segment of one curve reflects data deletions by BIH as a result of a data format misunderstanding.) Note that for these standards to operate at their most stable frequency, the frequency is slightly offset from UTC. This is acceptable to BIH. The important feature is how little the rate changes with time. The BIH bimonthly report provides rates for all contributing clocks at 60 day intervals for one year. The report is updated every 60 days by adding the most recent 60 day interval and deleting the oldest interval. The report also identifies the weight factor for each clock over the one year span. The weight factor is on a scale of 0 to 100 through 1980 and on a scale of 0 to 200 starting in January 1981. Figure 2 shows the BIH weight credit for the APL cesium standards over the total three-year reporting period. On occasion, APL's contribution has been as high as 4.5% of the total data used for the determination of the second. This is well above the average for contributions from 90 standards in 18 laboratories. In the United States, contributions to BIH come only from USNO, NBS, and APL.

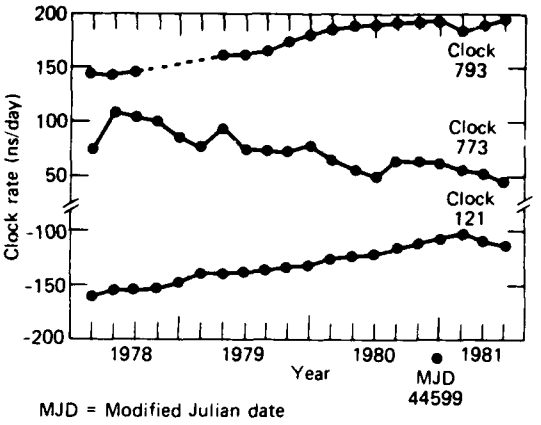

Fig. 1 BIH clock rates for APL cesium standards.

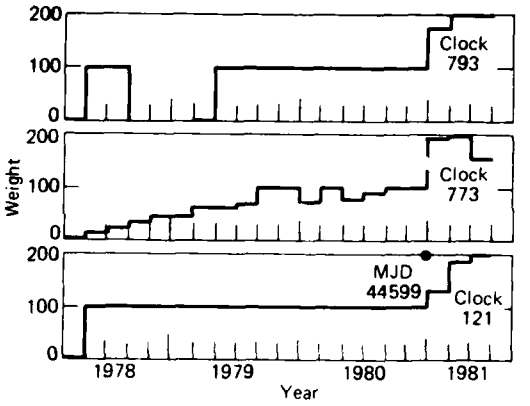

Fig. 2 APL cesium clock weight for BIH time scale.

REFERENCES

[1] *Bureau International de l'Heure Annual Report for 1978*, Federation of Astronomical and Geophysical Services, Paris (1979).
[2] *Bureau International de l'Heure Annual Report for 1979*, Federation of Astronomical and Geophysical Services, Paris (1980).
[3] *Bureau International de l'Heure Annual Report for 1980*, Federation of Astronomical and Geophysical Services, Paris (1981).

This work was supported by NASA and the Navy Special Projects Office.

AN AUTOMATED MEASUREMENT SYSTEM FOR THE SPACE SHUTTLE DATA RELAY LINKS

J. D. Colson

An automated, computer-controlled test and measurement system has been developed for the Goddard Space Flight Center to evaluate the performance of the Space Shuttle RF data relay at the Kennedy Space Center.

BACKGROUND

During preflight checkout of the NASA Space Shuttle at the Kennedy Space Center, Fla., command (forward) and telemetry (return) data must be transmitted to and from the Shuttle and the Johnson Space Center, Texas. The Tracking and Data Relay Satellite (TDRS) service is used for this transmission link. Two-way data flow from the Johnson Space Center to the White Sands Ground Terminal for TDRS is by way of a high-speed data link. The link extends from White Sands to the TDRS and then to the Merritt Island Launch Area TDRS Earth Terminal (Fig. 1).

The Shuttle is required to operate from various Kennedy Space Center facilities; therefore, it is necessary to use a "relay" to transfer the data between it and the TDRS Earth Terminal. The Goddard Space Flight Center (GSFC) Microwave System Group is responsible for the design, installation, and operation of the relay.

Early in 1979, GSFC requested that APL develop a Relay Test and Verification System (RTVS) to test the operational readiness of the relay.

DISCUSSION

The Merritt Island relay equipment consists of solid-state power amplifiers, high-power traveling-wave tube amplifiers, and waveguides. S and Ku frequency bands are used for data transmission. The forward links operate at 2.025 to 2.120 and 13.75 to 13.80 GHz. The return links are at 2.2 to 2.3 and 14.6 to 15.25 GHz. The simultaneous use of both bands is permitted.

The relay equipment is located in the satellite terminal and in the user's enclosure. As shown in Fig. 2, the RTVS equipment is also located in those two terminals, in the operations building, and in the collimation tower, which acts as a pseudo Shuttle. In operation, a forward signal is received at the satellite terminal from the TDRS, amplified, routed to the user's enclosure via waveguides, and retransmitted to the Shuttle by a 3 or 9 m antenna system. Similarly, a return telemetry signal is transmitted by the Shuttle, received at the same antenna, amplified, and retransmitted to TDRS via the satellite terminal.

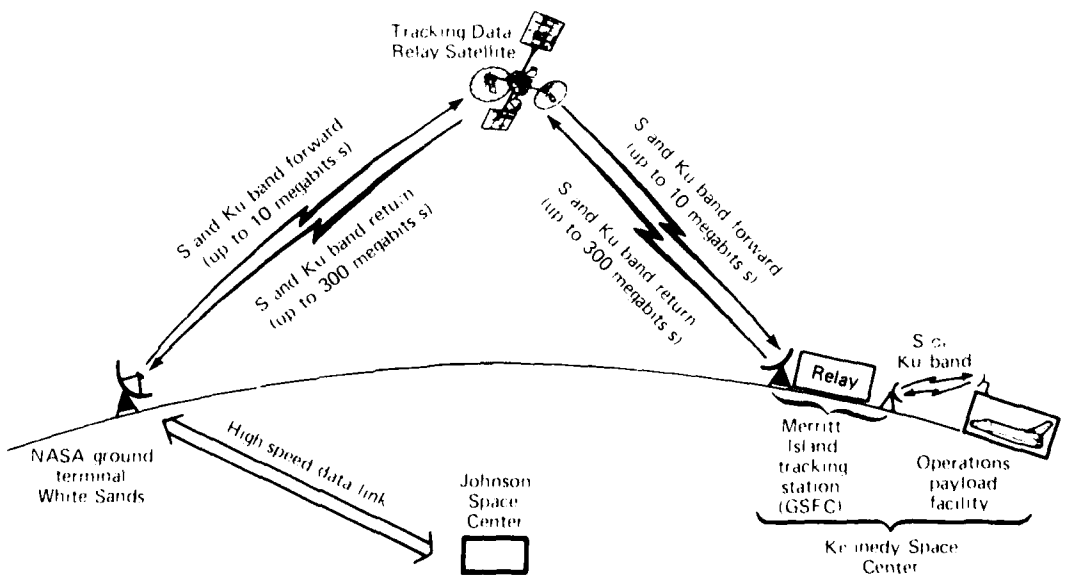

Fig. 1 Shuttle prelaunch data flow.

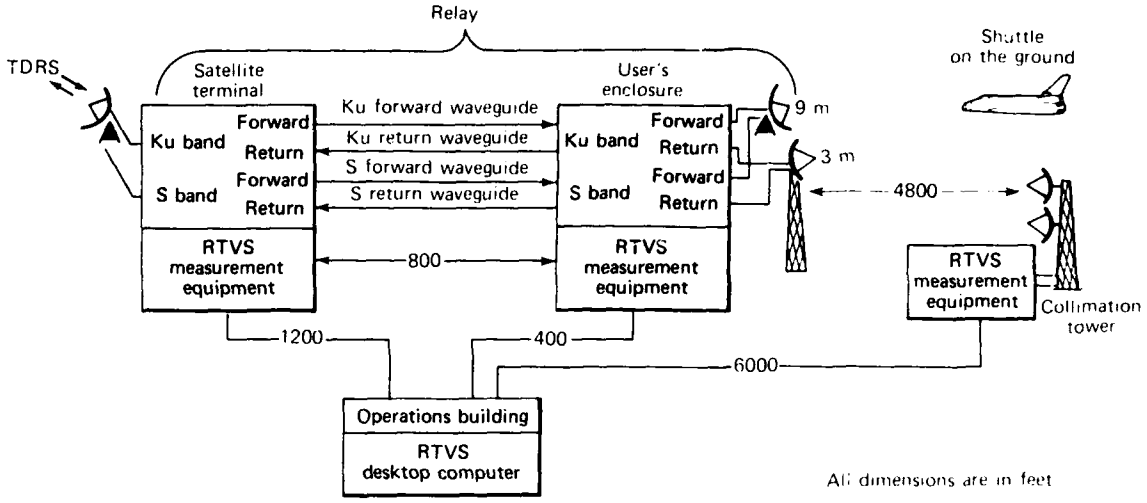

Fig. 2 Block diagram of Merritt Island Launch Area relay and RTVS equipment.

Description

The RTVS is totally automated. It consists of a Hewlett-Packard HP9845T desktop calculator/controller and an HP9895A flexible disk drive located in the operations building, plus special-purpose RF, control, and signal switching equipment located in the satellite terminal, the user's enclosure, and the collimation tower. All RTVS equipment is interconnected and controlled via the IEEE-488 interface bus. The RTVS software controls the self-testing and calibration of all RTVS equipment, the measurement of the relay operating parameters, and the analysis of the measured link characteristics to provide detailed performance criteria and status. By the selection of specific test modes, link failures in the relay can be partially isolated.

Design Concepts

The RTVS generates a known RF continuous wave signal that is injected at specific relay test points. The performance of the relay is determined by measuring the received signal at specific test points. Typically, only the magnitude and relative phase of the signal are measured.

Figure 3 is a functional block diagram of the RTVS. The measurement system is based on using two HP8505A network analyzers, one at the satellite terminal and one at the user's enclosure. The analyzers are used as an intermediate frequency (IF) device. For absolute frequency accuracy they are phase-locked to an HP8660C frequency synthesizer. The network analyzer RF output signal is frequency up-converted to S or Ku band by mixing it with the signal from an HP8672A programmable frequency synthesizer (i.e., local oscillator). The S or Ku band relay return signal is frequency down-converted to a signal identical to the one being generated by the network analyzer. This is accomplished by the careful selection of a specific local oscillator frequency. The forward signal is generated using the difference product of the IF and the local oscillator. The return signal is converted to IF by taking the difference between it and the local oscillator frequency. Using this technique, it is possible to generate and receive a series of frequencies at different RF bands, yet the intermediate frequencies are identical. All RTVS frequency-dependent equipment is phase-locked to a common stable reference. The down-converted return signal is input to channel B on the analyzer. The network analyzers are two-channel devices; thus, magnitude and phase are measured simultaneously. For magnitude data, the absolute power of the returned signal is measured, whereas for phase data, the return signal is measured with respect to the reference signal.

The RTVS can perform round-trip and one-way link testing. A round-trip test is the simultaneous measurement of the forward and the return link using either the 3 m or the 9 m antenna and the collimation tower dual-band linear frequency translator. These test paths are identical to Shuttle data flows, whereas one-way link testing is useful for making engineering measurements, isolating link problems, and conducting limited evaluations without having to radiate test signals during Shuttle operations.

Round-trip and one-way test paths are illustrated in Fig. 3. For a round-trip link evaluation, a forward test signal is injected at test point A and returned to test

AD-A125 288 DEVELOPMENTS IN SCIENCE AND TECHNOLOGY(U) JOHNS HOPKINS 2/3
UNIV LAUREL MD APPLIED PHYSICS LAB 1981 JHU/APL-DST-9
N00024-83-C-5301

UNCLASSIFIED F/G 5/2 NL

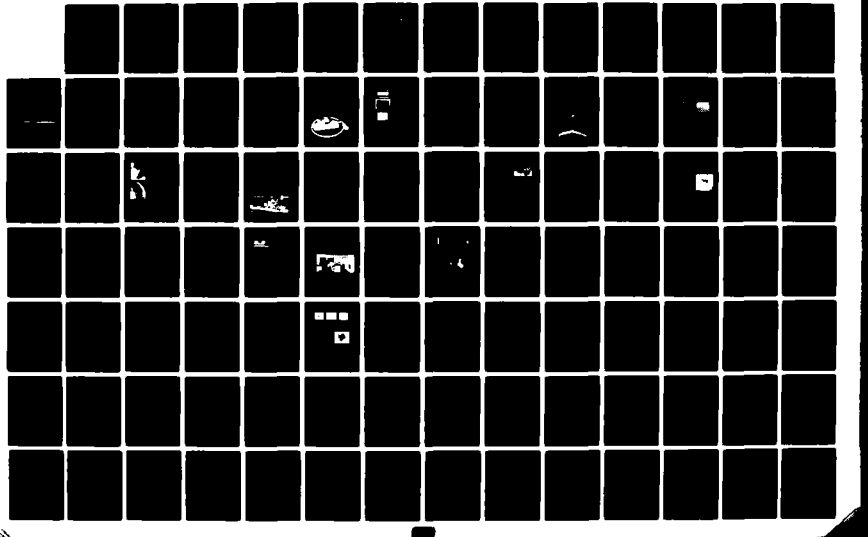

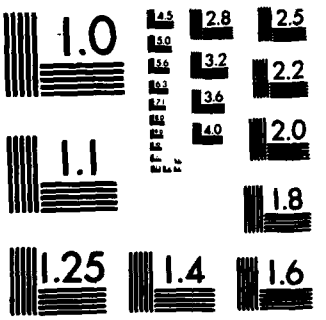

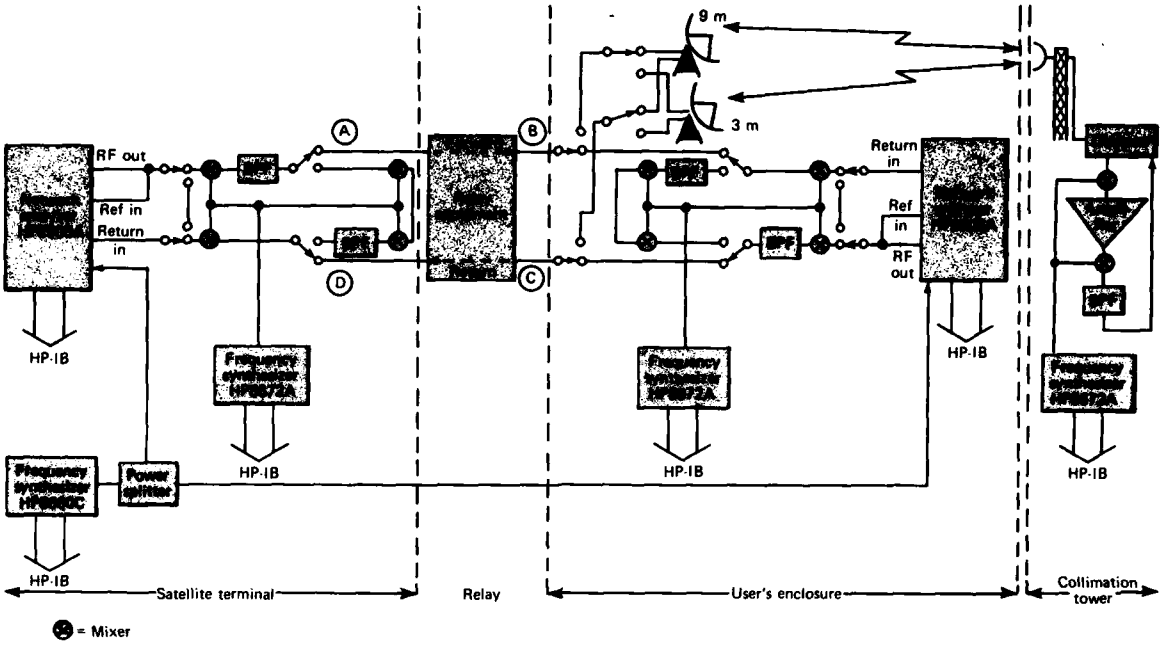

Fig. 3 Functional block diagram of RTVS.

point D. For a one-way evaluation, a return signal is injected at test point C at the user's enclosure and received at test point D for evaluation at the satellite terminal. Alternatively, a forward signal is injected at test point A and received at test point C for evaluation at the user's enclosure.

The RTVS collimation tower translator generates a return frequency signal when a proper forward signal is received. The translator uses the same mixing techniques and local oscillator frequencies as are used at the satellite terminal and the user's enclosure in order to preserve proper frequency relationships.

RF switches in the satellite terminal and user's enclosure allow the test signal to feed two additional mixers and a bandpass filter. The path is used to calibrate the up/down converters. A similar technique is used at IF to calibrate the network analyzers.

Evaluation Methodology

The methodology of the evaluation is to compute the signal loss that would occur in a digital bit stream if it were transmitted through the relay at a rate equivalent to that of the Shuttle for the measured link. A 31-bit pseudorandom bit sequence is generated in the computer and applied to a fast Fourier transform, which converts these time series data to the frequency domain. The normalized measured link data are then multiplied by the fast Fourier transform bit sequence data, and an inverse Fourier transform is run to return the data to the time domain. The group delay is removed, and the signal loss of the resulting waveform is calculated. The resultant data are displayed graphically. The energy per bit versus noise power is also calculated.

Performance Testing

The Ku band portion of the relay uses 800 ft of waveguide between the satellite terminal and the user's enclosure. Theoretical waveform degradations for 750 ft of waveguide using 100 megabit/s phase-shift-keyed data have been calculated. A 750 ft length of EW-132 elliptical waveguide has been measured using the RTVS system. The result of this measurement is almost identical with the theoretical prediction (Fig. 4). Thus, the RTVS, using RF substitution techniques, is producing almost identical results.

CONCLUSIONS

Although quite complex, the RTVS is an extremely powerful and flexible measurement system. The equipment has been stable and has provided reliable, consistent measurement and analysis results through repeated calibrations and rigorous testing. The major advantages of the computer-controlled measurement system are that it does not require a number of operators at widely separated locations to perform measure-

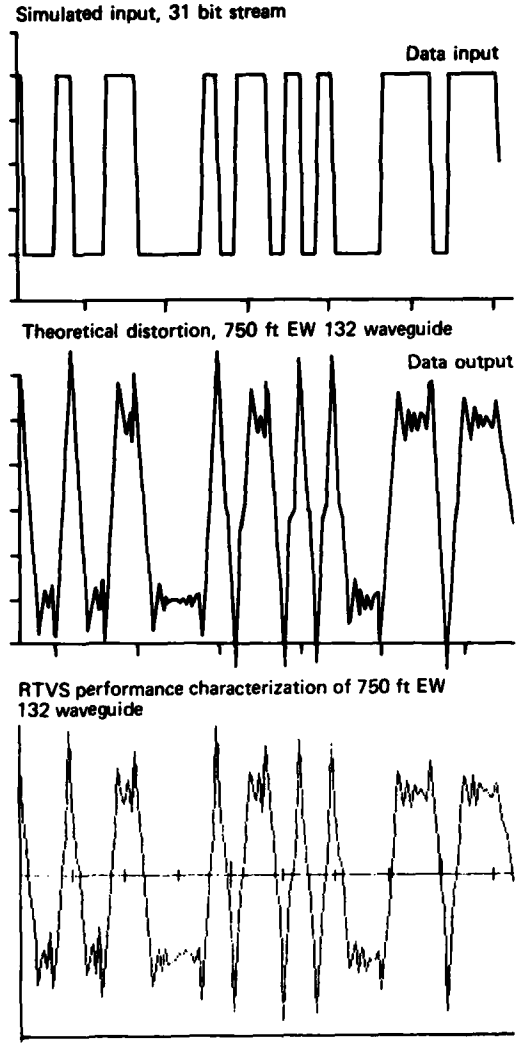

Fig. 4 Comparison of theoretical and input bit stream waveforms with that computed by RTVS.

ments, and large amounts of data can be collected and processed easily. Moreover, the system is configured and operated in the same manner each time the program is executed, and the operating characteristics are easily modified by means of software changes.

REFERENCES

[1] J. D. Colson, *Relay Test and Verification System*, JHU/APL S3C-3-103 (24 Aug 1981).
[2] J. D. Colson, *An Automated Measurement System for a Space Shuttle Data Relay Link*, JHU/APL CP 082 (Nov 1981).

This work was supported by NASA/Goddard Space Flight Center.

COMPUTER SIMULATION OF TDRS Ku-BAND AUTOTRACKING

S. C. Jones

A computer simulation model has been developed by APL to predict the performance of the automatic antenna pointing control system (autotrack) of the Tracking and Data Relay Satellite (TDRS). The ability of the satellite to point its single-access antennas toward a user spacecraft has been verified by this model.

BACKGROUND

The TDRS system is comprised of synchronous orbit satellites and a single ground station at White Sands, New Mexico. Figure 1 shows the configuration for single-access data relay between a user spacecraft and the ground station through a TDRS.

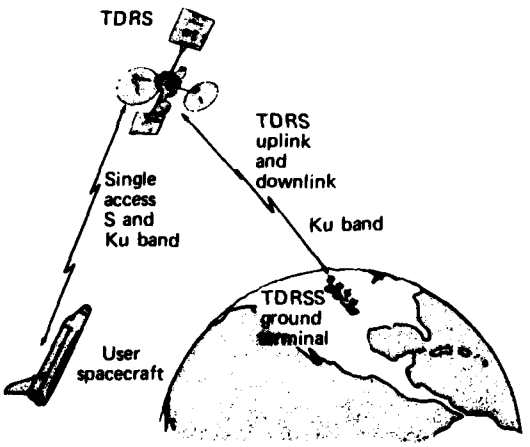

Fig. 1 Single-access data relay through TDRS.

Each TDRS has two 16-ft dish antennas with dual-frequency feeds so that they can transmit and receive at S and Ku bands. Autotracking is required on the Ku-band return link from user spacecraft in order to point the boresight of the very narrow (±0.14°) Ku-band beam of the dish antenna to within acceptable limits (±0.06°) about the user spacecraft. Open-loop Ku-band antenna tracking cannot be used because of its relatively high uncertainty (±0.22°) in pointing.

The TDRS autotracking design is complex. Antenna error signals are sent to the White Sands ground station, where the pointing control loop is closed through hardware and software. Antenna positioning commands from the ground station are sent to the TDRS on the forward command link.

The system will be verified prior to launch of the TDRS by computer simulation rather than by hardware testing. An overall system hardware test is impractical because of high costs, the distributed nature of the system, the late fabrication of some components, and antenna deformation in earth gravity. At the request of the NASA/Goddard Space Flight Center, APL developed the computer model described here to assist in the verification of the autotrack design.[1,2]

DISCUSSION

The TDRS autotrack system design is unique in that most of the autotrack equipment is on the ground rather than in the spacecraft. This permits optimum filters and processing parameters to be selected for each user.

The antenna Ku-band feed has a central horn and four horns on its perimeter. Elevation and azimuth error signals derived from the four perimeter horns are time multiplexed into a single RF signal that is linearly summed with the central horn signal in an RF coupler. This process results in an amplitude modulation (AM) of error signals upon the user's data-modulated return signal. The composite signal is then relayed from the TDRS to the ground station.

At the ground station, part of the AM signal is split off before it reaches the data detectors and is routed to the autotrack detector equipment (ADE). The ADE recovers the AM error signal by square law detection. It also uses square law detection to determine signal presence.

The error signal is demultiplexed into its separate elevation and azimuth components within the ground station autotrack interface processor (AIP). The AIP also integrates the error signals, performs thresholding functions, and corrects for small signal suppression effects that occur within the ADE square law detector.

The processed elevation and azimuth signals and the signal presence message from the AIP are sent to the automatic data processing equipment (ADPE) as digital words every 0.512 s. The ADPE software uses those signals, along with ephemeris data in two major modes (pull-in and autotrack), to provide antenna pointing commands.

The antenna pointing commands are formatted and uplinked to the TDRS and decoded in a command receiver. The commands are implemented into antenna

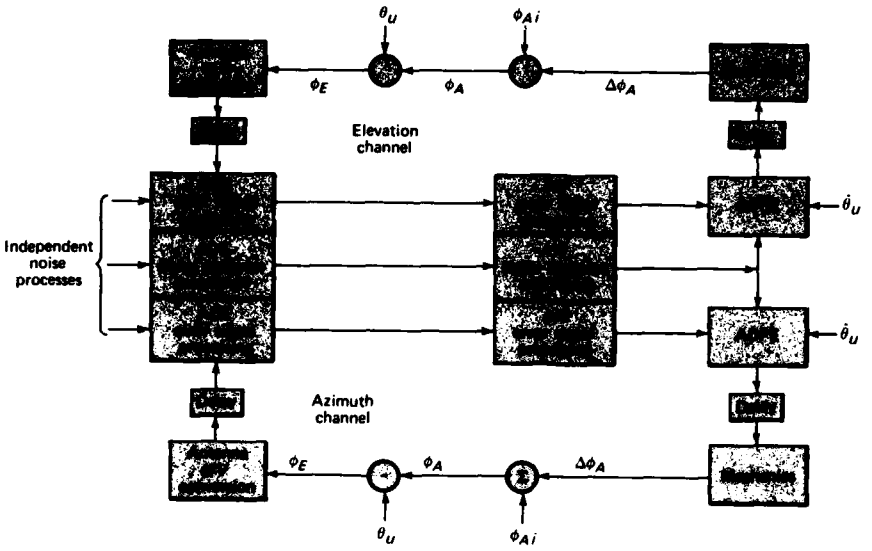

Fig. 2 Autotrack computer model.

motion by a stepper motor as a series of 0.0075° steps that move the antenna boresight toward the user spacecraft. The antenna steps excite mechanical motion in the TDRS body, which adversely affects antenna pointing and the resultant error signals.

Figure 2 is a block diagram of the computer model for the autotrack system. This is a two-channel simulation, the upper part is for the elevation axis and the lower part for the azimuth axis. Within each channel of the model, there is further division into a TDRS simulation and a ground simulation; these are separated by the time delay boxes. In the center of Fig. 2 is the signal presence processing, which is common to the ground equipment simulation for both channels.

The software is stepped in simulated time increments of 0.512 s. The timing is referenced to the times when the AIP model sends error samples to the ADPE software.

The TDRS model receives a series of antenna stepping commands from the ground simulation. The commands are implemented into incremental antenna motion, $\Delta\phi_A$, by a simple mechanical model. This incremental motion is added to previous antenna motion and the initial antenna angular position, ϕ_{Ai}, to obtain the actual antenna angular position, ϕ_A. The user look angle is subtracted from this to arrive at the antenna error angle, ϕ_E.

The error angle, ϕ_E, is converted into an effective AM modulation index by the model's antenna simulation. The signal-to-noise ratio is also calculated within the antenna simulation software.

The antenna error signal is delayed by the one-way transit time (0.14 s) and is applied to the ADE computer model, which simulates noise, accounts for square-law detection of the AM error signal, and generates signal-presence indications.

The error signals and the signal-presence indications are input to the AIP model, which does 0.512 s averaging of the error signal waveform. It also does 8.192 s averaging in the pull-in mode. In the autotrack, or fine-pointing, mode, the AIP model applies the correction factor for small signal-suppression effects computed for the ADE square-law detector. Finally, the AIP model performs a 5 out of 10 vote on the ADE signal-presence indications to obtain a single signal-presence signal to be input to the ADPE model.

The loop gain can have wide variations during a simulated pass and can vary as much as 20 dB during the pull-in and early autotrack stage.

The ADPE software model takes the averaged error signals, user angle rate information, $\dot{\theta}_u$, and the "voted" signal-presence indication from the AIP model and uses them to generate the antenna stepping command list, thereby closing the loop. It operates in two major modes, pull-in and autotrack, depending on its input signals, to generate the proper antenna stepping commands. The ADPE model closely simulates the planned ground software, which is essentially a rate following loop augmented by a position loop.

Figures 3 and 4 are sample results from executing the autotrack simulation model for a typical set of system input parameters and conditions as listed in Table 1.

Table 1

TYPICAL INPUT CONDITIONS FOR SIMULATION

Initial antenna error angles (deg)	−0.15, 0.15
User spacecraft angle rates (deg/s)	0.006, 0.006
User data rate, Manchester coding (megabits/s)	4.8
Antenna boresight error slope factor ((V/V)/deg)	0.12
Boresight signal-to-noise ratio (dB)	2.0
Effective signal-presence threshold bias (dB)	1.2

Figure 3 is a plot of the azimuth pointing angle of the antenna and the azimuth look angle of the user spacecraft versus time. The initial antenna offset from the user is 0.15° in this case. There is a 5 s interval of open-loop tracking in which the error angle is constant at about 0.15°, prior to activation of autotrack at $t = 0$. Note that the antenna pulls in and tracks the user spacecraft with a root mean square error of 0.01°. The acquisition time (the time it takes the antenna to pull to within 0.03° of the user) is less than 10 s.

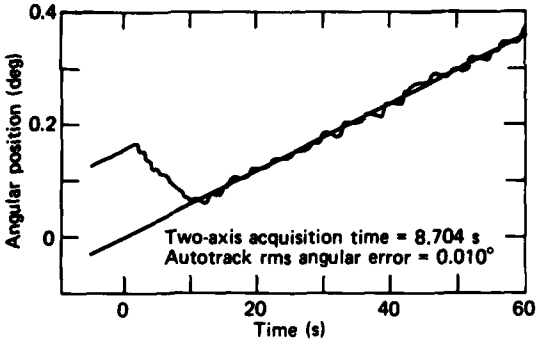

Fig. 3 Antenna boresight and user look angles versus time, azimuth axis.

Figure 4 plots the history of elevation versus azimuth error angle with time as an implicit parameter. In this figure, acquisition occurs during the transition from error angles at −0.15°,0.15° to error angles near 0°,0°. A smooth transition from the starting offsets to within the 0.03° error circle is desirable and is achieved in this example.

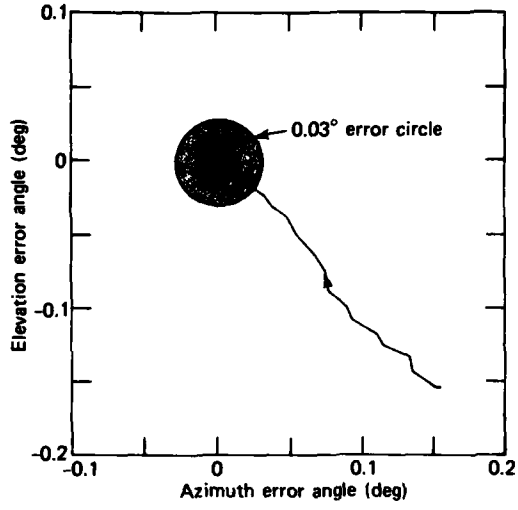

Fig. 4 Error angle history, elevation versus azimuth.

In general, the autotrack system, as simulated, has operated properly under the current system specifications. However, at the lower range of allowable gain the system has problems with slow acquisition or non-acquisition of the user spacecraft.[3] The computer model has been used to derive and evaluate software fixes for these problems.[4]

REFERENCES

[1] S. C. Jones, *TDRS Ku-Band Autotrack Computer Model*, JHU/APL S3C-5-042 (23 Feb 1981).
[2] S. C. Jones, *Computer Simulation of TDRS Ku-Band Autotracking*, JHU/APL S3C-5-044 (25 Feb 1981).
[3] S. C. Jones, *Evaluation of TDRS Ku-Band Autotracking Under New ADE Performance Bounds*, JHU/APL S3C-3-104 (10 Sep 1981).
[4] S. C. Jones, *Reducing the Effect of TDRS Autotrack Low Gain Pull-In Problems by Narrowing the Outer Deadzone and Reducing the YP Threshold*, JHU/APL S3C-3-105 (21 Sep 1981).

This work was supported by NASA/Goddard Space Flight Center.

STRATEGIC SYSTEMS AND TECHNOLOGY

INTRODUCTION

APL's first effort in the area of strategic weapon systems was in 1957 when it supported the U.S. Navy's Special Projects Office as a consultant in the development of the Polaris Fleet Ballistic Missile (FBM) Weapon System. In subsequent years, the main thrust of the Laboratory's work in this area was in developing and assisting in the conduct of an independent evaluation program for the FBM Weapon System that featured a combined technical and operational evaluation that is continuous throughout the life of the weapon system.

During the past year, APL has continued its evaluation of the Navy's operational FBM Weapon Systems (Poseidon, Trident I, and Trident I Backfit) to derive estimates of weapon system performance under operational patrol conditions, identify sources of system inaccuracy and unreliability for corrective action or future improvements, and determine weapon system readiness for operational deployment.

The Laboratory participates in the planning, conduct, and analysis of three major test programs for the U.S. Navy: the *Demonstration* and Shakedown Operation (DASO), the Operational Test, and the Patrol Performance Analysis Programs. The same functions are performed for the United Kingdom's Submarine-Launched Ballistic Missile DASO Program.

An annual report, based largely on the analysis of performance data from the test programs and prepared for each deployed weapon system for the Commanders-in-Chief of Atlantic and Pacific areas, quantifies performance planning factors for the Joint Chiefs of Staff in the targeting and use of the FBM forces. Many other reports provide feedback to the Navy and its contractors on the performance of the weapon systems.

The DASO and Operational Test programs are supported by two additional programs. In the Range Systems Program, APL evaluates the performance of the test range tracking ships and ground stations that record missile-flight telemetry data and provide for flight-test safety. In the LONARS program, APL developed the instrumentation used in DASO testing for the accurate measurement of SSBN position and velocity using loran signals and continues to support LONARS maintenance and improvements.

The Improved Accuracy Program (IAP) was initiated in 1975 to develop the technology required for more accurate SLBM Weapon Systems. The Laboratory's main effort was to investigate weapon system accuracy and develop the capability necessary to predict the accuracy of an improved weapon system over a wide range of untested operational conditions. The validation of accuracy models was a significant part of that effort. APL developed an advanced methodology for estimating error contributors and applied it to the analysis of data from weapon system tests. Major contributions by APL to this program were the development of SATRACK, an instrumentation system utilizing satellites for precise tracking of missiles in flight, and the processing and analysis of tracking data to measure or estimate errors in initial conditions and in the boost-phase guidance system.

A new program, just getting under way, is the Trident II Advanced Development Program. The design goals of the Trident II system are greater missile payload for a given range and a substantial increase in accuracy. The testing and analysis of this highly accurate system poses new challenges for the Laboratory. It will require advanced analysis techniques and instrumentation concepts and will draw heavily on technology developed in the IAP.

In 1969, the Laboratory initiated work on a technical program to investigate current and future technology that could jeopardize the future security of the FBM submarine force. This effort grew into a large program and resulted in the formation of the APL Submarine Technology Division. Developments in ocean science and technology arising from this program are discussed in more detail in the Ocean Science and Technology Section.

The command, control, and communications systems linking the National Command Authority with deployed FBM submarines are vital for the mission of the nation's strategic forces. APL began in the late 1960's to evaluate the efficacy and reliability of communications to FBM submarines. The first effort, the evaluation of the TACAMO airborne link, was later expanded and continues at present to cover other communication links to the deployed FBM submarine fleet.

As part of the Strategic Systems effort at the Laboratory, the SSBN Sonar Evaluation Program evaluates the performance and effectiveness of sonar systems aboard FBM submarines, to determine how well they contribute to the security of the FBM's as a strategic deterrent and to determine how they can better fill that vital role. Advanced recording systems have been developed and installed aboard two SSBN's to record, at very high rates, acoustic and environmental data throughout selected patrols. An advanced signal processing facility at APL processes the patrol sonar data; the processed output is compared with results obtained at sea to identify system and operational deficiencies.

In the mid-1960's, the Laboratory was requested by the U.S. Army to develop and conduct an evaluation program for the Pershing Weapon System in its strategic role in Europe, the program to be modeled as closely as possible after the Polaris program. This is a continuing program today; data are collected and analyzed from test exercises performed on "alert" sites in Europe and from Operational Tests conducted in the United States. Annual reports estimating the weapon system performance planning factors are prepared for the Commander-in-Chief, U.S. Army, Europe.

This introduction attempts to present an overall view of the ongoing work at APL in strategic systems programs. The articles in this section are only a small sampling of recent accomplishments in this area. The work in strategic systems and related programs is a substantial portion of the total Laboratory commitment to defense programs, underlining the importance APL attaches to the advancement of the deterrent capability of the nation's strategic forces.

NAVY STRATEGIC COMMUNICATIONS SIMULATOR

S. F. Czajkowski

The purpose of APL's Strategic Communications Continuing Assessment Program is to provide analytical support to the Navy in assessing the performance of radio communications systems for Navy Strategic Forces during all phases of a nuclear war. In order to provide an analysis tool capable of timely and technically rigorous evaluation of system performance, a computer model — the Navy Strategic Communications Simulator — has been designed and implemented.

BACKGROUND

The United States maintains military forces equipped with nuclear weapons continuously on the alert. The forces are divided into three categories: Intercontinental Ballistic Missiles (ICBM's) deployed in hardened underground silos in the northern midwest, FB-111 and B-52 bomber aircraft on runway alert at various U.S. military airfields, and Submarine-Launched Ballistic Missiles (SLBM's) carried on board nuclear-powered submarines (SSBN's) operating covertly throughout the Atlantic and Pacific Oceans. Typically referred to as the Triad, these forces act as a deterrent to attack on the United States by nuclear-capable foreign countries. Assured communications from the National Command Authority (NCA), i.e., the President and the Secretary of Defense or their successors, to the geographically dispersed weapon platforms is essential for preserving the validity of the Triad's deterrent capability. Moreover, the communications must be able to withstand jamming and/or physical attack by an enemy.

Over the last twelve years, the Laboratory has provided performance assessments for the many communications systems supporting the Navy leg of the Triad — the SLBM's. APL's analysis capabilities in this area have been substantially enhanced over the past year through the development of a computer model to evaluate quantitatively communications systems performance throughout all phases of a nuclear attack on the United States. This model, the Navy Strategic Communications Simulator (NSCS), is being used to assess the performance of both current and planned systems for communications with deployed (submerged) SSBN's.

DISCUSSION

The NSCS simulates the propagation of a highly structured Emergency Action Message (EAM) from the NCA to the SSBN forces through a communications network defined by the user, in this case the United States strategic communications network. The model, written in the PL/1 programming language, employs discrete-event Monte Carlo* techniques to simulate the survival of network nodes (fixed communications facilities, aircraft, ships, satellites, etc.) during a nuclear attack on the system, the reliability of the transmitting and receiving equipment, and the quality and time of acceptance of the EAM. Other factors affecting the ability of the communications network to deliver an EAM that are accounted for in the model include message transmission and reception protocols, message processing (manual error correction and piecing of multiple message copies), jamming effects, and antenna patterns.

The general structure of the computer program is shown in Fig. 1. The required inputs include the network structure, node availabilities (as functions of time), equipment reliability data, communications link quality data (as functions of time), message processing delay times, and the transmission sequences for each transmitting node.

For each run of the program, the user inputs a time relative to the initiation of an enemy attack on the network. That time represents the time of insertion of an EAM into the system by the NCA. On the basis of node survivability and endurance information and equipment reliability data, random numbers are drawn to determine available nodes and failure/repair times for transmitting and receiving equipment. The resulting time-dependent status of the network is called a *network realization*. The EAM is then propagated through the network realization many times, during which the number of messages accepted and the associated acceptance times are recorded for nodes of interest (e.g., SSBN's).

During the simulated flow of an EAM, a list of current and future events is maintained. It comprises message reception and acceptance events for the various nodes of the network, events identifying failure and repair times for all transmitting and receiving equipment, and events representing the physical destruction of friendly and jammer nodes. The events are processed in the order of increasing scheduled time, starting with

*"*Discrete event" means that calculations are performed only at the simulation times when events occur, where the list of possible events includes message reception at a communications facility, the failure or repair of transmitting or receiving equipment, and the physical destruction of a facility. "Monte Carlo" refers to the general technique of repeated simulated trials in which random numbers are chosen from probability distributions to determine the outcome of individual trials.

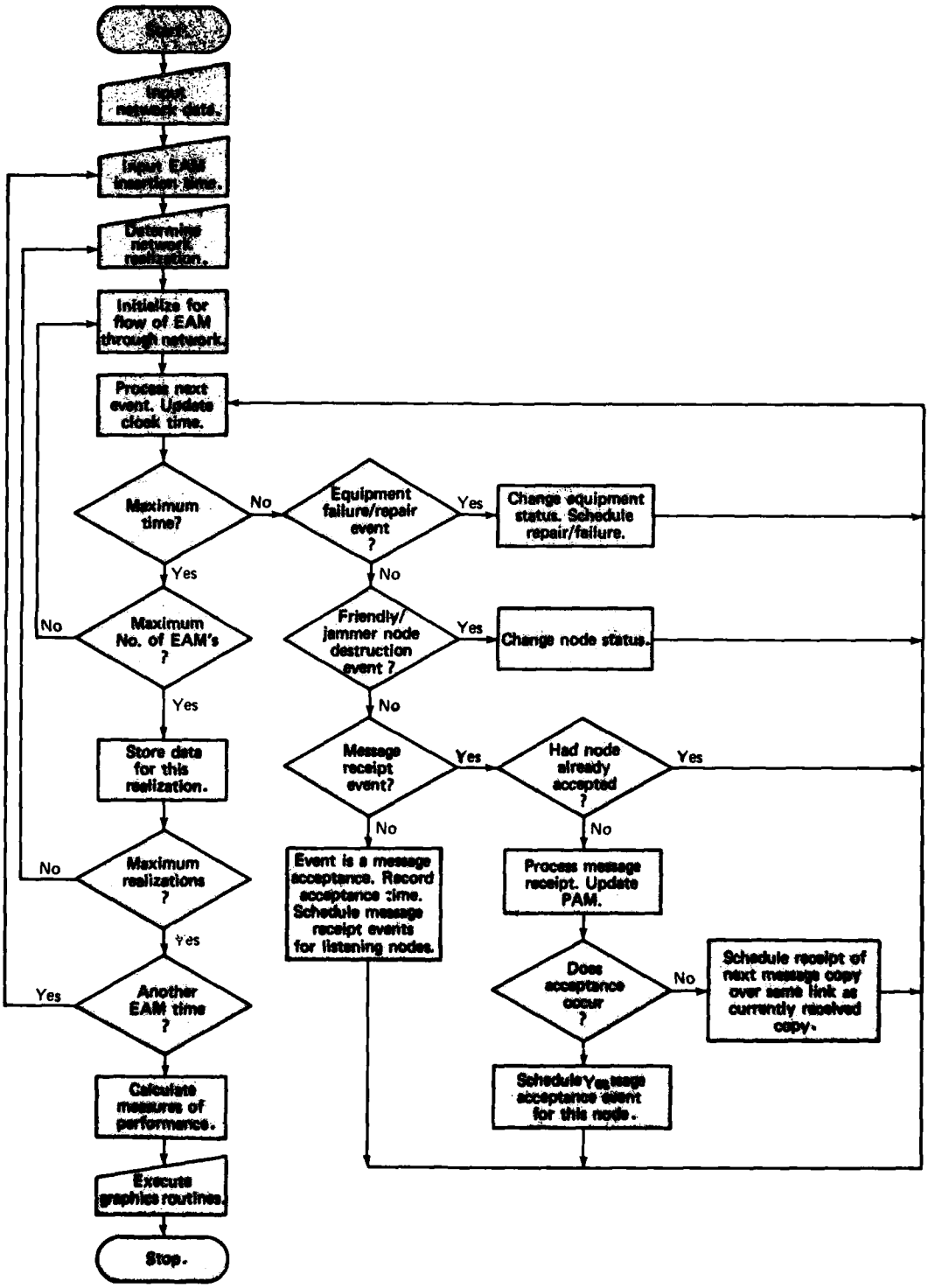

Fig. 1 Flow chart of computer program for the Navy Strategic Communications Simulator.

the event representing the acceptance of the EAM by the source node of the network at the EAM insertion time.

If an equipment failure or repair event is processed, a flag is set to signify that the equipment is unavailable or is available for sending or receiving messages, whichever the case may be. In addition, a new event that represents the next future failure/repair time for this equipment is scheduled. When a node destruction event is processed, a flag is set so that the "destroyed" node is no longer available for message processing or jamming.

When a message reception event is processed, the received message character error rate (CER) is used to update the information at the receiving node, and a check is made to determine if the message is accepted. The chance of acceptance is based on the value of the probability of an acceptable message (PAM) function, which is computed using the CER's of all received messages. The PAM function incorporates the prescribed EAM validity and piecing procedures. If message acceptance does not occur, reception of the next message copy over the same link is scheduled. If acceptance does occur, a message acceptance event for that node is scheduled for the appropriate time (accounting for message processing time). When that acceptance event is processed, the accepting node begins its transmission sequence, and message receptions are scheduled for appropriate times at the listening nodes.

For each transmission link, a random draw is made from the appropriate predicted signal-to-noise ratio (S/N) or signal-to-jamming ratio (S/J) distribution at the time of message transmission to determine an S/N or S/J value for each copy of the trial EAM sent over a given link. Each S/N or S/J value is converted to a CER by accessing the S/N (or S/J) to CER transform corresponding to the mode of transmission on the given link.

Event processing is terminated when a time limit (specified as a model input) is exceeded. A three-dimensional matrix of message acceptance times indexed by EAM insertion time, network realization, and SSBN location number is then transferred to graphics routines, and measures of system performance are calculated and output graphically.

The user has the option of displaying any of eight measures of end-to-end system performance. Four measures (connectivity, coverage, availability, and survivability) are hierarchical in nature and assess the ability of the system to achieve certain specified levels or thresholds of performance within a selected time period. The other four measures (message acceptance probability, message acceptance time, fraction of SSBN operating area accepting the message, and communications commit time) assess the absolute ability of the system to deliver EAM's to the SSBN's; i.e., the measures are not relative to preset thresholds.

Figure 2 is an example of the graphics output. It shows the message acceptance probability for a hypothetical SSBN operating area in the Atlantic Ocean 20 min after the message was released by the NCA. The message acceptance probability at any time after EAM insertion and at any SSBN location is computed as the fraction of trial EAM's received and accepted at the given location by that time.

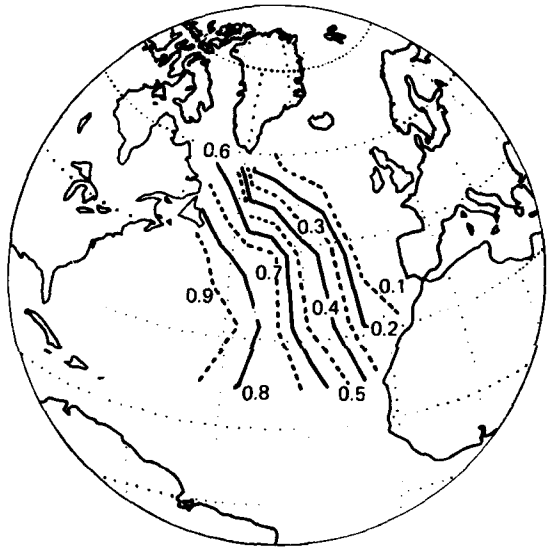

Fig. 2 Example graphics display showing message acceptance probability over an SSBN operating area; EAM insertion time is 15 min; time after EAM insertion is 20 min.

The results for the other measures of performance can be output in tabular form, as statistical distributions plotted graphically, or as geographic charts (e.g., Fig. 2), whichever is appropriate.

REFERENCES

[1] S. F. Czajkowski, *Navy Strategic Communications Simulator Description*, JHU/APL FS-81-031 (Feb 1981).
[2] P. M. Thompson and S. F. Czajkowski, *SCAP Computer Analysis System Specification*, JHU/APL FS-82-050 (Mar 1982).

This work was supported by the Chief of Naval Operations, OP-941D.

ANALYSIS OF MISSILE LAUNCH AND IMPACT LOCATION ACCURACY

T. L. Tomcsik, W. G. Innanen, and C. L. Rowland (APL)
and A. T. Massey and R. W. Morton (Science Applications, Inc.)

An error analysis scheme has been developed to estimate or verify the survey measurement accuracy of bottom-mounted transponder positions at Trident missile launch and Trident and MX missile impact sites in the Pacific. An additional error analysis scheme was developed to estimate or verify the scoring accuracy for reentry body positions at Trident and MX missile impact sites in the Pacific.

BACKGROUND

Trident (U.S. Navy) and MX (U.S. Air Force) missile testing programs in the Pacific Ocean have generated a need for error analyses that calculate how accurately impact location arrays determine reentry vehicle impact points and with what accuracy a launch location array finds the position of a submarine during a launch sequence. The impact location arrays consist of a surface sonobuoy array that is used to locate reentry vehicle impact points and a bottom-mounted transponder (BMT) array that is used as a geodetic reference to locate the sonobuoys. The BMT launch location array provides a precision navigation reference for positioning a submarine.

The classic technique for surveying the geodetic location of the BMT's in the launch and impact areas uses a least-squares approach to minimize the differences between measured and calculated acoustic travel times between the survey ship and the BMT's in order to determine the relative position of each BMT within the array. Subsequently (or simultaneously, depending on the specific computation used), the differences between the survey ship's locations determined from the array and those determined from a geodetic reference (NAVSAT etc.) are minimized, also using least-squares procedures, to offset and rotate the array to the most probable geodetic position.

The Sonobuoy Missile Impact Location System (SMILS) uses similar least-squares techniques to position the sonobuoys relative to the known BMT's in order to determine reentry vehicle impact points from the positioned sonobuoys. Different types of sonobuoys are used in order to identify which interaction is taking place: sonobuoy to BMT to sonobuoy, sonobuoy to sonobuoy, or reentry vehicle impact point to sonobuoy. Figure 1 illustrates the operation of SMILS.

DISCUSSION

The problem was approached in two parts. First, the error analysis called Missile Impact Location System Sensitivity Analysis (MILSSA) was developed to determine the geodetic accuracy of the BMT locations in the impact and launch areas. Second, the error analysis SMILS was developed to determine the accuracy of the reentry vehicle impact points. The primary output of MILSSA (BMT geodetic position error) is an input for SMILS. The error analyses were not combined into one program because of computer limitations.

MILSSA takes relative errors, geodetic errors, and parameters and calculates BMT and survey-ship relative position errors and BMT geodetic position errors. Figure 2 illustrates the logical flow of MILSSA. Essentially, the analysis scheme can be broken down into inputs, calculations, and outputs.

Before specifying error sources, it is important to define the different types of errors. Any error can consist of a bias error and a random error. Bias errors are constant or correlated over a series of measurements or fixes, whereas random errors are independent between fixes and are randomly distributed so that they cancel out with a sufficient number of measurements. All errors addressed in MILSSA and SMILS are evaluated for both bias and random components.

In MILSSA, the relative and geodetic error inputs are derived from the measurement errors inherent in the relative and geodetic surveys used to position the BMT's. In order to determine position errors from those measurement errors, operational parameters associated with the geometry of the array/survey configuration must also be considered. Therefore, three types of relative error sources (relative fixed parameters, relative survey parameters, and relative measurement errors) and three types of geodetic error sources (geodetic fixed parameters, geodetic survey parameters, and geodetic measurement errors) were identified.

The fixed parameters in both cases are associated with the geometry or setup of the particular navigation system used that might affect measurement errors. The survey parameters in both cases are associated with the conduct of the survey and operation of the navigation systems that also might affect the final measurement errors. The measurement errors in both cases are primarily associated with the empirical measurement of

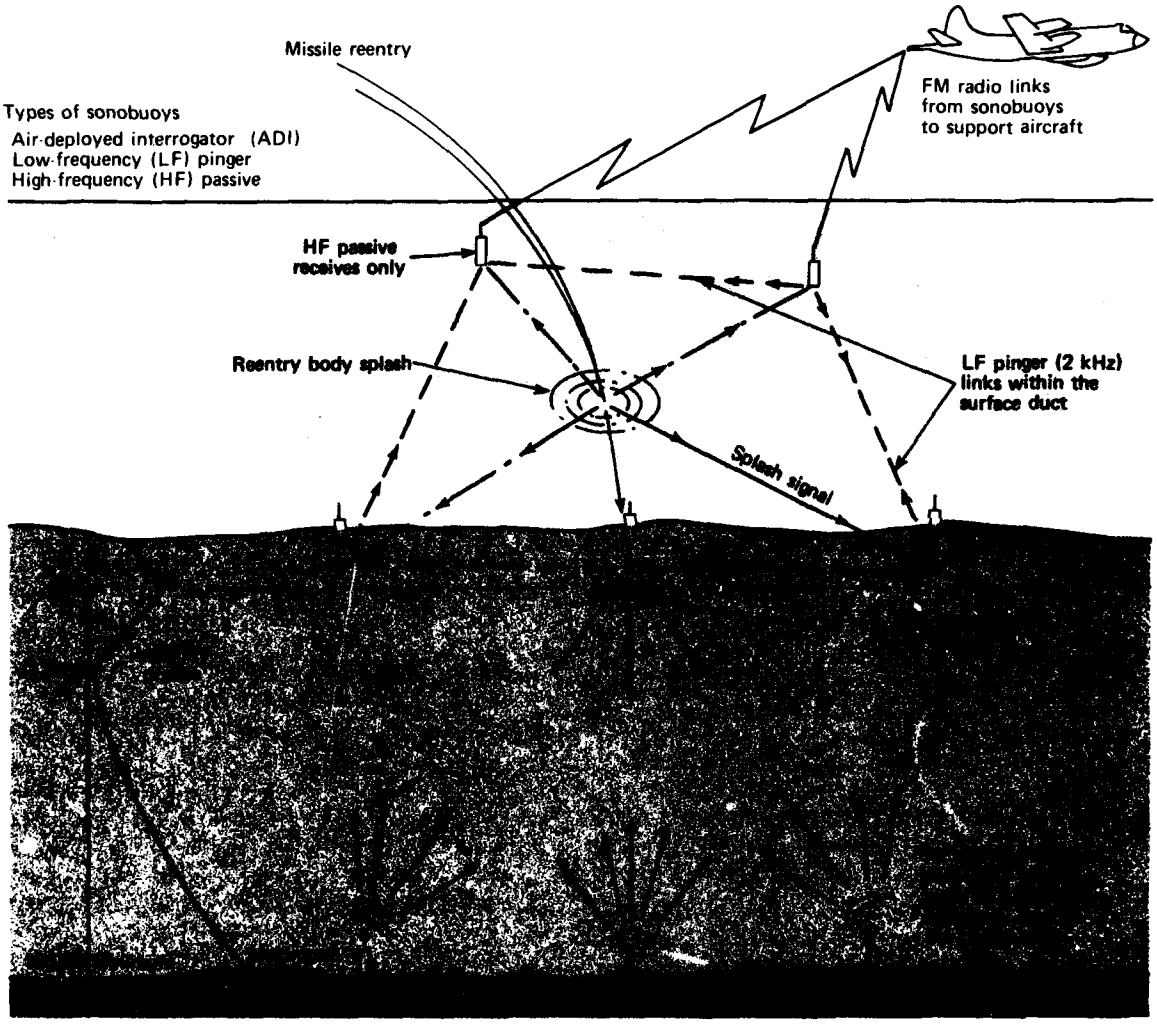

Fig. 1 Sonobuoy Missile Impact Location System.

position and the effect of those empirical measurements on the least-squares analysis procedures. Measurement errors have three major sources:

1. Systematic errors resulting from the inherent errors in the navigation system used,
2. Instrumentation errors resulting from the resolution capabilities of the system, and
3. Computational errors resulting from input and processing of navigation data within the analysis procedure.

In discussing the mathematical basis for the calculations in the MILSSA model, an important factor that must be considered is an awareness that the model is an error analysis, not a survey procedure. Consequently, although the mathematics deals with parameters measured during a survey, it deals, in fact, with errors in those parameters, not the actual measured quantities. This also applies to the SMILS model.

Using Fig. 2 as a guide, it is possible to outline quickly the mathematical steps taken to assess the overall sensitivity of the error in BMT position to a given error source. All parameters and error sources are input to the model according to the relative and geodetic error source classifications discussed above. The relative parameters and error sources are then used to calculate the relative errors in both the BMT and ship positions according to the following least-squares formulation:

$$t = \sum (T_m - T_c)^2 = \text{a minimum} , \qquad (1)$$

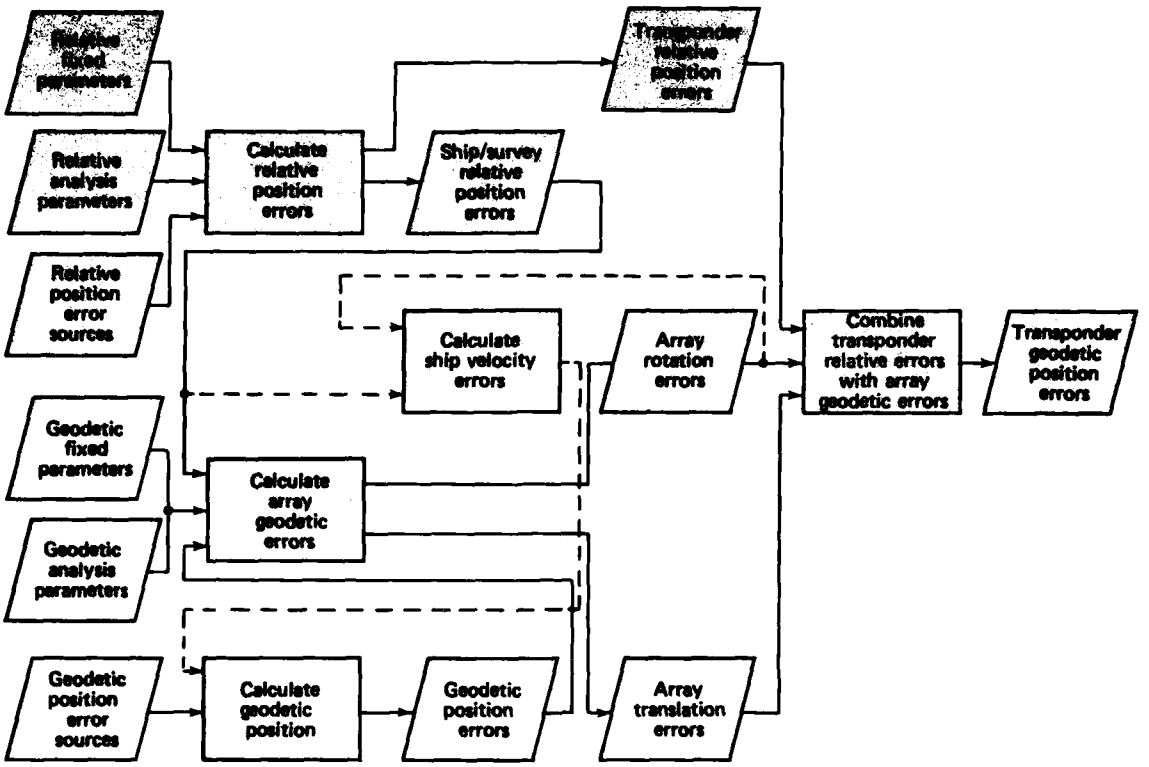

Fig. 2 Schematic of the MILSSA program.

where T_m is measured time delay and T_c is calculated time delay from the best estimate of ship/BMT relative positions. Likewise, the errors in geodetic position are calculated and input along with the relative ship position errors to another least-squares formulation:

$$G = \sum (X_G - X_r)^2 = \text{a minimum} , \qquad (2)$$

where X_G is measured geodetic position and X_r is calculated geodetic position from the best estimate of relative coordinate system translation and orientation. This determines the translation and rotation of the array as required to calculate array geodetic errors.

When NAVSAT provides the geodetic survey ship positions, the geodetic position calculation can be modified by an iterative procedure that decreases the error in X_G through the application of relative ship's velocity corrections resulting from array rotation and translation to NAVSAT errors. It thereby improves the calculation of X_r until convergence occurs, thus defining the geodetic errors in the array location and orientation.

These geodetic errors are then combined with the relative position errors to determine the overall geodetic position error of each BMT as an output. The model also outputs BMT relative position errors, survey ship relative position errors, array rotation geodetic errors, and array translation geodetic errors. MILSSA is used as a sensitivity analysis by varying specific inputs, either errors or parameters, and observing the effect on the outputs.

The SMILS model uses the following error and parameter inputs to calculate random and bias position and sound velocity errors:

1. BMT positions determined by survey;
2. Random and bias geodetic position errors for each BMT, generated by MILSSA;
3. Sonobuoy positions and reentry body splash positions determined at the impact site of interest;
4. Instrumentation and measurement random and bias errors incurred while determining sonobuoy and reentry body splash positions;
5. An appropriate sound velocity profile taken at the site of interest; and
6. The sonobuoy drift velocity.

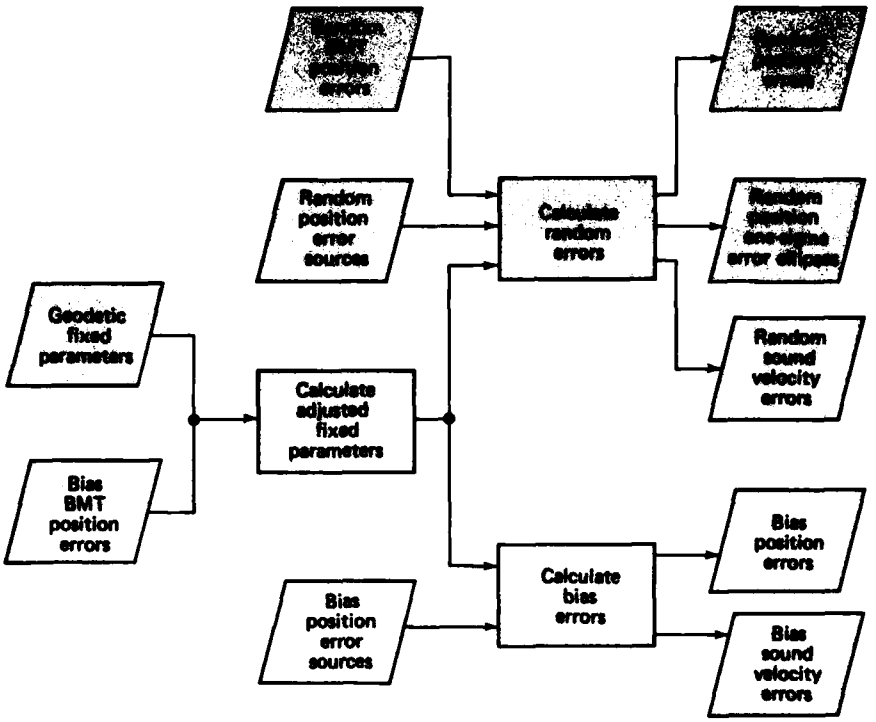

Fig 3 Schematic of the SMILS program.

Figure 3 illustrates the flow of events in SMILS. As in MILSSA, the analysis scheme can be broken down into inputs, calculations, and outputs.

The error and parameter inputs listed above are classified according to the type of response time measurement with which they are associated. There are three types:

1. Sonobuoy to BMT to sonobuoy (three-body interaction),
2. Sonobuoy to sonobuoy (two-body interaction), and
3. Reentry body splash to sonobuoy (two-body interaction).

All the different interactions inherent in the SMILS configuration are represented here. By specifying all the response time measurements possible in a SMILS configuration and all the errors and parameters associated with each response time measurement, one can calculate the random and bias errors in reentry body splash position, sonobuoy position, and sound velocity.

The SMILS model estimates the sound velocities, sonobuoy positions, reentry body splash positions, and BMT positions from the three types of expected response time measurements discussed. This is done by linearizing the differences between the measured and the expected response time about the true sound velocities, true sonobuoy positions, true reentry body splash positions, and true BMT positions. The variance-covariance matrices derived from this linearization by a least-squares estimation give random and bias errors of the sound velocity, sonobuoy position, and reentry body splash position.

The most straightforward results are derived from the variance-covariance matrices by taking the square root of the diagonal elements. In the case of the random error matrix, the root mean square (rms) random errors for sonobuoy and reentry body splash positions and the surface and deep sound velocities were derived. For the bias error matrix, the rms bias errors were derived. The output position errors are in X, Y, Z coordinates.

Since there is considerable interest in the one-sigma error ellipses formed by the random error for reentry body splash and sonobuoy positions, the eigenvalues and eigenvectors for those position errors were determined. For each, the square root of the eigenvalues provided the ellipse semiaxes, and the eigenvectors provided the orientation of the ellipse. SMILS, like MILSSA, is used as a sensitivity analysis by varying spe-

cific inputs, either errors or parameters, and observing the effect on the outputs.

The position errors output by MILSSA and SMILS compared favorably with the position errors provided by the Eastern Space and Missile Center and the Palisades Geophysical Institute for the same launch and impact events. No comparison data are available for the sound velocity errors calculated by the SMILS model. It is believed that the random ones are reasonable but that the bias ones are small. The SMILS model can easily be reconfigured to make sound velocity error an input instead of an unknown.

This work was supported by the Strategic Systems Project Office, SP-25, and the Air Force MX Ballistic Missile Office.

SYSTEM TO MEASURE TRIDENT SUBMARINE HULL VIBRATION

T. M. Rankin, R. L. Konigsberg, and W. F. Kujawa

A vibration survey for the Trident Ship Strategic Weapon System was conducted. An 81-channel vibration measurement system was developed to obtain accurate readings of the low-level hull vibrations in Trident submarines that result from submarine maneuvers such as missile launchings. The data were stored in a digital data acquisition system for future analysis. Hull vibration modes and the vibration of hull-borne equipment will be identified and used to determine the ship's reliability and to improve fleet ballistic missile performance.

BACKGROUND

A Trident Vibration Test (TVT) was performed on USS *Ohio* (SSBN 726) during a Demonstration and Shakedown Operation (DASO). The test included measurements of SSBN vibration levels during at-sea surfaced and submerged maneuvers and during DASO missile launches. The objective of the TVT was to determine the shipboard level and range of vibration that could be encountered in Trident SSBN's and to establish design and test criteria from these data for Trident I and II Missile components. The TVT was also used to verify analytical methods for determining the dynamic characteristics of the launch tube/missile interference.

As program manager, APL provided technical coordination for the design, fabrication, calibration, and installation of the instrumentation, and for conducting the test. Contractors, including Lockheed Missiles and Space Co., Westinghouse Electric Corp., Interstate Electronics Corp., General Electric Ordnance Systems Co., and Draper Laboratory, participated in the definition of data requirements and the performance of data analysis, and supplied various equipments.

APL designed and built the special vibration-measurement instrumentation system (accelerometers and associated signal conditioning) used on SSBN 726 to provide data relating to:

- The definition of the missile environment during normal patrol conditions,
- The transmissibility of vibration along the launcher interface and from decks to equipment during normal patrol conditions and during missile launches,
- The effect of launch-induced vibrations on the initialization of on-board guidance systems, and
- The determination of hull mode shapes and the validity of related modeling.

The design of this instrumentation was based on earlier experience with equipment designed for the Poseidon and Trident backfit submarines. The previous instrumentation for the program consisted of nine accelerometers and provided measurements of vibration only within the missile compartment. The system used for the Trident SSBN consists of 81 transducers distributed throughout the full length of the pressure hull, each cabled to a centrally located signal conditioning unit (SCU). The 81 channels of output, along with other signals related to submarine performance and time synchronizaion, are input to a data processor/recording system provided by Interstate Electronics Corp. The vibration data processor (VDP) formats and outputs the vibration data digitally to magnetic tape for future analysis.

A self-test circuit was designed into the TVT system to ensure proper operation of the distributed sensor systems. Upon receipt of the self-test command from the VDP operator, each of the 81 channels is verified for proper operation; in the event of a channel failure, the operator is alerted that a failure occurred and is supplied with its number. The automatic self-test mode can also be initiated at any time by the operator. The verification and calibration sequence is completed in 30 s, and successful completion is signaled to the operator. The TVT system measurement bandwidth is 100 Hz, with a low frequency accuracy of about ±1%.

DISCUSSION

The TVT instrumentation system (shown in simplified form in Fig. 1) consists of 81 measurement transducers (75 accelerometers and 6 strain gauges), a power conditioner unit, an SCU, a recording unit, the VDP, and an M42 data recording station. This equipment was distributed throughout the submarine. The 75 accelerometers are mounted as triads (see Fig. 2) on submarine hull members, on and in missile tubes, on ship's equipment and cabinets, and within an instrumented Active Inert Missile (AIM).

Six thousand feet of diversified cable, provided by several suppliers, are required to interconnect the equipment. Special kinds of cabling are required in certain areas; cabling for penetrating the two watertight bulkheads is supplied by the Electric Boat Division of General Dynamics Corp.; cabling for penetrating the missile tube is provided by Westinghouse Electric Corp.; cabling for the AIM Missile as well as for the triad mounts is provided by Lockheed Missile and Space Co.; and cabling for connections to the VDP are provided by Interstate Electronics Corp. (IEC). The Vitro Laboratories Division of Automation Industries, Inc., coordinated the interfacing of equipment supplied by the various contractors.

The vibration sensors must measure accurately both the very-low-frequency, low-level hull mode vibration and local higher frequency vibration at equipment locations. To ensure noise-free data over this broad dynamic range and bandwidth (DC to 100 Hz) when operating with such a widely distributed system, special consideration had to be given to the accelerometer measurement channel electronics. A linear-force feedback-type accelerometer that produces a current output proportional to linear accelerations along its sensitive

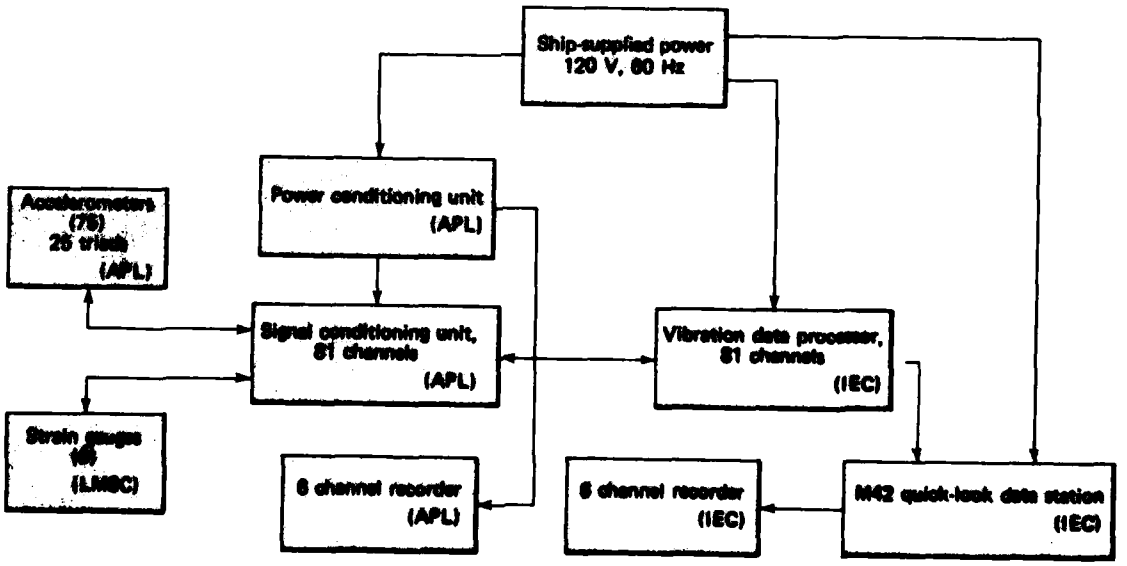

Fig. 1 Block diagram of TVT instrumentation.

axis was selected. By closing the current torque loop via a long cable to the SCU, using a precision resistor, the voltage proportional to the input acceleration could be monitored very accurately and was virtually noise free. This technique eliminated the need for special signal conditioning and transmission electronics at each measurement site. The Sundstrand QA-1100 accelerometer torque loop electronics (self-contained) was modified by the manufacturer to operate with these extremely long cables (about 1100 ft maximum) while still providing a measurement bandwidth from DC to greater than 100 Hz. The accelerometers also provide for current self-test of remote performance and electronic calibration controlled by the SCU. The SCU provides 1 g offset adjustment and range selection of 1 to 0.1 g full scale for each channel. Operating self-test provides a record of the range selected on the APL strip-chart recorder and the VDP data record because the self-test function provides a signal of 100 ms duration equivalent to +0.05 g followed by a signal of 100 ms duration equivalent to −0.05 g.

The triad mount of the accelerometers provides for heading alignment to the ship's centerline (ship's inertial navigation system (SINS) reference) and for accelerometer alignment to the SINS pitch and roll axes. The accelerometers are aligned orthogonally in the laboratory to better than 6 arcmin and are calibrated to better than ±0.5 arcmin. The triads are aligned in heading on the submarine by optical transfer techniques and for pitch and roll by means of a precision clinometer. One triad is mounted on the SINS bedplate to correlate the special TVT data with navigation system data during tests. During installation on USS *Ohio*, it was found convenient to align the SINS bedplate reference unit with the SINS pitch and roll repeaters and then to align all other units to this reference unit electronically.

Six Lockheed strain gauge bridges and associated amplifiers are mounted within the AIM Missile to measure very small changes in load; the gauge is AC coupled to the amplifier to remove the offset at the amplifier induced by static strain. The signal conditioner provides for range selection from 50 to 500 microstrains (a microstrain is one millionth of an inch per inch) full scale for each strain gauge channel. Also, during self-test the signal conditioner control electronics commands a step change in the bridge equivalent to 100 microstrains, producing an output transient signal that is monitored at the SCU and recorded by the IEC equipment on magnetic tape.

Both the APL and the IEC equipments contain six-channel strip-chart recorders that fulfill a quick-look function, ensuring that data are transmitted from the SCU to the VDP. The digital data recorded at the VDP can be played back through the IEC strip-chart recorder for quality evaluation.

The complete self-test operation is as follows. The 75 accelerometers are subject to a sequential +0.05 and −0.05 g equivalent acceleration for 100 ms duration each, and the response of each accelerometer is

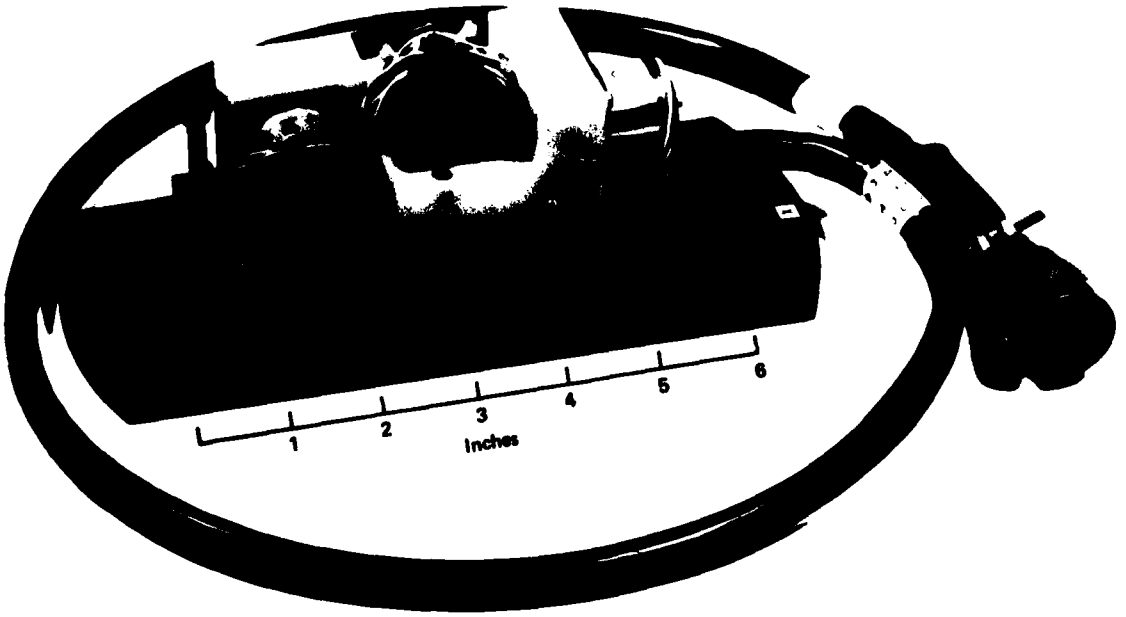

Fig. 2 Typical accelerometer triad with cover removed to show the heading reference scribe lines in the baseplate, the dual sets of jack screws, and a flexure for independent roll and pitch alignment adjustment.

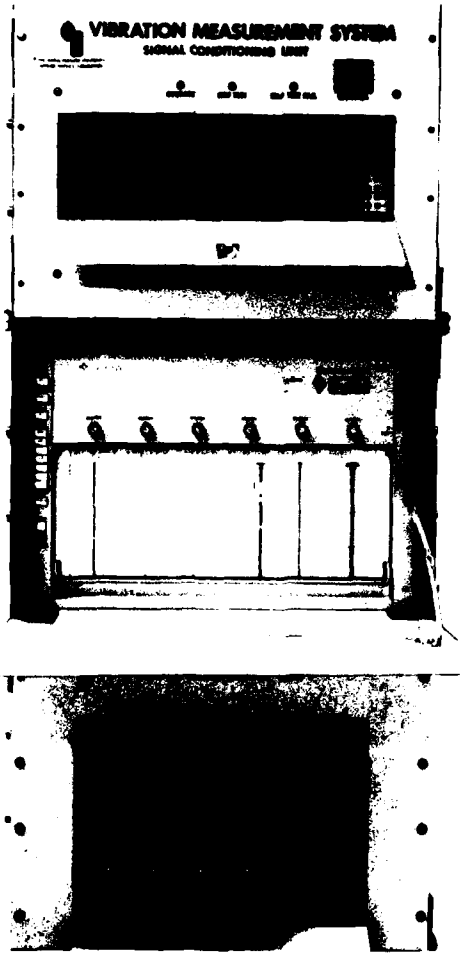

Fig. 3 The TVT system. The SCU, recorder, and power conditioner are stacked using standard IEC submarine enclosures and fasteners. (The width of the units must be less than 25 in.)

verified. Then the six strain gauges are self-tested by being subjected to a +100 microstrain equivalent step change at the bridge for 5.5 s. The entire test is completed approximately 30 s following its initiation at the front panel of the SCU or remotely at the VDP. If an accelerometer self-test is not verified, the self-test stops at the failed channel and that channel is indicated on a display on the SCU front panel. At that time, the cause may be investigated or the remaining self-tests may be completed by resuming self-test via a RESTART pushbutton on the SCU.

The VDP built by IEC provides the 81 channel third-order Butterworth anti-aliasing filters, the multiplexing, and the 8-bit analog-to-digital conversion for input to the M42 data handling and recording system.

The APL equipment (Fig. 3) was installed during the first Trident DASO in early 1982. All test runs were completed successfully. Quick-look data taken from strip-chart playback of the digital vibration data tapes have been evaluated. The evaluation indicates that all instrumentation functioned properly with the exception of one accelerometer triad, which failed due to contamination in the connector during a 5-min run. The system's noise levels were very low compared to the signal levels that were measured.

The data recorded during the test are now being analyzed by several contractors as well as APL. Final test results are expected in late 1982.

ACKNOWLEDGMENTS

The authors would like to acknowledge the special contributions of E. B. Cope for overall fabrication and testing and F. Jurgens for the mechanical design and fabrication of the triads and the submarine mounting interfaces.

This work was supported by the Strategic Systems Projects Office.

OCEAN SCIENCE AND TECHNOLOGY

INTRODUCTION

> "It is particularly important that submarines have become the main arm of the forces of modern navies."
>
> Sergei G. Gorshkov

The impact of Admiral Gorshkov's incisive observation is recognized worldwide. Advances in technology, sometimes revolutionary and frequently motivated by the lessons of two World Wars, allow modern navies to assign submarines central roles in both strategic and tactical mission areas. To fulfill these missions, it is axiomatic that submarines must be able to operate largely undetected by their adversaries.

For a number of years, the Laboratory has been engaged in efforts aimed at developing a more complete understanding of those elements of technology and ocean science related to submarine detection. In the early years of this effort, the focus quite naturally was on developing better measures of the performance of currently deployed Navy anti-submarine-warfare systems. However, as the effort matured, the scope was broadened to include other technology areas that appeared to offer potential in submarine detection. The breadth of the subject areas under investigation has been matched by the range of techniques applied, running the gamut from purely theoretical analyses to full-scale ocean experiments, and including laboratory experiments, computer simulations, and large-scale data-processing methods.

Analysis, simulation, and laboratory research are extremely useful, but many phenomena of interest must be studied at sea. Accordingly, APL has developed the ability to conduct large-scale scientific studies in the open ocean. Through its ocean exercise activities, APL has acquired unique capabilities in the development and application of oceanographic instrumentation as well as in the analysis of data derived from it. Central to APL's effort is the development of sensing and data-processing systems to detect and characterize ocean-generated signals from subsurface, airborne, and satellite platforms.

An understanding of the physics of the ocean environment is essential for APL to perform its mission in support of the Fleet. This area of physics includes the propagation of electromagnetic and acoustic radiation; absorption and scattering both within and at the surface of the ocean; hydrodynamic phenomena such as surface waves, internal waves, and currents; and the effects of such physical variables as water temperature, pressure, salinity, and density. The pursuit and application of the requisite knowledge and understanding in this physical field are the fundamental objectives of the Laboratory's work in ocean science and technology.

AN OCEANOGRAPHIC MISSION FOR GEOSAT

B. E. Raff and J. J. Ousborne

The ability of a satellite altimeter system to provide oceanographic data depends in part on the satellite orbit parameters. The optimal oceanographic orbits for detecting and mapping mesoscale features have been identified for the GEOSAT satellite. Their compatability with the primary geodesy mission has been examined.

BACKGROUND

GEOSAT is a geodesy satellite that will carry a high-resolution altimeter system; it is scheduled for launch in the spring of 1984. The basic principle of satellite geodesy is to use the satellite as a stable platform from which vertical measurements to the ocean surface are made (Fig. 1). When the altimeter data are merged with accurate orbital information, undulations in the mean sea level caused mainly by the geoid are revealed.

In addition to being a sensor for measuring the geoid, the GEOSAT altimeter is, unavoidably, an environmental sensor. The sea surface topography contains fluctuations caused by the mesoscale eddy field, tides, circulations, storms, barometric pressure systems, and surface wave systems. The global surveillance of mesoscale eddies is a goal that is attainable only through remote sensing. The eddies are most readily delineated by changes in vertical stratification that are manifested at the ocean surface as depressions and elevations. An altimeter system such as GEOSAT could provide data for the surveillance of the mesoscale eddy field. The compatability of such a mission with the primary one of geodesy is the question that was investigated.

The detectability of mesoscale eddies is a strong function of the temporal and spatial sampling scheme determined by the satellite orbit parameters. The fundamental parameters of the GEOSAT orbit are given below:

Period	6045 ± 47 s
Inclination	108°
Eccentricity	0.0015

The orbit is basically an ellipse defined by the orbit period and eccentricity. The angle between the plane of the ellipse and the equatorial plane is called the inclination angle. For GEOSAT, the inclination angle and eccentricity are fixed by the geodesy mission. The orbit period remains a free parameter within a particular interval

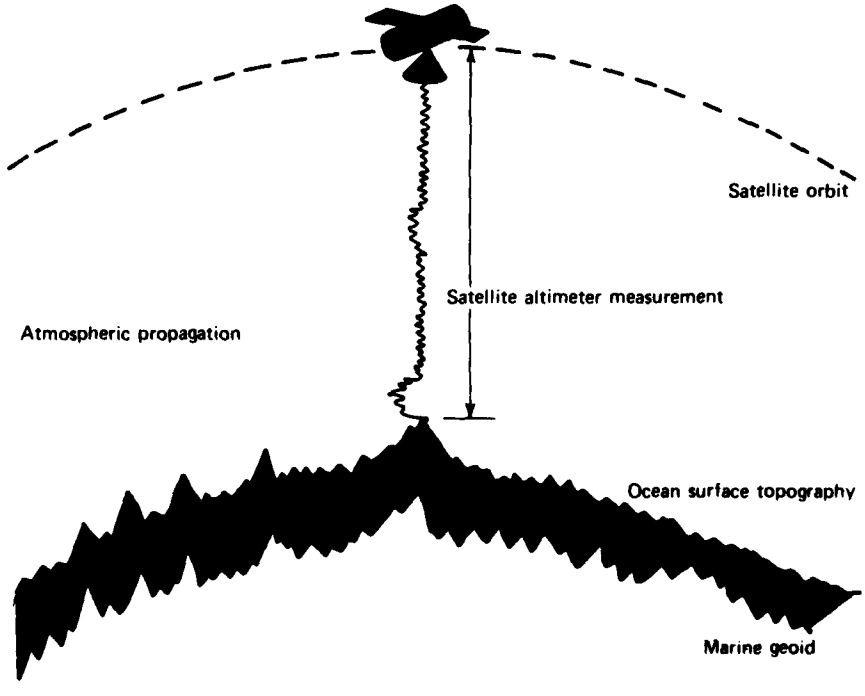

Fig. 1 The altimeter system.

and has a strong influence on eddy detectability. A figure of merit was developed to provide a reference for selecting optimal oceanographic orbit periods.

DISCUSSION

Consider the problem of detecting an eddy when its parameters (amplitude, radius, speed, and location) are unknown. For this problem, one in which a reasonable *a priori* density function for the signal parameters can be assumed, a generalized likelihood detector can be formulated. Such a detection algorithm was implemented; partial results are shown in Fig. 2. The calculations represented by this figure include various statistical models of eddies and noise from both geophysical processes and system sources. There are two major implications. First, the mesoscale eddy signature embedded in a noise background must be sampled four to six times to achieve reasonable detection performance. Second, the ground-trace crossings must be accumulated within a specified time interval (the sampling time). If the sampling time becomes excessive, the eddy will have moved far enough to degrade the processor's detection performance. Figure 2 suggests that 20 to 30 days is a maximum eddy sampling time. The time required to accumulate a global data set is longer, perhaps 60 days.

As Fig. 2 demonstrates, eddy detectability is a function of the number of samples and the sampling time. More frequent eddy crossings provide better detection performance. A maximum level of detectability results from a particular sampling frequency, which is a parameter in the figure of merit. The figure of merit is the probability, expected over an eddy population, that a candidate orbit will provide a certain detection performance. An optimal orbit provides the highest figure of merit and the greatest probability of achieving a performance goal. Symmetries in orbital mechanics result in several orbits with a high figure of merit. As a result, there are several period bands or zones that are optimal for mesoscale eddy detection.

A search for optimal orbits was conducted over the domain of allowed GEOSAT periods. Figure 3 illustrates the calculations. The figure of merit is shown for two sampling frequencies. As the sampling frequency increases, only three narrow bands provide a high figure of merit within the domain of interest. Those bands represent the optimal zones for a secondary GEOSAT mission. The optimal zones correspond to orbits that generate a sequence of ground tracks that evolve progressively in either an eastward or a westward direction. Figure 4 shows how the ground-trace pattern evolves for one of those orbits.

Central to this investigation is the degree to which there is compatability between optimal oceanographic orbit periods and orbit periods involved in the primary geodesy mission. In the latter, the objective is to accumulate a ground-trace pattern with 10-nmi equa-

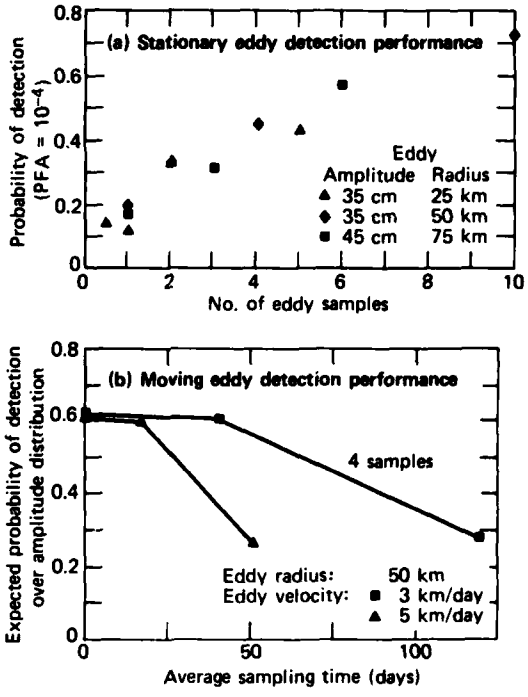

Fig. 2 Detection performance predictions.

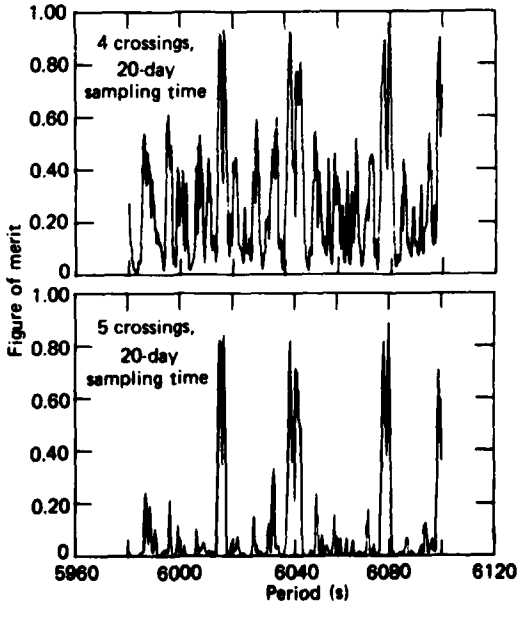

Fig. 3 Figure of merit versus orbit period (50° latitude).

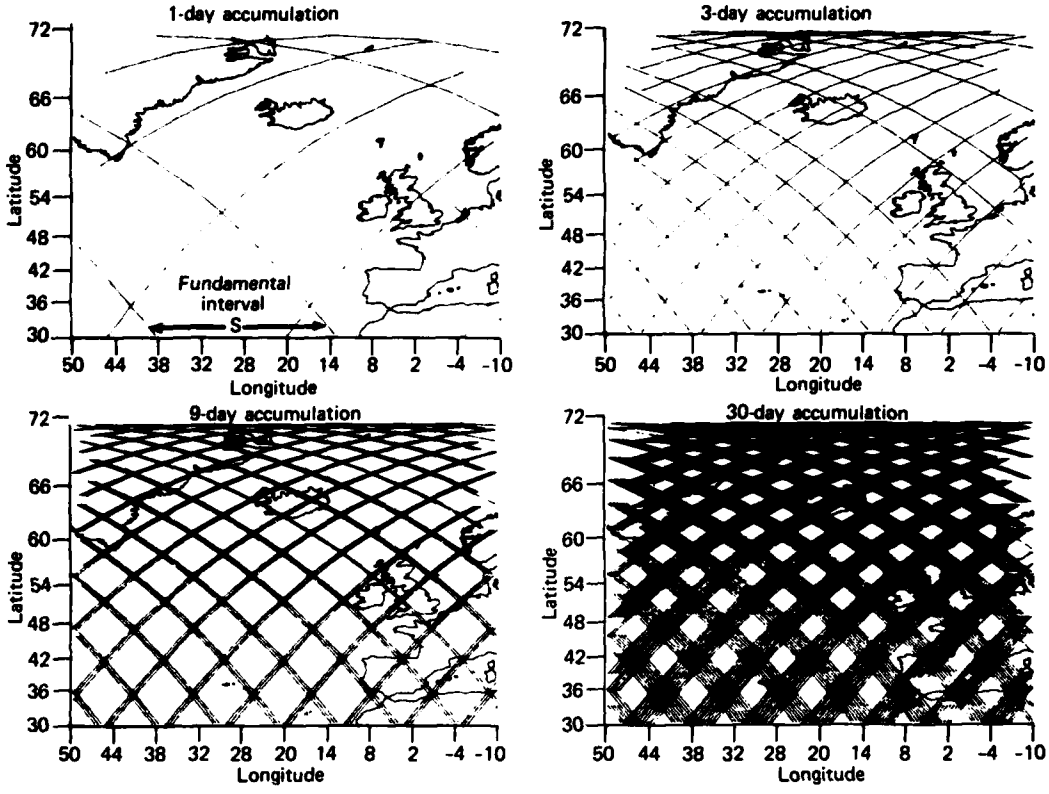

Fig. 4 Ground-trace pattern accumulated over various intervals.

torial separations in a six-month sampling time. Figure 5 shows that many orbit periods fulfill the coverage requirements of the geodesy mission. Many that meet the geodesy objective are not suitable for mesoscale eddy detection. Nevertheless, some oceanographic orbit periods do correspond closely to orbit periods that also provide optimal coverage for the geodesy mission.

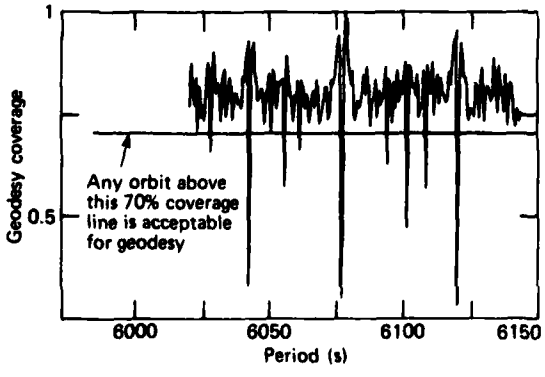

Fig. 5 Geodesy coverage versus orbit period.

There are two other possible conflicts between an oceanographic mission and a geodesy mission. First, an initial maneuver would be required to position the spacecraft in an oceanographic orbit. The maneuver would employ the spacecraft cold-gas propulsion system and partially deplete the cold-gas supply. However, it is estimated that the required cold-gas expenditure would easily be accommodated by the spacecraft's capacity. Second, drag eventually will move the spacecraft from the desired oceanographic period, and a repositioning maneuver would be required. Such a maneuver would interrupt the geodesy mission for perhaps two weeks. It is adjudged that the frequency of the interruptions, approximately every six months, would be tolerable.

It was concluded from the investigation that the operational requirements of a secondary oceanographic mission could be satisfied acceptably within the scope of the GEOSAT mission.

This work was supported by the Department of the Navy.

THE GENERATION OF RAY-LIKE PICTURES BY FULL-WAVE METHODS

R. F. Henrick and H. S. Burkom

Ray pictures have been used extensively as an interpretive aid in visualizing and understanding wave propagation, although important effects arising from the diffraction of wave energy are neglected in this form of presentation. However, the application of contouring algorithms together with a full-wave theoretical treatment not only yields useful ray-like pictures that illustrate wave propagation but does so with the greater accuracy inherent in those methods.

BACKGROUND

Wave propagation is a commonly studied topic, particularly in areas concerned with electromagnetic radiation or acoustic propagation. The complex refraction of wave energy is evidenced by the sporadic reception of distant radio stations under certain atmospheric conditions and the recording of whale and dolphin noises across ocean basins. The bending of wave propagation paths has been long known and is utilized in the manufacture of eyeglasses and cameras. Using the concept of rays (lines perpendicular to propagating wavefronts) to indicate the direction of wave propagation permits a better understanding of how refracted energy propagates. One can, for example, predict the focusing properties of a lens or predict radio propagation in the atmosphere or acoustic propagation through the ocean.

By assuming that a wave remains intact so that the perpendicular ray is clearly defined, ray theory neglects diffractive effects typified by the distortion of wavefronts or the leakage of energy from locally intense focusing points. These effects can be very significant in the environments that are often encountered in electromagnetic or acoustic propagation. More complex calculational techniques include these effects and can give very accurate quantitative values of intensity levels. Those methods do not propagate waves individually, as the ray method does; instead, they solve at each point for the intensity levels arising from the sum of all waves intersecting the point. Therefore, one cannot visualize how each wave reached that point. However, because high intensity levels may be expected along each wave path, contouring of the intensity levels (i.e., drawing lines of constant intensity or propagation loss) should indicate how energy propagates. Such images have appeared previously.[1] The application of a sophisticated contouring routine developed previously at APL[2] along with interactive computer graphics provides significant new insight into how the energy propagates.

DISCUSSION

Wave propagation is of primary importance in the propagation of sound in the ocean. Light and radio waves are severely attenuated in seawater, and significant work has been conducted on using sound waves to remotely sense the interior features of the ocean, to detect submarines, and to communicate underwater. The success of these endeavors is due in great part to the presence of naturally occurring waveguides, known as sound channels, in the ocean. The sound channels, which arise from vertical density and temperature stratifications in the ocean, cause the speed at which sound propagates to vary with depth.

A typical vertical sound-speed profile taken in the deep ocean at northern latitudes is shown in Fig. 1a. The sound speed initially increases in a near-surface mixed layer, then decreases as the water cools in the ocean's thermocline, and finally increases with increasing pressure in the deep ocean where the water is uniformly cold. The associated ray trace in Fig. 1b indicates that two sound channels are present. Some rays (representing the direction of acoustic wave propagation) are trapped in a surface sound channel, while others cycle deep into the ocean and return every 30 miles or so from the deep sound channel. The surface acoustic duct provides continuous reception for a shallow receiver. The deep energy returning periodically in what are known as convergence zones provides intermittent reception for deep receivers. Shadow zones are areas where no rays are present; they represent large areas where the source would not be perceived. This ray picture is independent of acoustic frequency.

Such diagrams provide a useful but qualitative representation of the intensity of the wave field as a function of range and depth. To provide quantitative intensity levels using ray theory, the intensity of the wavefront corresponding to each ray intersecting a point must be computed, the relative phases of each wavefront determined, and all wavefronts added coherently. Only when this process is carried out for many points (a computationally expensive task) can the audibility of the source really be determined.

Nonray methods typically solve for intensity levels directly at all points in depth and range, but they lack the simple, clear imagery afforded by ray pictures. One technique, the parabolic equation (PE) method, is often used in underwater acoustics and radar propagation studies. Using an approximation to the wave equation, PE permits an efficient numerical solution that

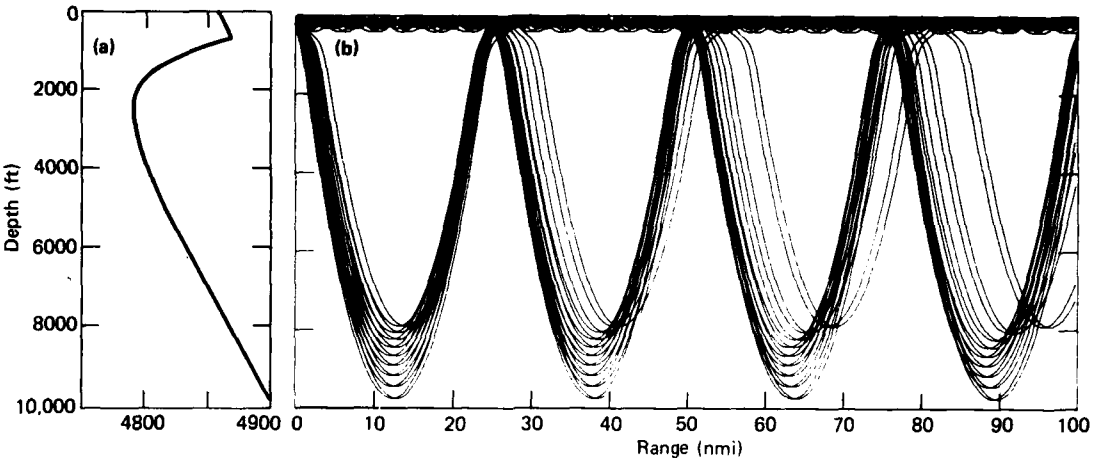

Fig. 1 (a) Typical sound speed profile taken in the Norwegian Sea. (b) Corresponding ray trace for a 65-ft-deep source.

includes diffractive effects ignored in ray theory. If the output of PE is contoured, areas of different intensity or transmission loss may be identified. In particular, by restricting the contours to transmission loss levels within the tolerance of a receiver, the audibility of the source by that receiver can be determined.

The application of the contouring routine developed at APL[2] yields ray-like images that provide both direction of propagation and intensity levels. Figure 2 illustrates a PE contour for the same geometry as Fig. 1 but at a frequency (60 Hz) where diffractive effects are important. Here, the maximum transmission-loss contour is at the 95 dB level; contours are drawn every 5 dB. The pattern is the same type as in Fig. 1, but there are notable differences. The surface duct energy is much weaker than that predicted by Fig. 1. Theory[3] indicates that diffraction makes this duct leaky, so that the energy is not trapped strongly. The contour edges are scalloped, again distinct from a smooth ray image. Areas also exist where rays are present but energy levels are low, particularly at long ranges. Positions where a source is audible are obvious from Fig. 2; Fig. 1 is less clear and definitely not as quantitative.

The utility of a contouring routine is increased when it is coupled with interactive graphics. A scientist can model different source levels or receiver capabilities

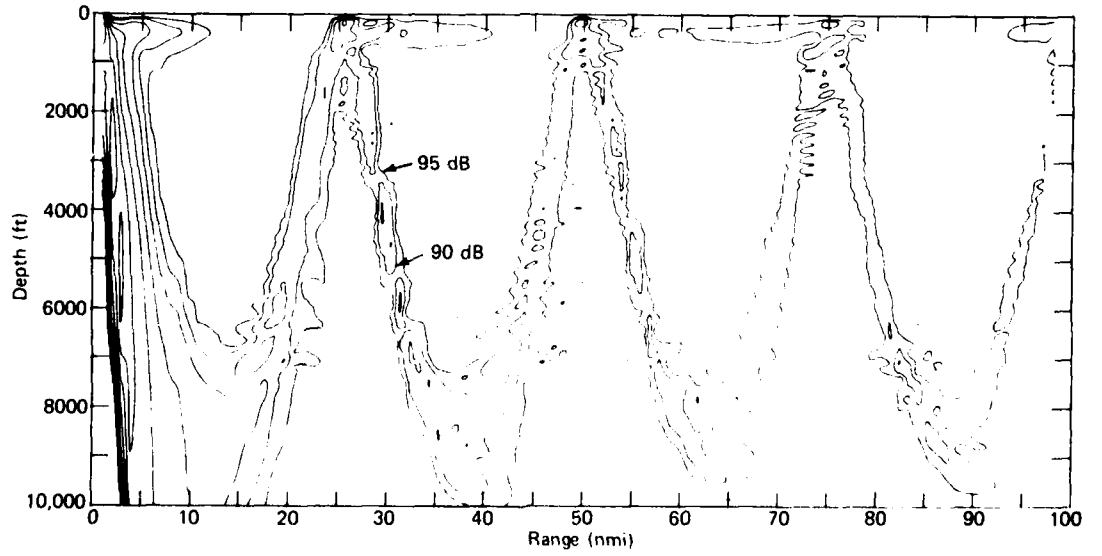

Fig. 2 Contour of PE transmission loss for same geometry as Fig. 1. Maximum contour is 95 dB; contour interval is 5 dB.

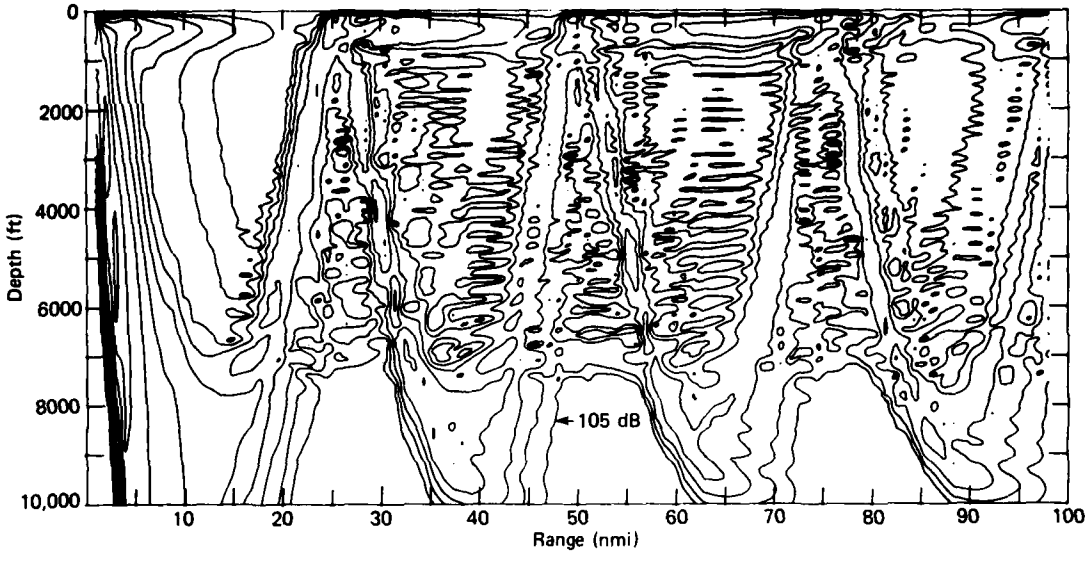

Fig. 3 Transmission-loss contour for same case as Fig. 2, except that the maximum contour level is now 105 dB.

by varying the contour level. Contours may be labeled or colored to indicate their levels. Zoom options can be used to study areas of interest, all within minutes on a single computer terminal. Figure 3 shows the effect of varying the contour level. A maximum contour of 105 dB transmission loss is chosen, perhaps corresponding to a sensitive receiver. Much of the area predicted by Fig. 1 to be in a shadow zone is now seen to be filled in. The gains achieved by deploying the improved receiver (Fig. 3) over the capability implied in Fig. 2 are now immediately obvious.

The contouring algorithm implemented here is not generally specific to PE simulations or to underwater acoustic-propagation simulations. Potential applications include other areas of interest to APL, such as radar ducting. By means of the algorithms, the researcher can understand how the energy propagates and can obtain acurate numerical results.

REFERENCES

[1] F. D. Tappert, "The Parabolic Approximation Method," *Lecture Notes in Physics 70: Wave Propagation and Underwater Acoustics*, Springer-Verlag, New York, pp. 224-285 (1977).
[2] L. E. Klein and N. Rubinstein, *CONPLT Calcomp Contour Plotting Subroutine*, JHU/APL FIC(2)-75 U-29 (1975).
[3] F. M. Labianca, "Normal modes, virtual modes, and alternative representations in the theory of surface duct propagation," *J. Acoust. Soc. Am.* **53**, 1137-1147 (1973).

This work was supported by the Department of the Navy.

HEATED ANEMOMETRY FOR OCEAN MEASUREMENTS

R. E. Dingwell, F. B. Weiskopf, R. W. Spangler, and W. I. Sternberger

The measurement of microscale velocity fluctuations in the ocean requires a transducer with high-frequency response and good resolution — requirements that usually lead to a fragile instrument. The need for a sensor to make such measurements over long periods of time has led the Ocean Data Acquisition Program (ODAP) to develop two systems, each using the principles of heated anemometry.

BACKGROUND

Hot-wire and hot-film anemometry have long been used for the laboratory investigation of fluid turbulence. Such anemometer systems typically use a small probe with a metal wire or film resistor. The measurement transducer is maintained at a constant, higher-than-ambient temperature by means of an instrumentation bridge with a high-gain feedback amplifier. More recently, the development of thermistors with short thermal time constants has made practical their use as transducers in thermal anemometry.

ODAP has followed two directions in developing instrumentation for the measurement of ocean turbulence. An effort was undertaken to modify standard laboratory hot-film probes to ensure their ruggedness in the ocean without seriously degrading their known performance characteristics. Another effort addressed the development of a velocity measuring instrument using a field-proven thermistor probe.

DISCUSSION

Hot-Film Probe Development

Hot-film probes consist of a thin-metal sensing element with a resistance of 5 to 20 Ω, deposited on a substrate with high electrical and thermal insulating qualities (see Fig. 1). The probe coating is an insulating layer that prevents shorting to the fluid but is very thin to allow good heat transfer. The coating is usually silicon dioxide (SiO_2). There are several choices of probe geometry; however, the conical geometry with its insensitivity to small variations in angle of attack and favorable hydrodynamic characteristics was chosen for this application. The ODAP hot-film-probe development effort was devoted to modifying this basic configuration

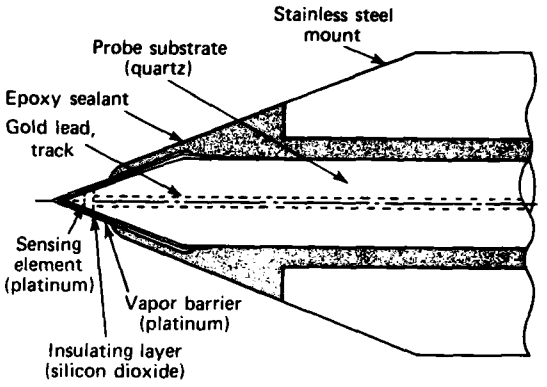

Fig. 1 Tip of thin-film probe.

in order to improve mean lifetime and also to develop a suitable mount for the probes.

To establish baseline standards for mean lifetime of the probes, standard commercial probes (manufactured by TSI and DISA) were tested to failure. They had lifetimes ranging from 10 to 100 hours, consistent with estimates by others using hot-film probes in laboratory environments. All other hot-film probes were lifetime tested in the same manner as the standard commercial probes.

TSI, one of the two leading probe manufacturers, recommended a design modification to make their standard commercial probes more rugged. The modification was to deposit a platinum vapor barrier over the SiO_2. It was postulated by TSI that seawater attacks the quartz insulating layer of the probes, particularly at pinholes, and the vapor barrier would seal off any pinholes in the quartz. Platinum was chosen because it is inert in seawater.

ODAP life tested several of the modified probes manufactured by TSI over the course of the development project. The first two lasted for 625 and 950 hours. The dramatic improvement in lifetime is attributed, in part, to the platinum vapor barrier, which was 300 to 900 nm thick. The other contribution is the lower overheat (probe operating temperature minus ambient temperature) at which the ruggedized probes were tested compared to the recommended operating temperature (67°C).

Two modified probes were used to measure velocity fluctuations in the ocean. They failed when the insulating layer broke away from the substrate. The

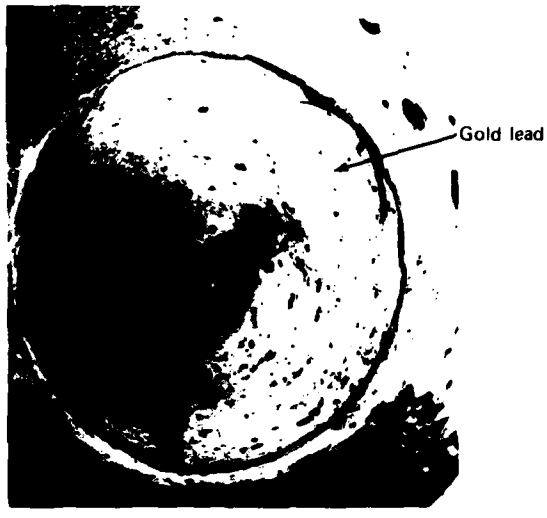

(a) 50 X magnification

(b) 200 X magnification

Fig. 2 Failed TSI modified probe; blown-out patch reveals gold lead. The area of gold indicated in (a) is enlarged in (b).

separation occurred directly over the gold lead that extends aft from the sensing element (see Fig. 2). This area of the probe is particularly susceptible to this type of failure because of the poor bond between quartz and gold. To reduce the probability of this failure mode, the sealant was brought further forward toward the tip. The sealant encapsulates the probe and fixes the substrate in the stainless steel housing.

The quality of the platinum vapor barrier, particularly its adhesion to the insulating layer, was critical to probe lifetime. The second design modification was aimed at improving the adhesion of the materials. APL procured from TSI some unmounted substrates with sensing element and insulating layer applied but without the platinum vapor barrier. The deposition of the platinum vapor barrier was preceded by the deposition of a very thin layer of chromium to act as a wetting agent.

One probe of this design (S/N 9134 of Fig. 3) exhibited excellent lifetime, it survived 1200 hours exposed to seawater (of this time, 243 hours were powered) plus further time under simulated conditions. Eventually the probe failed at the probe/sealant interface.

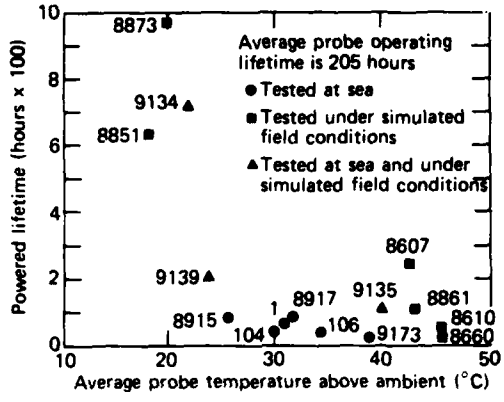

Fig. 3 Probe lifetime versus average probe temperature above ambient.

The most recent modification to the modified design is aimed at corrosion and leakage failures. A simpler mount was designed and a new sealant selected.

Our experience and discussions with other experimenters suggest a strong correlation between operating temperature and probe lifetime. The correlation is shown in Fig. 3, which is a plot of number of hours of powered lifetime versus average temperature above ambient for all the probes that were lifetime tested. Operating temperatures ranged from 67° (recommended by TSI) to 40°C.

Fifteen conical thin-film probes with platinum vapor barriers have been tested to failure under both simulated and actual at-sea conditions. Parameters that were varied include methods for establishing the vapor barrier, mount designs, and asssembly techniques. Parameters that were not controlled but may be of importance include sensing element definition and insulator quality. Overall, these designs offer better lifetimes than those of standard commercial versions and thus are more appropriate for use in the ocean. However, a unit for long-term deployment remains a goal.

Heated Thermistor Development

In many instances, a thermistor transducer is an acceptable alternative to a thin-film transducer. By virtue of their construction, thermistors are mechanically more rugged and are well insulated from conducting fluids. Unfortunately, the frequency response of a thermistor, even when heated, does not approach that of a thin film.

The ODAP versions of heated thermistor anemometers use a novel implementation of the constant current and constant temperature operating modes. Figure 4 is a functional diagram of the ODAP implementation of the drive and sense electronics. The major distinguishing features are a two-arm (versus four-arm) sensor bridge and a differential bridge drive.

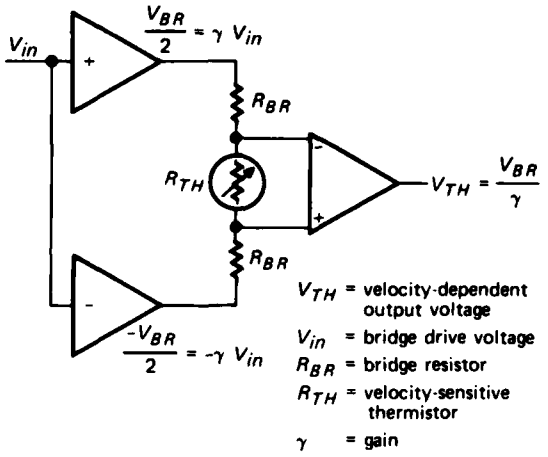

Fig. 4 Bridge circuitry of thermistor anemometer.

Constant current operation is straightforward: V_{TH} versus fluid speed is measured for a constant V_{BR}. Constant temperature operation requires the incorporation of a feedback loop. Specifically, the internally heated thermistor must maintain a constant operating temperature, which further implies that R_{TH} must remain constant. When V_{TH} is fed back to the V_{BR} input, the relationship $R_{TH} = 2\,R_{BR}$ holds for all conditions. The operating temperature is determined by selecting appropriate R_{BR} values and is defined by the thermistor's resistance-temperature curve.

It is well recognized that thermal anemometers are sensitive to changes in the ambient fluid temperature as well as fluid speed.[1,2] Lueck and Osborne have observed that the relationship

$$\frac{T-\theta}{Q} = f(v^{-1/2}) \qquad (1)$$

holds for thermistor beads, where T is the internal temperature of the thermistor, θ is the ambient fluid temperature, Q is the power dissipation in the thermistor, and v is the fluid speed. It is desirable to eliminate the effects of changes in θ (temperature compensate), thereby reducing Eq. 1 to

$$Q = f(v^{1/2}) \qquad (2)$$

for constant-temperature operation.

By including the circuit in Fig. 5 in the constant-temperature feedback loop, one generates a constant-overheat operating mode. In such a mode, the feedback voltage is modified in response to changes in the ambient temperature. The effect is to maintain $T - \theta$ = constant. Values of the gain-determining components for the Fig. 5 circuit are a function of the nominal resistance of the overheated thermistors.[3]

Empirical evaluation of the various operating modes has shown that the anemometers

1. Have predictable, reproducible DC response to speed;
2. Exhibit turbulent velocity response, identical to a thin film, to approximately 150 Hz; and
3. Are readily adaptable to a microprocessor-based control and data-assimilation system.

In particular, the constant-overheat operating mode has demonstrated a 25-fold improvement over the constant-temperature mode in reducing ambient temperature dependency. Initial indications are that this improvement will increase as further data become available.

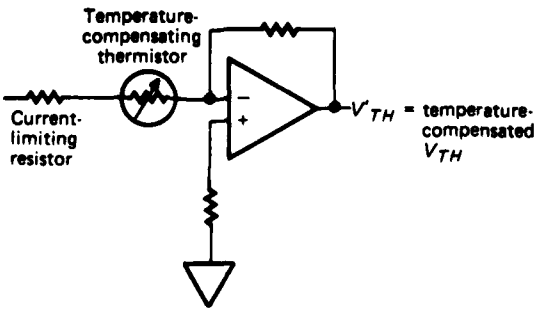

Fig. 5 Temperature compensation network of thermistor anemometer.

REFERENCES

[1] H. B. Sache, *Semiconductor Temperature Sensors and Their Applications*, Wiley and Sons, New York (1975).
[2] R. G. Lueck and T. R. Osborne, "The Characteristics of Internally Heated Thermistors," *Deep-Sea Res.* 27A (1980).
[3] W. I. Sternberger, *Heated Thermistor Anemometers for Ocean Measurement Applications*, JHU/APL ODAP-R-045 (Sep 1981).
[4] R. E. Dingwell and F. B. Weiskopf, *A Hot Film Anemometer for Ocean Measurement*, JHU/APL ODAP-R-027U (Oct 1980).
[5] R. E. Dingwell and F. B. Weiskopf, *Hot Film Anemometer Development Project Summary*, JHU/APL ODAP-R-038 (Feb 1981).

This work was supported by the Chief of Naval Operations, OP-009E.

A MOTION-COMPENSATED LAUNCH/RECOVERY CRANE

E. H. Kidera

Oceanographic instrumentation towed from a surface platform is normally subjected to unwanted vertical motion imparted by the rolling, heaving, and pitching of the platform. This motion can cause severe shock-loading conditions in the tow cable and induces unplanned depth variations that reduce the instruments' resolution. This article discusses a unique motion-compensation system for use with towed instrumentation that eliminates shock loading and minimizes depth variation. The system is operational in sea states as high as 5 and effectively decouples 96% of the vessel's motion.

BACKGROUND

One of the primary oceanographic instrumentation systems used by APL's Submarine Technology Division is a faired cable system instrumented over much of its length with thermistors, fluorometers, and conductivity cells (hence, "TFC chain"); the chain is towed from a surface vessel. The use of a depressor combined with the low drag of the chain results in a nearly vertical catenary. Components of surface platform motion (pitch, roll, and heave) are transferred to the chain through the tow sheave. The resultant vertical motion of the chain has limited its utility for wave physics measurements and has restricted its safe operation to low sea states to avoid excessively high shock loading. A passive boom-motion compensator was conceived, designed, and built to handle the TFC chain and reduce the vertical sensor motion. Figure 1 shows the articulated crane that was modified to provide motion compensation in addition to normal launch/recovery functions.

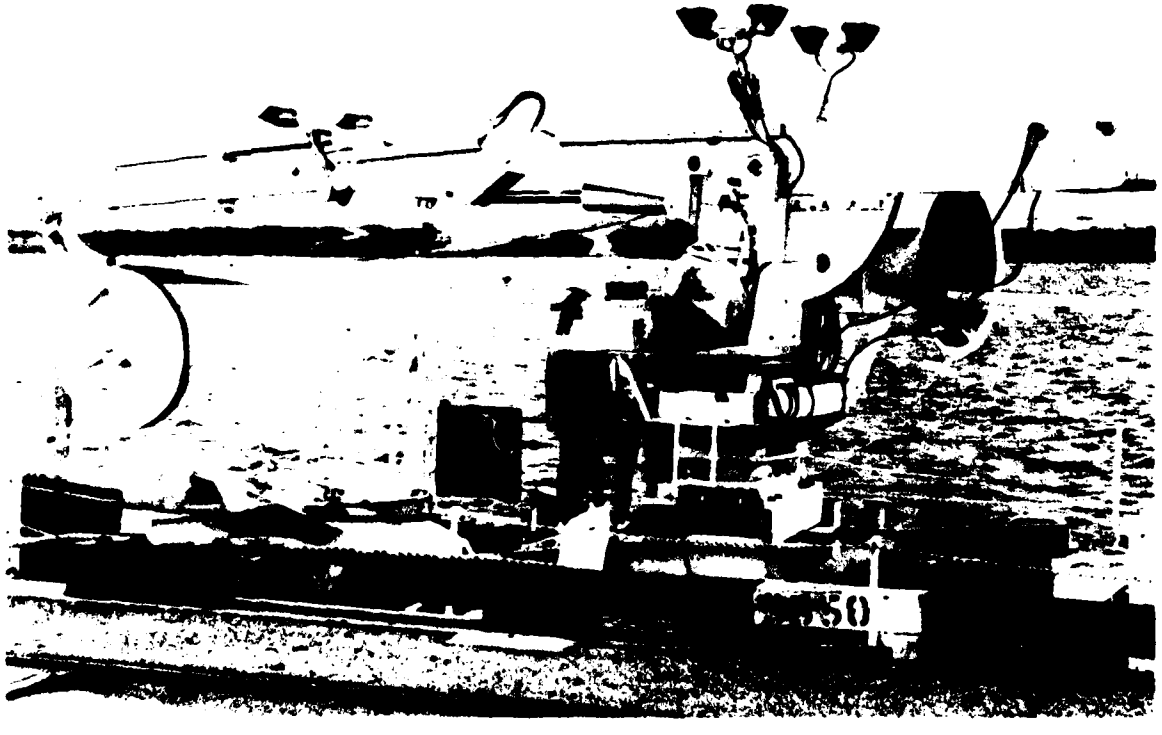

Fig. 1 Motion-compensated crane shown in tow position during dockside equipment checkout.

At APL, further changes were made to the crane to allow its use at sea. It was oceanized, a 4-ft-diameter towing sheave and a depressor saddle were mounted, and a fairlead was added to restrain the thermistor chain during operation. However, the primary modifications were to allow its operation as a motion compensator. Accumulators were added via the special porting to the extension side of the main-boom cylinders. The accumulators act as an interface between the hydraulic oil in the cylinder and the nitrogen that provides the spring. Bladder accumulators were chosen because of their high sensitivity to pressure change. In the event of failure of the motion compensation system, all components can be isolated and the launch/recovery operations carried out normally.

A bottle rack connected to the accumulators supplied a large adjustable gas volume. This configuration allowed the spring constant to be varied at will. The bottle rack includes a high-pressure source and a low-pressure sink for adjustment of system pressure to match the tow loads at any given time. Adjustment is through solenoid valves controlled either manually from the operator's console or automatically from boom-position limit switches. The automatic feature allows the system to operate unattended for hours because changes in loading and boom position are adjusted by the limit switch to maintain the boom in the desired position.

DISCUSSION

The motion-compensated launch/recovery system had its maiden voyage in April 1981 aboard R/V *Cape* off the Florida coast. It was tested extensively and performed admirably. The system is capable of a 25-ft stroke and has a 25-second natural period. In sea state 3, the system limited the motion of the depressor to 4 cm rms for periods of 10 seconds or less.

After the April test, several significant improvements were made to the system. They resulted in a reduced boom-sensitivity threshold and in a substantially reduced system-damping value. The unit was taken to sea in August 1981 in support of an instrumentation checkout. A sea state 5 was encountered, during which the boom performed flawlessly. Motion was reduced from 4 to 3 cm rms in band. This performance corresponds to up to a 96% reduction in vessel-induced vertical motion at the characteristic ship pitch period. Figure 2, a power spectrum of depressor depth, shows the significant reduction in motion between compensated and uncompensated tow. Note the absence of motion peaks on the compensated spectrum. The run shown is for a 6 kt tow in sea state 4.

A passive compensator acts as a soft spring with a natural period significantly longer than the natural period of platform motion. Theoretically, this action allows it to maintain constant cable tension, independent of platform motion, thus minimizing depth variations. System performance is limited by several factors so that the actual cable tension is not constant but varies slightly about some nominal value determined by the pressure in the system. The following are key design factors:

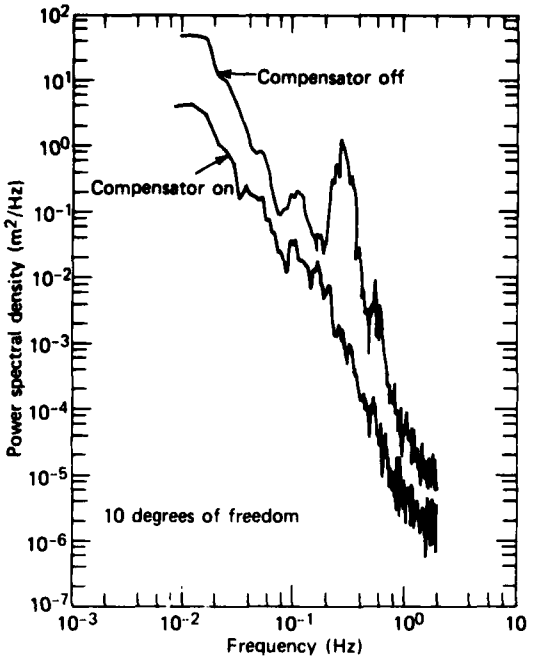

Fig. 2 Depth spectral density for compensator on and for rigid tow (compensator off).

1. Boom sensitivity threshold — the force required to initiate movement of the boom. "Stiction" (static friction) in the pivot bearings and piston seals determines the sensitivity.
2. Natural period of the boom — determined by the length of the boom and the volume of the support gas. A soft spring that corresponds to a large volume is desired.
3. System damping — primarily a result of losses in the hydraulic oil flow. It should be kept to a minimum for best performance.
4. Boom stroke — the dynamic range of the boom. Sufficient stroke is needed to allow operation in the most adverse sea states that will be encountered.
5. Depressor effective mass (DEM) — the mass of the depressor itself plus the entrained water mass. For optimum performance, a depressor with a high DEM and low weight in

seawater is desirable. A winged depressor has a high DEM because of the water above the wing that must be accelerated with the depressor. Since the boom sensitivity threshold is fixed, the larger the DEM the smaller the acceleration will be and, thus, the smaller the amplitude of depth variation.

Passive compensation is simple in theory but relatively tricky in practice. In designing a motion compensation system, all of the above factors must be carefully weighed and matched to the platform characteristics, chain catenary, and ocean conditions that are involved. As in most such matters, compromises dictated by limitations of time and funds must also be made.

System Description

The launch/recovery motion-compensated crane incorporates several key components:

1. The IMTCO model 1725 crane,
2. Motion-compensation modifications and equipment added to the crane,
3. Bottle rack for a large gas volume and adjustment, and
4. Power pack for launch/recovery and general crane use.

The basic crane is an articulated, hydraulic truck crane. Features such as dual main-boom cylinders, a high capacity, a long reach, a rotation system, and low cost make it the ideal choice for modification to shipboard use as a launch/recovery motion compensator. The crane was modified by the factory to APL's specifications. A counterweight was added to balance the boom, and the main boom cylinders were ported for connection to the motion-compensation components.

CONCLUSIONS

The motion compensator has proved itself to be a highly useful tool in the study of ocean structure and a valuable piece of equipment for launch/recovery and towing. It offers several advantages over alternate methods:

1. Reduction in chain motion over a wide frequency range of platform motion;
2. Combined launch/recovery and motion-compensation capabilities in one efficient unit;
3. Minimum cable fatigue through reduction in bending rates and shock loading, even in rough seas;
4. High sensitivity combined with low damping, providing chain-motion reduction in low and high sea states;
5. The capability of continuous compensation operation, with only intermittent attention; and
6. Fail-safe features that permit continued launch and recovery operations in case of malfunction.

Further improvements of the system are possible; they will be carried out if and as time and funding permit. Ultimately, it may be feasible to limit chain motion to only a few centimeters overall.

This work was supported by the Department of the Navy.

MOTION COMPENSATION SYSTEM FOR OCEAN PROFILING

E. H. Kidera and S. A. Mack

The vertical profiles of ocean temperature and salinity measured with instruments lowered by cable from surface ships can be seriously affected by the nonuniform drop rate caused by ship motion. This paper describes a motion compensation system developed for conductivity, temperature, and depth profilers that significantly reduces the effect of ship motion on profiler drop rates, thereby enhancing the measurement capabilities of vertical profilers.

INTRODUCTION

The measurement of the vertical profiles of ocean parameters from surface ships is an important technique for addressing scientific issues of interest to oceanographers and the Navy. The ocean's temperature and salinity structure represents a complex field varying in space and time on scales that span several orders of magnitude. Much work in recent years has been focused on understanding the relationship between the large-scale temperature-salinity structure (scales on the order of one to hundreds of meters) and the small-scale structure (scales less than 1 m). The presence of small-scale features called ocean microstructure indicates mixing processes that are driven by the large-scale features. Mixing can be caused by several mechanisms including velocity shear instabilities and convective instabilities.[1]

To understand the mechanisms causing ocean microstructure, high-quality vertical measurements of temperature and salinity over both large and small scales are required. It is further necessary to map out the horizontal extent of the observed microstructure patches. This paper describes a recent development that advances the capability of ship-lowered instruments to probe the microstructure range of vertical profiling by decoupling the sensor from the effects of surface ship motions. Although the motion compensation system was specifically designed for use with a particular APL/Neil Brown Instruments Systems, Inc. conductivity, temperature, and depth (CTD) instrument system that included a fluorometer, it can be used for many other systems that require vertical profiling from surface ships. The motion compensation system was designed and built at APL. The prototype system was tested and subsequently used during an oceanographic mission in the Pacific in November 1980.

DISCUSSION

Effects of Ship Motion

The motion of a surface ship resulting from surface and atmospheric dynamics imposes effects on vertical profile measurements ranging from the obvious to the subtle. The degree to which the resulting data contamination becomes a problem is a function of the vertical scales over which the data are to be interpreted. The effect of the surface ship roll, pitch, and heave is to vary the descent rate of the sensor. With slow descent rates and moderate sea states, the sensor can reverse direction periodically. For deep measurements of large-scale temperature features, these sensor reversals cause a resampling of parts of the profile and a lower overall resolution and sampling efficiency. In this case, the data are usually resampled later at a lower rate and are made uniform in depth. Although the efficiency of the data sampling is lower owing to the ship motion, large-scale temperature data are relatively unaffected.

The more subtle effects of reversals and nonuniform descent rate become significant when one is trying to measure the small-scale temperature and/or conductivity microstructure, particularly when attempting to compute salinity and density from the separately measured temperature and conductivity. CTD systems are designed with the sensor arm extending from the lower portion of the electronics pressure housing. Reversals in the descent will cause the sensors to resample regions that have been mixed by the pressure housing itself, thus contaminating the microstructure measurements. Data processing algorithms can be used to identify and partly remove such regions from further data analysis, but the advantage of eliminating sensor reversals with a motion compensation system is clear.

The most subtle effect, one not easily addressed in data analysis, is that arising from a nonuniform, but monotonic, descent rate. The computation of salinity requires independent measurements of temperature and conductivity from sensors whose frequency responses are well matched. However, the frequency response of thermistors is a function of speed.[2] Nonuniform drop rates thus will vary the frequency response of thermistors, creating fluctuating differences in the relationship of thermistor and conductivity frequency responses. The well-known effect called "salinity spiking" (artificial salinity peaks in regions of high temperature gradients) can result from this response mismatch.

A further complication of nonuniform drop rate can arise even when only temperature or conductivity data are being analyzed. A uniformly sampled space series is required in order to compute the vertical wavenumber spectrum of temperature. While an equispaced spatial series can be obtained by interpolation, so doing creates an effective attenuation at high wave numbers

and a resultant artificial change in spectral slope. The problem can be avoided by a totally free-fall device with internal power and recording, but these systems have their own limitations, including limited battery lifetime, limited recording capabilities, lack of real-time processing, a need for ballast release for multiple profiling, and a need for recovery before horizontal repositioning. The motion compensation system offers an alternative to free-fall devices for many applications that otherwise would not be possible in any but the most benign sea states.

System Description

The unit discussed in this paper serves as a launch/recovery device and also decouples surface vessel motion from the CTD sensor package during vertical profiling. This motion compensator, known as a bobbing-boom type, is a passive compensation sysem that can be modeled as a single-degree-of-freedom spring mass system. The CTD sensor package acts as the mass, and the boom/pneumatic cylinder combination serves as a very soft spring. If the unit is properly designed, the mass is not excited and remains stationary at periods of vessel motion shorter than the natural period of the boom.

This type of compensator was built because it offers several key advantages:

1. Simplicity and reliability inherent in a passive system,
2. Inherently low friction of boom design and thus high sensitivity,
3. Efficiency of operation in the dual role of launch/recovery gear and motion compensator,
4. Excellent motion compensation performance.

The system consists primarily of the boom, support column, tow sheave, pneumatic cylinders, volume tanks, air supply, and control circuit (Fig. 1). The unit is mounted on deck near the CTD winch and can be fully assembled in half a day by two people. The components are described briefly below.

Boom. The boom is pivoted on the inboard end and supports the tow sheave on the outboard end. It is constructed of aluminum for light weight and resistance to corrosion. The balanced design offers better performance as a motion compensator by removing the boom weight from the support cylinder loading. A special pivot bearing system minimizes stiction (static friction).

Support Column. The boom is held by the support column on which all the other components, with the exception of the air supply, are mounted. The column pivots freely for launch/recovery and during CTD casts to allow for the drift of the vessel and the resulting cable angle. The free-pivot feature minimizes side loading of the entire unit that otherwise could twist the boom and support column.

Fig. 1 CTD unit and motion compensator shown during a launch.

Tow Sheave. A light sheave is used to support the ⅛-in. CTD cable. A limit switch in the sheave is set as a safety to turn off the CTD winch and prevent damage should the profiler be raised too high.

Pneumatic Cylinders. The boom is supported by pneumatic cylinders that are pressurized to support the load of the CTD unit and cable. Bladder cylinders are used because of their exceptionally low breakaway friction. They are of limited stroke (6 in.), and two were used in series to achieve the desired boom stroke of 9 ft.

Volume Tanks. The pneumatic cylinders are connected by hose to several air tanks to supply a large volume and thus a soft spring. For test purposes, the system volume can be varied from 0 to 18 gallons in 3-gallon increments. This feature allows the compensator to be operated with varying spring stiffness. For general system use, a soft spring is preferred.

Air Supply. An air compressor developing 175 psi and delivering 4 ft^3/min supplies the motion compensator with air pressure to adjust the system.

Control Circuit. Solenoid valves provide adjustment of system pressure and thus load capacity. One valve dumps the system to atmosphere for reducing pressure; the other is connected to the air supply line to increase pressure. The two valves are controlled either manually from a hand-held control box or automatically from limit switches that respond to boom position. The manual control is used for launch and recovery of the CTD. Automatic control provides adjustment of the system pressure to match load conditions. During a long cast, as the cable is payed out, the load on the end

of the boom increases, causing the boom to be displaced downward. If the load change is large enough, the boom trips a limit switch that admits more air to the system, thus returning the boom to a neutral position. A similar sequence occurs as the cable is retrieved.

At-Sea Performance

The CTD compensator performed exceptionally well in minimizing drop-rate fluctuations and in handling the CTD unit during launch and recovery. It allows an operator to position the profiler overboard with minimal effort because the weight of the unit is carried by the boom.

Preinstallation testing of the system revealed a natural period of 12 to 13 s and a sensitivity of under 3 lb. The natural period, sensitivity, and damping are key factors in determining the system's performance as a motion compensator. It is desirable to have a long natural period and very low sensitivity and damping.

Preoperation tests were conducted at sea to determine actual system performance. Two basic tests were carried out, the first with the profiler at a fixed cable length, the second in a yo-yo mode for repeated profiling.

Figure 2 shows the depth power spectral density obtained with the compensator on and off during the first at-sea test with the CTD unit at a fixed cable length. A clear difference in motion between passive and rigid operation is evident. Overall motion excursions were reduced from 29 to 13 cm rms. Note that the compensator performs best at periods somewhat shorter than its natural period. At about 1 Hz, the sensor depth variation is reduced to the noise level of the depth sensor. A proper volume setting for optimum performance is important. A softer than optimal spring results in long-period drift caused by boom stiction. A stiffer spring results in increased motion and even permits resonance to occur at progressively shorter periods as the volume is reduced.

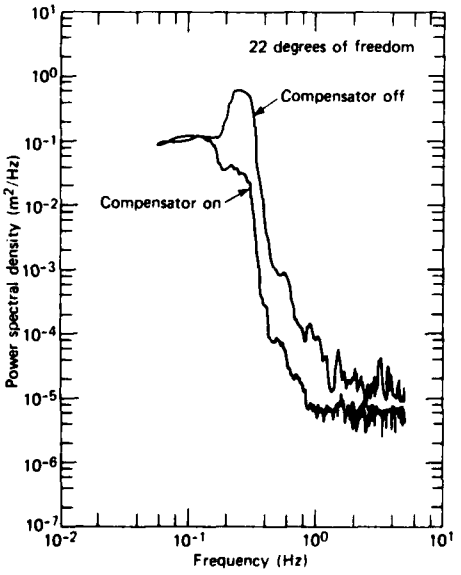

Fig 2 Depth power spectral density for compensator on and compensator off with the CTD profiler kept at a fixed cable length.

The second at-sea test simulated normal profiler operations. The unit was winched up and down between 20 and 50 m at a drop rate of about 50 cm/s. Figure 3 shows depth versus time for eight casts (only the down portion is shown). The first four casts (left to right) are with the unit rigid; the second four are with the boom in compensation mode. Note the substantial decrease in sensor motion and the total elimination of sensor turnarounds when the compensator is turned on. A further appreciation of the reduction of depth variations may be gained from Fig. 4 by comparing the depth power spectral density (after detrending) for the fourth profile (uncompensated) and the fifth profile (with compensator on). The rms depth fluctuations are reduced from 34 to 14 cm. Figure 5 shows the same eight casts as Fig. 3, this time as drop rate versus depth. With the system on and compensating, the fall rate is much more nearly constant.

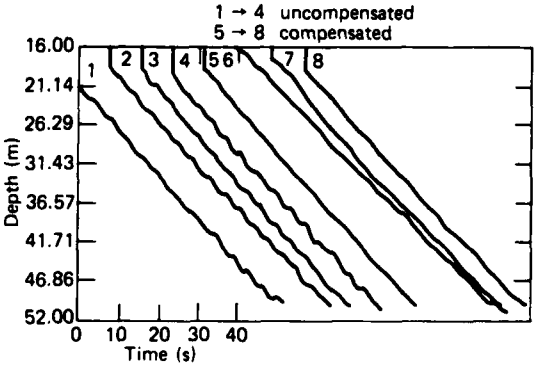

Fig. 3 Profiler in yo-yo mode, the first four casts (left to right) with system rigid (compensator off), and the second four casts with compensator on.

CONCLUSIONS

The present motion compensation boom has proven to be a valuable and reliable system that enhances the quality of vertical profile measurements from surface ships under a variety of sea conditions. The more uniform drop rate afforded by the system allows reliable vertical measurements of temperature and

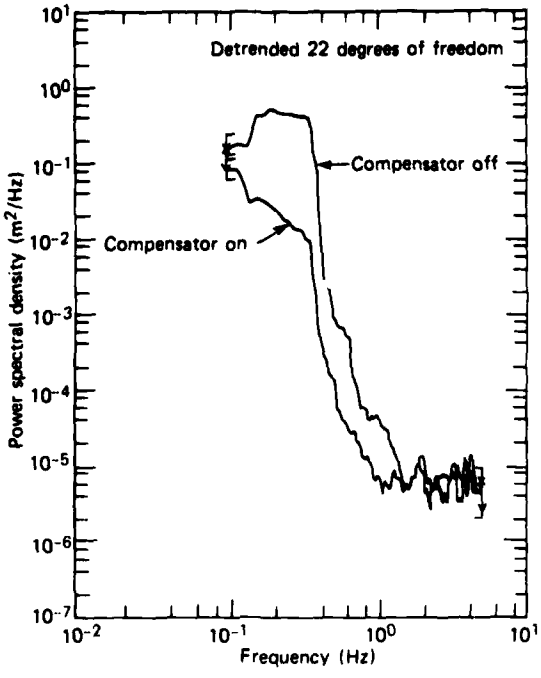

Fig. 4 Depth power spectral density for profile 4 (uncompensated) and profile 5 (compensator on) of Fig. 3.

conductivity over scales not previously attainable for ship-lowered instruments. The measurements thus obtained are uncontaminated by sensor reversals and are less affected by a nonuniform drop rate. While specifically designed for use with a particular API/Neil Brown Instruments Systems, Inc. profiler, the motion compensation device should be useful for a variety of ship-lowered instruments that require decoupling from ship motion.

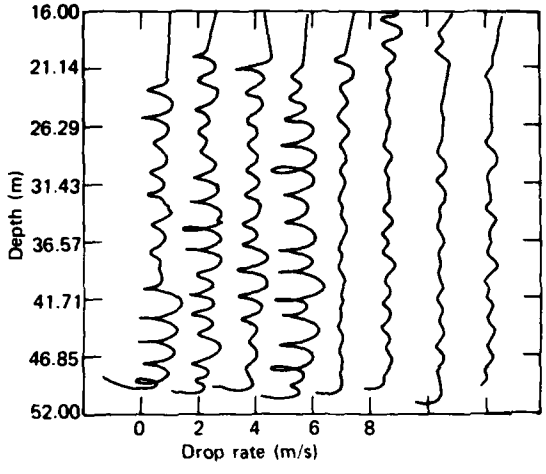

Fig. 5 Drop rate versus depth for CTD casts, the first four (left to right) with system rigid, and the second four with compensator on.

ACKNOWLEDGMENTS

The authors wish to thank Bryce Troy for developing much of the data processing software.

REFERENCES

[1] J. S. Turner, *Buoyance Effects in Fluids*, Cambridge University Press (1973).
[2] M. C. Gregg and T. B. Meagher, "The Dynamic Response of Glass Rod Thermistors," *J. Geophys. Res.* **85**, 2779-2786 (1980).

This work was supported by the Department of the Navy.

SURFACE-OPERATED CONTROLLED-DEPTH PARAVANE

C. W. Anderson

A surface-controlled paravane system was built to serve as a submerged platform for towing a buoyant cable. APL modeled the paravane after a helicopter-towed minesweeping vehicle designed at the David Taylor Naval Ship Research and Development Center. The APL system differs in that it is surface-controlled and unbiased with respect to port and starboard operation. A shipboard operator may direct the vehicle to hold a constant depth, to change depth, and to change between port and starboard tow-off directions. The reliability of the system is good; less than 3% of nearly 400 hours of towing was lost because of all difficulties related to paravane operations.

DISCUSSION

The system consists of a towed, instrumented paravane, a topside control console, and an electromechanical tow cable. Figure 1 shows the paravane just before launch; attached above the vehicle is a sample buoyant cable. The paravane is approximately 0.9 m long; it has a 0.88-m wing span and a mass of 20 kg. The cylindrical body is constructed of flotation material that gives an in-water positive buoyancy of 13.3 N. Dynamic lift is provided by a biwing configuration; a small motor-driven vane extending from the vehicle's underside provides dynamic control. Electronics and the vane motor drive are housed inside the body. An electromechanical tow cable and a deck cable couple the paravane to the topside electronics.

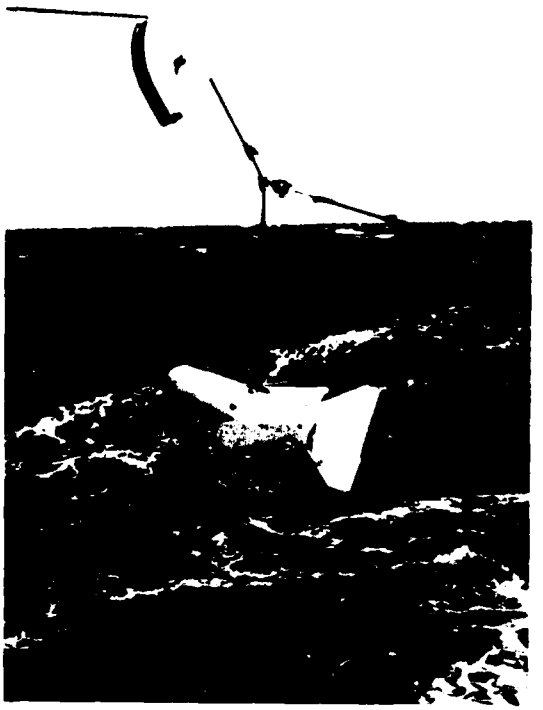

Fig. 1 Surface-controlled paravane during launch.

System Operation

Commands to the paravane come from the control console where an operator can set running depth and tow-off direction and also can monitor depth, roll, and vane angle. The operation of the paravane is simple because the only control surface is the small movable vane. The vane holds or changes the roll angle of the paravane. With a given tow-cable scope and ship speed, the paravane's depth is determined by roll because the roll angle determines the relative magnitude of the horizontal and vertical lift components. When the roll angle is zero, all lift is directed vertically downward, moving the paravane deeper. As the roll angle increases, the horizontal lift component increases, causing an increase in tow-off from the ship that results in a decrease in depth.

Automatic depth keeping is provided by the electronics subsystem that accepts depth and tow-off instructions from the operator and receives inputs from the paravane sensors: a depth transducer, a roll sensor, and a vane angle potentiometer. The operator-set depth and the actual depth are compared, and the vane angle of attack is set proportional to the depth error by a servo-controller. Manual override is required to change between port and starboard tow-off directions. Automatic depth keeping is resumed once the vehicle has passed through the zero-degree roll attitude.

System Performance

Typical variations in the measured depth of the paravane are ±0.3 to ±0.6 m when operating in 2- to 3-m seas at depths of 15 to 23 m. Actual depth stability and the ability to determine depth stability depend in large part on wave height, wave frequency, and operating depth because the feedback source is a pressure transducer. Pressure fluctuations from some surface waves are significant and will influence paravane depth control and apparent stability. For the test involving the buoyant cable, the paravane's worst-case measured depth variations were acceptable because motion in-

duced on the cable damped out before it could cause any problems. Improving the paravane's depth-keeping capability was therefore not warranted.

In addition to running the paravane at constant depth, as in the cable test, the system offers the capability of operation in a continuously changing depth mode. Such operation could be useful for oceanographic surveys if the paravane is instrumented with environmental sensors and if its towing characteristics are acceptable. Several profiling test runs were made at tow speeds from 5 to 11 knots over a 25-m vertical aperture. Climb/dive angles of about 20° were typical when averaged over two or more profiling cycles. A maximum angle of 38° was measured during the climb leg at 9 knots. The average profiling angles were lower than the 38° maximum because built-in roll limits override some of the manual profiling commands. Modification of the roll-override circuit appears feasible and would improve the average climb angles without diminishing other towing characteristics.

Consideration of the paravane for use in data collection requires an understanding of the vehicle's trajectory during depth changes. Motion is in three dimensions: in the direction of tow, in the vertical direction, and in the lateral direction. Lateral displacement defines the amount of tow-off from the centerline of the ship; for very shallow depths, it will be nearly equal in magnitude to the maximum attainable depth. In a simple model considered in a reference frame moving with the tow ship, the paravane traverses an arc drawn in a vertical plane perpendicular to the centerline of the tow ship. Thus, the trajectory is a compound curve with respect to an absolute reference frame, and the suitability of using the paravane in environmental surveys must be decided with this operational attribute in mind.

SUMMARY

A surface-controlled paravane has proven to be a versatile submerged test platform for towing buoyant cables. The vehicle demonstrates compatibility with the cruise speeds of most research vessels in both a constant-depth and a profiling mode of operation because it may be towed at speeds from 4 to 11 knots. The paravane may also be an excellent sensor platform for applications requiring a small, lightweight, easily handled, towed profiler.

This work was supported by the Department of the Navy.

DIGITAL ARRAY TAPE RECORDING AND REPRODUCING SYSTEM

J. L. Machamer and M. Davidson

The high-density Digital Array Tape Recording and Reproducing System was developed for use in APL's oceanographic measurement programs. APL designed and developed the electronic interface equipment that enables any standard 14-track wideband analog tape recorder/reproducer to be used as a digital recorder with a high throughput rate. Data with throughput rates of up to 45 megabits per second are recorded on magnetic tape at bit packing densities of 33 kilobits per inch per track. The recorded data can be reproduced at or below the recorded rate with an average bit error rate of 1 in 10^7.

BACKGROUND

The Digital Array Tape Recording and Reproducing System (DATARRS) was developed to record large quantities of data received from an underwater acoustical array. The digital interface was packaged for field use with APL-owned portable tape recorders/reproducers; however, the interface can be used with the laboratory or portable standard instrumentation of any manufacturer. DATARRS can be used with error correction equipment at a throughput rate of 38 megabits per

second to provide a reduced bit error rate of 1 in 10^{10} (Ref. 1). It provides a high-density digital recording capability for most data acquisition and processing applications where low error rates are required.

DISCUSSION

Recording Operation

Figure 1 is a simplified block diagram of the system in which DATARRS was designed to operate. Control lines are omitted for simplicity. Fourteen data channels (U0 to U13) can be accommodated, although error correction is possible only if 8 or 12 channels are used. The record digital interface inputs 14 data channels (V0 to V13) with or without error correction encoding (parity tracks). It converts the data to a recording code that is more suitable for the channel bandwidth of the tape recorder/reproducer and controls the recorder speed. The encoded data are recorded on magnetic tape using standard analog techniques.

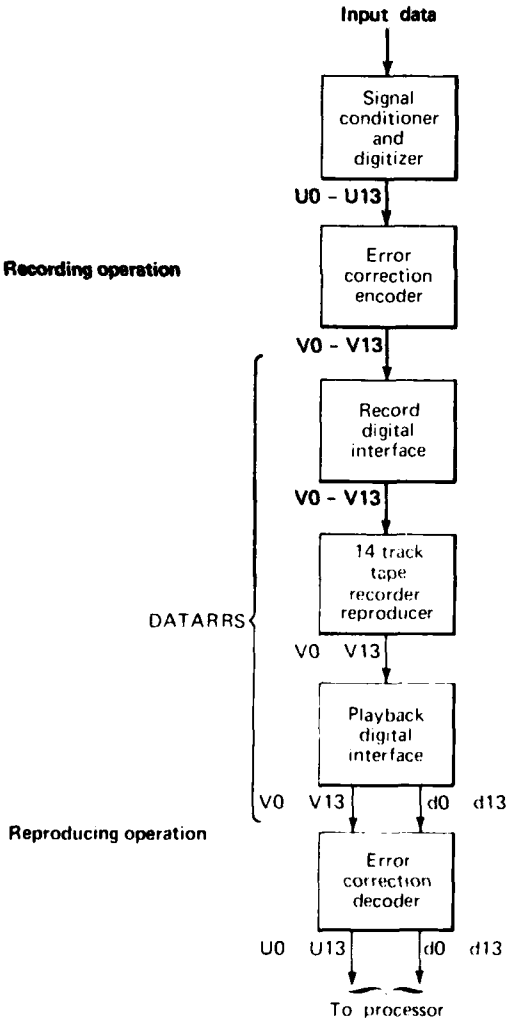

Fig. 1 Simplified block diagram of high-density digital array tape recording/reproducing system.

The data are recorded at bit packing densities that depend on the data bit rates and the tape speed. Figure 2 indicates the operating points for the specified upper limit of 33 kilobits per inch per track and a typical density of 21.5 kilobits per inch per track. The points are indicated for operation with and without error correction equipment.

Reproducing Operation

During tape playback, the DATARRS playback digital interface controls the tape recorder playback speed; synchronizes, channel decodes, and organizes the data; and checks the data for channel coding errors. As a result of the last operation, the playback digital interface generates information on data quality (d0 to d13) on a line-for-line basis with channel decoded data. The playback digital interface data and data-quality information are output to the error correction equipment for correction and transfer to a processor. DATARRS will function with the tape recorder/reproducer as a stand-alone unit or in conjunction with APL error correction equipment.

Channel Encoding

The tape recorders/reproducers for DATARRS are longitudinal multitrack instruments that use a nonsaturation, direct-record method with bias to record the digital data on tape. The channel is essentially a baseband digital system that usually requires the source binary information to be encoded in a format more suitable for transmission. The selected coding scheme is a low-disparity block code $(N,c;D)$. Such codes are defined as one-to-one mappings from the input code blocks of bit length N to the channel code words of bit length c, where $c \geq N$. The disparity, D, is defined as the excess of binary 1's to 0's in the channel code word. The code is a combination of the (5,6; 0) and (5,6; ± 2) block codes[2]; it contains a set of zero disparity words and a set of word pairs with complementary disparities of ± 2.

The code words, with zero disparity or alternating ± 2 bit disparity, are grouped with a unique tape synchronization word and are output as continuous data bit streams. These encoded data match the channel bandwidth better than the source data, while maintaining a reasonable overall efficiency. The decrease in data throughput when overhead bits are used is shown in

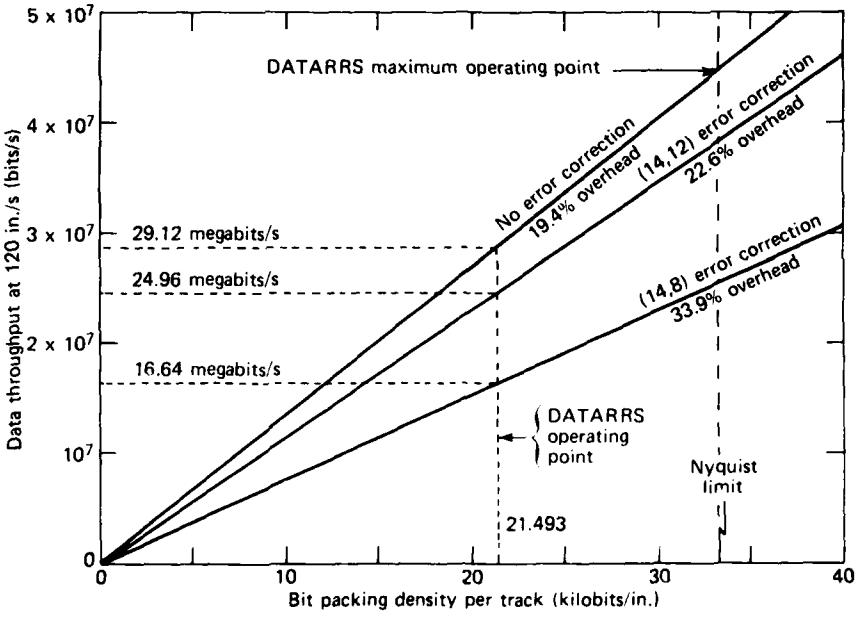

Fig. 2 Throughput rate versus bit packing density.

Fig. 2 for the channel encoding with and without the error correction bits.

REFERENCES

[1] P. J. Luke, J. L. Machamer, and W. A. Becraft, "Error Correction Encoder Error Correction Decoder," *Developments in Science and Technology, Fiscal Year 1975*, JHU/APL DST-3.

[2] M. Davidson and J. L. Machamer, "High-Density Digital Magnetic Recording Using the (5,6) Alternating Disparity Block Code," *Electron. Lett.* **14**, No. 15 (Jul 1978).

This work was supported by the Department of the Navy.

COMPUTER TECHNOLOGY APPLICATIONS

INTRODUCTION

Computer systems play an important role in APL's contributions both to national defense and to the solution of civil problems. Extensive computational facilities are maintained by the Laboratory to support the work of its scientists and engineers.

The central digital computer facility consists of an IBM 3033 multiprocessor with high-speed large-scale dual processors. The 3033 has a basic machine cycle time of 58 ns with overlapped instruction execution, and it has an advanced virtual memory operating system. Its main memories, which contain 16 million bytes, are supplemented by auxiliary direct access storage totaling 115 billion bytes (disk and mass storage). The facility serves a wide variety of tasks including large-scale simulations, complex analyses, and data processing and reduction. Extensive use is made of interactive processing for the real-time solution of problems; about 700 remote terminals are available.

APL also supports two analog/hybrid computer laboratories. Analog and hybrid computations are esential to the solution of complex problems, particularly when large numbers of simultaneous differential equations must be solved. Hybrid facilities can economically simulate large physical systems comprising continuous and discrete processes as well as real-time simulations that include hardware in the loop. APL's two hybrid computer laboratories are the Interactive Simulation Laboratory (ISL) and the Guidance System Evaluation Laboratory. The EAI 680 analog computers in the ISL are interfaced with an IBM 3033 digital machine that is part of the multiprocessor configuration. The other hybrid system, consisting of an EAI PACER 600 system interfaced to missile hardware and a radio-frequency test-chamber darkroom, is used primarily to test missile guidance hardware.

A computer-based image processing laboratory that has now reached routine operational level is reported in one of the papers in this section. That laboratory is a part of the Data Processing Center. The image processing capability is a major, long-term commitment by APL.

Other papers in this section deal with the development of better security for data and programs, the development of a network known as APLnet, uniting a variety of computers including the central IBM 3033 multiprocessor, and the development of a database maintenance processor to automate management information system updating.

Many articles that might have been placed in this section cover application-specific uses of computers; therefore, they have been placed in other sections of this volume. Most of the papers in the other sections discuss applications based on the use of computers, testifying to the central role this technology plays in the work of this Laboratory.

THE BID IMAGE PROCESSING LABORATORY

J. P. Randolph and D. G. Tilley

The burgeoning field of digital image processing has many diverse applications in the scientific work performed by APL. A newly established, central Image Processing Laboratory now provides APL with a powerful resource for the pursuit of ongoing programs and for the attraction of new and challenging tasks; applications already have included space science, oceanography, missile technology, and biomedical image analysis.

BACKGROUND

The capabilities of the Image Processing Laboratory (IPL) developed by the Instrumentation Development Group (BID) are divided into three basic areas of image processing:

Image Digitizing. Images are subdivided into an orthogonal array of square picture elements (pixels) as small as 12.5 μm. Each pixel is digitally recorded on magnetic tape or disk as an 8-bit byte of data that defines its density or color intensity as one of 256 levels.

Digital Image Processing. Digitized imagery, either monochrome or color, may be processed on line interactively or off line via the IBM 3033MP computer. In either case, extensive software exists to provide such algorithms as edge enhancement, contrast enhancement, contouring, convolution, and pseudocolor encoding. Special application software can also be written.

Digital Image Output. Digital imagery and graphics, either color or monochrone, may be output as soft displays on cathode ray tube (CRT) terminals or in a wide variety of hard-copy formats. Annotated graphics may be output on paper or microforms, and imagery may be output as either prints or transparencies up to 10 by 10 in. Both graphics and imagery may be output on 16, 35, and 105 mm roll film. Computer-generated color movies may also be produced.

The equipment used to provide the above capabilities is described below, and an example of an application is cited.

DISCUSSION

DEC PDP-11/70 Computer

A DEC PDP-11/70 computer serves as the controlling element for the IPL. This computer has 640 kilobytes of metal-oxide semiconductor memory, a hardware floating point unit, and five disk units providing a total of 130 megabytes of disk storage. It is equipped with a nine-track tape drive, a DECwriter terminal, and six CRT terminals.

As the central node of the APLnet computer network[1] (reported elsewhere in this volume), this computer has direct communication with the IBM 3033MP computer system in the Frank T. McClure Computing Center and also with the other PDP-11 and VAX computers at APL that share the network.

The IPL equipment described below is interfaced to the unibus of the PDP-11/70, which makes it possible for these devices to share the resources of that computer and to pass imagery from one device to another. In addition to serving as the control element of the IPL, the PDP-11/70 also provides an image-processing capability via resident software operating under the RSX-11M operating system. Special application software is written and added to the system as the need arises.

Optronics Film Scanner/Writer

Image digitization is performed on the Optronics P-1700 drum scanner/writer (Fig. 1), which accepts monochrome or color imagery, transparent or opaque, up to 10 by 10 in. During the scanning process, by means of appropriate optics, a beam of light is caused to pass through or be reflected from the imagery. The light that is transmitted or reflected is sensed by a photomultiplier tube, the output of which is fed through a logarithmic amplifier and an analog-to-digital converter to produce an 8-bit byte of data proportional to the optical density of the pixel being sensed. A precision lead screw driven by an incremental motor causes the image to be subdivided into an orthogonal array of square pixels. Six pixel sizes from 12.5 to 400 μm may be selected. In the case of color imagery, three scans are made using red, green, and blue filters in turn.

The digital output of the scanner is fed via the unibus to the PDP-11/70 computer where it is stored on disk or magnetic tape or transmitted to another computer via the APLnet link.

The P-1700 may also be used to write monochrome imagery from digital data onto film up to 10 by 10 in. with the same choices of pixel size. During the write operation, the process is reversed. Each 8-bit byte of data passes from the unibus to a digital-to-analog converter, which produces a voltage proportional to the density of the represented pixel. That voltage modulates a light-emitting-diode light source, which impinges on

film contained in a light-tight rotating drum driven by the same mechanical system as was used in the scanning operation.

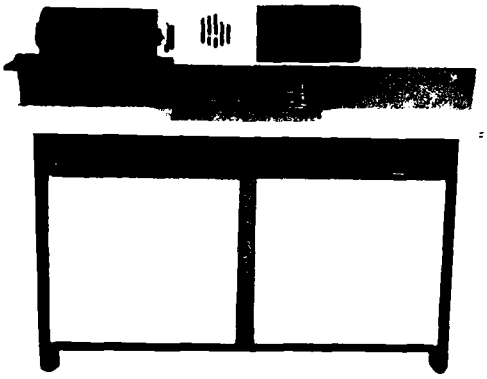

Fig. 1 The Optronics P-1700 film scanner/writer.

The Optronics C-4300 system is used to output color imagery. It is similar to the writing section of the P-1700 but uses a glow-crater tube to produce a white light source. Again, three passes are required, one each with red, green, and blue filters in the light path. The system is restricted to four pixel sizes from 25 to 200 μm. The output imagery is written as a positive or negative color transparency up to 10 by 10 in. or as an 8 by 10 in. color Polaroid print or transparency.

Comtal Vision One/20

The Comtal Vision One/20 System is an interactive image processor that can be used in standalone operation or with the PDP-11/70 computer. It also serves as a monitor to display imagery being scanned or written by the Optronics equipment. It contains an embedded LSI-11 microprocessor, pipeline processors, and a refresh memory that can store up to 1024 by 2048 8-bit pixels. Because it is a two-channel system, it will accommodate two users concurrently. Each of the two 19-in. color monitors can display any 512 by 512 pixel image stored in the refresh memory.

Digital images are loaded into the Comtal via a dedicated nine-track tape drive or from the unibus of the PDP-11/70. In the latter case, the imagery may be resident in the PDP-11/70 disks or may be transmitted from the IBM 3033MP computer system or another computer in the APLnet network.

The Comtal is controlled interactively by means of a keyboard, data tablet, or track ball. Resident software provides over 100 image processing functions, including roaming, zooming, scrolling, convolution, iterative filtering, and pseudocoloring. The display is recalculated and refreshed in one-thirtieth of a second. Additional application software may be written to perform other operations on the PDP-11/70 with subsequent display on the Comtal.

Overlays and annotation may be added to the displayed image. When the processing is complete, the resultant image may be written back into memory, written on magnetic tape, output via the unibus to the PDP-11/70, or sent via APLnet to another computer. The image may also be output in any of a variety of hard-copy formats via the Matrix camera.

Matrix 4007 Camera

A Matrix model 4007 camera provides high-quality hard-copy output of monochrome or color imagery in a variety of formats from either of the two Comtal monitors or from a Tektronix 4027 color graphics terminal connected to the IBM 3033MP computer.

The Matrix camera uses a composite exposure method to produce full-color hard copy. The red, green, and blue video components of the image are acquired and displayed sequentially on a built-in high-resolution monochrome monitor. The three primary color components of the monitor are photographed sequentially through corresponding red, green, and blue filters that are automatically rotated into the light path. Black and white recording can also be selected.

Three cameras are included in the system. A multiple-image camera allows from 1 to 25 images to be recorded in orderly arrays on a single 8 by 10 in. sheet. Outputs may be Polaroid color transparencies or prints or conventional positive or negative transparencies in black and white or color. A 35 mm camera also records positive or negative transparencies in black and white or color. Finally, a Polaroid SX-70 pop-up camera quickly produces 3 by 3 in. color prints.

Dicomed Computer Output to Microfilm System

The Dicomed D48C Color Graphic Recorder, operating under the control of the PDP-11/70 computer, is a precision, high-resolution, computer output to microfilm system. Data may be input from nine-track magnetic tape written in proper format by any digital computer or from the PDP-11/70 disk units. Digital data in either vector or raster form produce an image on a built-in monochrome monitor having a resolution of 4096 by 4096 pixels. The image is photographed as it is being written. Color images are recorded by making multiple exposures through one or more of seven computer-selectable color filters.

Interchangeable film transports and optical assemblies allow the system to be configured to handle

the following standard roll film formats: 16 and 35 mm (black and white or color, sprocketed or unsprocketed) and 105 mm microfiche (black and white only) in either page or legal format with reduction ratios of 24, 42, and 48 times.

In the raster mode, the D48C can produce high quality 35 mm images with a resolution of up to 40 line pairs per millimeter. In the vector mode, it can be used to produce 35 mm slides or 16 mm movies by using the TELL-A-GRAF software recently installed on the IBM 3033MP computer; that software allows a user to create his own graphics, either monochrome or color, from essentially any graphics terminal connected to the IBM 3033MP computer.

Figure 2 shows all of the IPL equipment except the Optronics equipment already shown in Fig. 1.

Fig. 2 Partial view of the Image Processing Laboratory showing the COMTAL system (left center), Matrix camera (left rear), PDP-11/70 computer (right foreground), and Dicomed system (right rear).

System Integration

Since the systems described above are all interfaced to the unibus of the PDP-11/70 computer, intercommunication between systems is readily accomplished. Digital imagery may be input to the unibus from digital tape, the Optronics P-1700 scanner, the Comtal, the PDP-11/70 disk, or via APLnet from the IBM 3033MP or any other connected computer. Once the data are on the unibus, they may be displayed and processed on the Comtal and then output as hard copy on the Matrix camera or via the unibus on the Dicomed or Optronics systems. Imagery may also be processed on the PDP-11/70 or any other computer connected to APLnet and then returned to the unibus for output as hard copy or for recording on magnetic tape or disk. Figure 3 shows the interconnections of the equipment making up the IPL.

Many image-processing applications have arisen that require the kind of interaction between the systems that is described above. One such application is described briefly below.

AN APPLICATION OF THE IPL

The Space Sciences Branch of the Space Department has applied the resources of the IPL to the display and analysis of synthetic aperture radar (SAR) data recorded during the NASA SEASAT mission in 1978. Ocean swell systems with wavelengths between 50 and 400 m have been identified in the radar data recorded by a satellite 800 km above the earth to confirm measurements made by NOAA wave buoys and laser profilometers. Temperature gradients and current boundaries have been observed in the SAR imagery, and their effects on surface waves are being investigated. The results of the data analysis have been documented in various technical publications.[2-6]

The SAR image data were acquired as digital tapes in a 16-bit per pixel format and were converted to an 8-bit format to produce high-resolution prints and transparencies using the Optronics P-1700 and 35 mm slides using the Dicomed D48C. The IBM 3033MP computer and the Small Interactive Image Processing System/Video Image Communication and Retrieval (SMIPS/VICAR) software were used to apply fast Fourier transforms to the SAR data, to generate power spec-

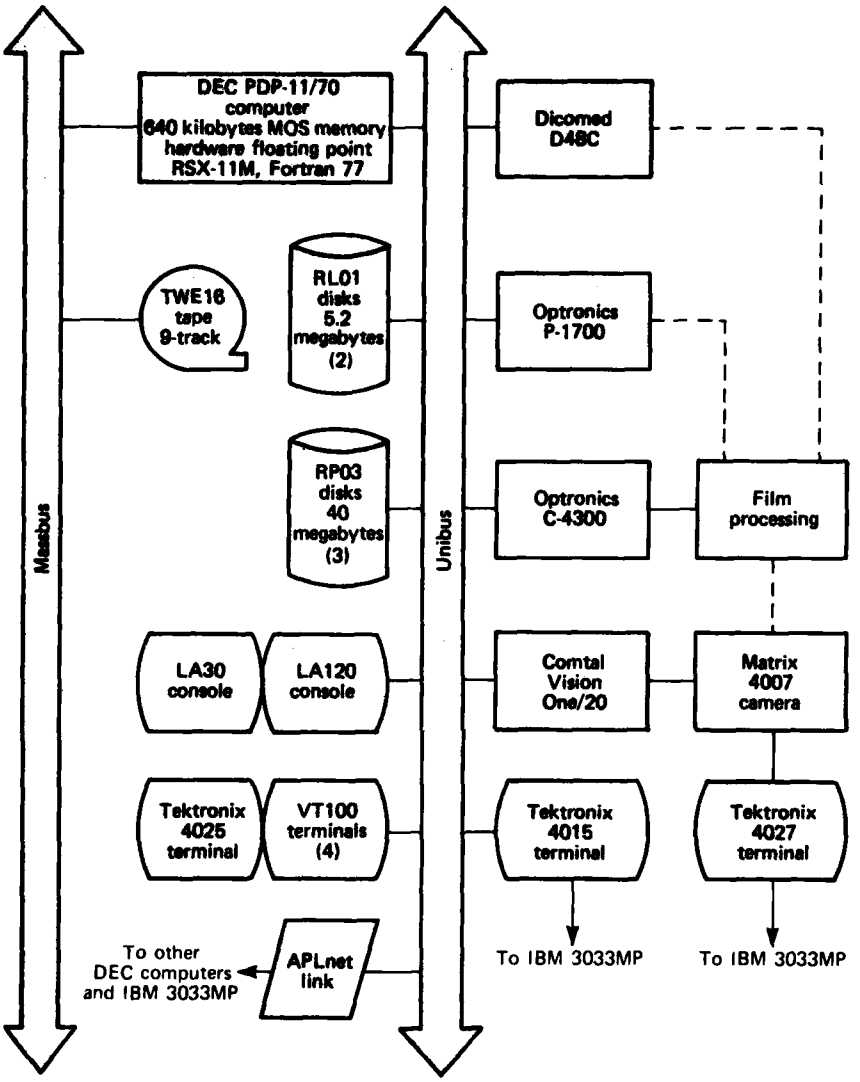

Fig. 3 Block diagram of the Image Processing Laboratory.

tra from the transformed data, and to filter the spectra digitally with a Gaussian convolution. The PDP-11/70 computer was used to estimate the characteristic range and azimuth response of the SAR imaging system as two fourth-order polynomials optimized separately in each dimension to minimize their variance with SAR data representing Chesapeake Bay. The Comtal was used to remove this systematic bias from the fast Fourier transform power spectra and to better approximate true ocean wave conditions. Ocean wave spectra have been generated in this manner for numerous locations along the Atlantic Coast of the United States. These spectra have been displayed as 512 by 512 pixel images on the Comtal monitor and photographed with the Matrix camera to produce 35 mm slides, Polaroid SX-70 prints, and multiple image formats on 8 by 10 in. sheet film. The spectra have also been displayed sequentially on the Comtal monitor as a loop movie and recorded on ½ and ¾ in. video tape using a video camera and cassette recorders.

Figure 4 shows an ocean wave spectrum obtained for an area off the North Carolina coast. Eight shades of gray are used to represent wave intensity as a function of wavelength. In this polar plot, the radial lines show the direction of wave propagation in degrees with respect to the satellite heading, and the circular lines show wavelengths in meters. A high intensity of 200 m

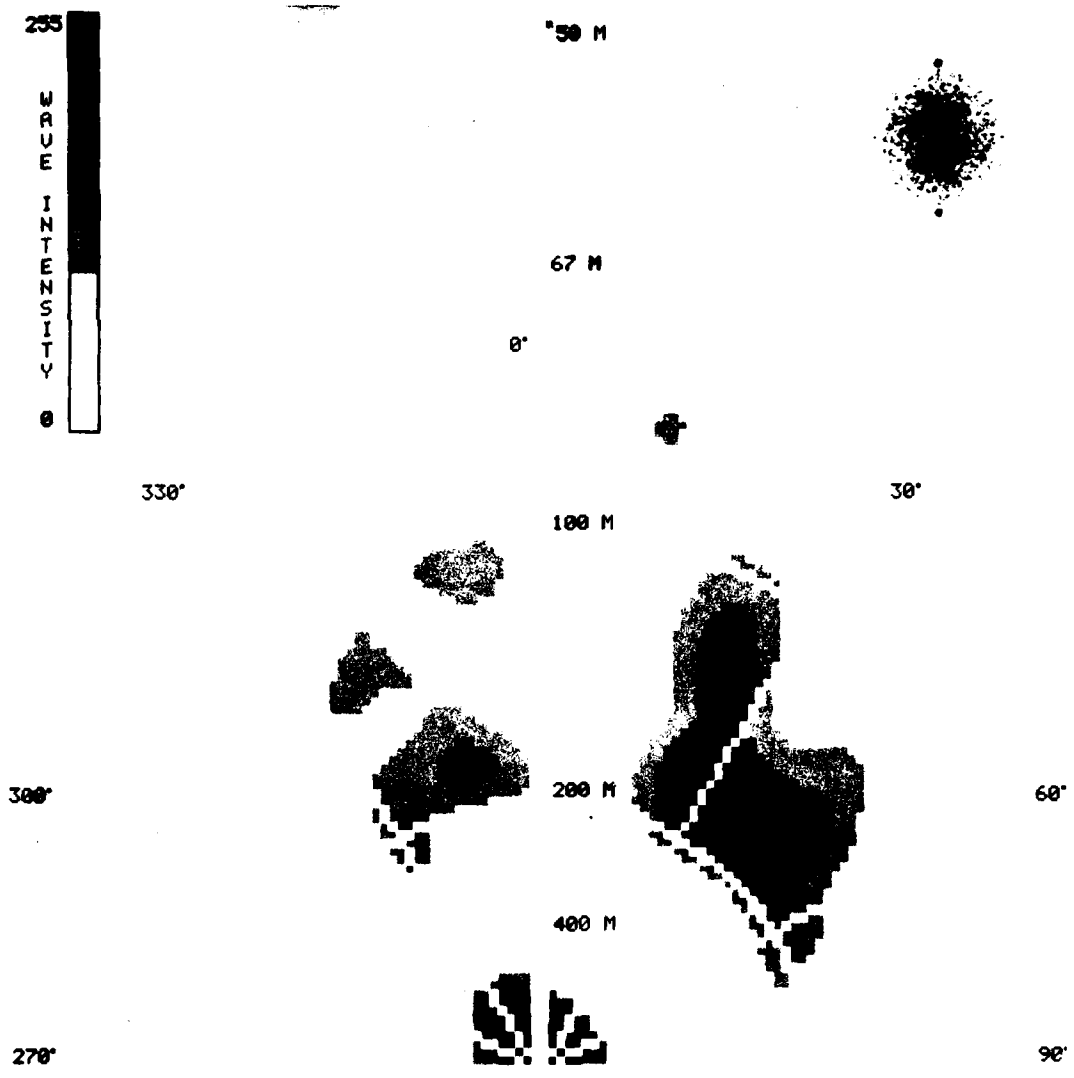

Fig. 4 Typical SEASAT SAR ocean wave spectrum.

waves propagating at an angle of 30° is depicted. The power spectrum in the upper right-hand corner is an 8X minification of the SMIPS/VICAR FFT data that were computer enhanced to produce the ocean wave spectrum. The graphic overlay and image combinations were accomplished with the Comtal, and the 512 by 512 pixel negative was produced using the Optronics P-1700.

FUTURE PLANS

The APL Space Department expects to continue using the IPL in 1982 for the analysis and display of SAR oceanographic data. Color illustrations for a special SEASAT SAR issue in the *Journal of Geophysical Research* will be produced on the Matrix camera during January 1982.

A 16 mm color movie, also planned for the first part of the year, will display SAR imagery recorded during September of 1978 (SEASAT orbit 1339) along a track extending from the Bahama Islands to the mouth of Chesapeake Bay. Ocean wave spectra will be calculated along the satellite track using the SMIPS/VICAR software on the IBM 3033MP computer. Image processing software will be developed on the PDP 11/70 computer to produce the movie on the Dicomed D48C recorder.

During the second half of 1982, it is expected that optical SAR data obtained by the second flight of the Space Shuttle, Columbia, will be acquired by the Space Department and analyzed using the resources of the IPL. Significant results will be reported during the September 1982 meeting of the International Society for Photogrammetry in Ottawa.

REFERENCES

[1] H. D. Pixler, *APLnet (System Description)*, JHU/APL BCS-1-021, BCE-T-1018 (Mar 1981).

[2] R. C. Beal, A. D. Goldfinger, D. G. Tilley, and W. J. Geckle, *Calibration Strategies for Spaceborne Synthetic Aperture Radar*, JHU/APL CP 084 (Dec 1981).

[3] R. C. Beal, P. S. DeLeonibus, and I. Katz, eds., *Spaceborne Synthetic Aperture Radar for Oceanography*, No. 7 of the Johns Hopkins Oceanographic Studies, Johns Hopkins University Press, Baltimore (1981).

[4] A. D. Goldfinger, R. C. Beal, and D. G. Tilley, "Optimal Spatial Filtering and Transfer Function for SAR Ocean Wave Spectra," *Proc. Fifteenth International Symp. on Remote Sensing of the Environment*, Ann Arbor, Mich. (May 1981).

[5] R. C. Beal and D. G. Tilley, "Optimal Spatial Filtering and Transfer Function of SAR Ocean Wave Spectra," *Proc. Third SEASAT SAR Workshop on SAR Quality*, Frascati, Italy (Dec 1980).

[6] R. C. Beal, "The Potential of Spaceborne Synthetic Aperture Radar for Oceanography," *Johns Hopkins APL Tech. Dig.* 1, No. 2, 148-156 (Apr-Jun 1980).

This work was supported by Indirectly Funded R&D.

DATA SET ACCESS CONTROL

D. G. Sager

There are controls to protect data sets from access in an unauthorized manner or by unauthorized persons. To be accepted and used, the controls should be transparent to the user, they should not hinder the sharing of data sets, they should be easy to maintain, and they should perform well. The data set access control facility described here was developed by APL to meet these objectives.

BACKGROUND

In 1976, the IBM Corporation announced the availability of the Resource Access Control Facility (RACF) program for the Multiple Virtual Operating System (MVS). RACF was designed to provide access controls for computer-related resources such as data sets, tape volumes, disk volumes, and interactive terminals. However, the data set access control facility proved to be difficult to use and manage, and it generated considerable computer overhead. Its data set access controls require that a profile be constructed for every data set to be protected. The profiles reside in the RACF data base and contain information about how the data set may be accessed.

The many data sets in a computing center as large as the Frank T. McClure Computing Center of APL make such a facility unworkable. At the McClure Computing Center, more than 500 permanent data sets are created each day, over 16,000 data sets reside on high-speed disk volumes, over 32,000 reside on slower mass storage volumes, and over 150,000 reside on tape as part of the Computing Center Archive Facility. To use the RACF data set access control facility would require nearly 200,000 data set profiles to be created initially and over 500 more to be added each day. The profiles would have to be maintained and updated either by computing center personnel or by the users themselves. The scope of such an endeavor is mind-boggling. The education and personnel resources required would be more than could be expended. It was therefore decided to use the RACF framework but to develop our own data set access control facility.

DISCUSSION

RACF allows an installation to tailor the access control facility to meet its own needs by providing exits both before and after major functions are performed. These exits must be written by the installation and may

be used to control the function. The APL data set access control facility was designed and implemented to use only the provided exits, and the standard IBM program code was not modified.

Instead of using a RACF data set profile to determine the access authorization for a data set, the authorization can be inferred from the access allowed to an alternate entity. The alternate entity, in this case, was chosen to be the data set qualifier. A data set qualifier is defined as the first 1 through *n* nodes of a data set name, where *n* is the total number of nodes in the data set name. For example, the data set name GROUP.USER.PROJECT.SUBPROJ.DATA has five data set qualifiers. Listed in order of most specific to least specific, the qualifiers are:

GROUP.USER.PROJECT.SUBPROJ.DATA,
GROUP.USER.PROJECT.SUBPROJ,
GROUP.USER.PROJECT,
GROUP.USER, and
GROUP.

The APL data set naming conventions are well suited to such an implementation for access control because a data set name unambiguously identifies the owner of the data set. The naming conventions state:

1. A data set name is a character string (maximum of 44 characters) composed of nodes (maximum of eight characters per node) separated by periods.
2. A data set name must have at least three nodes but no more than eight.
3. The first node (high-level index) must identify the Laboratory group or the outside organization that owns the data set.
4. The second node must identify the user or the project responsible for the data set. If the data set is of group scope, such as a group load module library, the second node should be the same as the first.
5. The third and subsequent nodes may be chosen by the owner and should describe the contents or function of the data set.

The access control facility protects data sets by limiting access to them; that is, it permits only authorized users to perform authorized actions, such as reading or writing. All accesses to data sets are entered in a journal, and security variances can be identified. All data sets are protected by default. The owner of a data set has the responsibility for determining who is authorized to access the data set and how they may access it. Rules are created by the data set owner and enforced by the access control facility.

Each user of the McClure Computing Center has a rule (or a set of rules) that governs the access to his data sets. Two types of access rules may be defined: specific and universal. A specific rule is one by which a user or group (Laboratory group or outside organization) is given a particular type of authority to access a data set or a collection of data sets. A universal rule is one by which all users are given a specified access authority. Access to a data set for which no specific rule has been defined is governed by the universal rule for that data set. Similarly, if a user is not explicitly named in a specific access rule for a data set, his access to that data set is governed by the universal rule.

When a user's account is established initially, a universal access rule is defined that allows no one but himself to access any of his data sets. The user may change his universal access rule, and he may define additional universal and/or specific rules for any of his data sets.

The access authorities supported are hierarchical in structure; that is, a granted authority permits access at all lower authorities. The authorities that can be specified in either universal or specific access rules are:

ALTER - Authorization is granted for complete control over the data set including the ability to create, delete, and rename the data set.
UPDATE - Authorization is granted to read or write the data set.
READ - Authorization is granted to read the data set.
CONTROL - Authorization is granted to execute a load module from the data set.
NONE - All access is denied.

Access rules associate data set qualifiers with user or group identifiers and levels of authority. The search for a data set qualifier that governs the access for a particular data set starts with the entire data set name (most specific qualifier) and proceeds to each shorter qualifier until either an access rule is found for that qualifier or the data set name is depleted. Thus, if more than one access rule could apply, the one with the most specific qualifier will be used. Once an access rule for a qualifier of the data set is found, access will be determined by either the specific rules or the universal access authority for that qualifier.

Example 1

If user SMITH in group ZZZ wants to allow all of his data sets to be read but would like to prohibit access to data sets with the qualifier ZZZ.SMITH.PROJA, then the following universal rules would be required:

Data Set Qualifier	Universal Access Authority
ZZZ.SMITH	READ
ZZZ.SMITH.PROJA	NONE

If user SMITH subsequently wants to permit all users in group XXX as well as user JONES to read data sets with the qualifier ZZZ.SMITH.PROJA, then the following specific rules would have to be established:

Data Set Qualifier	Access Authority	Userid or Groupid
ZZZ.SMITH.PROJA	READ	XXX
ZZZ.SMITH.PROJA	READ	JONES

Example 2

If the manager of project PROJA within group AAA wants to allow all the members of groups AAA and BBB to have ALTER authority to the data sets of PROJA, then the following rules would be required:

Data Set Qualifier	Universal Access Authority
AAA.PROJA	NONE

Data Set Qualifier	Access Authority	Userid or Groupid
AAA.PROJA	ALTER	AAA
AAA.PROJA	ALTER	BBB

If, in addition, the project manager wants to grant user SMITH in group CCC authority to READ the data set AAA.PROJA.MASTER, then the following rules would be required:

Data Set Qualifier	Universal Access Authority
AAA.PROJA.MASTER	NONE

Data Set Qualifier	Access Authority	Userid or Groupid
AAA.PROJA.MASTER	ALTER	AAA
AAA.PROJA.MASTER	ALTER	BBB
AAA.PROJA.MASTER	READ	SMITH

CONCLUSION

The API data set access control facility has been written and implemented. It is both automatic and transparent to the user. All data sets are protected automatically and may be shared with other users in accordance with rules the owner can establish. The facility has proven to be easily managed, and the incurred overhead is low. The McClure Computing Center currently has over 2000 registered users and more than 200 defined groups. Fewer than 1500 data set qualifier profiles had to be created to control access to the 200,000 data sets.

REFERENCE

[1] *OS/VS2 MVS Resource Access Control Facility (RACF): General Information Manual*, SC28-0722, IBM Corp. (Apr 1978).

This work was supported by Indirectly Funded R&D.

A LOCAL COMPUTER NETWORK FOR APL

**H. D. Pixler, M. D. Lasky, D. Brocklebank,
B. W. Ballard, R. W. Rumsey, R. R. Potter, and S. M. Schaaf**

APLnet, a network based on a generic and user-transparent architecture, has been developed to connect the many computers at APL. This high-data-rate digital communication system is designed to connect dissimilar computers in order to share computer resources and functions in a common framework.

Currently, the network includes the IBM 3033MP and several Digital Equipment Corp. (DEC) minicomputers. System-level software programs have been developed by APL to control the input and output across the network and to provide a system that is easy to use. A technology transfer has been negotiated with Network Systems Corp. to make the APL DEC modifications available commercially.

BACKGROUND

Computer systems such as the IBM 3033MP, DEC PDP-11/70, and PDP-11/55 can handle, internal to each system, large numbers of reliable data transfers at high data rates. However, when data must be transferred at high rates between dissimilar computers or when the distance between similar equipment is greater than 200 ft, additional hardware and software are required. In the past, wide-bandwidth data communications between dissimilar computer architectures required links that were both very expensive and technically difficult to implement and use.

A local network was needed in order to meet APL's requirements for image processing, large database transfers, advanced graphic processing, and sharing of resources.

DISCUSSION

The goal in the development of APLnet was to provide a user-oriented, high-performance, local computer network, using standard software and hardware where possible. This goal was realized through the use of DIGITAL Network Architecture (DNA) as a common framework for the network software and the commercially available HYPERchannel as the communications hardware.

DNA is a "layered" network architecture, each layer defining a distinct set of functions as well as rules for implementing those functions. Figure 1 shows the relationship between the layers of DNA. This architecture has been implemented by APL engineers for the IBM 3033 computer and by DEC as DECnet for most of its computers.

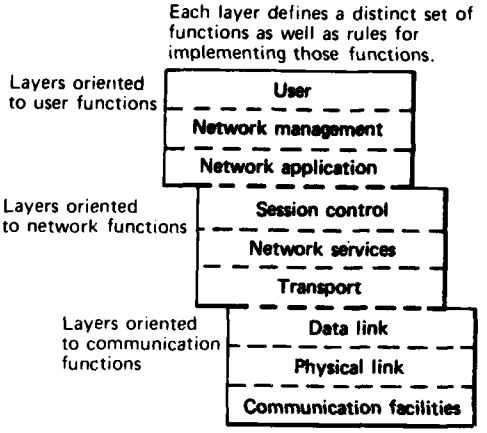

Fig. 1 DIGITAL Network Architecture (illustration from DEC).

DECnet, a seasoned network implementation with consistent and simple user interfaces, provides the following services:

1. Task-to-task communications,
2. Remote file access and transfer,
3. Remote terminal facilities, and
4. Network maintenance and management tools.

The use of DECnet software minimized the task of developing well-documented user-oriented network software. While it was necessary for APL to enhance the software to support HYPERchannel, the modifications are transparent to the DECnet user.

HYPERchannel provides a general-purpose, high-speed data communications path between multiple computers that may be separated by as much as 5000 ft. Connections are made to HYPERchannel's coaxial transmission trunks via intelligent network adapters that buffer data, route messages, and detect and correct errors. Adapters are available to connect almost any computer to HYPERchannel through standard input/output (I/O) interfaces or channels. Each adapter supports the maximum data transfer rate of the I/O device with which it interfaces; the transmission rate between adapters is 50 million bits per second. The use of commercially available HYPERchannel communications hardware for APLnet eliminated the need for special-purpose hardware.

The initial APLnet hardware configuration included three DEC PDP-11 computers and the IBM 3033 (Fig. 2). (Development of software to support the future VAX computer is now under way.) The software to support the initial APLnet configuration fell into two categories: PDP-11 software in support of the HYPERchannel hardware, and 3033 software to replicate DECnet functions.

The PDP-11 software consists of two modules, HCP and HY, which fit into the DECnet structure as shown in Fig. 3. HCP implements the HYPERchannel protocol, which was defined as a modification of the digital data communications message protocol of DNA, to ensure delivery and sequentiality of messages. HY performs low-level physical control of the HYPERchannel hardware. The PDP-11 development effort also in-

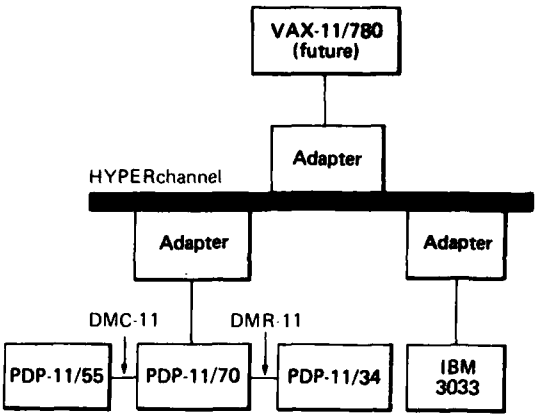

Fig. 2 Initial configuration of APLnet hardware.

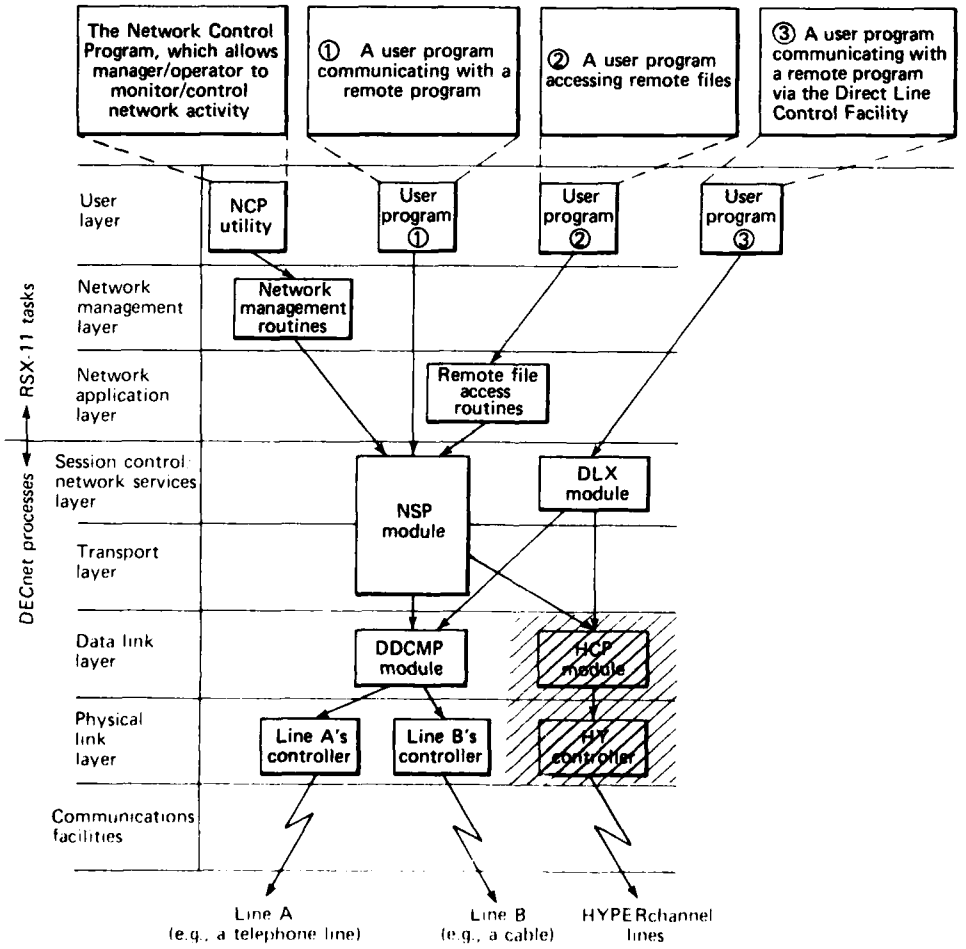

Fig. 3 Vertical interaction of DECnet software modules, with HYPERchannel support (illustration from DEC).

cluded modification of the DECnet generation procedure that directs the configuration of DECnet software for a particular node. The procedure also was modified to support the HYPERchannel software modules.

APLnet software developed for the 3033 includes the HCP protocol and device control, the session control, and the XRNET facility, which allows network access to the 3033 files. This software makes use of the shared variable manager (SVM) to mediate its communications with user tasks. SVM was developed at APL to provide a standard mechanism for intertask communications in the operating system environment. Figure 4 shows the structure of the IBM APLnet software.

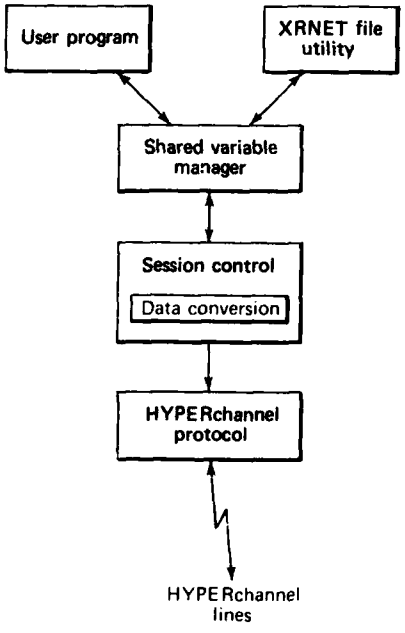

Fig. 4 Structure of IBM APLnet software.

The HCP protocol and device control module implements the same HYPERchannel protocol as its PDP-11 counterpart. It also interacts with the operating system to provide physical control of the HYPERchannel adapter.

Session control implements the user interface to the IBM APLnet software, allowing the IBM user to submit requests for network functions and to receive responses. A generalized data conversion facility, implemented under session control, allows the IBM user to request the conversion of data from one machine representation to another, on transmission to and/or reception from a remote node.

A common language interface has been developed for the IBM APLnet software. It is compatible with the popular IBM programming languages APL, Fortran, PL/1, and Assembler.

XRNET is a utility program that functions as a user task in the 3033. It makes use of the APLnet modules described above to provide remote access to data files stored in the 3033.

CONCLUSION

The APLnet system currently provides intercomputer communications for DEC and IBM computers via HYPERchannel. HYPERchannel adapters are available from most major vendors. The software needed in order to add other vendors' computers to APLnet can be developed by means of the DNA model.

This work was supported by NAVSEASYSCOM.

GENERALIZED FULL-SCREEN INPUT PROCESSOR

B. J. Pride and R. R. Potter

If the question were asked, "What is the single most-time-consuming programming job that returns the least for the investment in time?" many programmers and data processing managers would answer, "Data maintenance programs." To reduce the development time of database applications, a generalized package of maintenance software was conceived, designed, and implemented.

BACKGROUND

Several years ago, the Frank T. McClure Computing Center at APL installed a database management system (DBMS), a set of computer programs that provides an environment for organizing, storing, retrieving, and securing data. This DBMS, called INQUIRE,[1] provides an easy-to-use English-like language for report generation as well as the usual data organization functions. Reporting needs can be satisfied quickly and easily with minimal involvement of data-processing professionals. But data processing had to be very much involved with writing maintenance programs (programs that maintain the accuracy and currency of the data in a database). A database application that could be designed, be implemented, and have reporting functions completed in a matter of days would sometimes be held up for months while a data-maintenance program was written and tested.

Generalized, on-line data maintenance is a relatively new concept; the number of commercially available software packages that perform this function are relatively few. Those that are available are generally specific in terms of th· file structures or DBMS's they will support. All these factors led to the development of a generalized maintenance processor for INQUIRE databases.

DISCUSSION

The goal was to design computer software that would not only be easy to use but would also be comprehensive enough to handle a wide variety of database applications. It was desired to keep the level of complications low so that even people with little data-processing background could use the programs readily.

The result was a package called the Generalized Full-Screen Input Package (GFSIP). GFSIP is a data-maintenance tool with two basic functions: provide the mechanism for designing electronic input forms and change databases based on those forms. Usually two types of people use GFSIP, the form designer (most often the database administrator or systems analyst of a database project) and data-entry personnel (clerical, secretarial, etc.).

The form designer virtually "draws" a picture on an IBM 3270 series cathode ray tube (CRT) screen of how he would like the form to look. In this drawing, he can include line titles, column headings, etc. to clarify the purpose of the form and the type of information to be entered. He indicates with "field markers" (Fig. 1) where information from the database will be placed on the form and also what information from the database corresponds to which markers. This is all he has to do to create a form layout. The physical location of data on the form (row and column) is determined automatically by the form processor program, and all the physical attributes of the data (length, type, and validation criteria) are extracted from the APL/Data Dictionary System.[2] Therefore, the form designer need not be concerned about the actual screen locations of data and does not have to duplicate the information already known by the system.

Once the form is designed, data-entry personnel can use it immediately. The form is called up by the data processing program, and the terminal operator can request to add, update, or delete database records via a processing selection menu (Fig. 2). If the operator wishes to add records, he selects the appropriate option, and a blank form is displayed on the screen. He then types in all or any part of the requested information.

```
CMD: _                    INQUIRE FULL SCREEN FORMATTER     PANEL: SAMPLE SCREEN

NAME:  @01                        @02

HOME ADDRESS: @03

PHONE NUMBER: @04

_ _ _ _ _ _ _ _ _ _ _ _ _ _ _ _ _ _ _ _ _ _ _ _ _ _ _ _ _ _ _ _ _ _ _ _ _ _ _ _ _

 CV  NAME      S  K  TITLE          CV  NAME      S  K  TITLE
 @01 LASTNAM   1  M  LAST NAME:    @02 FIRSTNAM1
 @03 ADDRESS   _  _  _             @04 PHONE     _  _  _
```

Fig. 1 Example of form design. The field markers begin with @. The table below the dashed line relates field markers to database fields.

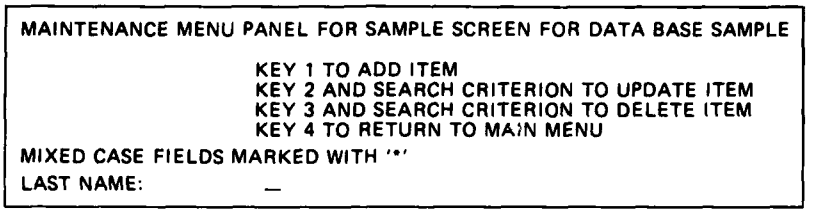

Fig. 2 Sample processing-selection menu.

When he is satisfied with the information he has entered, he depresses the ENTER key, and the information is added to the database.

If, by chance, he enters the information incorrectly, the program, using validation criteria from the APL/Data Dictionary, notifies him of the errors and allows him to make corrections before the database is modified. In this way, many data entry errors can be prevented, and the database is a more reliable source of information.

When the operator wishes to change or delete records in the database, he specifies the criteria the records must satisfy (such as records for "employee Jones" or for "part number 123"). Qualifying records are displayed on the form (one at a time), and the operator can change information by simply typing over the old information or he can verify the record for deletion. Changed information is still subject to validation, so errors are prevented.

METHOD

GFSIP is a combination of computer software written in the PL/I programming language and a set of INQUIRE databases. It combines the electronic "form-fill-in" capability of the IBM 3270 series (or compatible) CRT terminal with the data definition information stored in the APL/Data Dictionary System to provide an easy-to-use mechanism for changing an application database and to ensure the accuracy of the data.

The forms are sorted in an INQUIRE database, which links the two processor programs. The forms can be created or changed and used immediately since the processor interprets the form at execution time. This means that

1. The forms always have access to the most current data definitions and validation,
2. New features in the processor are immediately applicable to all existing forms,
3. The form designer does not have to know job-control language or linkage editor controls, and
4. Data-entry personnel do not have to know or understand the operating environment.

CONCLUSION

The generalized screen processor benefits many types of people. It gives the screen designer an opportunity to experiment in real time with new ideas for data-entry screens. It relieves programmers of a large portion of database maintenance programs. The database administrator benefits from the reduction in turnover time. The data-entry operator has a simple way to maintain a database, and the skills learned for one database application can be transferred to the next without retraining. In short, GFSIP spells productivity.

REFERENCES

[1] *INQUIRE Concepts and Facilities*, Infodata Systems Inc. (Dec 1977).
[2] B. J. Pride, *Applied Physics Laboratory Data Dictionary System (APL/DDS)*, JHU/APL BCS-1-100-79 (1 Oct 1979).
[3] R. R. Potter and B. J. Pride, *Generalized Full Screen Input Package (GFSIP)*, JHU/APL BCS-1-018-80 (12 Jun 1980).

This work was supported by NAVSEASYSCOM.

BIOMEDICAL SCIENCE AND ENGINEERING

INTRODUCTION

The collaborative biomedical program between the Applied Physics Laboratory and The Johns Hopkins University's School of Medicine began in 1965. The program brings together the expertise in medical and biological sciences found at the Medical School with that in the physical sciences, engineering, and mathematics found at APL, in order to solve significant problems in biomedical science and health care delivery. From the beginning, this collaboration has received strong support from the University's leadership and encouragement from the Navy, APL's principal sponsor. The strength of the collaboration is evidenced by the joint appointments made within the two University divisions: 17 members of the APL staff have appointments at the Medical School, and 16 members of the medical faculty have Principal Staff appointments at APL.

Currently there are active projects in ophthalmology, neurosensory research and instrumentation development, cardiovascular systems, patient monitoring, therapy and rehabilitation, clinical information systems, clinical engineering, and biomedical image analysis. Fifty-six APL physical scientists and engineers are working in collaboration with 50 medical school biomedical scientists and clinicians on these projects. Their research and development results are published in the peer-reviewed scientific and medical literature. Since the program's inception, over 250 papers have been published, and there are even more published abstracts and presentations at major scientific and medical meetings.

The articles selected for this year's *Accomplishments* indicate the breadth of the collaborative biomedical effort. In ophthalmology, there is an article describing how the scattering of polarized light at small angles can be used to obtain information about the ultrastructure of the cornea. Part of the neurosensory research effort is described in an article on the responses of two types of nerve fibers following a mild burn to the hand. Cardiovascular research at the Medical School on control of arterial blood pressure and flow has been aided by the microprocessor-controlled blood pump described in the third article. As a result of the effort in clinical information systems, there is an article describing a generalized computer network for hospital record-keeping. The final article describes an audio filing system for the blind that combines a personal computer with a low-cost cassette tape recorder.

STRUCTURAL IMPLICATIONS OF SMALL-ANGLE LIGHT SCATTERING FROM THE CORNEA

R. L. McCally and R. A. Farrell

We have used the scattering of polarized laser light at small angles, together with measurements of corneal birefringence properties, to deduce characteristics of the cornea's lamellar structure. We have shown that such scattering depends on the lamellar waviness that occurs whenever the tension on the constituent collagen fibrils is reduced and that the lamellae of central rabbit and bovine corneas have preferred orientations.

BACKGROUND

The cornea is the transparent window in the wall of the eye through which we see. The corneal stroma, which concerns us in this article, is sandwiched between two thin cellular layers. It accounts for 90% of the cornea's thickness. The stroma is made up of about 200 stacked sheets, called lamellae, each about 2 μm thick. These lamellae are composed of cylindrical collagen fibrils embedded in a ground substance. The 20-nm-diameter fibrils lie parallel to one another within each lamella and make large angles with those in adjacent lamellae.

Healthy corneas scatter very little light. Indeed, about 98% of red light and 90% of blue light pass undeviated through a rabbit cornea. Nevertheless, the characteristics of this scattering are quite sensitive to the arrangement of the structural elements that scatter the incident light. Several years ago, we recognized that measurements of scattering properties can be used to test the predictions of the various proposed models of stromal structure and to deduce structural features.[1,2]

In the beginning, we used the wavelength dependence of the scattering of unpolarized light to deduce characteristics of the distribution of the collagen fibrils about one another in the lamellae.[1,2] Those findings were of basic physiologic importance because they related the basic structure of the corneal stroma to one of its major functional properties—transparency. In this report, we discuss our recent use of the scattering of polarized light at small angles and our measurements of the cornea's birefringent properties to probe the characteristics of its lamellar structure.[3,4] We have shown that polarized light scattering at small angles depends on the lamellar waviness that occurs whenever the tension in the constituent collagen fibrils is relaxed and that the lamellae of central rabbit and bovine corneas have preferred orientations. These findings should provide a better understanding of the cornea's mechanical properties.

DISCUSSION

In the small angle light scattering (SALS) method,[3,4] the tissue is illuminated by a collimated beam of polarized light from a laser, and light scattered with polarization either parallel ($I_\parallel$ configuration) or perpendicular ($I_\perp$ configuration) to that of the incident beam is observed at scattering angles of less than 5°. This scattered light forms characteristic patterns like the cloverleaf $I_\perp$ pattern in Fig. 1a. Previous attempts by other investigators to interpret these patterns in terms of structures known histologically had not been fruitful.[5,6]

Early in our investigations of corneal SALS, we noted that standard electron micrographs of the cornea showed that the corneal lamellae undulated in a quasiperiodic fashion with a mean wavelength of about 14 μm. We were told by J. Francois (private communication) that these undulations disappeared if the cornea was fixed for microscopy with an applied transcorneal pressure. Suspecting that the undulating lamellae might somehow act like a diffraction grating and thereby produce the lobed SALS patterns, we performed experiments that confirmed that the SALS pattern disappeared if a transcorneal pressure equal to the normal intraocular pressure was applied (Fig. 1). Subsequently, we confirmed that the lamellae did straighten if the corneas were fixed with an applied pressure.[4] Because of this evidence and the fact that the angular position of the intensity maxima in the patterns is consistent with a Bragg spacing of 14 μm, we concluded that the quasiperiodic waviness of the lamellae was the histological feature responsible for the corneal SALS patterns.[4] The theory of SALS,[7] recently completed at APL, removes the mystery of exactly how the lamellar undulations act like a diffraction grating. It also aided other structural interpretations in Ref. 4, discussed below.

The transmission through the cornea in the $I_\perp$ configuration, as well as the appearance of the $I_\perp$ SALS patterns, varies periodically as the polarization direction of the incident light is rotated. The data in Fig. 2 show that the transmission maxima and minima are 45° apart and that their angular positions remain fixed as the transcorneal pressure is varied. The most distinct SALS patterns, like those in Fig. 1, are observed at the minimum $I_\perp$ transmission setting, which, we found, bears a fixed relationship to overall corneal geometry. At the setting that produces maximum transmission, the patterns are blurred and indistinct (Fig. 3).

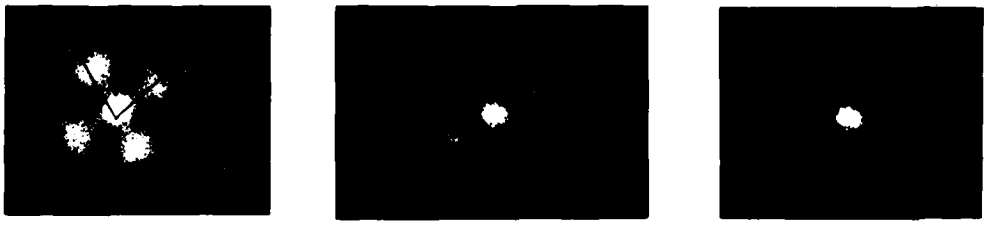

Fig. 1 The effect of increasing transcorneal pressure on the $I_\perp$ scattering from rabbit cornea. The outer lobes define the axes shown by the arrows. Experimentally, we find that these axes coincide with the polarizer and analyzer directions that, here, are aligned to produce minimum $I_\perp$ transmission. The true scattering angle is shown on the first plate. Each plate received the same photographic exposure and processing.

In Ref. 4, we used the manifestations of corneal birefringence illustrated by Figs. 2 and 3 to deduce characteristics of the orientation of the corneal lamellae. We argued that the lamellar orientations could not be random; rather, the lamellae must be oriented in either one preferred direction or two preferred directions at right angles, and that they are superimposed on a random background of lamellar orientations.[4] Specifically, in bovine corneas the preferred lamellar orientations are either at 45°, 135°, or both to the long axis of the ovoid-shaped cornea. In rabbit corneas, they are at 45°, 135°, or both to a line drawn from the center of the cornea to the midpoint of the slightly flattened portion of the limbus. (The limbus is the region where the clear cornea blends into the white sclera.)

The distribution of lamellar orientations must determine, at least in part, the mechanical properties of the cornea. The cornea's curvature, which provides 75% of the eye's refractive power, is determined by these properties; thus, our research could lead to a better understanding of the basis of corneal curvature. In addition, the relationship that we found between the tension on the collagen fibrils and corneal SALS could be exploited to devise an optical method for monitoring wound strength after the fibrils are cut in corneal surgery.

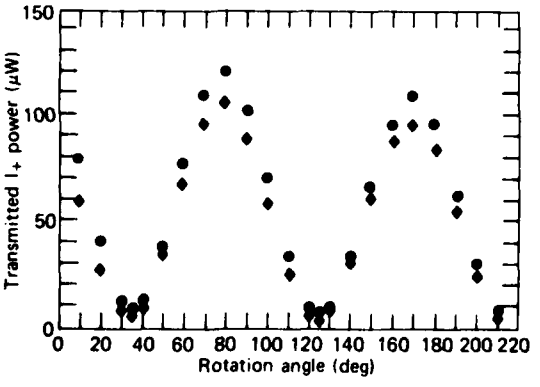

Fig. 2 The variation of transmitted $I_\perp$ power (for the same cornea as in Fig. 1) as a function of the polarization direction of the incident beam. The circles are at zero transcorneal pressure; the squares are at 18 mmHg pressure.

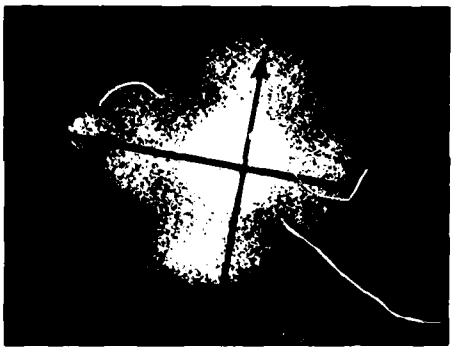

Fig. 3 The zero pressure $I_\perp$ scattering pattern at the maximum $I_\perp$ transmission setting for the same cornea as in Fig. 1. The photographic exposure and processing are the same as in Fig. 1.

REFERENCES

[1] R. A. Farrell, R. L. McCally, and P. E. R. Tatham, "Wavelength Dependencies of Light Scattering in Normal and Cold-Swollen Rabbit Corneas and their Structural Implications," *J. Physiol.* **233**, 589-612 (1973).
[2] R. A. Farrell and R. L. McCally, "On Corneal Transparency and its Loss with Swelling," *J. Opt. Soc. Am.* **66**, 342-345 (1976).
[3] R. L. McCally and R. A. Farrell, "Effect of Transcorneal Pressure on Small-Angle Light Scattering from Rabbit Cornea," *Polymer* **18**, 444-448 (1977).
[4] R. L. McCally and R. A. Farrell, "Structural Implications of Small-Angle Light Scattering from Cornea," *Exp. Eye Res.* **34**, 99-114 (1982).
[5] E. P. Chang, D. A. Keedy, and J. C. W. Chien, "Ultrastructure of Rabbit Corneal Stroma: Mapping of Optical and Morphological Anisotropies," *Biochim. Biophys. Acta* **343**, 615-626 (1974).
[6] F. A. Bettelheim and R. Magrill, "Small-Angle Light Scattering Patterns of Corneas of Different Species," *Invest. Ophthalmol.* **16**, 236-240 (1977).
[7] R. H. Andero and R. A. Farrell, "Calculated Corneal Small-Angle Light Scattering Patterns: Wavy Fibril Models," *J. Opt. Soc. Am.* (in press).

This work was supported by the National Eye Institute Grant EY01019.

NEURAL MECHANISMS OF HYPERALGESIA

R. A. Meyer (APL) and J. N. Campbell (JHMI)

Pain sensation is coded by signals in a specific group of peripheral nerve fibers. The increase in pain sensitivity (called hyperalgesia) following a burn to the skin is signaled by the increased responsiveness of a subset of these nerve fibers.

BACKGROUND

Anyone who has burned himself on the stove knows that such an injury to the skin often alters the pain sensibility at the site of the injury. This hyperalgesia is characterized by spontaneous pain and a decrease in pain threshold. Stimuli that before the burn were not painful (e.g., gentle warming or light touching) can be quite painful after the burn. Hyperalgesia is believed to be the result of an increased responsiveness (called sensitization) of the receptors of the peripheral nerve fibers responsible for pain sensation.

In the past, it was thought that there was only one class of nerve fiber that coded for burning pain sensation.[1-4] These nociceptive afferents (a general term for nerve fibers responsive to injurious stimuli), have relatively slow nerve impulse conduction velocities, in the range 0.5 to 2.0 m/s, and are called C-fibers. The thermal threshold for neural activity in these C-fibers occurs at a temperature near the pain threshold in man (i.e., about 45°C, which is about 12°C above skin temperature), and the slow conduction velocities of the C-fibers are consistent with the long latency to burning pain sensation in man. Recently we described another group of nociceptive afferents that are responsive to intense heat stimuli.[5] They have conduction velocities ranging from 5 to 55 m/s and therefore are classified as A-fibers. Although their initial thermal thresholds are typically greater than 50°C, those thresholds are significantly reduced following exposure to intense heat stimuli.

In this study, monkey C-fibers and A-fibers and human subjects were exposed to a series of thermal stimuli before and after a 53°C, 30-s burn to the glabrous skin of the hand (i.e., nonhairy skin, such as the palm). The burn resulted in increased sensitivity of the A-fibers, decreased sensitivity of the C-fibers, and increased pain sensibility in human subjects. Thus, A-fiber and not C-fiber nociceptive afferents appear to code for the hyperalgesia that follows a burn.[6]

METHODS

This research is based on comparing the subjective judgments of pain in human subjects with the recorded neural responses of single nociceptive afferents in monkey. The human subjects and the receptive fields of the nerve fibers under investigation were exposed to an identical sequence of test stimuli before and after a 53°C, 30-s burn. A laser thermal stimulator developed at APL[7] provided step increases in skin temperature over a 7.5-mm-diameter spot. The first stimulus of the test sequence was always 45°C, and the remaining nine stimuli of the test sequence were presented in random order and ranged from 41 to 49°C in 1°C increments. The stimuli were of 3-s duration and were delivered every 30 s. Test sequences were presented according to the following schedule: test, 10-min rest, test, 5-min rest, burn, 10-min rest, test, 10-min rest, test.

Human subjects were instructed to assign an arbitrary number (the modulus) to the magnitude of pain associated with the first stimulus (45°C) of the first test sequence. Subjects judged the painfulness of subsequent stimuli relative to this modulus.[8] Nonpainful stimuli were assigned a value of zero.

Standard techniques[1,6] were used to record from single peripheral nerve fibers of the anesthetized monkey. Only fibers whose receptive fields were restricted to the glabrous skin were considered.

RESULTS

The mean responses of the C-fibers, A-fibers, and human subjects before and after the burn are shown in Fig. 1. To compare the various responses, the data were normalized by dividing the response to a given stimulus by the response to the first 45°C stimulus. After the burn, the skin of human subjects became hyperalgesic within minutes, and pain was present even without stimulation. As shown in Fig. 1a, the threshold for pain decreased significantly; the 41°C stimulus, which before the injury was barely detected, was more painful after the injury than was the 49°C stimulus before the injury. The magnitude of pain also increased significantly. Stimuli that were only slightly painful before the burn became much more painful afterward; the mean rating for the 49°C stimulus increased to four times its value before the burn.

A-fibers gave only a meager response before the burn; however, after the burn their response was greatly enhanced. Their response threshold decreased significantly and their response to the more intense stimuli increased. In addition, some of the A-fibers developed spontaneous activity. In contrast, the activity in the C-fibers was suppressed following the burn; their thresh-

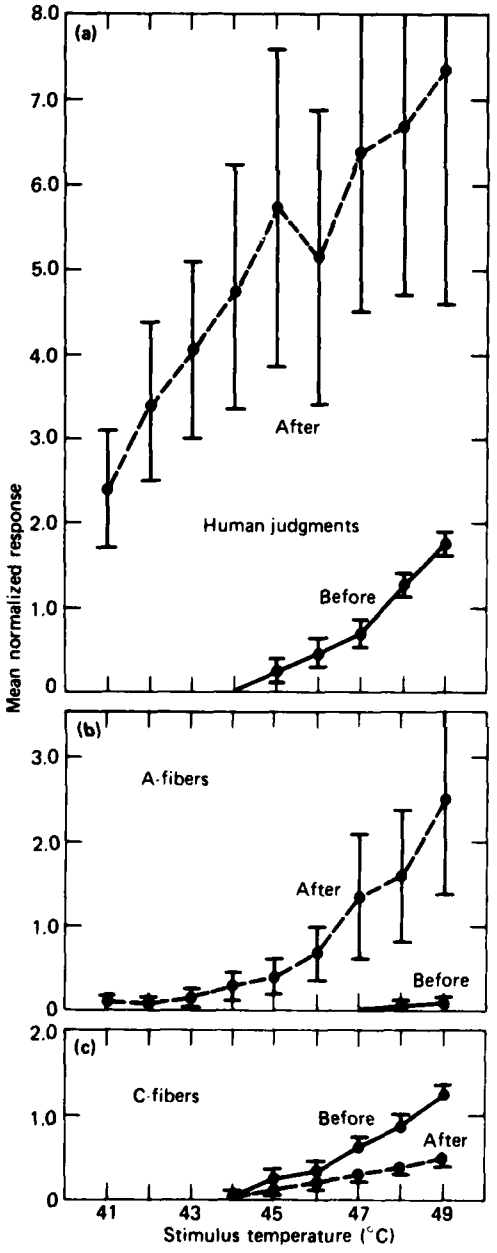

Fig. 1 Normalized response of human subjects, A-fibers, and C-fibers to thermal test sequence before and after a 53°C, 30-s burn to the hand; (a) human judgments of pain (N = 8), (b) responses of A-fibers (N = 14), (c) responses of C-fibers (N = 15). The burn resulted in increased pain sensation (hyperalgesia) in human subjects and an enhanced response (sensitization) of the A-fibers. In contrast, the burn resulted in a decreased response of the C-fibers.

old for neural activity was increased and the response to the more intense stimuli decreased. Thus, the A-fibers appear to code for hyperalgesia in man.

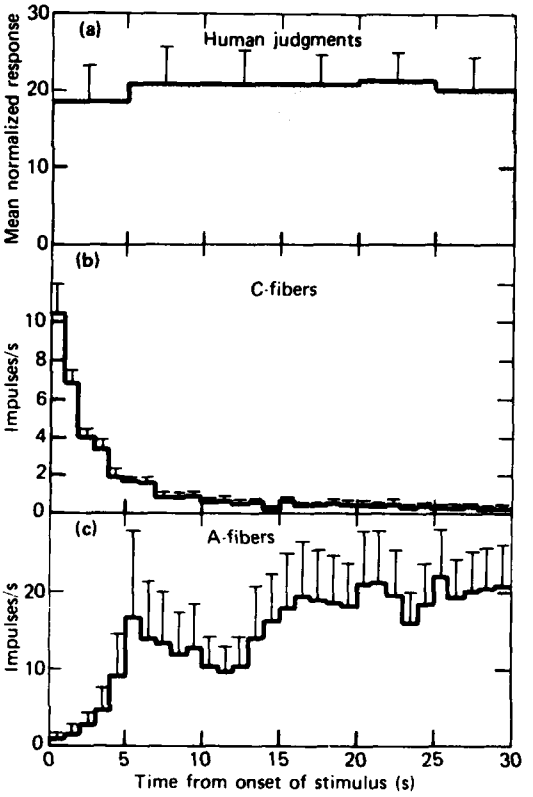

Fig. 2 Histogram of the responses during the burn for the human subjects (N = 8), the C-fibers (N = 15), and the A-fibers (N = 14). The pain was intense throughout the stimulus. The C-fibers exhibited a large response at the beginning of the stimulus that quickly diminished to a low rate within 5 s. In contrast, the A-fiber response increased during the first 5 s and remained at a high level throughout the stimulus.

The average responses of the human subjects and the two fiber types during the 53°C, 30-s burn are shown in Fig. 2. For the human subjects, the pain remained intense throughout the burn at a level ten times that for the 49°C stimulus before the burn (cf, Fig. 1). The response of the A-fibers increased during the first 5 s and remained at a high level for the remainder of the stimulus. The C-fibers had a significant initial response that diminished to a low level within 5 s. Thus, the A-fibers also appear to code for the pain during a prolonged, intense stimulus.

As an additional test of the role of A- and C-fibers in pain sensation, a separate experiment was performed on two subjects. Twenty minutes after the burn, a blood pressure cuff was placed on the upper arm and inflated to 250 mmHg pressure, which was sufficient to stop blood flow in the arm and also resulted in a gradual block of action potential conduction in the nerve fibers. After 40 min, light-touch and cold sen-

sitivity and motor function were gone, indicating that conduction in the A-fibers was at least partially blocked. At that time, a thermal test sequence at the site of the burn indicated that the hyperalgesia was markedly decreased, yet the pain evoked by a thermal test sequence at nearby uninjured skin was not reduced, suggesting that C-fiber function was still intact. These data imply that the A-fibers were blocked before the C-fibers and lend further support to the view that hyperalgesia is signaled by A-fibers. Furthermore, since the pain in uninjured skin was not altered, the data also support the view that pain in uninjured skin is signaled by C-fibers.

CONCLUSIONS

C-fiber nociceptive afferents appear to code for the intensity of thermal pain near pain threshold in the uninjured hand, but A-fiber nociceptive afferents appear to code for the pain during intense, prolonged stimuli and also for the hyperalgesia following a burn to the glabrous hand.

REFERENCES

[1] R. E. Beitel and R. Dubner, "Response of Unmyelinated (C) Polymodal Nociceptors to Thermal Stimuli Applied to Monkey's Face," *J. Neurophysiol.* **39**, 1160-1175 (1976).

[2] P. Bessou and E. R. Perl, "Response of Cutaneous Sensory Units with Unmyelinated Fibers to Noxious Stimuli," *J. Neurophysiol.* **32**, 1025-1043 (1969).

[3] R. H. LaMotte and J. N. Campbell, "Comparison of Responses of Warm and Nociceptive C-Fiber Afferents in Monkey with Human Judgments of Thermal Pain," *J. Neurophysiol.* **41**, 509-528 (1978).

[4] R. A. Meyer and J. N. Campbell, "Peripheral Neural Coding of Pain Sensation," *Johns Hopkins APL Tech. Dig.* **2**, 164-171 (1981).

[5] J. N. Campbell, R. A. Meyer, and R. H. LaMotte, "Sensitization of Myelinated Nociceptive Afferents that Innervate Monkey Hand," *J. Neurophysiol.* **42**, 1669-1679 (1979).

[6] R. A. Meyer and J. N. Campbell, "Myelinated Nociceptive Afferents Account for the Hyperalgesia that Follows a Burn to the Hand," *Science* **213**, 1527-1529 (1981).

[7] R. A. Meyer, R. E. Walker, and V. B. Mountcastle, "A Laser Stimulator for the Study of Cutaneous Thermal and Pain Sensations," *IEEE Trans. Biomed. Eng.* **23**, 54-60 (1976).

[8] S. S. Stevens and D. Galanter, "Ratio Scales and Category Scales for a Dozen Perceptual Continua," *J. Exp. Psych.* **54**, 377-411 (1957).

This work was supported by the National Institutes of Health, Grant NS-14447.

AUTOMATIC CONTROL OF PHASIC AORTIC PRESSURE IN THE EXPERIMENTAL ANIMAL

W. Schneider, W. H. Guier, and R. S. Carlson

A hybrid servo-controlled blood pump has been developed that can maintain the time dependence of arterial blood pressure at specified values in an experimental animal. The pump is intended for research on how information from the arterial pressure sensors is processed in the animal's natural cardiovascular-neural-hormonal reflex control system.

BACKGROUND

Other investigators have emphasized the desirability of selectively and reversibly perturbing various cardiovascular control loops to obtain further information about the system.[1] The relevant cardiovascular receptors (sensors) are in both the arterial and the venous circulations and are sensitive to pressure (stretch), rate of change of pressure, and a wide variety of chemicals including hormones secreted by the endocrine system. Information from these receptors in the form of neural spike trains is integrated in the central nervous system to produce the appropriate reflex (closed-loop) responses. Although these reflex control loops are exceedingly complex, they can be usefully simplified by holding selected parameters at physiologically normal (or extreme) values while forcing others to change via carefully designed interventions. The pressure control system described here is designed specifically to do this for the time-varying arterial blood pressure in the vicinity of arterial pressure receptors. The information will aid research on understanding the role played by the arterial pressure sensors in the response of the cardiovascular system to various stresses such as hemorrhage.

METHODS

The first application of the blood pressure control system is shown schematically in Fig. 1. The pulsatile blood pump is used in a total heart-lung bypass preparation. Venous blood is taken from the right atrium, oxygenated, and delivered by the pump to the aortic root via a cannula that is surgically inserted through the apex of the left ventricle and aortic valve so that the valve remains open and the coronary arteries are occluded. Also, as shown in Fig. 1, the pulmonary artery is tied just above the right ventricle to prevent any blood from being delivered to the aorta via the lungs and left heart. Consequently, no chemical "signals" from the lungs or myocardium are returned to the circulation and, in the absence of pulsatile pressure, the cardiopulmonary receptors are quiescent.

The microcomputer controls the aortic arch pressure to a desired time profile, affording a way to change the desired profile and to monitor the experiment on a CRT or to archive it, or both.

Pump and Pump Driver Electronics

The major requirements for the blood pump used to control the pressure-time dependence are:

1. A stable relationship must exist between flow increment and pump shaft position,
2. The pump chamber must have reasonably low compliance,
3. The pump must do minimal damage to the fragile red blood cells, and
4. It must be able to deliver an average flow of 6 ml/s, a peak flow of 35 ml/s, and a peak rate of change of flow of 1000 ml/s^2.

The pump that best fulfilled these requirements was a dual-roller pump actuated by a high-performance permanent-magnet torque motor with velocity and position feedback. The rollers "packetize" blood in medical-grade Tygon tubing of 1/4 or 3/8 in. ID to achieve the desired capacity.

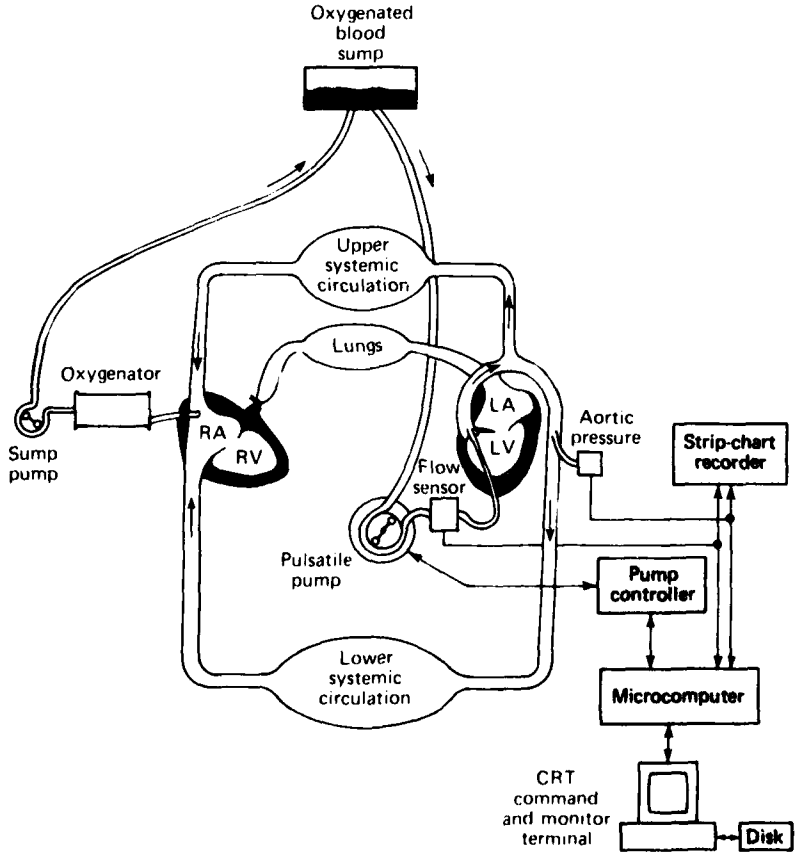

Fig. 1 Total heart bypass preparation of rabbit for aortic arch pressure control.

Velocity is the control variable for the pump driver electronics. A high-gain velocity loop gives the pump a 10 ms step response to achieve 90% of the commanded value in the linear region of operation, a bandwidth sufficient for reasonable outer loop response.

Position feedback from a 12-bit incremental shaft encoder with index indication provides the capability to compensate for flow loss arising from pump driver saturation, as may occur for extreme flow rate commands. The position of the pump shaft is the control variable for the loop external to the pump driver electronics implemented in the microcomputer software.

Position feedback also provides for autocalibration of nonlinearities in the pump's flow-position increments. These nonlinearities, caused by disengagement of the roller from the tubing, have been minimized by special contouring of the pump retaining wall. With the aid of an electromagnetic flowmeter, a correction table for the nonlinearities can be constructed during a microcomputer-generated calibration cycle.

The output compliance of the roller pump is largely due to the compliance of the tubing from the "pinch" roller in the pump to the cannula in the experimental animal. Care has been taken to minimize this compliance to prevent pressure oscillations.

Microcomputer and Software

To understand better how the microcomputer controls the time dependence of pressure in the aortic arch, refer to Fig. 2, which shows the major elements, physical and mathematical, that perform this task. Aortic arch pressure is the primary observed variable. From it are derived, on a beat-by-beat analysis of the observed hemodynamics, the mean arterial pressure (MAP), the end diastolic pressure (EDP), the mean diastolic pressure (MDP), and the systemic vascular dynamic resistance (SVDR).

The pump command for the current beat is based on these parameters computed two beats previously. The command-generation computation for the current beat is achieved during the previous beat. The commanded parameters to the pump command-generation software are stroke volume (SV) and ejection time (ET). They are functions of the experimenter's com-

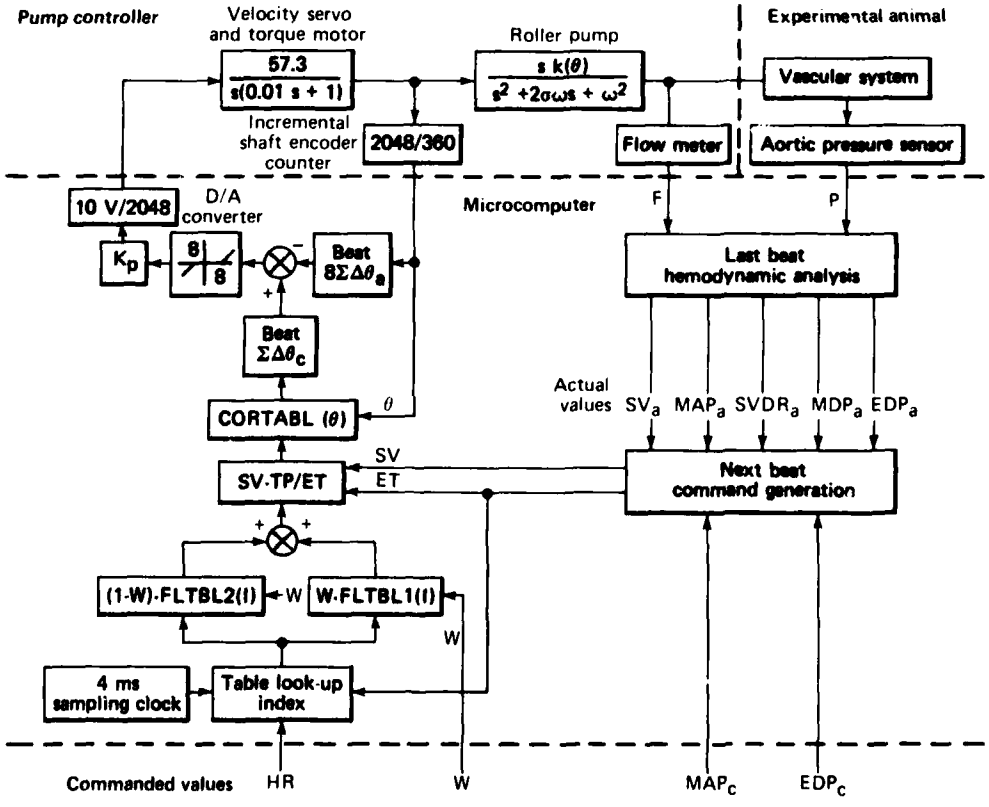

Fig. 2 Block diagram of phasic pressure controller.

manded values, the commanded mean arterial pressure (MAP_c), and the commanded end diastolic pressure (EDP_c).

The main task of the pump command-generation software is to generate the pulsatile drive signal to the pump driver electronics. A 4 ms clock translates the experimenter's commanded heart rate (HR) to a sequence of index integers that generates "ideal" normalized flow increments from two appropriately weighted flow-increment tables. The weighting factor, and thus the shape of the resulting flow, is controlled by the experimenter.

The ideal normalized flow increments per sample are then scaled by the computed stroke volume and ejection time commands as well as by the tube parameter. The tube parameter scales the ideal flow increments to ideal pump-shaft-position increments.

The pump correction multiplier adjusts the ideal position command to compensate for the inherent roller pump nonlinearities, which depend on position.

The adjusted position increments are summed and compared to the pump's summed position increments, on a beat-by-beat basis, to develop an error signal that, when appropriately scaled, results in a velocity command to the pump driver electronics.

All software was written in assembly language to achieve the desired 250 Hz sampling rate in the presence of much mathematical calculation. Most software is interrupt-driven. First priority is given to the sampling clock and second priority to the communications controller for command and monitoring of the experiment.

By the end of the NIH grant period, the pump had been used successfully to control mean pulsatile pressure in several total heart-lung bypass experiments at the Johns Hopkins Medical Institution's School of Biomedical Engineering.

REFERENCE

[1] D. S. Gann and W. M. Guier, "A Simulation Approach to the Study of Neurohumoral Control of Blood Volume," presented at 1981 Summer Simulation Conf., Washington (15-17 Jul 1981).

This work was supported by the National Institutes of Health, Grant NS-0726.

DISTRIBUTED PROCESSING/LOCAL NETWORK TECHNOLOGY FOR HOSPITALS

S. G. Tolchin, R. L. Stewart, S. A. Kahn, E. S. Bergan, and G. P. Gafke

A demonstration of a distributed data processing hospital information system has begun at the University of California, San Francisco (UCSF) Hospitals and Clinics. The project is a collaborative effort on the part of UCSF and APL. A highly intelligent, local area communication network permits the integration of heterogeneous minicomputer systems that support the clinical ancillary and administrative areas of the UCSF Medical Center. The application level design is being provided by UCSF, and the fiber-optic-based, intelligent, local area communication network is being provided by APL.

BACKGROUND

Hospitals are some of the most prodigious generators and consumers of information in existence. Certain characteristics distinguish them from virtually all other computing environments. The wide spectrum of financial, management, and clinical functions that hospitals must fulfill gives rise to a vast and heterogeneous array of information problems and processing needs. Typically, those needs are serviced by independent computer systems chosen to be the best functional modules to support an area.

At the same time, there is a need for communication among the various functions. Because most hospital functions deal with the same patients, there is a small but highly significant subset of identical information in each functional system. To avoid the entry of redundant information with its subsequent costs and errors, it is important that the shared information be ob-

tained from a single source within the group of hospital functions. Furthermore, since the output of many functions is required by practitioners for patient management, it is important that access to information on all functional systems be without undue difficulty, cost, or error.

Thus, the hospital information environment can be characterized as having two conflicting needs. The first is for modularity and heterogeneity of hardware and software for various functions; the second is for integration.

Although approaches to a total hospital information system have been studied for many years, no solution to the information processing needs of a "typical" hospital that is readily available, comprehensive, functionally integrated, and individualized has been demonstrated.

Recently, distributed data processing approaches to the problem have been considered. They support modular, distributed hospital information system development under in-house control as a viable alternative to the costly, centralized mainframe approach. A particularly important feature is the possibility for the institution to build its own hospital information system as an integrated system composed of existing or planned heterogeneous functional area systems. Each component system may be chosen to best serve the needs of a given hospital area, within an overall design that is tailored to the needs of the institution. The component systems may be off the shelf, developed in house, or developed by a vendor to specifications prepared in house.

Although such component systems are apparently incompatible, it is feasible for them to be networked together inexpensively (along with peripherals and other computing devices) using recently developed local area communication network (LACN) technology. This approach is designed to support the integration of functions and data and to facilitate the reconfiguration of the physical plant, user processing, controlled growth, and upgrading of the component systems.

Applications Environment

The demonstration project involves four minicomputers (hosts) interfaced with LACN support to achieve a level of functional integration that forms an extensible core for a comprehensive hospital information system. Figure 1 shows the four application hosts and the general system configuration.

The system is completely heterogeneous with respect to machine vendors/models, operating systems,

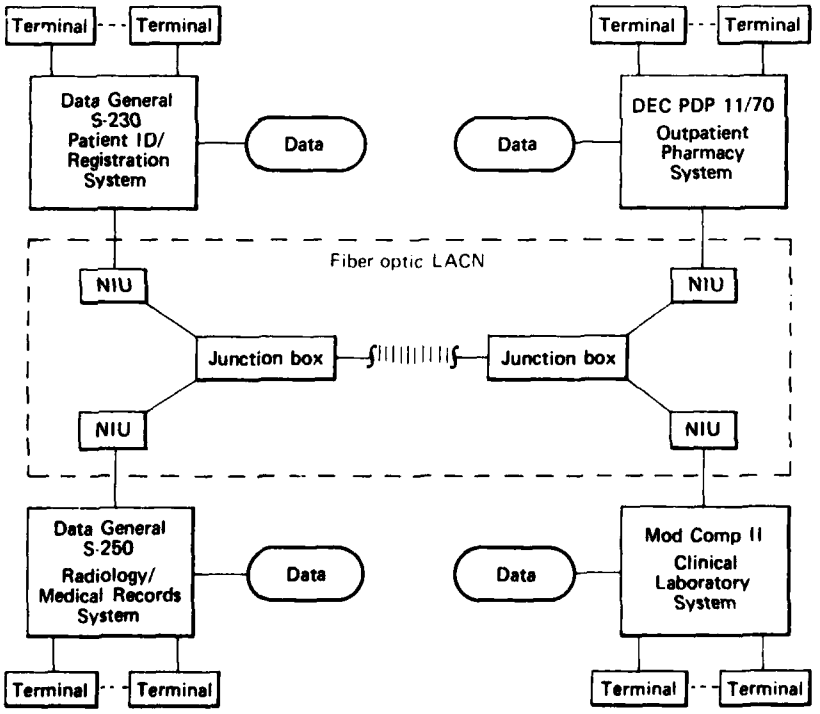

Fig. 1 Schematic of LCSI implementation.

application software systems, and local database or file access systems. As indicated in Fig. 1, the logical and physical interconnections among the host computers are accomplished by means of an LACN. Each host computer system retains its own terminals and its own local database. Although the LACN can support terminals directly, at present all remote access from a given terminal is through that terminal's defined host.

The integrated system applications design is implemented by means of transaction exchanges among hosts using services provided by the LACN. A transaction consists of data and control information in a single message. Transactions are associated with session types known to the LACN "permanently" or created interactively by some host or network manager. A session consists of transaction event identifiers and specifications of transaction interactions for participants. The sessions constitute processing agreements between hosts of different capacities and functions. A host may honor multiple session requests from remote nodes (computers, terminals, or devices) using a prearranged permanent session structure. The processing attributes of a session may be associated between a host and its network interface unit (NIU) to achieve the processing required for a number of applications.

A variety of error conditions (excluding LACN faults) may prevent normal operations. If a host is temporarily down, messages cannot be delivered, and originators must be so advised by the LACN. Similarly, a reversal of this condition must be reported. The LACN performs some error detection on messages delivered to it and rejects messages for length errors, incorrect transaction or session identifiers, incorrect addresses, etc.

Flow control is established at various levels in the integrated system, for example, between the host and its NIU. Also defined are restore and recovery procedures for handling problems resulting from network fragmentation, network component failures, and host failures.

Local Area Communications Network

An LACN called a Duplex Bus Communications Service (DBCS) has been developed at APL (Fig. 1). It uses fiber optics as the communications medium to provide potentially high-capacity data communications while permitting ease of installation, physical expansion, and reconfiguration of devices. In addition, fiber optics is relatively immune to electromagnetic interference (it can be used near radiology equipment) and provides enhanced security and reliability. By means of microprocessors and comprehensive software support at each network connection, DBCS provides a range of communications services, from simple message exchange to managing the temporary integration of processes in different computers. The physical architecture of the network permits it to overcome localized component failures (e.g., link or node failures). The software provides secure data communications. In addition, the DBCS is an "open system" in that new members may be added easily without modifying existing members.

The DBCS architecture consists of (a) NIU's, which permit computers, terminals, and other devices to be connected to the network; (b) dual-strand fiber-optic cable links; and (c) junction boxes, which direct all incoming data on a given fiber (encoded as light pulses) to all other outbound fibers. The fiber-optic links and junction boxes, operating at the same optical frequency, comprise a common communications channel. Figure 2 illustrates a possible network configuration. Computers and other devices such as terminals or printers are connected to the network by means of the programmable NIU's, which are interconnected by means of junction boxes and fiber-optic cables.

An NIU transmits data from its host(s) to the receiver of its junction box. The junction box retransmits the data to all other outgoing fibers but not back to the originating source. Because all other junction boxes follow the same rule, data are transmitted to all nodes on the network except back to the sender. Data are passed on the network in discrete packets containing source and destination addresses. Only packets addressed to a given NIU are read by that unit.

Each NIU competes with all others for use of the common communications channel. It listens on the channel until no signal is detected and thereby determines when to begin transmitting data. Another NIU may also attempt to transmit at approximately the same time, which might result in the superposition of two or more messages on the common channel. Such an event, called a collision, is detected by the sending NIU's, which issue a network abort. The abort is achieved by flooding the network with a pulse of light that directs all receiving NIU's to disregard the packet. Each sending unit then waits a randomly determined time before attempting retransmission, to avoid recurrence of the collision.

Two data packets may exist simultaneously without causing a collision when two NIU's are sending messages to each other. The receive lines of the two units do not contain superposed data, although the receive lines of all others do. This scheme permits simultaneous exchange or full-duplex, within the DBCS architecture.

In the scheme presented above, each NIU contends with all others for access to the shared communications channel. Thus, DBCS uses a contention bus topology. The combination of collision detection logic and listen-while-talk for access is known as carrier sense multiple access with collision detection. The basic algo-

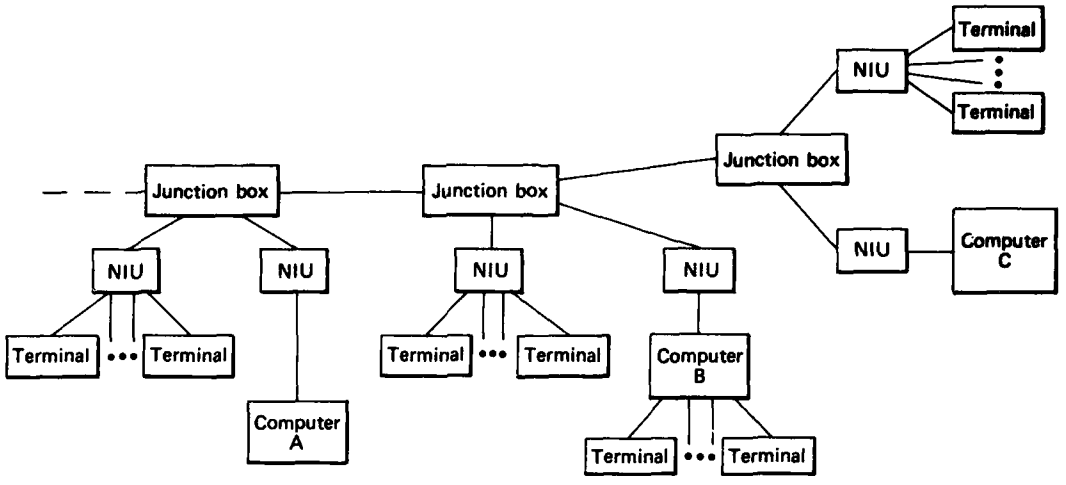

Fig. 2 A fiber-optic computer network.

rithm has been modified in DBCS to permit full-duplex communications.

Communications functions, which are performed according to rules known as protocols, range from managing the physical transfer of bit streams at a low level through to high-level functions such as controlling integrated and structured data exchanges among cooperating programs in different computers. These protocol functions are accomplished by the hardware and software within each NIU. Distributed network control is achieved by means of a common network protocol system within each unit. The protocol design is based on the proposed International Standards Organization/Open Systems Interconnection Reference Model.

The decision to perform most protocol functions within the NIU rather than within the host computer provides significant advantages, including a simplification of development and maintenance activities. Rather than having to develop protocols within a computer host for every other host with which it may need to communicate, only one interface (to the network) is needed.

The protocols provide various communications services. Simple message exchange without receipt acknowledgment (like a letter dropped in a mailbox) is known as datagram service. In the next level of service, called virtual circuit service, message sequencing and delivery are assured. Finally, to link two computing devices across the network, the content and time reference of messages as well as their associated virtual circuit must be monitored; the administration of such an event-oriented circuit is called session management.

Major protocol program modules are depicted in Fig. 3 in their relative functional location within an NIU.

In terms of the integrated hospital system application, Fig. 4 shows the functional relationship of the NIU to the parent host and its input/output handlers, operating system, and data calls. Each of the four hospital computers serves its local user community in a dedicated or a time-sharing mode of operation. For an active process running on the host computer, remote data calls or other messages to remote hosts are accomplished by building a transaction and writing to the NIU. Transfers are made across a physical and a data link path between the NIU and its host under the interface flow control protocol for that host. Upon acceptance of the transaction, the NIU assumes responsibility for a proper response or an error message. On the return path, the NIU signals the host input/output handler when a transaction addressed to a resident of the host is available for transfer. When signaled that the host is ready to receive, the NIU makes the necessary code/format changes and performs the transaction.

The fiber-optic LACN described above uses five NIU's (one for the monitoring node), two junction boxes, and approximately 1000 m of dual fiber-optic cabling. The cost, including NIU interfaces and NIU software for transaction processing, installation, and checkout, is on the order of $100,000.

SUMMARY

An applications design and a technology for a generalized LACN are being implemented to achieve a

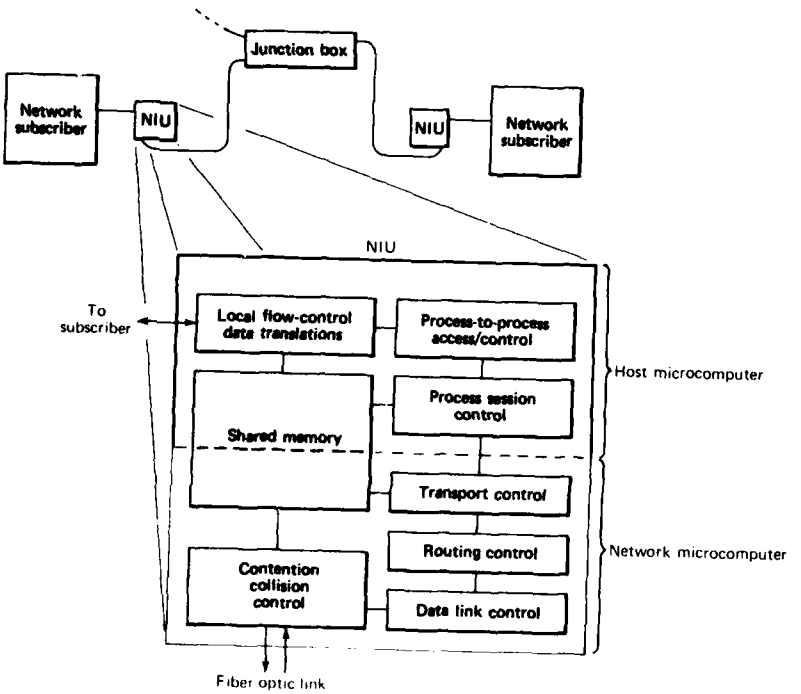

Fig. 3 NIU protocol modules.

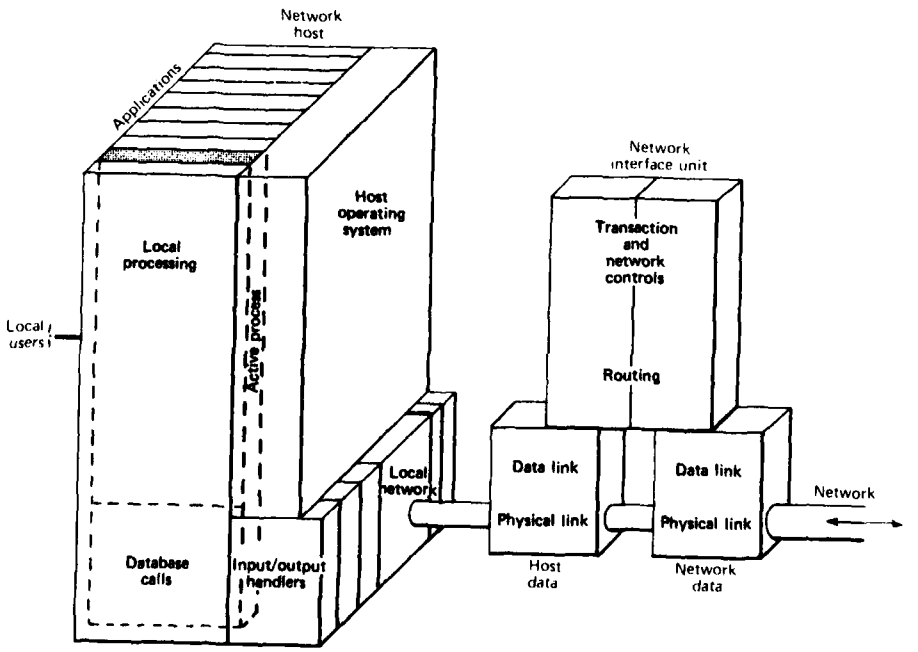

Fig. 4 A functional node.

flexible distributed hospital system capability. The approach integrates heterogeneous stand-alone computer systems within an expandable, reconfigurable architecture while maintaining the autonomy of the individual systems. The applications design, LACN physical architecture, fiber-optic communications medium, communications protocols, and NIU's have been reviewed. The application integrates a Patient ID/Registration System, Outpatient Pharmacy System, Clinical Laboratory System, and Radiology/Medical Records System.

REFERENCES

[1] S. G. Tolchin, R. L. Stewart, S. A. Kahn, D. W. Simborg, M. E. Chadwick, and Q. E. Whiting-O'Keefe, "A Generalized Network Technology for Hospitals: Initial Implementation," presented at Fifteenth Annual Hawaii Conf. on Systems Sciences (Jan 1981).

[2] S. A. Kahn, R. L. Stewart, S. G. Tolchin, E. S. Bergan, and G. P. Gafke, "Design and Implementation of a Fiber-Optic Contention Bus Network," presented at Fifteenth Annual Hawaii Conf. on Systems Sciences (Jan 1981).

[3] S. G. Tolchin and R. L. Stewart, "The Distributed Processing Approach to Hospital Information Processing," *J. Med. Syst.* **5**, No. 4, 345-360 (1981).

[4] S. G. Tolchin, R. L. Stewart, S. A. Kahn, E. S. Bergan, G. P. Gafke, D. W. Simborg, Q. E. Whiting-O'Keefe, M. E. Chadwick, and G. E. McCue, "Implementation of a Generalized Network Technology for Hospitals," presented at Fifth Annual Symp. on Computer Applications in Medical Care (Nov 1981).

[5] Q. E. Whiting-O'Keefe, D. W. Simborg, and S. G. Tolchin, "The Argument for a Modular Distributed Hospital Information System" presented at Fifth Annual Symp. on Computer Applications in Medical Care (Nov 1981).

[6] S. J. Healy, R. L. Stewart, S. A. Kahn, and S. G. Tolchin, "Description of a Fiber-Optic Contention Network," *JHU/APL Tech. Dig.* **2**, No. 2, 84-86 (1981).

[7] R. L. Stewart and S. G. Tolchin, "A Distributed Processing/Fiber-Optic Hospital Information System," presented at Fourth Annual Symp. on Computer Applications in Medical Care (Nov 1980).

[8] S. A. Kahn, R. L. Stewart, S. G. Tolchin, and S. J. Healy, "Functional and Logical Description of a New Fiber-Optic Contention Bus Network," *Fall COMPCON*, 268-272 (1980).

[9] M. L. Zichner, P. J. Brusil, and S. G. Tolchin, "Distributed Processing Architecture for a Hospital Information System," presented at Third Annual Symp. on Computer Applications in Medical Care (Oct 1979).

This work was supported by the National Center for Health Services Research.

AUDIO FILING SYSTEM FOR THE BLIND

J. H. Kuck

The development of the Audio Filing System for the Blind was in response to the national search contest sponsored by APL to bring forth ideas for the use of personal computers to aid the handicapped. It won Honorable Mention in the contest.

Although the system is a simple concept based on readily available technology, it is believed that it could have a major effect on the ability of blind persons to obtain employment and to manage their personal affairs. This short-term development was not formally funded.

BACKGROUND

Although the cassette tape recorder has been around for a long time, its potential as a medium for storage of voice information by blind persons does not appear to be fully utilized. This shortfall results from the excessive amount of time required to search for a specific piece of information in a file (the cassette) that contains many entries on each tape track.

The Library of Congress, in connection with their talking book program, developed a method of tone indexing in which short bursts of low-frequency tone (about 60 Hz) are superimposed on the tape at normal playing speed. When played at the high FAST-FORWARD speed on a special tape recorder for the blind, the tones can easily be heard. Because they are converted to a higher frequency, the midaudio range, they can be easily heard and readily distinguished by ear from the even-higher-frequency squeaky voice sounds. By counting the tonebursts, the blind person can quickly access major sections of a recorded book or magazine with the aid of a voice-recorded table of contents.

The special tape recorder has the feature that the playback head remains in contact with the tape in the FAST-FORWARD and REWIND modes. This is not true of ordinary, low-cost cassette recorders. The special recorder for tone indexing is now commercially available from the American Printing House for the Blind. It has a pushbutton for manual tone indexing and raised

tactile symbols on the control keys for identification by the blind user.

DISCUSSION

The Audio Filing System uses a personal computer to enhance the capabilities of the tone-indexing technique. It provides automatic computer control of the file-search operation in a way that should make it easier for a blind person to cope with files containing a large number of file sections on each tape track. Although manual tone indexing is quite satisfactory if there are only a few major sections to be indexed on each tape track, the search operation becomes burdensome when there are 50 to 100 small file sections on each. If the user does not remember the index number of a file section, he must listen to a lengthy voice index to find it. He must then keep his attention focused on counting while listening to the tonebursts, and he must react quickly to stop the recorder at the right moment to avoid overshooting the start of the voice data. Computer control relieves him of these burdens in the following ways:

1. The computer counts the tones and stops the recorder automatically at the right spot.
2. During the creation of a file, the index of names and numbers recorded on the tape can be typed manually on the computer keyboard and stored on a disk file. This file will be used later by the computer when it is automatically searching the tape for a particular entry that has been typed on the keyboard.
3. When a tape is being indexed, standard-length tonebursts are automatically generated by the computer. A specified delay is automatically provided after each toneburst before voice recording starts. This delay allows time for the motor to stop, when a search ends.

To search for an item, all the blind user has to do is type the command RUN SNAME on the computer keyboard and, when alerted by a distinctive audible cue, put the recorder in FAST-FORWARD, type the name of the file section, and press the RETURN key. The computer starts the tape recorder motor and stops it at the right moment (when the wanted file is located).

The demonstration model uses the special APH Model 3-5194A tape recorder, an APPLE II PLUS computer with a monitor, a disk drive, and a custom circuit board that plugs into one of the vacant slots in the computer. The circuit board contains six integrated circuit packages and a few passive components. Four of the integrated circuits form a low-pass filter and a threshold detector. The remaining two packages are a buffer and relay that control the tape recorder motor. The tape recorder uses ordinary cassettes, but a special recording head allows four tracks to be recorded instead of the usual two. At the slowest tape speed, each track is 90 minutes long.

To index a tape, the computer is programmed to generate a 27 Hz square wave that is fed into the tape recorder through the microphone jack. On playback, the waveform of this signal suffers considerable distortion, but when fed through the low-pass filter, the envelope of the toneburst can be obtained with a diode detector. The toneburst output level is high enough (compared to the residual voice sounds that get through the filter and the diode detector) to enable a comparator functioning as a threshold detector to separate the toneburst from voice interference.

Figure 1 shows the frequency response of the low-pass filter. The filtering problem is made more difficult by the two-to-one change in tape speed that occurs in the FAST-FORWARD mode between the beginning and end of the tape. Nevertheless, the filter has been used successfully at a recording speed of 1-7/8 in./s. At the slower speed of 15/16 in./s, the system failed to function correctly.

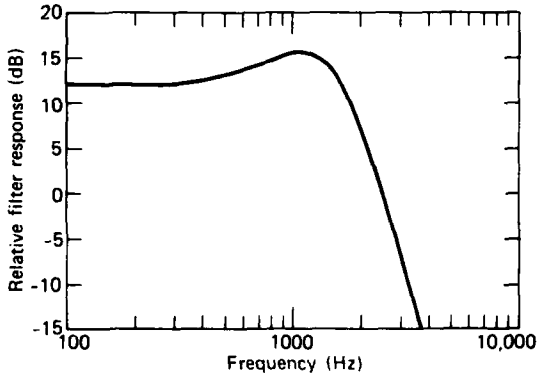

Fig. 1 Frequency response of filter for Audio Filing System.

Computer programs are a necessary part of a complete system. The ones that have been written so far for this system provide for searching by name or number, putting indexing tones on the tape, and creating the disk index. These programs cause the computer speaker to issue single-letter Morse code cues to let the blind user know when to perform various operations.

In order to operate the system, a blind person must know touch-typing. The system should be most useful to students and blind professionals in fields such as law, teaching, and psychology who need fast access to large quantities of information. It might also open up employment opportunities in nonprofessional areas such as order-taking. Thought is being given to im-

provements in the system that might make it even simpler to operate and less expensive; for example:

1. A machine-language program might be able to perform the functions of the filter/detector circuit and make possible the elimination of the custom interface circuit board.
2. If the assemblage of computer components were replaced by a dedicated "black box," the typing of a computer command could be replaced by a single key stroke on a special key, and the necessary programs could be permanently stored in memory.

These improvements would reduce the possibilities of operator error. If a dedicated system could be mass produced, the cost could probably be brought down to a point well below the cost of a personal computer.

ACKNOWLEDGMENT

Credit is due to Norman Crouch and Alan Mergenthaler for their valuable voluntary contributions of technical advice and assistance in the construction of the working model.

This work was supported by Indirectly Funded R&D.

FUNDAMENTAL RESEARCH

INTRODUCTION

Fundamental research has been firmly established at APL for many years as one of the Laboratory's principal missions, which include the application of advanced science and technology to the enhancement of the security of the United States and the pursuit of basic research to which the Laboratory's facilities can make an especially favorable contribution. The incorporation of basic research into the Laboratory's mission recognizes that such research will play a vital role in future technological achievements and that it is needed to avoid institutional obsolescence.

Much of the basic research conducted at APL is done in the Research Center, which was formally established in 1947. Its initial objectives, still valid today, were to establish APL as a contributor to scientific knowledge, to develop and provide fundamental understanding basic to fields of present and potential interest to the Laboratory, and to enhance the professional competence of the staff by serving as a doorway to science. Since its inception, the Research Center has spawned new programs that are now carried out in other units of the Laboratory. Most notable are the Space Department and the Biomedical Research Program.

Today, the Milton S. Eisenhower Research Center is comprised of 60 staff members organized into eight groups. These scientists report their research in the professional scientific literature; typically, 60 papers are published each year. The articles in this section describe some recent accomplishments in basic research by staff members of the Research Center and of other Laboratory units.

The program on new methods in wave physics conducted by the Theoretical Problems Group is represented by an article on variational calculations of scattering from random objects that have general electrical and magnetic properties. This article is the result of a collaborative effort between the Fleet Systems Department and the Research Center. Research on fluid mechanics within the Theoretical Problems Group has resulted in the article that demonstrates there are three types of two-dimensional separation. Another fluid mechanical problem investigated by members of the Applied Mathematics Group is described in the article on sloshing frequencies of fluids in containers. The research effort in surface science is represented by the article on internal energy transfer in molecules colliding with heated surfaces. The article on the theory of electron spin resonance line broadening in one-dimensional organic conductors is from the program on electromagnetic effects in thin films. Finally, the article on solute flow through heteroporous membranes describes research done by scientists within the Biomedical Programs Office.

In addition to these selected accomplishments in basic research, other Research Center investigations are reported elsewhere in this volume. They include Bird's work on the effects of finite length on the magnetic levitations of a cylindrical metal shell encircling an alternating current filament (in the Space Science and Technology Section), the work of Feldman, Satkiewicz, and Blum on polycrystalline silicon solar cells (in the Energy, Environmental, and Urban Technology Section), and the research of McCally and Farrell on the structural implications of small-angle light scattering from cornea (in the Biomedical Science and Engineering Section).

EVALUATION OF VARIATIONAL EXPRESSIONS OF ELECTROMAGNETIC WAVE SCATTERING FROM RANDOM OBJECTS WITH GENERAL ELECTRIC AND MAGNETIC PROPERTIES

J. A. Krill, R. H. Andreo, and R. A. Farrell

The vector stochastic variational principle for calculating electromagnetic wave scattering from random objects and surfaces was extended to include linear magnetic materials. Calculational difficulties associated with the singular behavior of the dyadic Green function were resolved by reexpressing the vector variational principles in terms of the scalar Helmholtz Green function.

BACKGROUND

Of continued interest in many diverse fields is the study and modeling of the random scattering and propagation phenomena that are present in a wide variety of systems including communications, radar, and other remote sensors. Because comprehensive exact solutions to the equations describing these complex phenomena generally do not exist, a variety of approximation techniques has been used. Many of these techniques require estimating the field at the surface of or within the scattering medium; however, the conditions for the validity of such a scattering approximation may be limited or unknown.

The development of the variational approximation method for random scattering has been pursued at APL for several years. Variational approximations are well known to be inherently less sensitive to errors in the initial field estimates than are other approximations because first-order errors in these estimates lead to only second- and higher-order errors in the variational approximation for the scattered field. A tractable general application of variational methods to random scattering was made possible in 1977 when Hart and Farrell[1] developed stochastic variational principles for the mean scattering amplitude and differential scattering cross section for scalar waves with homogeneous boundary conditions. Their general method was extended to vector wave scattering from random conducting dielectric objects and surfaces on which the field satisfies inhomogeneous boundary conditions.[2]

During the past year, we have generalized the vector stochastic variational principles to include magnetic materials such as obscurant magnetic filaments, that is, materials with permeability as well as permittivity and conductivity.[3] We have found a dyadic Green function formalism convenient for expressing the vector variational principles; however, we encountered some calculational difficulties in our attempts at a straightforward evaluation of the expressions for scattering from cylinders. The singular nature of the dyadic Green function proved to be the source of the difficulties, and they were removed by recasting the vector variational principles in terms of the scalar Helmholtz Green function.[4]

DISCUSSION

The scattering, absorption, and propagation of electromagnetic radiation (such as light and radar emissions) by assemblies of objects (such as aerosols, chaff, other obscurants, and rough surfaces) is of continued interest. The objects are usually specified in a statistical or probabilistic sense and exemplify random scatterers. The prototype volume scattering problem is illustrated in Fig. 1; it depicts a plane wave, $\boldsymbol{E}_i$, polarized in the direction $\hat{e}_i$, propagating in the direction $\hat{k}_i$, and incident on a random inhomogeneous and anisotropic scatterer. Interest lies in the total field, $\boldsymbol{E}$, propagating in the direction $\hat{k}_s$; the usual dyadic Green function formalism can be used to write it as the sum of an incident and scattered field, that is,

$$\boldsymbol{E} = \boldsymbol{E}_i + \int_{V_0} dV\, \bar{\bar{G}}_0 \cdot \bar{\bar{\mathbf{O}}} \cdot \boldsymbol{E} \,, \qquad (1)$$

where V_0 is the volume of the scatterer, $\bar{\bar{G}}_0$ is the appropriate dyadic Green function, and the dyadic $\bar{\bar{\mathbf{O}}}$ characterizes the scatterer and depends on its (tensor) permeability $\bar{\bar{\mu}}$, permittivity $\bar{\bar{\epsilon}}$, and conductivity $\bar{\bar{\sigma}}$. The $\hat{e}_s$ component of the vector scattering amplitude $\boldsymbol{T}$ can be obtained from the far field limit of Eq. 1 in the usual fashion.

For random scattering problems, Eq. 1 can be used to derive an invariant expression for the average differential scattering cross section, which is of the form[1,3]

$$\langle |\hat{e}_s \cdot \boldsymbol{T}|^2 \rangle = \frac{1}{(4\pi)^2} \frac{\langle |N_1|^2 \rangle \langle |N_2|^2 \rangle}{\langle |D|^2 \rangle} \,. \qquad (2)$$

The quantities N_1, N_2, and D are volume integrals involving the electric field $\boldsymbol{E}$ and the adjoint field $\tilde{\boldsymbol{E}}$ inside the scatterer, the Green dyadic $\bar{\bar{G}}_0$, the dyadic $\bar{\bar{\mathbf{O}}}$, and its adjoint $\bar{\bar{\mathbf{O}}}\ddagger$. The adjoint field is simply related to $\boldsymbol{E}$ by reciprocity, i.e., by the replacements $\hat{k}_i \rightarrow -\hat{k}_s$, $\hat{e}_i \rightarrow \hat{e}_s$, and $\bar{\bar{\mathbf{O}}} \rightarrow \bar{\bar{\mathbf{O}}}\ddagger$. For the nonmagnetic case,[2] $\bar{\bar{\mathbf{O}}}$ is an algebraic matrix and it is readily verified that $\bar{\bar{\mathbf{O}}}\ddagger = \bar{\bar{\mathbf{O}}}^{tr}$, where tr denotes matrix transposition.

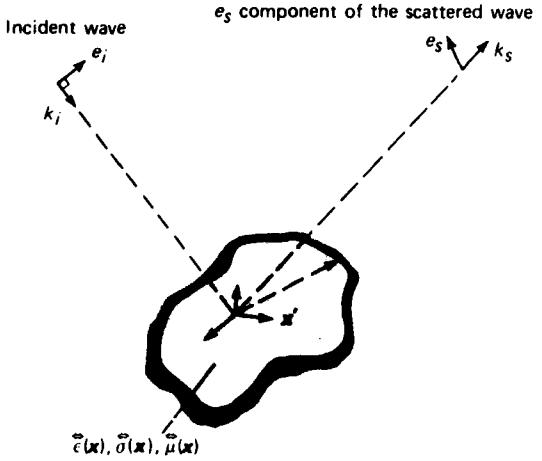

Fig. 1 The geometry is illustrated for plane wave scattering by an arbitrary volume, V_0, with inhomogeneous, anisotropic permittivity $\vec{\epsilon}(\mathcal{X})$, conductivity $\vec{\sigma}(\mathcal{X})$, and permeability $\vec{\mu}(\mathcal{X})$.

For linear magnetic materials, the dyadic $\vec{\mathbf{O}}$ is the sum of an algebraic matrix $\vec{\mathbf{O}}_E$, which contains the electrical properties of the scatterer, and a differential dyadic operator $\vec{\mathbf{O}}_M$, which contains the magnetic permeability.[3] The variational expression (Eq. 2) requires the determination of the adjoint operator $\vec{\mathbf{O}}\ddagger$. This was achieved by applying integration by parts to the usual definition of an adjoint operator, as encountered in quantum mechanics, for example. The result is that $\vec{\mathbf{O}}\ddagger$ has the same form as $\vec{\mathbf{O}}$ but with the algebraic matrices $\vec{\epsilon}$, $\vec{\sigma}$, and $\vec{\mu}$ replaced by their transposes.[3] Thus, all of the ingredients are available to evaluate Eq. 2 for magnetic materials.

The Green dyadic is convenient for deriving variationally invariant expressions for the scattering amplitude statistics, such as the one just discussed, and it enters through the double volume integral

$$D_2 = \int_{V_0} dV\,[\vec{\mathbf{O}}\ddagger \cdot \vec{E}] \cdot \int_{V_0} dV'\,\vec{G}_0 \cdot [\vec{\mathbf{O}} \cdot E] \quad , \quad (3)$$

which appears in D of Eq. 2. The inner integral over the Green dyadic $\vec{G}_0$ can be expressed as a principal value integral over the free-space Green dyadic minus a term that is proportional to the depolarization tensor[5] $\vec{L}$. The principal value integral excludes a small volume, V_ϵ, about the field point where the source and field points coincide, and $\vec{L}$ is the depolarization tensor appropriate to V_ϵ.[6] Straightforward evaluation of this principal value integral and of $\vec{L}$ proved difficult when we attempted to calculate the scattering from cylinders as a test case. Consequently, we examined other methods for evaluating Eq. 3.

The free-space Green dyadic can be written as a dyadic differential operator acting on the usual scalar Helmholtz Green function. Inserting this result into the inner integral of Eq. 3 and using dyadic identities to integrate by parts twice allows this integral to be written as the sum of three terms[4]: a volume integral whose integrand contains the scalar Green function as a multiplicative factor, a nonsingular integral over the surface of the scatterer, and a term that is essentially the polarization charge density induced in the scatterer. Thus, we can eliminate the need to evaluate the depolarization tensor and the principal value integral at the cost of evaluating the three terms. If the scatterers have soft boundaries, the surface integrals can be evaluated at infinity, where they vanish because the scatterers are localized, so that evaluating the reformulated expressions should be simpler in those cases. Our preliminary results[7] for a test case of scattering from two parallel cylinders (hard scatterers) show that calculating the three terms is straightforward and that the vector stochastic variational principle can account for known polarization, interference, and multiple scattering effects. We plan to complete these preliminary calculations for this special test case and then to apply this procedure to more realistic systems.

REFERENCES

[1] R. W. Hart and R. A. Farrell, "A variational principle for scattering from rough surfaces," *IEEE Trans. Antennas Propag.* **AP-25**, 708-710 (1977).

[2] J. A. Krill and R. H. Andreo, "Vector stochastic variational principles for electromagnetic wave scattering," *IEEE Trans. Antennas Propag.* **AP-28**, 770-776 (1980).

[3] R. H. Andreo and J. A. Krill, "Vector stochastic variational expressions for scatterers with dielectric, magnetic, and conductive properties," *J. Opt. Soc. Am.* **71**, 978-982 (1981).

[4] J. A. Krill, R. H. Andreo, and R. A. Farrell, "A computational alternative for variational expressions that involve dyadic Green functions" (to be published in *IEEE Trans. Antennas Propag.*, 1982).

[5] H. C. Van de Hulst, *Light Scattering by Small Particles*, Chap. 6, Wiley and Sons, New York (1957).

[6] A. D. Yaghjian, "Electric dyadic Green's functions in the source region," *Proc. IEEE* **68**, 248-263 (1980).

[7] J. A. Krill, R. H. Andreo, and R. A. Farrell, "Variational and exact solutions for electromagnetic scattering from two randomly separated cylinders," *Proc. 1981 CSL Scientific Conf. on Obscuration and Aerosol Research* (to be published by Ronald H. Kohl and Associates, 1982).

This work was supported by Indirectly Funded R&D.

CLASSIFYING TWO-DIMENSIONAL LAMINAR SEPARATION

V. O'Brien

Although steady flow separation from a stationary surface is reasonably well understood, unsteady separation or recirculation zones near moving boundaries are not. A review of our data and the data of others and of viscous flow theory for two-dimensional laminar incompressible flows indicates that just three kinds of stagnation regions are associated with separation.

SUMMARY

Regions of separated backward flow immersed in a larger domain of forward flow have been recognized since the time of Prandtl. They can be very important for they occur at all Reynolds numbers, in internal and external flows, whether steady or unsteady, and in both laminar and turbulent flows. Let the present discussion be confined to laminar incompressible flow that is two dimensional. Even under this restriction there is no agreement on criteria for the inception of reverse flow when the flow is unsteady or the boundary wall is in motion. Yet the unity of fluid dynamics suggests that there is only a minimum number of constraints to describe the local stagnation regions at the heads (or tails) of recirculation regions. In recent work at APL, vorticity contours have been used to show that two-dimensional separation falls into three stagnation region classes for steady flows, one type associated with fixed walls and the two others with moving walls (Figs. 1 to 3). The existing data on laminar unsteady flows indicate that they also fall into the same three classes.[1]

DISCUSSION

A recent publication,[1] reviews the published literature of theoretical solutions involving separation ranging from Stokes flow to numerical analyses of the full Navier-Stokes equation for laminar flows of high Reynolds number. After a survey of the confirming experimental data for both steady and unsteady flows, I concluded that two-dimensional laminar flows have only three types of stagnation regions.

The most familiar type of recirculation region is the one for which the bounding streamline, ψ_s, intersects the stationary wall as shown in Fig. 1. There is universal acceptance of Prandtl's criterion (see Oswatitsch[2]) for the location of separation from a fixed solid surface in steady flow; e.g.,

$$\frac{\partial u(s)}{\partial n} = 0 ,$$

where u is the velocity vector parallel to s, and n is the normal direction (Fig. 1). This defines a wall stagnation point, S, but using the definition of vorticity ($\Omega = \nabla \times q$), it can also be interpreted as the intersection of the null vorticity curve, $\Omega(s,n) = (\partial v/\partial s) - (\partial u/\partial n) = 0$, with the wall. For the attached vortex (separation bubble), there are universal angular relationships near S among the curves $\psi_s = 0$, $u = 0$, and $\Omega = 0$ as well as for the direction of the maximum pressure gradient at the wall.[2,3] At the reattachment in the separation bubble, the angular relationships among the streamfunction, velocity, and vorticity curves are the same, except that the direction along $\psi_s = 0$ is reversed (Fig. 1).

Numerical analyses of unsteady flows in terms of the streamfunction, ψ, and vorticity, Ω, show the movement of stagnation points on the wall for attached recirculation regions (cf. Ref. 4). The accompanying null vorticity curves and bounding streamlines meet at the stagnation points. In coordinates moving with them, the local field is like the steady one (Fig. 1 and Refs. 2 and 3).

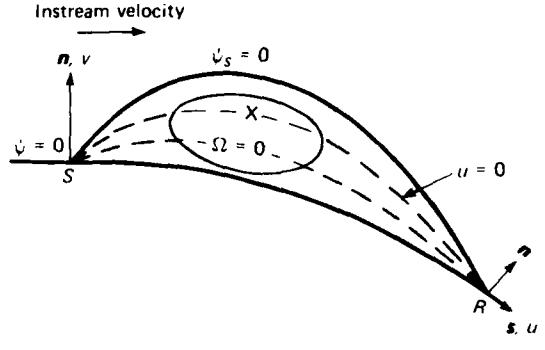

Fig. 1 An attached recirculation bubble; *S*, *R* are stagnation points of separation and reattachment, respectively, on the stationary wall.

Two types of recirculation, both occurring in stream, are associated with moving walls. The first, illustrated in Fig. 2, is related to a conjecture by Moore,[5] Rott,[6] and Sears[7] that the separation stagnation point occurs where $u = 0 = du/dn$ (coordinate axes referred to the moving wall). There is an orthogonal intersection where the null vorticity contour ($\Omega = 0$) coincides with one of the pair of streamlines through the stagnation point. Here, in local von Mises coordinates (ξ, η), u' is the local streamward component, and at S the conditions are $u' = 0 = \Omega\,[= -(\partial u'/\partial \eta)]$. Similar conditions hold at R. The Moore-Rott-Sears

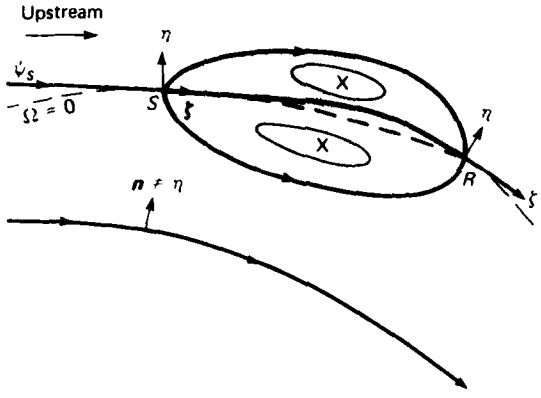

Fig. 2 Closed recirculation regions associated with a dividing streamline with stagnation regions of the orthogonal saddlepoint type; Ω = 0 is the null vorticity curve, X marks the vortex centers, and ξ, η are local von Mises coordinates at *S* and *R*.

implication that this streamline saddlepoint must be aligned parallel and perpendicular to the moving wall is too restrictive in general, and a second type of in-stream separation is discussed below.

The orthogonal type of in-stream stagnation saddlepoint also occurs in unsteady flow solutions in terms of ψ and Ω (Refs. 4, 8, and 9) and has been confirmed by flow visualization. Instantaneous streamlines and null vorticity curves coincide at the stagnation points.

The second type of single vortex in-stream separation does not involve the $\Omega = 0$ contour. In addition, the intersection need not be orthogonal, and often the angles are quite unequal as in Fig. 3. The exact global solution of Stokes flow between nonconcentric cylinders rotating in opposite directions[10] is perhaps the best example of such a "trifurcating flow." The single recirculation region can also occur with "upstream-moving walls" in a uniform flow,[11] where it is acknowledged that the Moore-Rott-Sears conjecture is inadequate (see also Ref. 12).

The second type of in-stream separation also occurs in unsteady flows and has been observed experimentally in the oscillatory flow above a plate with an attached disturbance bar moving in harmonic horizontal motion.[13] (The flow visualization confirmed recirculation regions attached to the moving disturbance bar.) Moreover, various numerical analyses of unsteady flows have shown detaching vortices that have the nonzero vorticity stagnation point.[14-16]

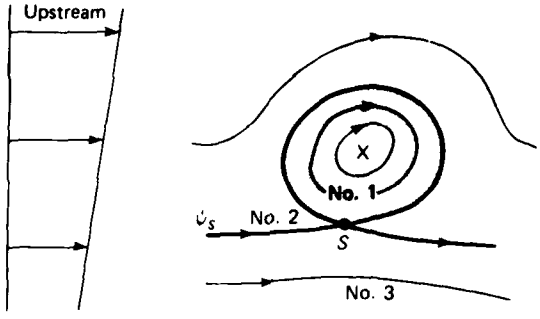

Fig. 3 Single recirculation region associated with nonorthogonal in-stream dividing streamline saddlepoint; one stagnation region in a "trifurcation" flow.

REFERENCES

[1] V. O'Brien, "Stagnation Regions of Separation," *Phys. Fluids* **24**, 1005-1009 (1981).
[2] K. Oswatitch, in *Symp. on Boundary Layer Research*, H. Gortler, ed., Springer-Verlag, Berlin, p. 357 (1958).
[3] V. O'Brien, "Analytic Description of Steady Separation from Curved Surfaces," *Phys. Fluids* **20**, 1045-1049 (1977).
[4] V. O'Brien, "Unsteady Separation Phenomena in a Two-Dimensional Cavity," *AIAA J.* **13**, 415-416 (1975).
[5] F. K. Moore, in *Symp. on Boundary Layer Research*, H. Gortler, ed., Springer-Verlag, Berlin, p. 296 (1958).
[6] N. Rott, "Unsteady Viscous Flow in the Vicinity of a Stagnation Point," *Q. Appl. Math.* **13**, 441-451 (1956).
[7] W. R. Sears, "Some Recent Developments in Airfoil Theory," *J. Aeronaut. Sci.* **23**, 490-499 (1956).
[8] T. D. Brown and T-K. Hung, in *ASME 1977 Biomechanics Symp.* (ASME AMD-23), pp. 35-38 (1977).
[9] I. J. Sobey, "On Flow through Furrowed Channels," *J. Fluid Mech.* **96**, 1-26 (1980).
[10] W. Müller, "Beitrag zur Theorie der Langsamen Stromung Zwiet Exzentrischer Kreiszylinder in der Zähen Flussigkeit," *Z. Angew. Math. Mech.* **22**, 177-189 (1942).
[11] O. Inoue, "MRS Criterion for Flow Separation over Moving Walls," *AIAA J.* **19**, 1108-1111 (1981).
[12] C. A. Koromilas and D. P. Telionis, "Unsteady Laminar Separation: An Experimental Study," *J. Fluid Mech.* **97**, 347-384 (1980).
[13] V. O'Brien, *Periodic Boundary Layer Flows over a Flat Plate, Part III: With Disturbance Bars*, JHU/APL TG 944 (Aug 1967).
[14] H. J. Lugt and S. Ohring, in *4th International Conf. on Numerical Methods in Fluid Dynamics*, Springer-Verlag, Berlin, pp. 275-281 (1975).
[15] U. B. Mehta, in *AGARD Symp. on Unsteady Aerodynamics* (Ottawa), Paper No. 23 (1977).
[16] S. E. Hurlbut, M. L. Spaulding, and F. M. White, "Numerical Solution of the Time-Dependent Navier-Stokes Equations in the Presence of an Oscillating Cylinder," in *Nonsteady Fluid Dynamics* (ASME Winter Meeting), pp. 201-206 (1978).

This work was supported by Indirectly Funded R&D.

UPPER AND LOWER BOUNDS FOR SLOSHING FREQUENCIES BY INTERMEDIATE PROBLEMS

D. W. Fox and J. R. Kuttler

Very good, rigorous, numerical estimates are given for the characteristic frequencies of the vertical oscillations of the surface of an ideal fluid in a canal or tank under the influence of gravity. The estimates are obtained by using conformal transformations to cast the problem in a form suitable for employing the method of intermediate problems. The first ten or more frequencies of a wide variety of regions are estimated to six or more significant figures.

BACKGROUND

The "sloshing problem" is a classical problem in fluid dynamics, originally studied in the nineteenth century,[1,2] that describes the characteristic frequencies of the vertical oscillations of the surface of an ideal fluid in a container under the influence of gravity.[3] It has application to aircraft and missile fuel tanks, canals, and so forth. Nevertheless, solutions had heretofore been known only for a few special cases.

In terms of the velocity potential, the sloshing problem is a differential equation with an eigenvalue in the boundary condition. We have obtained very good, rigorous, numerical estimates for these eigenvalues by using conformal transformations on the crosssections of the sloshing regions to cast the problem into a form suitable for the method of intermediate problems.[4,5] We have determined the first dozen or more eigenvalues of a wide variety of regions to six or more significant figures with a modest amount of calculation.[6]

DISCUSSION

A two-dimensional sloshing problem is a linear eigenvalue problem that describes small plane irrotational oscillations under gravity of an ideal fluid with a free surface. In Fig. 1, the cross section of the region occupied by the fluid is G with horizontal free boundary, $\partial_1 G$, and impermeable boundary, $\partial_2 G$. In terms of a velocity potential, ϕ, the sloshing problem is

$$\begin{aligned} \Delta\phi &= 0 \quad \text{in } G , \\ \frac{\partial\phi}{\partial n} &= \lambda\phi \quad \text{on } \partial_1 G , \\ \frac{\partial\phi}{\partial n} &= 0 \quad \text{on } \partial_2 G , \end{aligned} \tag{1}$$

where Δ is the Laplace operator and $\partial/\partial n$ is the normal derivative. Note that the eigenvalue, λ, appears only in the boundary condition on $\partial_1 G$.

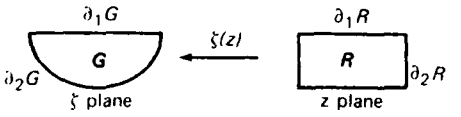

Fig. 1 The conformal transformation $\zeta(z)$ takes the rectangle R onto the region G, mapping the top $\partial_1 R$ onto $\partial_1 G$.

Let $\zeta(z)$ be an analytic function that transforms the rectangle R in the z plane conformally onto the region G in the ζ plane so that the top edge, $\partial_1 R$, has image $\partial_1 G$ and the remainder, $\partial_2 R$, of the boundary of the rectangle has image $\partial_2 G$ (see Fig. 1). The sloshing problem (Eqs. 1) is then transformed into an eigenvalue problem for the image function $\psi(z) = \phi[\zeta(z)]$ stated by

$$\begin{aligned} \Delta\psi &= 0 \quad \text{in } R , \\ \frac{\partial\psi}{\partial n} &= \lambda\sigma\psi \quad \text{on } \partial_1 R , \\ \frac{\partial\psi}{\partial n} &= 0 \quad \text{on } \partial_2 R , \end{aligned} \tag{2}$$

where $\sigma = d\zeta/dz$ on $\partial_1 R$. In operator formulation, this is the relative eigenvalue problem

$$Au = \lambda Bu . \tag{3}$$

Now the eigenvalues and eigenvectors of A that satisfy the simpler equation $Au = \lambda u$ are easily found by a separation of variables. Thus Eq. 3 is in an ideal form for applying the *method of intermediate problems*.[4,5] This method finds lower bounds for the eigenvalues of Eq. 3 in the following manner.

Let σ_0 be the maximum of σ on $\partial_1 R$ and write B as

$$B \equiv \sigma_0(I - T^2) .$$

Let P^k be the operator of orthogonal projection on a subspace spanned by a set of functions $\{p_1, \ldots, p_k\}$ in $L^2(\partial_1 R)$. When problem 3 is modified by the projection P^k, the resulting problem,

$$Au = \lambda\sigma_0(I - TP^k T)u , \tag{4}$$

has eigenvalues that are lower bounds for the eigenvalues of Eq. 3. As more functions $\{p_1, \ldots, p_k\}$ are used, the bounds get better. Moreover, if we choose the functions p_i properly, we can solve Eq. 4 exactly by matrix methods. Such a special choice is

$$Tp_i = \sum_{\nu=1}^{n} \beta_{i\nu} u_\nu \ , \tag{5}$$

where the u_ν are the known eigenvectors of A. Then the eigenvalues of Eq. 4 are found by solving the finite-dimensional matrix eigenvalue problem:

$$\det|\Lambda - \lambda\sigma_0(I - \beta^T B^{-1}\beta)| = 0 \ , \tag{6}$$

where Λ is the diagonal matrix of the known first n eigenvalues of A, β is defined by Eq. 5, and B is the Gram matrix of the p_i, given by

$$B_{ij} = \int_{\partial_1 R} p_i(x) p_j(x)\, dx \ .$$

Equation 3 is also in a very convenient form to find upper bounds by the familiar Rayleigh-Ritz method. The eigenfunctions of A are used as trial functions in this method, which leads to the finite matrix problem:

$$\det|\Lambda - \lambda M| = 0 \ , \tag{7}$$

where Λ is as before and M is defined by

$$M_{ij} = \int_{\partial_1 R} \sigma(x) u_i(x) u_j(x)\, dx \ .$$

We have applied this method with great success to a variety of sloshing regions,[6] including images of some nonrectangular regions for which the sloshing problem is solvable. We have been able to determine the first ten to twenty eigenvalues with agreement between the lower and upper bounds to six to eight significant figures using only matrices with orders in the range 20 to 40. Calculations were done on the Laboratory's IBM 3033 computer using the LINPACK and EISPACK standard matrix packages. Figure 2 shows some of the regions considered; also shown are the map, $\zeta(z)$; the first nonzero eigenvalue, λ_1, to the number of places determined; and the order of the matrix that was solved.

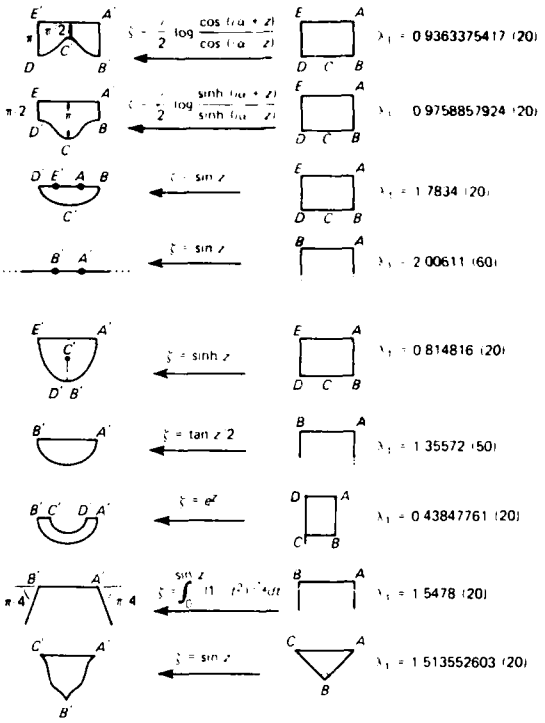

Fig. 2 Regions G, conformal maps $\zeta(z)$, regions R, and first nonzero eigenvalue to the number of places for which the upper and lower bounds agree (order of matrix solved).

REFERENCES

[1] A. G. Greenhill, "Wave Motion in Hydrodynamics," *Am. J. Math.* **9**, 62-112 (1887).

[2] H. Lamb, *Hydrodynamics*, 6th ed., Dover Co., New York, pp. 444-450 (1945).

[3] J. R. Kuttler and V. G. Sigillito, "Lower Bounds for Sloshing Frequencies," *Q. Appl. Math.* **27**, 405-408 (1969).

[4] N. W. Bazley and D. W. Fox, "Lower Bounds to Eigenvalues Using Operator Decomposition of the Form B^*B," *Arch. Rat. Mech. Anal.* **10**, 352-360 (1962).

[5] D. W. Fox and W. C. Rheinboldt, "Computational Methods for Determining Lower Bounds for Eigenvalues of Operators in Hilbert Space," *SIAM Rev.* **8**, 427-462 (1966).

[6] D. W. Fox and J. R. Kuttler, "Upper and Lower Bounds for Sloshing Frequencies by Intermediate Problems," *ZAMP* **32**, 667-682 (1981).

This work was supported by Indirectly Funded R&D.

INTERNAL ENERGY TRANSFER IN MOLECULE-SURFACE COLLISIONS

S. N. Foner and R. L. Hudson

Energy transfer in molecule-surface collisions is a fundamental interaction in heterogeneous chemical processes. Using a modulated molecular beam mass spectrometer, we have carried out the first quantitative measurements on the internal energy excitation of polyatomic molecules in single collisions with heated surfaces.

BACKGROUND

Information on energy transfer in molecule-surface collisions is important for the development of a microscopic understanding of the dynamics of heterogeneous processes. Although considerable experimental information exists on the translational energy accommodation of atoms and molecules on surfaces, rather limited data are available on internal energy accommodation (essentially restricted to the rotational energy accommodation of a few diatomic molecules),[1-4] and prior to this work[5] virtually no quantitative information had existed on internal energy transfer to polyatomic molecules. Recently, considerable attention has been focused on a closely related area, the energy distribution in the desorbed products of heterogeneous reactions.[6-9]

DISCUSSION

When a molecule collides with a heated surface, it experiences changes in its translational and internal (rotational and vibrational) energies. In general, the molecule will not be brought into thermal equilibrium with the surface before being reflected. From kinematic arguments, one expects that translational and rotational energy transfers will be more efficient than vibrational energy transfer.

To carry out the experiments on energy transfer to polyatomic molecules, we used a mass spectrometer that had been developed to detect and characterize free radicals and other transient chemical intermediates. Two major issues had to be addressed: how to assure that the molecules being studied had suffered collisions with the heated surface, and how to measure the internal energy of the molecules. The first issue was solved by the geometrical design of the apparatus. The internal energy was measured by observing the changes produced in the energy required for the dissociative ionization of the molecules.

Figure 1 is a schematic diagram of the mass spectrometer and molecular beam system. The heated surface is a polycrystalline platinum ribbon filament (0.0025 cm thick by 0.075 cm wide) positioned in front of a 0.020-cm-diameter beam sampling aperture (slit 1). A unique feature of the experimental arrangement is that if the ambient gas pressure is kept low enough to avoid gas scattering in the filament to the slit 1 region, only molecules that have collided with the filament can enter the molecular beam and be ionized and subsequently detected by the mass spectrometer. All other molecules entering through slit 1 are geometrically excluded by the additional collimating slits.

The beam chopper is used in two distinct operational modes. In the first, or traditional, mode it is used for background suppression and low-level signal mea-

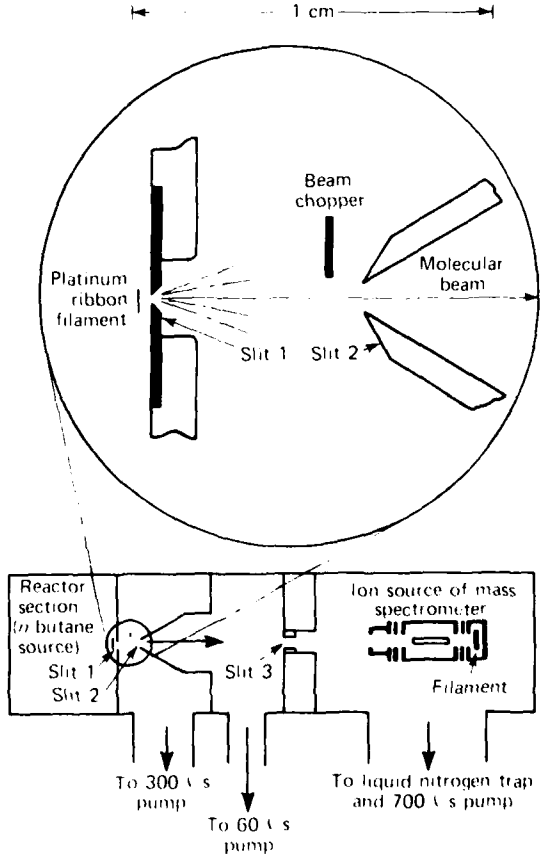

Fig. 1 Mass spectrometer and molecular beam system for studying energy transfer in molecule-surface collisions.

surements, such as are required for ionization potential measurements and free radical detection. The beam chopper modulates the beam on and off at 170 Hz. The electron multiplier counting circuits are synchronously gated to provide the signal and the background level.[10-12] In the second mode, which is used here for translational energy measurements, the ion current is sampled at 20 μs intervals to obtain the displacements of the leading and trailing edges of the beam pulse, from which one determines the transit times of the molecules into the ion source. (At 300 K, for example, the transit time for an *n*-butane molecule, $M = 58$, that has the most probable velocity is 324 μs.)

The method we have used to measure internal energy relies on the fact that a molecule with internal energy is more easily fragmented than one without internal energy. For mass spectrometric measurements, we actually study dissociative ionization processes, where internal energy is most directly manifested by changes in ionization energy and in the shapes of the ionization curves near threshold. Because a large fraction of the molecule's internal energy is available for fragmentation, less energy has to be supplied by the ionizing electrons, and this results in a lowering of the ionization energy. To provide molecules with known internal energy, the heated filament is replaced by an effusive oven source in the calibration procedure. In the oven, the molecules suffer many collisions with each other and with the walls; when they leave, they are in thermal equilibrium with the oven.

We have chosen *n*-butane as a typical polyatomic molecule. Figure 2 shows data on appearance potential for the peak corresponding to the $C_3H_7^+$ ion fragment from the *n*-butane at room temperature, after collision with a platinum filament at 1000°C and after effusion from an oven at 300°C. In the heated filament experiments the *n*-butane pressure was intentionally kept low, between 0.004 and 0.010 Torr, to eliminate gas scattering effects. Although the platinum filament had been cleaned by being heated in oxygen at 1100°C, the formation of a carbon overlayer on the surface is not unlikely at these pressures. The observed energy shift for the oven-heated $C_3H_7^+$ ionization curve is consistent with previously published photoionization data taken at a lower temperature.[13] It is obvious that the internal energy acquired by an *n*-butane molecule in a single collision is only a small fraction of that appropriate to the filament's temperature.

The increase in internal temperature of an *n*-butane molecule on collision with the 1000°C filament, determined using internal energy interpolation between the equilibrium curves for the oven source at 30 and 300°C, was about 130°C. Because the heat capacity of *n*-butane is a very nonlinear function of temperature, the internal energy accommodation is substantially lower than the 13% (130°C temperature rise upon collision with the 1000°C filament) suggested by the above result. In particular, the vibrational energy accommodation coefficient is only about 5%, as we shall see.

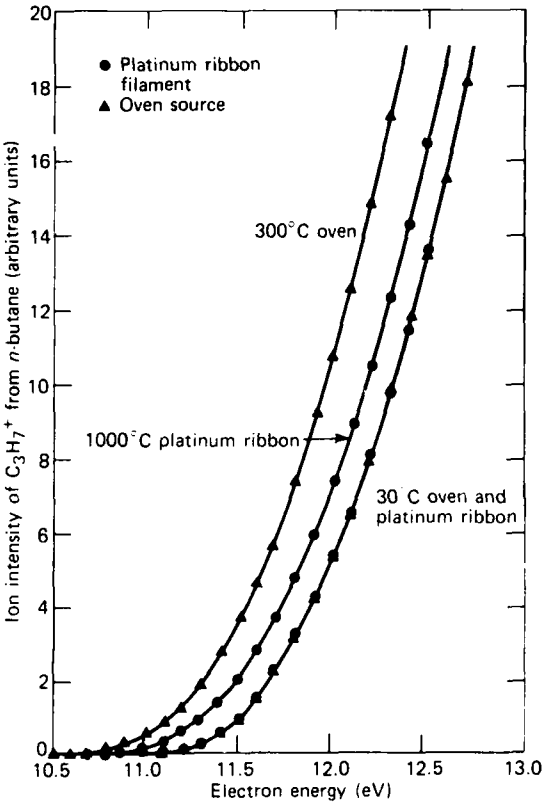

Fig. 2 Appearance potential curves for the $C_3H_7^+$ ion from *n*-butane at room temperature, after collision with a platinum filament at 1000°C and after effusion from an oven at 300°C. The data have been subjected to "deboltzmannization" to remove the thermal energy spread in the electron beam,[12] and the energy scale has been standardized using argon, ionization potential = 15.76 eV.

The translational energy accommodation coefficient is $\alpha_t = (E_i - E_r)/(E_i - E_s)$, where E is the translational energy and i refers to incident molecules, r to reflected molecules, and s to molecules in equilibrium with the surface. Similar expressions apply for the vibrational, α_v, and rotational, α_r, energy accommodation coefficients. For *n*-butane impinging on platinum, α_t was determined from transit time measurements as described above and was found to be a decreasing function of temperature, having a value of 0.48 at low temperatures and dropping to 0.34 at 1000°C.

The difference between the equilibrium internal energies for *n*-butane at 1000°C and at 30°C is 39.7 kcal/mole.[5] The total internal energy acquired by *n*-bu-

tane molecules on collision with the 1000°C platinum filament is found from the interpolation discussed above; its value is 3.0 kcal/mole. Thus, if one assumes that rotational accommodation parallels that of translation (i.e., $\alpha_r = 0.34$), then the rotational energy contribution is 0.98 kcal/mole, leaving 2.0 kcal/mole for vibration, which corresponds to a vibrational energy accommodation coefficient of 0.05. It is perhaps not too surprising that it is difficult for a molecule like *n*-butane, with 36 vibrational modes, to achieve thermalization in a single collision.

REFERENCES

[1] C. W. Draper and G. M. Rosenblatt, "Thermal Accommodation Coefficients by High Speed Vibration of Solid Samples," *Surface Sci.* **99**, 671 (1980).
[2] V. Ramesh and D. J. Marsden, "Rotational and Translational Accommodation Coefficients of Nitrogen on Nickel, Silver, and Gold," *Vacuum* **24**, 291 (1974).
[3] W. Allison and B. Feuerbacher, "Rotationally Inelastic Molecule-Surface Scattering," *Phys. Rev. Lett.* **45**, 2040 (1980).
[4] F. Frenkel, J. Hager, W. Krieger, H. Walther, C. T. Campbell, G. Ertl, H. Kuipers, and J. Segner, "Rotationally Inelastic Gas-Surface Scattering Investigated by Laser-Induced Fluorescence," *Phys. Rev. Lett.* **46**, 152 (1981).
[5] S. N. Foner and R. L. Hudson, "Internal Energy Transfer in Molecule-Surface Collisions," *J. Chem. Phys.* **75**, 4727 (1981).
[6] G. Comsa, R. David, and B. J. Schumacher, "The Angular Dependence of Flux and Velocity Distribution for D_2 Molecules Desorbing from the Ni(111) Surface," *Surface Sci.* **85**, 45 (1979).
[7] C. A. Becker, J. P. Cowin, L. Wharton, and D. J. Auerbach, "CO_2 Product Velocity Distributions for CO Oxidation on Platinum," *J. Chem. Phys.* **67**, 3394 (1977).
[8] R. P. Thorman and S. L. Bernasek, "The Internal Energy Distribution of Atom-Recombination Product N_2 Desorbing from Polycrystalline Fe," *J. Chem. Phys.* **74**, 6498 (1981).
[9] L. D. Talley, W. A. Sanders, D. J. Bogan, and M. C. Lin, "Internal Energy of Hydroxyl Radicals Desorbing from Polycrystalline Pt Surfaces," *Chem. Phys. Lett.* **78**, 500 (1981).
[10] S. N. Foner and R. L. Hudson, "Mass Spectrometric Studies of Atom-Molecule Reactions Using High Intensity Crossed Molecular Beams," *J. Chem. Phys.* **53**, 4377 (1970).
[11] S. N. Foner and R. L. Hudson, "Mass Spectrometry of the HO_2 Free Radical," *J. Chem. Phys.* **36**, 2681 (1962).
[12] S. N. Foner and R. L. Hudson, "On the Heat of Formation of Diimide," *J. Chem. Phys.* **68**, 3162 (1978).
[13] B. Steiner, C. F. Giese, and M. G. Inghram, "Photoionization of Alkanes. Dissociation of Excited Molecular Ions," *J. Chem. Phys.* **34**, 189 (1961).

This work was supported by Indirectly Funded R&D.

INTERSTACK SPIN-ORBIT COUPLING AND ELECTRON-SPIN-RESONANCE LINE BROADENING IN ORGANIC METALS

F. J. Adrian

The electron spin resonance (ESR) line widths (ΔH) of the one-dimensional organic conductors tetrathiofulvalenium-tetracyanoquinodimethanide (TTF-TCNQ) and its isostructural selenium analog (TSeF-TCNQ) are explained in terms of spin-orbit coupled electronic transitions between the one-dimensional conduction bands of adjoining electron-donor (TTF) and electron-acceptor (TCNQ) molecular stacks.[1] The fact that ΔH depends only slightly on magnetic field orientation suggests that the transition involves a spin-correlated electron pair rather than a single electron.

BACKGROUND

Organic metals are formed by the reaction of an electron-donating molecule and an electron-accepting molecule to form a partially ionic charge-transfer compound.[2] Either the donor or the acceptor must be (and often both are) planar, highly conjugated molecules (i.e., benzene-like) in which the donated and accepted electrons occupy π molecular orbitals (MO's) constructed from *p*-type atomic orbitals (AO's) oriented perpendicular to the molecular plane. The organic metal crystal structure consists of individual stacks of the donor and acceptor molecules, as illustrated in Fig. 1 for TTF-TCNQ. This stacking pattern enables the π MO's of adjoining molecules in the donor stack to interact (and similarly for the MO's of the acceptor stack), causing the electrons in those MO's to become delocalized into separate donor and acceptor conduction bands. Obviously, the electrons conduct efficiently only in the stacking direction, so the materials are one-dimensional conductors. The substances are of great interest from the standpoint of their fundamental physics and chemistry and because of their potential electronic

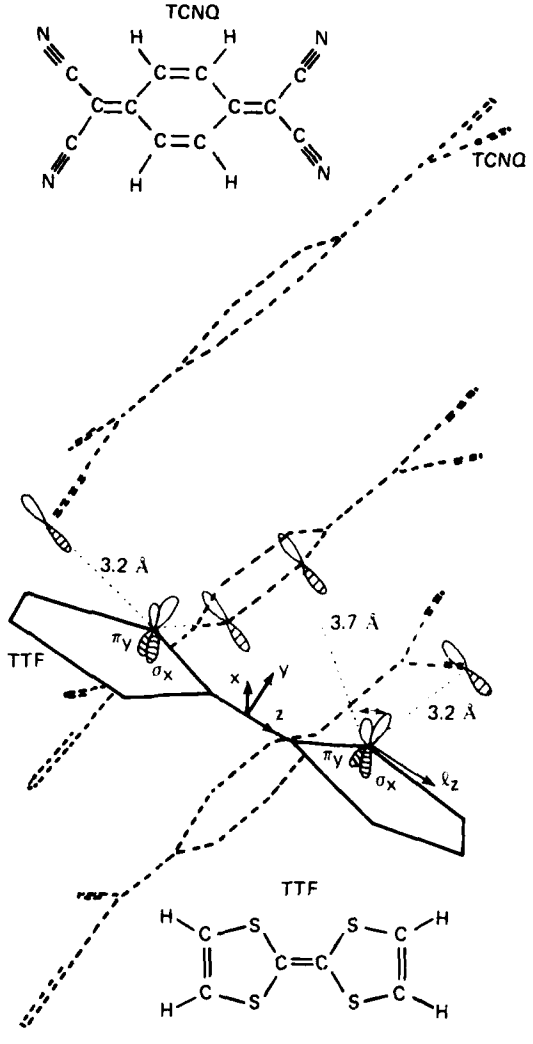

Fig. 1 TTF-TCNQ crystal structure and effects of spin-orbit interactions and interstack overlap in TTF-TCNQ. Each molecule in a TTF donor stack (only one molecule shown) interacts with three TCNQ molecules of each acceptor stack. The nearest-neighbor overlapping orbitals, indicated by dotted lines, are the *S-N* and *S-C* orbitals separated by 3.20 and 3.73 Å, respectively.

applications; consequently, they have been subjected to extensive experimental and theoretical investigation.

The electron spin magnetic moments of the unpaired conduction band electrons (as constrasted with the paired electrons of opposite spin and hence zero net magnetic moment found in localized chemical bonds) make these materials paramagnetic and amenable to investigation by ESR. This technique observes transitions between the two magnetic sublevels of an unpaired electron for which its spin (s) and associated magnetic moment (μ_e) are, respectively, parallel and antiparallel to an external magnetic field (H). For $H = 3000\ G$, the transition frequency is in the microwave range at 9000 GHz. The precise ESR line frequency, its width, and various fine-structure splittings are related to magnetic interactions between the electron and its molecular environment; thus, the measured quantities can be translated, with the aid of theory, into detailed structural information. Although the delocalization of the electron in a conduction band obliterates the electron-molecule interactions responsible for the fine-structure splittings, there remains ΔH and the effective electronic magnetic moment, which differs somewhat from the free-spin value because of small contributions from the orbital motions of the electrons. Experiment shows that in the organic metals, ΔH is the result of donor heavy-atom (sulfur in TTF, selenium in TSeF) spin-orbit interactions that scatter the conduction electrons between conduction band states with an accompanying change in electron spin state.[3] These processes limit the lifetime of an electron in a particular spin state and consequently broaden the ESR line in accordance with the Heisenberg Uncertainty Principle.

However, the spin-orbit origin of ΔH was puzzling because spin-orbit interactions are ineffective for electrons confined to a one-dimensional band. Although it was fairly obvious that weak interstack interactions had to be involved, previous theories attempted to incorporate the limited two-dimensional character of the organic metals into the theory of spin-orbit coupled transitions in isotropic metals.[3] This approach is incorrect because it neglects the molecular character of the units comprising the organic metals (as contrasted with atoms in ordinary metals) and thus fails to consider important features of the spin-orbit interaction of an atom when bound in a molecule.

DISCUSSION

The spin-orbit interaction is between the electron spin magnetic moment and the magnetic field created at the electron by its orbital motion with respect to the other charged particles in the system. Fortunately, all elements of this very complicated interaction can be neglected except for terms involving the orbitals of the heaviest atom(s) in the system, where the combined effects of a large nuclear charge and the very rapid orbital motion of the electron in the coulomb field of this nucleus yield a very large orbital magnetic field. The spin-orbit interaction energy of a single sulfur or selenium atom is $\lambda \mathbf{l} \cdot \mathbf{s}$, where $(h/2\pi)\mathbf{l}$ and $(h/2\pi)\mathbf{s}$ are the orbital and spin angular momentum of the electron, h is Planck's constant, and $2\pi\lambda/h = 7.2 \times 10^{13}$ and $3.8 \times 10^{14}\ s^{-1}$ for sulfur and selenium, respectively. As depicted in Fig. 1 for the zth component of $\mathbf{l}$, this operator rotates a p orbital 90° about the operator axis,

except that the result is zero if the orbital is parallel to the operator axis. Thus, l can only couple the donor π orbitals with in-plane bonding sulfur or selenium σ AO's, and these σ states are too far removed energywise from the π states to be directly involved in the ΔH producing transitions.

However, the donor σ AO's overlap slightly with the acceptor π orbitals, as is also depicted in Fig. 1. The overlap corresponds to a partial attempt by two electrons to occupy the same region of space. This is forbidden for electrons of the same spin by the Pauli Exclusion Principle. The remedy is to eliminate the overlap by Schmidt orthogonalization of the acceptor π MO's to the donor σ AO's, i.e., $\pi_A^{or} = \pi_A - \langle \pi_A | \sigma_D \rangle \sigma_D$. This obviously admixes a small donor σ component into the acceptor π states and enables donor spin-orbit coupled transitions between the donor and the acceptor π states. Since these transitions can be accompanied by an electron spin transition generated by the spin operator s, they can lead to ESR line broadening.

A static coupling of the donor and acceptor π states cannot produce transitions. The spin-orbit coupling must be time varying, much as an oscillating electromagnetic field is required to stimulate atomic and molecular transitions. The time variation here is provided by electron-electron and electron-molecular-vibration interactions that scatter the electrons between intrastack conduction band states. The resulting transition rate is

$$W = 2(2\pi\lambda/h)^2 |\langle s' | s_z | s'' \rangle|^2 \langle \pi_A | \sigma_D \rangle^2 \tau_1 , \qquad (1)$$

where $1/\tau_1$ is the electron scattering rate and $\langle s' | s_z | s'' \rangle$ is the electron spin transition matrix element. From the Heisenberg Uncertainty Principle, $\mu_e \Delta H = (h/2\pi W)$. The results for TTF-TCNQ and TSeF-TCNQ at 300 K are 6 and 470 G,[1] respectively, in good agreement with the observed line widths of 7 and 508 G.[3]

Although there is good agreement between the calculated and observed line widths, there remains the question why ΔH is often independent of the orientation of the exter' l field, H, despite the very anisotropic crystal structures of the organic metals. As shown in Fig. 1, the σ_1 donor AO's, which have the only significant overlaps with the acceptor π states, are coupled to the donor σ states by the orbital operator l_z. The accompanying spin operator is s_z. If the transition involves a single unpaired electron whose spin is parallel or antiparallel to H, then s_z can change the spin state, as required for line broadening, only if H is perpendicular to z. For this case, ΔH should depend strongly on the orientation of H.

A possible answer to this problem begins by noting that there are several types of spin transition, depending on the occupancy of the donor and acceptor states.[1] They are:

I $\quad (D: A\bullet) \rightharpoonup (D\bullet\ A:)$,

II $\quad (D: A) \rightharpoonup (D\bullet\ A\bullet) \rightharpoonup (D\ A:)$,

III $\quad (D\bullet\ A) \rightharpoonup (D\ A\bullet)$,

where the dots denote electrons in the donor and acceptor states. Case III is obviously a single electron transition. Case I is effectively a single electron spin transition because the Pauli Exclusion Principle requires the two electrons in the same state to be nonmagnetically paired. However, in case II, the (D• A•) electrons may be either a nonmagnetic (singlet) or a magnetic (triplet) pair. The line broadening in case II is due to a spin transition from the triplet part of (D• A•) to the pure singlet (D: A) and (D A:) states. It can be shown that the spin matrix element $|\langle s' = \text{singlet} | s_z | s'' = \text{triplet} \rangle|^2 = 1/16$, independent of the orientation of H.[1] Furthermore, it is reasonable to expect that (D: A)⇀(D• A•) will be the only significant transition because all other transitions involve either a doubly occupied acceptor state or a vacant donor state.[1] These states are energetically unfavorable because the first electron received by an acceptor state tends to repel a second electron and, similarly, the loss of one electron by a donor state renders it positively charged and less likely to yield a second electron.

REFERENCES

[1] F. J. Adrian, "Interstack Spin-Orbit Coupling and ESR Line Broadening in Tetrathiofulvalenium-Tetracyanoquinodimethanide" (to be published).

[2] H. J. Keller, ed., *Physics and Chemistry of One-Dimensional Metals*, Plenum Press, New York (1977).

[3] Y. Tomkiewicz, "ESR of Organic Conductors," in *The Physics and Chemistry of Low Dimensional Solids*, L. Alcacer, ed., D. Reidel Co., Boston, pp. 187-195 (1980).

This work was supported by Indirectly Funded R&D.

MEMBRANE TRANSPORT IN NONIDEAL, NONDILUTE SOLUTIONS

M. H. Friedman and R. A. Meyer

Using irreversible thermodynamics, we have developed a set of transport equations for membranes bounded by concentrated solutions. We have confirmed the validity of the equations experimentally.

BACKGROUND

Conventional techniques for measuring membrane transport properties are based on the implicit assumptions that the membrane is homogeneous (i.e., it contains only one kind of transport pathway) and that the solutions bounding the membrane are dilute and ideal. However, those assumptions often are not valid and can lead to significant errors in predicting membrane performance. Earlier theoretical studies[1] showed that the errors introduced by membrane structure are greater in more concentrated solutions, even when the effects of solution nonideality are ignored. A better understanding of the influence of membrane structure and solution nonideality on membrane transport should permit the more rigorous interpretation of transport experiments and the more confident design of separation devices.

We have developed equations that describe the transport across a structured membrane bounded by concentrated solutions of a single solute.[2,3] The equations show that the membrane reflection coefficients for volume and solute flow are unequal but related by a simple expression that depends on the concentration of the bounding solutions. Experimental measurements of these reflection coefficients for sucrose transport across Cuprophan dialysis membrane verify this relationship. A simplified expression for membrane transport in nonideal, nondilute solutions was developed based upon the use of a modified osmotic driving force.

DISCUSSION

Most studies of nonelectrolyte transport through membranes are interpreted in terms of the Kedem-Katchalsky equations[4] derived from irreversible thermodynamics. If only a single solute is present,

$$J_v = -L_p(\Delta P - \sigma_f RT\Delta c_s) \qquad (1a)$$

and

$$J_s = J_v(1 - \sigma_s)c_s - \omega_p RT\Delta c_s \ , \qquad (1b)$$

where J_v is volume flux, J_s is solute flux, L_p is the hydraulic conductivity of the membrane, ω_p is the phenomenological permeability of the membrane for the solute, c_s is a mean solute concentration, R is the gas constant, and T is absolute temperature. When the solutions are ideal and dilute ($c_s V_s << 1$, where V_s is the partial molar volume of the solute), the reflection coefficients for volume flow and solute flow, σ_f and σ_s, respectively, are equal.

The physical significance of the reflection coefficients, whose value in ideal dilute solutions lies between zero and unity, is most clearly seen from Eq. 1b. The first term in the equation can be regarded as the flux of solute convected across the membrane in the volume flux. In an "open" membrane whose pores are much larger than the solute diameter, $\sigma_s \approx 0$ and the convected solute flux is simply the product of the volume flux and the solute concentration. When the membrane pores are closer in size to that of the solute, the membrane exerts a sieving effect so that the convected flux of solute is less; σ_s becomes greater than zero. The reflection coefficient of an impermeable membrane is unity, and no solute is passed. Thus, the reflection coefficient measures the ability of the membrane to separate the solute from the solvent.

The derivation of equations analogous to Eqs. 1 for transport in nonideal, nondilute solutions is based on the Kirkwood formulation of the Stefan-Maxwell equations.[5] The fluxes of solvent and solute are expressed in terms of generalized diffusivities and the exact chemical potential gradients of the two components. The equations are linearized and integrated across the membrane to yield flux equations from which the following relationship between σ_s and σ_f is obtained[2]:

$$\sigma_s = \sigma_f \frac{1 - \nu_s}{1 + \Gamma} \ , \qquad (2)$$

where $\nu_s \equiv c_s V_s$ is a measure of the nondiluteness of the solutions bounding the membrane, and $\Gamma \equiv d \ln \gamma_s / d \ln c_s$ is a measure of the influence of nonideality on the transport process (γ_s is the activity coefficient of the solute). This relationship between σ_s and σ_f is independent of heteroporous membrane structure and the presence of boundary layers. Thus σ_s is expected to be a concentration-dependent fraction of σ_f, approaching σ_f as the solutions become more dilute ($\nu_s \to 0$) and more ideal ($\Gamma \to 0$).

Equation 2 was tested experimentally to verify the newly developed theory. The membrane transport

apparatus described previously[6] was used to measure σ_t and σ_s simultaneously for the solute/membrane system sucrose/Cuprophan 150PM. Transport measurements were made at four mean sucrose concentrations. As shown in Fig. 1, σ_s is essentially independent of c_s, whereas σ_t decreases as c_s decreases and at low values of c_s approaches σ_s. The experimental values of σ_s/σ_t are plotted against c_s in Fig. 2. The measured ratios correlate well with those predicted by Eq. 2 and thus provide experimental evidence for the validity of the theory on which it is based.

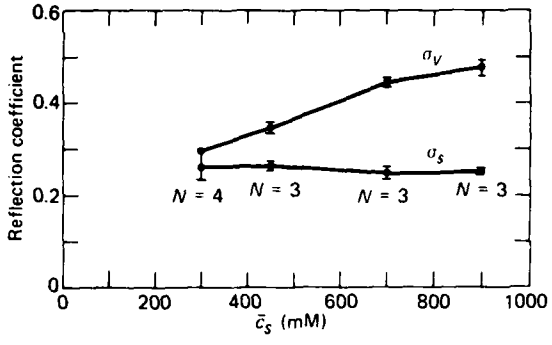

Fig. 1 Concentration dependence of reflection coefficients for sucrose transport across Cuprophan. *N* designates the number of experiments at each sucrose concentration; error bars are ± 1 standard error of the mean.

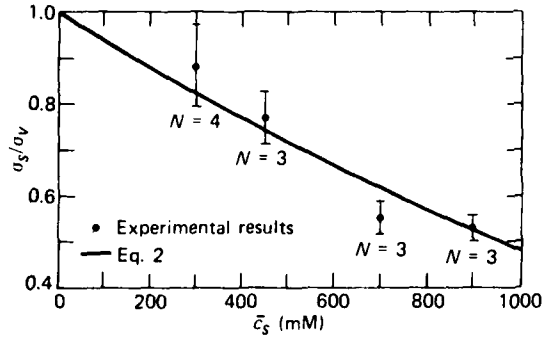

Fig. 2 Concentration dependence of σ_s/σ_t for sucrose transport across Cuprophan. Error bars are ± 1 standard error of the mean.

The analysis leading to Eq. 2 can also be used to convert Eqs. 1 into a form that describes transport in nonideal, nondilute solutions in terms of a single reflection coefficient. The quantity $RT\Delta c_s$ in Eqs. 1 is commonly termed the "osmotic pressure" difference, $\Delta\Pi$. By defining a modified osmotic driving force, $\Delta\Pi_m = (1 + \Gamma)\Delta\Pi/(1 - \nu_s)$, one obtains

$$J_t = -L_p(\Delta P - \sigma_s\Delta\Pi_m) \tag{3a}$$

and

$$J_s = J_t(1 - \sigma_s)c_s - \omega_{pm}\Delta\Pi_m \ , \tag{3b}$$

where ω_{pm} is a modified phenomenological permeability. Equations 3 reduce to Eqs. 1 for ideal dilute solutions.

REFERENCES

[1] M. H. Friedman, "The Effect of Membrane Heterogeneity on the Predictability of Fluxes, with Application to the Cornea," *J. Theor. Biol.* **61**, 307-328 (1976).

[2] M. H. Friedman and R. A. Meyer, "Transport Across Homoporous and Heteroporous Membranes in Nonideal, Nondilute Solutions. I. Inequality of Reflection Coefficients for Volume Flow and Solute Flow," *Biophys. J.* **34**, 535-544 (1981).

[3] M. H. Friedman and R. A. Meyer, "Transport Across Homoporous and Heteroporous Membranes in Nonideal, Nondilute Solutions. II. Inequality of Phenomenological and Tracer Solute Permeabilities," *Biophys. J.* **34**, 545-557 (1981).

[4] O. Kedem and A. Katchalsky, "Thermodynamic Analysis of the Permeability of Biological Membranes to Non-electrolytes," *Biochim. Biophys. Acta* **27**, 229-246 (1958).

[5] E. N. Lightfoot, *Transport Phenomena and Living Systems*, John Wiley and Sons, New York (1974).

[6] R. A. Meyer and M. H. Friedman, "Interferometric Technique for the Simultaneous Measurement of Passive Membrane Transport Coefficients," *Rev. Sci. Instrum.* **48**, 1317-1321 (1977).

This work was supported by Indirectly Funded R&D.

ENERGY, ENVIRONMENT, AND URBAN TECHNOLOGY

INTRODUCTION

Efficient energy generation and utilization are implicit in much of APL's defense work and satellite systems, particularly in missile propulsion. An APL evaluation of alternative, long-range, nondepleting sources of energy identified solar and geothermal energy sources as being especially attractive to meet future national requirements. Studies of the exploitation of one aspect of solar energy, the thermal gradient between the surface and the deep ocean, indicate that Ocean Thermal Energy Conversion (OTEC) may provide a practical and economical way to produce electricity and chemical products. The APL Ocean Energy Program assists the Department of Energy in the technical assessment of this concept.

APL also assists the Department of Energy in the assessment of geothermal resources and applications in the eastern United States. Knowledge gained from these two programs, along with the analysis of worldwide geothermal resources, has suggested the potential of hybrid geothermal/ocean thermal energy conversion (GEOTEC) plants. The GEOTEC system combines geothermal resources with OTEC power cycle technology and seawater cooling. It may permit the useful production of electric power or energy-intensive products at sites where neither technology alone would be suitable.

Other energy projects have included investigations of the reentry safety aspects of radioisotope heat sources used in spacecraft, the development of a sensing/shutoff system to eliminate the effects of arc faults in ship service switchboards, the development of methods to evaluate methane gas resources and to recover this gas from landfills, the development and testing of high-speed flywheels for energy storage, and fundamental photovoltaic research to develop thin-film techniques leading to inexpensive solar cells.

APL has been studying the environmental effects of energy facilities since 1971. A major activity has been the evaluation for the State of Maryland of the potential environmental, economic, and social impacts of all power-generating facilities proposed for development and construction in the state. In addition, generic studies are conducted for the State of Maryland and other public agencies in technical areas related to the location of energy facilities, their impact, and the mitigation of that impact.

Through a variety of special projects, APL has participated in and contributed to programs for developing and applying modern technology to several civil problems, including public transit and the movement of hazardous materials. The APL Transportation Program has been active since 1969. Its efforts have included research directed at the development of automated guideway transit command and control systems and at the provision of technical assistance to public agencies in the conduct of their automated transit and other transportation programs.

MODEL BASIN TESTS OF A 40 MW OTEC PILOT PLANT

J. F. George and D. Richards

A 1/30-scale model of a floating 40-MW ocean thermal energy conversion (OTEC) pilot plant has been subjected to wave conditions that the prototype would experience as a plant moored off Puerto Rico or Hawaii, or as a cruising plantship in the South Atlantic Ocean east of Brazil. The model survived the design wave conditions, but the measured data and test observations suggest that if the plant is to be moored at an island site, hull form modifications are required in order to prevent large "green water" waves from breaking over the bulwarks and damaging critical OTEC equipment located topside.

BACKGROUND

APL has been involved in OTEC development programs since 1973. Most of the work has emphasized a system in which OTEC plantships cruise slowly in tropical waters, using the ocean thermal gradient to run a heat engine, produce electricity, and then synthesize an energy-intensive product (e.g., ammonia or methanol) for storage and later shipment to market.[1,2] This approach seems to offer advantages over other OTEC systems in that the greatest temperature difference can be obtained in tropical waters, there are large operating areas where hurricanes have never been observed, and the energy-intensive product option eliminates the need to develop costly mooring and electric cable systems.

In 1980, APL completed the baseline design of a pilot plantship[3] that could produce up to 40 MW_e (net) of OTEC power while cruising in the South Atlantic approximately 500 nmi east of Recife, Brazil, or as a moored plant at an island site, with the electricity supplied by undersea cable to a shore utility grid. The barge-like hull is 135 m long and has a full-load displacement of 97,100 metric tons, including seawater ballast. The moored version of this pilot plant is shown in Fig. 1. The most stringent design condition is the 100-year-return, "most probable" hurricane at the Punta Tuna, Puerto Rico, site where the significant wave height (H_s) is 11 m and the modal period (T_m) is 13 s. There is no record of hurricanes at the Brazil site, and the design condition is characterized by long-period, swell-dominated waves with H_s = 8.5 m and T_m = 18 s.

Computer codes were used to predict the response of the platform and its attached cold water pipe (CWP), but inherent limitations in these simulations do not give sufficient confidence that the pilot plant can survive the severe hurricane conditions at Puerto Rico. For this reason, scale-model basin tests were conducted.

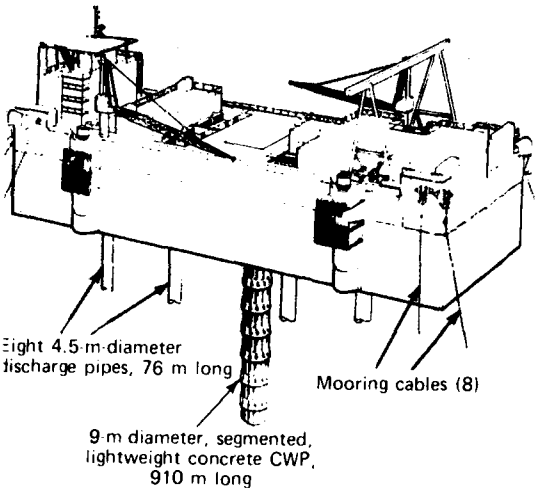

Fig. 1 Moored version of 40 MW (nominal) OTEC pilot plant.

DISCUSSION

The objectives of the model basin tests were to (a) verify the seaworthiness of the baseline pilot plant design under the extreme 100-year storm conditions; (b) measure mooring line tension, CWP angular rotation and axial force, and seawater system pressures; and (c) observe the behavior of the OTEC seawater system as a function of sea state and heading.

Model Description

Because the primary objective was to quantify the seakeeping characteristics of the pilot plant hull, particularly in large waves where nonlinear effects may be significant, it was important to use as large a model as practical, and a 1/30th-scale size was selected. At this scale, only the upper portion of the CWP could be modeled, and a ballast slug was added to the bottom to represent the mass effect of the missing length. The tests were conducted in the deep model basin of the Offshore Technology Corp., Escondido, Calif. Both regular and random wave seas were generated; the wave flap was driven by a hydraulic ram.

Principal Observations

The platform responded smoothly to the long-period, swell-dominated waves of the Brazilian site.

There was very little water on deck. The response to the hurricane sea conditions of Hawaii and Puerto Rico was very different. There the periods of peak wave energy fell directly in the range of the platform's natural periods in heave, pitch, and roll. The motions of the platform were large, and waves broke above the bulwark deck on all headings. When subjected to beam seas, the platform was pounded severely by the large waves.

Considerable difficulty was encountered with the mooring system during simulated hurricane conditions. When groups of large waves encountered the model, it was displaced substantially in surge and sway. This behavior was, in fact, consistent with predictions of the Lockheed study[4] that extreme conditions could displace the platform by as much as 335 m.

The action of the CWP and eight seawater discharge pipes could be viewed through an underwater window to the test pit. The response of the CWP was unremarkable. The platform appears to roll and pitch about the gimbal connection. No vibration modes were apparent.

Platform Motions and Seakeeping

The maximum platform responses measured in 16 tests at survival conditions are shown in Table 1. Maximum roll values were well within stability limits, and maximum heave accelerations do not exceed 0.25 g.

Table 1

MAXIMUM BASELINE PLATFORM RESPONSES AT 100-YEAR STORM CONDITIONS*

	Brazil	*Hawaii*	*Puerto Rico*
Roll (deg)	10.8	14.0	15.1
Pitch (deg)	7.6	11.9	12.7
Heave (m)	8.0	7.5	9.0
Heave acceleration ($m\ s^{-2}$)	1.7	2.2	2.4

*These maximum values do not occur at a single ship heading.

A shaped bow section and large bilge keels were added to the baseline platform. The additions improved the platform response for head and bow seas, but the response in beam seas, which is critical because of the frequent occurrence of green water coming over the gunwales at this heading, was virtually unaffected. Figure 2, a plot of the relative wave height amidships during the Puerto Rico hurricane, shows that the bulwark level would be exceeded approximately once a minute. Without protective modifications to the hull configuration, the OTEC heat exchangers and power system equipment probably would be damaged.

Response of the CWP

A critical design element is the attachment of the CWP to the hull. In most design concepts, the pipe is attached by a gimbal, universal, or ball-in-socket joint that permits relative roll and pitch angular motion. These angles were measured during tests; Fig. 3 shows a sequence of data for a simulated hurricane at Puerto Rico, with seas on the bow. The maximum values observed during the test sequence were −4.0° roll and +12.7° pitch and a maximum combined rotation of 13.3°. Allowance must be made for the rotation arising from current forces and platform heel. Although these contributing factors have not been analyzed completely, a CWP/platform joint with an angular capability of ±18° apparently is adequate for a cruising plantship in the Brazil operating area, but additional rotational capability (i.e., ±20 to ±25°) is required at the island sites.

Seawater Systems

The model had no seawater pumps or flowing systems, but heat exchanger resistances, warm water pump inlet screens, and the pump water column were represented. Seawater system pressures were measured at the center of the warm water intake grill, and the variation in pressure was used to estimate the effect on power requirements to pump warm water. For sea

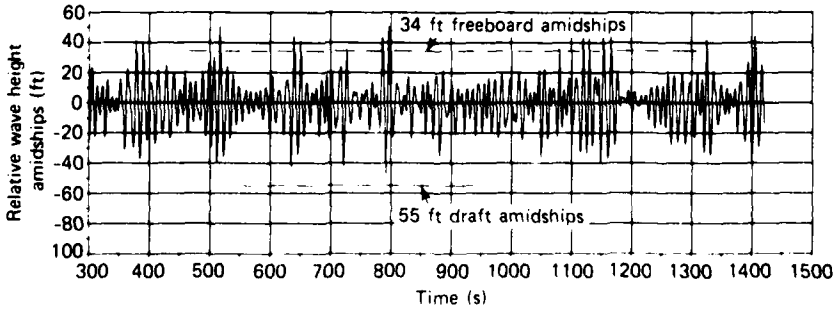

Fig. 2 Relative wave height amidships (test 115, Puerto Rico hurricane, beam seas).

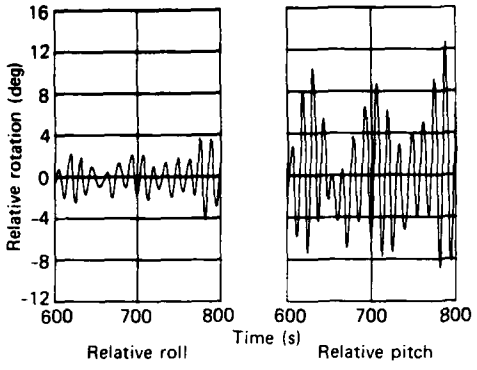

Fig. 3 Relative rotation at the CWP/platform connection (test 307, Puerto Rico hurricane, bow seas).

states near the expected limit of OTEC operation (H_s = 5 m), the power variation is approximately ±20%, or ±2% of the gross OTEC turbine generator load at the design temperature differential. Open-top pond trays were added in one test series to obtain qualitative observations of pond surface behavior. The observed surface waves in the prototype-timed movies rarely exceeded the main deck line in limiting sea states and usually were less than ±1 m.

CONCLUSION

This series of model basin tests proved valuable in demonstrating the seakeeping characteristics of a floating 40 MW OTEC pilot plant. It was shown that a barge-shaped ship of this size is suitable for use as a cruising plantship in the South Atlantic Ocean east of Brazil, where the significant wave height is not expected to exceed 8.5 m and the seas are characterized by long-period swells (T_z = 18 s). On the other hand, it was demonstrated clearly that modifications to the hull form would be required if the ship were moored near the islands of Puerto Rico or Hawaii, where it would be subject to more severe wind and wave conditions (e.g., H_s = 11 m).

REFERENCES

[1] W. H. Avery et al., *Maritime and Construction Aspects of Ocean Thermal Energy Conversion (OTEC) Plant Ships*, JHU APL SR 76-1B (Apr 1976).
[2] E. J. Francis, *Investment in Commercial Development of Ocean Thermal Energy Conversion (OTEC) Plant-Ships*, JHU APL SR 77-3 (Dec 1977).
[3] J. F. George and D. Richards, *Baseline Designs of Moored and Grazing 40-MW OTEC Pilot Plants*, JHU APL SR-80-1 A and B (Jun 1980).
[4] *Preliminary Design Report for OTEC Stationkeeping Subsystems (SKSS)*, Lockheed Ocean Systems, Sunnyvale, Calif. (Oct 1979).

This work was supported by the Department of Energy, Ocean Technology Division.

GEOTHERMAL/OCEAN-THERMAL ENERGY CONVERSION (GEOTEC) POWER PLANTS

G. L. Dugger, L. L. Perini, and F. C. Paddison

For locations far from the equator where conventional ocean thermal energy conversion (OTEC) cannot be used (no warm surface water) but where a moderate-quality (140 to 200°C) geothermal water exists near a shoreline, there could be advantages in combining the OTEC and geothermal binary cycle technologies. Such hybrid GEOTEC plants could be particularly attractive for remote military bases having a modest power demand (10 to 40 MWe) now satisfied by an oil-fired plant, such as the Naval Air Station at Adak, Alaska.

BACKGROUND

Seventy percent of the world's installed capacity for the geothermal production of electricity (2475 MWe[1]) is based on geothermal resources that produce steam directly; 30% is produced by geothermal water (geofluid) that is hot enough so that 20% or more can be flashed to steam without intolerable precipitation of dissolved solids. However, electricity can be produced economically with moderate-quality (≤200°C) re-

sources by means of a binary cycle in which the geofluid, kept under pressure, transfers some of its heat to a working fluid that is vaporized to drive the power turbine in a closed Rankine cycle of the same type used in OTEC plants. Since the supply of makeup cooling water is a problem for conventional inland binary geothermal plants, GEOTEC plants with seawater for cooling will have an important advantage.

The geothermal resource regions tend to lie in bands that include islands and island arcs, e.g., the Aleutian Islands of Alaska, and many of the continental coastal regions, e.g., the west coast of Mexico (see Fig. 1, taken from Ref. 2). These regions usually coincide with the boundaries of the earth's large crustal (tectonic) plates. The plates may come together with one subducting below the other, forming magma that can rise in fingers toward the surface and result in strings of volcanoes.[1] When the plates separate, the void formed may provide access to magma from the earth's interior.

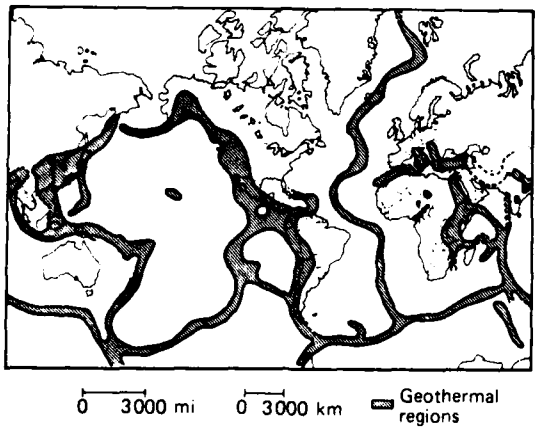

Fig. 1 Geothermal regions of the world (from Ref. 2).

For GEOTEC plants, the practical, continuous geofluid withdrawal rate may be more important than the geofluid wellhead temperature, T_{GH}, in determining the economic feasibility at a given site. Reasonable rates per well may be near 65 kg/s (1000 gpm) based on experience in the Philippines. Other Pacific Ocean sites that may be of interest to the Navy are Oahu (Hawaii) and Okinawa.

DISCUSSION

Preliminary Performance Estimates

As geofluid is withdrawn by downhole pumps, it is replaced by water from other parts of the reservoir. Because the permeability and recharge mechanism cannot easily be generalized, we treat well drawdown as a parameter and assume that the geofluid will be reinjected for environmental reasons and in order to stabilize the well drawdown with time. We assume that for each production well there is a reinjection well located far enough away to avoid thermal breakthrough during the economic life of the system. However, for a low T_{GH} geofluid resource (say 120°C) with low silica and salt contents, the used geofluid could be discharged into the ocean. We have developed simple computer programs for a GEOTEC binary isobutane (iC_4) cycle (Fig. 2a) and for a GEOTEC dual-binary cycle using isobutane in the high-temperature loop A and ammonia (NH_3, the most frequently chosen working fluid in closed-cycle OTEC systems) in the low-temperature loop B (Fig. 2b).

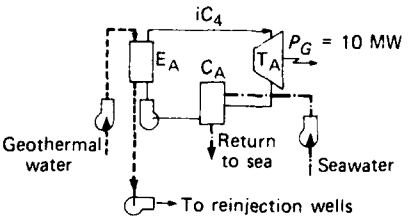

(a) GEOTEC binary cycle using isobutane loop

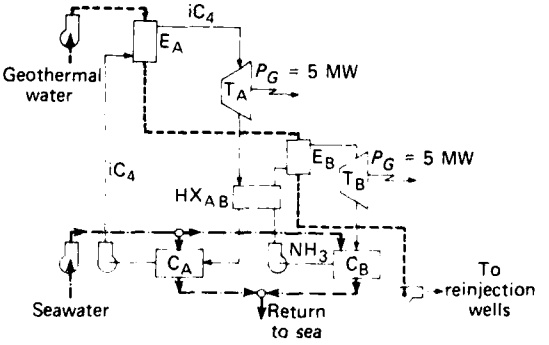

(b) GEOTEC dual-binary cycle using isobutane (iC_4) and ammonia (NH_3) loops

Fig. 2 Power cycles.

The major capital cost items for a GEOTEC plant will be the geothermal production wells and the reinjection wells; therefore, our calculation approach is aimed at minimizing the geofluid flow rate, $\dot{w}_{GH}$, needed to develop the required net power. The independent parameters are the gross turbine power, P_G (10 MW for the binary cycle, 5 MW for each fluid in the dual-binary system); T_{GH} (104 to 200°C); the seawater temperature, T_{SW} (assumed here to be 0°C for simplicity); the working fluid pump and turbine efficiencies, η_I (assumed here to be 80%); the reinjection temperature, T_{inj} (54 to 88°C); the "pinch" temperature difference, ΔT_p (the ΔT allowable between the two fluids in any heat ex-

changer, assumed here to be 5.6°C); and one pressure or saturation temperature in each loop.

For the binary cycle, the condenser pressure, P_{cA}, is treated as an independent parameter (assumed here to be 345 kN/m^2, corresponding to a saturation temperature for isobutane of 24.6°C).

The temperature of the geofluid exiting from the evaporator is equal to T_{inj}. The turbine inlet pressure is equal to the evaporator pressure, p_{tA}, which is also determined by T_{inj} because the saturation temperature of isobutane in the evaporator, T_{tA}, is $T_{inj} - \Delta T_p$, and $p_{tA} = f(T_{tA})$, according to the thermodynamic saturation properties of isobutane. The seawater coolant flow, $\dot{w}_{SW}$, decreases as T_{inj} increases (Fig. 3) because the condenser operates at a higher temperature, and the ΔT between isobutane and seawater increases.

The required $\dot{w}_{GW}$ is equal to $\dot{w}_t \Delta h_{tA} / \Delta h_{GW}$, where Δh_{GW} is the enthalpy drop of the geofluid,

$$\Delta h_{GW} = c_{pGW} \Delta T_{GW} = c_{pGW} (T_{GW} - T_{inj}) \quad (1)$$

and $\dot{w}_t$ is the isobutane flow rate determined from the required gross power (10 MW) because $\dot{w}_t = P_e /$ $\eta_{tA} \Delta h_{tA}$. As shown by the dashed curves in Fig. 4, this analytical approach indicates that for the binary cycle with $T_{GW} \leq 200$°C, $T_{inj} = 75$ to 90°C will be appropriate. The geofluid flow rates suggest that three to six production wells will be needed.

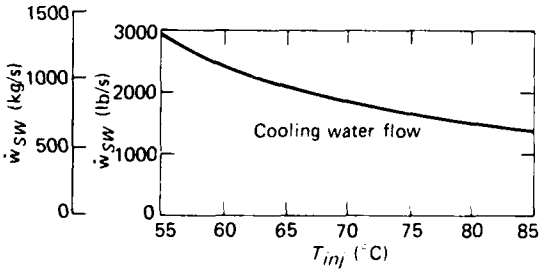

Fig. 3 Required seawater flow versus geofluid reinjection temperature for binary cycle GEOTEC plant with 10 MWe gross power output.

For the dual-binary cycle, the evaporator pressure in loop A and the condenser pressure in loop B (assumed here to be 690 kN/m^2) are treated as independent parameters. The corresponding saturation temperature for the condensing ammonia in loop B is 13.3°C. The condenser pressure for loop A and the evaporator pressure for loop B are dictated by T_{inj} and the ΔT between the isobutane and the ammonia in the heat exchanger, HX. The geothermal water is passed through the isobutane evaporator and then a sufficient amount is used in the ammonia evaporator. If the geofluid flow rate is insufficient for the ammonia evaporation, the remaining required heat is extracted from the isobutane in the heat exchanger, which is sized accordingly. If all the heat needed is available in the geothermal water, the heat exchanger is deleted.

With $\eta_{tA} = \eta_{tB} = 0.8$, the isobutane ($\dot{w}_t$) and ammonia ($\dot{w}_B$) weight flow rates are $\dot{w}_t = P_e /$ $\eta_{tA} \Delta h_{tA}$ and $\dot{w}_B = P_e / \eta_{tB} \Delta h_{tB}$, where $P_e = 5$ MW for each. The geofluid flow rate is calculated in the same way as for the binary plant, but now the temperature (and corresponding saturation pressure) in the ammonia-boiling section of the heat exchanger and the ammonia evaporator is controlled by T_{inj}:

$$T_{HXB} = T_{tB} = T_{inj} - \Delta T_p \; ; \qquad p_{HXB} = p_{tB} = f(T_{tB}) \; . \quad (2)$$

The temperature and corresponding saturation pressure of isobutane in the heat exchanger and condenser are:

$$T_{HXA} = T_{cA} = T_{HXB} + \Delta T_p \; ; \qquad p_{HXA} = p_{cA} = f(T_{cA}) \; . \quad (3)$$

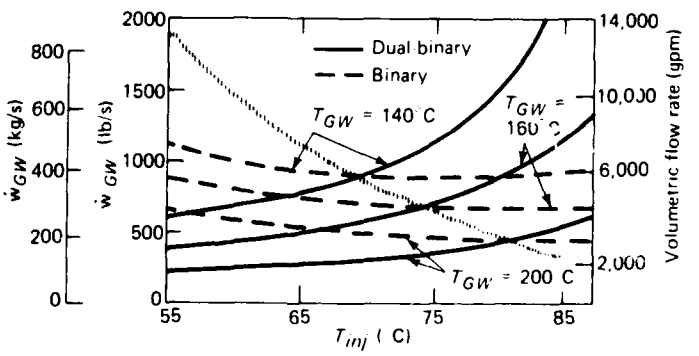

Fig. 4 Comparison of binary and dual-binary geothermal flow requirements to produce 10 MWe gross power.

The temperature of the seawater leaving the isobutane condenser equals $T_{c,i} - \Delta T_p$. Runs were made for various isobutane evaporator pressures for each T_{GH} and T_{inj}. Near-optimal values of $\dot{w}_{GH}$ are shown by the solid curves in Fig. 4, where the curves for the binary and dual-binary cycles are overlaid. For each value of T_{GH} there is a crossover point at some value of T_{inj}. The crossover points (including those outside the T_{GH} range shown) have been connected by the shaded line, to the left of which the dual-binary cycle is better (lower $\dot{w}_{GH}$) and to the right of which (if higher T_{inj} has to be used) the simpler binary cycle is better. The choice of cycles will depend on the geofluid resource conditions, including relative pumping power requirements, equipment costs, and operating and maintenance costs. However, a broad conclusion is that if a T_{GH} of about 200°C is available, the binary cycle should be used; the required geofluid flow for 10 MWe gross will be in the 140 to 200 kg/s range, and two or three production wells should suffice. If T_{GH} is about 120°C, other calculations not represented in Fig. 4 show that the dual-binary cycle would be needed, and two or three times as many production wells may be needed, but it may be feasible to avoid reinjection by discharging the spent geofluid into the ocean.

Parasitic Pumping Requirements and Net Power Output

The foregoing results were for a fixed gross power output of 10 MWe. The net power output will be smaller because of the parasitic power required to pump the geofluid, the seawater, and the working fluids. The power required to pump the geofluid to the surface is directly related to the required geofluid flow rate and the well drawdown depth. For a flow of 360 kg/s (corresponding to T_{GH} about 140°C) and for $T_{c,i}$ = 66°C, with a 10 m drawdown, P_{GH} = 0.09 MW. For a 150 m drawdown, it is 1.32 MW. In comparison, the geofluid head loss through the two evaporators is ≤1.5 m each, or ≤0.033 MW for the pair, based on our experience with OTEC heat exchangers. Frictional losses in the piping will also be small. Thus, 10 MWe gross power will yield between 8 and 9.5 MWe net power, depending on T_{GH} and well drawdown depth.

CONCLUSION

The combination of OTEC technology (including seawater cooling) with geothermal water resources may be attractive for coastal and island sites along the intersection lines of the earth's crustal plates. The heat exchangers will be one-eighth to one-fourth as large per kilowatt (for a given working fluid) as those for OTEC plants, with correspondingly lower specific cost. The turbines and generators will also be smaller, but reductions in the cost per kilowatt will be less impressive. The cold-water intake and return pipes will be much smaller in diameter than the OTEC cold-water pipes (0.6 m versus 4 m for 10 MWe) and will cost less. On the other hand, the multiple geofluid production and reinjection wells may add a few thousand dollars per kilowatt to GEOTEC plant costs. The high cost of plant construction at remote sites could be alleviated by constructing the power-cycle portion of the plant on a barge at a United States shipyard and towing it to the site.

In addition to directly planned use, GEOTEC plants could be used to exploit well fields that had been developed for intended flash-steam plants but proved to have temperatures too low for efficient power production by the flashing approach. Furthermore, successful early GEOTEC implementation at sites where modest amounts of baseload energy, independent of imported fuels, are needed may facilitate OTEC commercialization and vice versa. Moreover, participation by DoD in a GEOTEC development program would be advantageous. The Naval Weapons Center, China Lake, Calif., and the Naval Civil Engineering Laboratory, Port Hueneme, Calif., are now working with API on this program under DOE support.

Further information on geothermal resources is given in Refs. 1 through 4, examples of existing geothermal binary plants are given in Ref. 4, and additional details of our analysis are given in Ref. 5.

REFERENCES

[1] E. A. Peterson and M. Reed, "Direct Use of Geothermal Energy—An International Review," in *Renewable Energy Sources for Developing Nations*, Heliotechnic Press, London (May 1983).

[2] M. J. Aldrich, A. W. Laughlin, and D. L. Gambill, *Geothermal Resource Base of the World—A Revision of the Electric Power Research Institute's Estimate*, Los Alamos Scientific Laboratory, U. of Calif., LA-8801-MS, UC-66a (Apr. 1981).

[3] B. D. Marsh, "Island Arc Volcanism," *Am. Sci.* 67 (May–Apr. 1979).

[4] R. DiPippo, *Geothermal Energy as a Source of Electricity*, U.S. Department of Energy, DOE/RA/28320-1, pp. 342–353 (Jan. 1980).

[5] C. J. Dugger, J. C. Paddison, and J. H. Peters, "Geothermal Enhanced OTEC (GEOTEC) Resources and Plant Concepts," presented at 8th Ocean Energy Conf., Washington, D.C. (June 1983).

This work was supported by the Department of Energy, Ocean Energy Technology Division.

AD-A125 288 DEVELOPMENTS IN SCIENCE AND TECHNOLOGY(U) JOHNS HOPKINS 3/3
UNIV LAUREL MD APPLIED PHYSICS LAB 1981 JHU/APL-DST-9
N00024-83-C-5301

UNCLASSIFIED F/G 5/2 NL

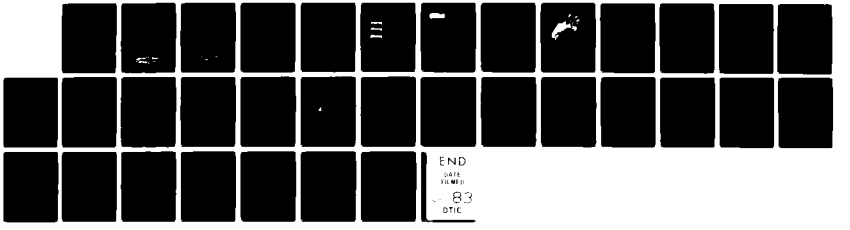

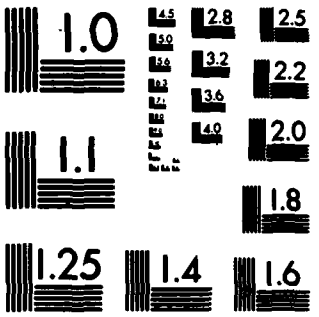

MICROCOPY RESOLUTION TEST CHART
NATIONAL BUREAU OF STANDARDS-1963-A

ENVIRONMENTAL IMPACT ASSESSMENT OF PROPOSED POWER PLANT AT VIENNA, MARYLAND

E. M. Portner

An environmental impact assessment has been performed of a proposed 500 MW coal-fired power plant next to an existing plant at Vienna, Md., adjacent to the Nanticoke River. The principal issues included the effects on the spawning of striped bass in the river, methods for the disposal of large quantities of combustion wastes, and the prediction of dust emissions from coal-handling operations.

BACKGROUND

Since 1972, APL has performed environmental impact studies of all proposed power plants in the state for the Maryland Power Plant Siting Program. The objectives are to provide the technical basis for policy decisions by the state government regarding environmental issues and to present the technical analyses in public hearings before the Public Service Commission (PSC) and other regulatory bodies. Other divisions of Johns Hopkins frequently participate in such studies; the Chesapeake Bay Institute assisted in the aquatic part of this evaluation.

DISCUSSION

The siting of a power plant involves many considerations and trade-offs, including the study of alternative sites and of design modifications to mitigate harmful effects. The proposed addition of a new unit at the existing Vienna plant site was less expensive than construction at a new site because existing facilities such as rail lines and transmission line corridors were already in place; however, the Vienna site is more sensitive environmentally than the other sites considered. Conversely, the proposed alternative sites are more expensive to develop but may have fewer harmful effects. All sites have some disadvantages. APL's responsibility was to perform a detailed evaluation of the proposed Vienna site, including design alternatives, and to study selectively the major features of several alternative sites. The results are documented in topical reports and summarized in an overview report.[1] A summary of several principal issues is presented here. Figure 1 is an artist's concept of the plant.

The proposed plant would withdraw cooling water from the Nanticoke River at a location centered in a striped bass spawning area. The siting of plants in such areas is common because utilities frequently locate plants as far downstream as possible to get a large supply of fresh water, and anadromous fish travel upstream to the fresh water boundary region to spawn. The proposed plant would use a cooling tower to reduce the withdrawal rate of water to 0.5 m^3/s, which is approximately 2% of the water required by a comparable

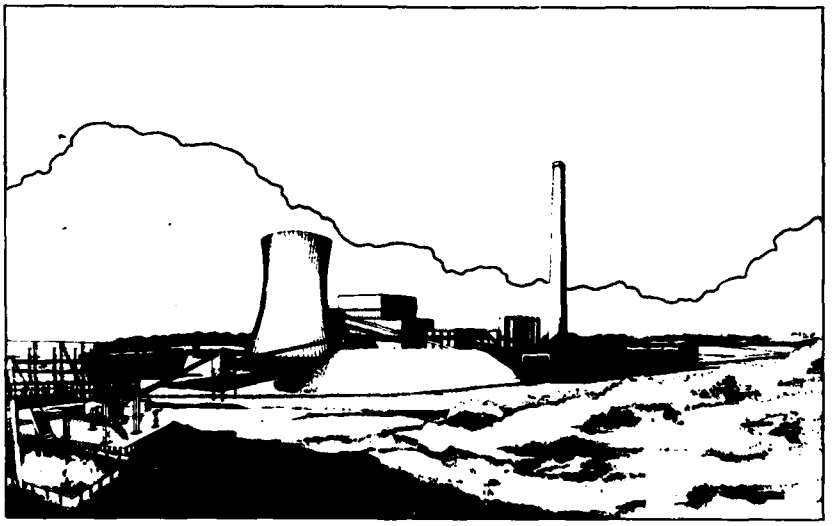

Fig. 1 Artist's concept of proposed power plant at Vienna.

older plant with once-through cooling. Passive intake screens would be used to prevent the entrainment of most eggs, older larvae, and juvenile fish. Such screens are a new technology only recently tested by Delmarva Power in the Chesapeake Bay area. Each screen consists of a frame of ribs in a cylindrical shape with triangular wire wrapped helically around the frame to form 1 mm slots. Most organisms are physically excluded from entrainment by the slot width, and the intake velocity is low enough so that organisms contacting the screen can swim away. The early stages of larvae without swimming ability are still vulnerable to entrainment. The screen face is kept clean by the passage of tidal currents and by occasional backwashing.

APL reviewed the laboratory and field data on screen performance. An entrainment model developed during earlier site evaluations was applied, using a screen performance estimate and thirteen years of data on the distribution of eggs and larvae in the river. Based on a number of conservative factors that would overpredict the effect of the plant, the model predicted that the new unit would entrain 2% of the eggs and larvae in the Nanticoke. A sensitivity analysis of the factors affecting entrainment was also performed. The effect on the adult fish population was estimated using a population dynamics model developed at APL. For perspective, we were able to show that the effect on the fish population of a 2% entrainment loss would be comparable to that of a single average commercial fisherman.

The estimated effect on striped bass became the major environmental impact issue contested by intervenors in the PSC hearing. Substantial effort was devoted to analyzing the costs and benefits of intake alternatives proposed in the course of the hearing and to reviewing the technical analyses of other parties. For example, a proposal to shut down the plant for routine maintenance during the spawning season led to an examination of the causes of plant outages and the increment in generation cost when a major baseload unit is off line. The resolution of the aquatic issue awaits the decision of the PSC and possible appeals.

Concern about the atmospheric emissions from power plants has created requirements for the efficient collection of flyash by electrostatic precipitators and the limitation of sulphur emissions, usually by a lime-based scrubber system. The wastes generated by such processes for the proposed Vienna plant over a period of 30 years are projected to cover 165 acres to a height of 45 ft. A potential air pollution problem has thus been transformed into a solid-waste disposal problem, which usually implies possible ground-water pollution unless suitable disposal methods are found. Conditions at Vienna (and in most of the surrounding area on the Eastern Shore) are not conducive to simple waste disposal techniques. The ground water level at times comes up to the ground surface, and the water table aquifer at Vienna has the highest quality drinking water available. The town of Vienna is one mile from the proposed waste disposal area. In future years, the municipal well will probably draw from the water table aquifer. In addition, discharges to surface waters could have an adverse effect on spawning and on the resident aquatic species. The disposal problem is complicated by the fact that the technology for such waste disposal is new and developing rapidly, and the regulatory requirements for disposal are in a state of flux.

The utility initially proposed to dispose of the waste by mixing flyash, oxidized scrubber sludge (gypsum), and lime to form a solid, relatively impervious mass of "fixed" material to be stored at a site near the plant. An artist's concept of the completed disposal area is shown in Fig. 2. Extensive field and laboratory tests and analyses were conducted by the utility and APL to determine the engineering properties of the waste, characterize the leachate from the waste, deter-

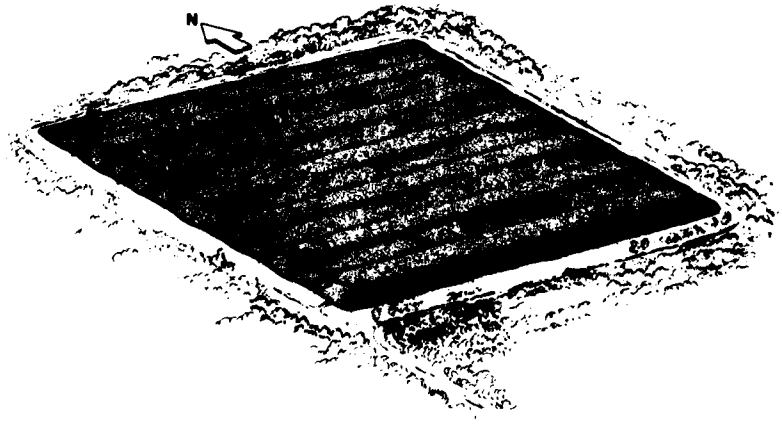

Fig. 2 Artist's concept of solid-waste disposal area.

mine the flow of rainwater through and over the waste, estimate the water quality and hydraulics of the ground water system, and predict the concentration of contaminants in the ground water down gradient from the waste.

It eventually became apparent that the proposed disposal approach would have difficulty meeting state water-quality regulations because the fixation process was not as effective as vendor literature suggested. The extent of the problem is indicated in Table 1, which shows the predicted initial leachate concentrations at the bottom of the waste pile and the probable regulatory standards that would be applied at some unspecified distance (perhaps zero) from the waste. Another problem is that differential settling would cause cracking of the waste and increase the bulk permeability and leachate quantity. Because of such factors and of uncertainties in the technical analyses and regulatory situation, it would have been very difficult to resolve the issues in an adjudicatory proceeding. The utility and the Power Plant Siting Program therefore agreed to study disposal alternatives jointly.

Table 1

PREDICTED LEACHATE CONCENTRATIONS AND REGULATORY STANDARDS

Constituent	Concentration (mg/l)	
	Predicted Leachate	Regulatory Standard
Total dissolved solids	8800	500
Sulfate	1350	250
Chloride	2970	250
Manganese	5.4	5.0
Barium	1.0	1.0
Iron	0.86	0.3
Arsenic	0.094	0.05
Chromium	0.001	0.05
Lead	0.005	0.05
Silver	<0.001	0.05
Cadmium	0.21	0.01
Selenium	0.12	0.01
Mercury	0.0005	0.002

The approach that eventually was adopted was tailored to site specific conditions and should result in negligible discharges to ground and surface waters. The flyash and scrubber sludge will be mixed but no lime will be added. The waste will be placed on a base of porous material to prevent direct contact with the water table (and thereby prevent contamination by capillary action). During emplacement of the waste, runoff from rainfall will be collected in a basin and used for scrubber makeup. When each section of the disposal area has been completed, the waste will be covered with an impermeable liner and a layer of soil, which will be vegetated. This revised design costs less than the original design because lime is no longer required, and the environmental isolation of the disposal has been greatly improved.

Another area of recent regulatory emphasis is the control of fugitive dust emissions emanating primarily from coal- and flyash-handling operations. Very little reliable quantitative information exists on the amount of dust emitted, the normal ambient dust levels, the effectiveness of various dust control technologies, and the accuracy of dust dispersion models. APL's study of these problems was directed mainly at the reliability of available information. The regulatory situation was also uncertain because the Environmental Protection Agency was in the process of developing regulations and transferring their administration to the states. There also were several unusual local features, such as a proposed highway that would traverse the site. A joint effort with the utility eventually produced a design that probably will meet dust standards. In addition, research needs were identified; APL has since begun a detailed study for Maryland of dust emission rates from various coal-handling operations such as rail-car dumping.

Other topics studied by APL for the Vienna site include noise, the effect on air quality of stack emissions, fogging of a nearby bridge by the cooling tower plume, salt deposition from the cooling tower, socioeconomics, the potential for site expansion, and comparison with alternative sites. Many of the studies indicated potential regulatory difficulties in the course of the technical evaluations, but in each case the problems were resolved through discussions among the Power Plant Siting Program, Delmarva Power, and the various regulatory agencies. The technical alternatives analyzed by APL provided the basis for discussing and resolving most of the issues.

The Vienna proceeding is typical in the scope of the issues addressed during the siting of a modern power plant. But it is unusual for a state government to support the detailed technical studies that resulted in a Vienna plant design tailored to local conditions and providing adequate environmental protection. Considering previous experience, in the absence of such studies a number of undesirable actions could have occurred: the utility could have been denied a permit to locate the plant at an economically advantageous site because of general concerns that the sensitive aquatic and groundwater resources might be damaged; the plant could have been sited at Vienna without a suitable design, resulting in substantial environmental damage; or the plant could have been sited at Vienna with a host of expensive but unnecessary environmental safeguards. The good news is that the plant has been sited by means of a process that reduces uncertainty in decision-making and allows costs to be controlled, while affording adequate environmental protection.

The bad news is that the utility filed its applications with the PSC almost four years ago, a decision is only now imminent, and appeals by various parties are likely. Furthermore, the utility must obtain at least ten other permits from federal, state, and local agencies for issues substantially the same as those already addressed in the PSC proceeding. (The licensing situation in Maryland is probably simpler than in most other states because Maryland has consolidated many of its permits under the PSC proceeding.) APL's role for the state in some of the subsequent proceedings may be to readdress the key technical issues if substantial changes occur in the technology, the regulatory requirements, or the body of scientific knowledge.

REFERENCE

[1] E. M. Portner, *Impacts of the Proposed Vienna Unit No. 9 — An Overview of Vienna and Alternative Sites*, JHU/APL PPSE 8-8, Rev. 1 (1981).

This work was supported by the Maryland Power Plant Siting Program.

VACUUM-DEPOSITED POLYCRYSTALLINE SILICON SOLAR CELLS

C. Feldman, F. G. Satkiewicz, and N. A. Blum

Thin-film solar cells represent one possible solution to the problem of providing a low-cost, environmentally safe, and reliable source of renewable electrical energy. Commercial single-crystal silicon solar cells having over 10% efficiencies have proved satisfactory in all respects except for cost. Thin-film polycrystalline silicon solar cells on inexpensive substrates would use a much smaller quantity of highly pure silicon than is used by single-crystal cells and would be potentially suitable for low-cost, large-scale fabrication. This article reviews a vacuum deposition approach to constructing polycrystalline silicon solar cells that have exhibited photovoltaic efficiencies of about 3%.

BACKGROUND

A major goal of present research on photovoltaic devices is to develop low-cost, thin-film fabrication techniques that would make solar cells practical for widespread use. One approach to this goal is to use physical vapor deposition, a technique already used in the manufacture of commercial single-crystal solar cells for making electrical contacts as well as for depositing antireflection coatings. It seems reasonable to researchers at APL to construct the entire device using those same techniques. One could visualize a vacuum deposition system in which cells would be continuously produced in interconnecting vacuum chambers — beginning with the insertion of blank substrates and ending with the completed cell.

Commercial solar cells consist of a semiconducting single-crystal silicon wafer containing a *p-n* junction, a continuous opaque electrode on the back side, and a finger-type electrode on the illuminated side. In order to emulate this cell configuration, a polycrystalline silicon layer must be deposited on a conducting base or on an insulating substrate coated with a conducting layer. Large silicon crystallites are needed for high photovoltaic efficiency, and depositions must be accomplished at high substrate temperatures in order to promote crystal growth. A suitable nonreacting, conducting substrate or conduction layer (back electrode) was not known at the time this research program was initiated.

The work described here deals with the solution of the back electrode problem and describes some of the separate vacuum deposition steps required for the fabrication of a complete solar cell.[1]

DISCUSSION

The experimental cell configuration is illustrated schematically in Fig. 1. The substrates were single-crystal Al_2O_3 (sapphire) or polycrystalline Al_2O_3 (alumina).

A layer of TiB_2 on alumina or sapphire substrates was found to meet the requirements for the back electrode.[2,3] The expansion coefficient of TiB_2 is be-

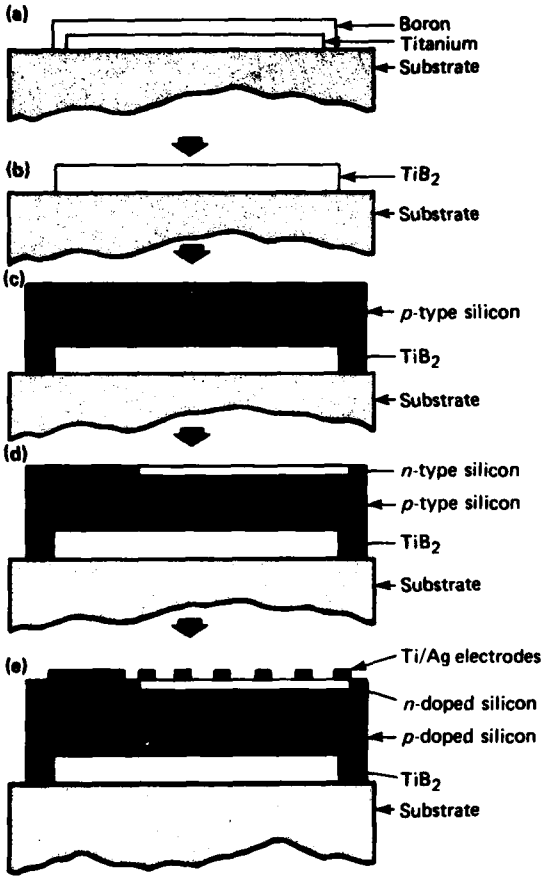

Fig. 1 Schematic of thin-film layers in silicon solar cell on insulating substrate.

tween those of silicon and sapphire. TiB_2 has excellent conductivity, is stable at high temperatures, and adheres well to the substrate. The silicon deposited on top of the TiB_2 layers also adheres well, even at high temperatures. In contrast, silicon films deposited at substrate temperatures greater than approximately 1100°C do not adhere to uncoated sapphire. TiB_2 layers were formed by depositing on the substrate a layer of titanium followed by a layer of boron and reacting the couple at high temperature (950°C) until TiB_2 was formed by a diffusion reaction.

Silicon films were deposited on top of the TiB_2 layer by electron beam heating of silicon in a tantalum-lined, water-cooled, nickel crucible. In order to obtain crystalline films with the large grains required for high efficiency, substrate temperatures were generally greater than 1000°C. Considerable effort was spent on producing very pure silicon films.

It was observed that silicon crystallites grown on the substrates coated with TiB_2 at high temperatures were considerably larger than those grown on uncoated substrates. In order to understand this, silicon crystallites grown on coated and uncoated substrates were studied by various experimental techniques including scanning electron microscopy (SEM), secondary ion mass spectrometry (SIMS), and x-ray diffraction. As a result of this work,[3] it was concluded that silicon atoms arriving at the TiB_2 surface at high substrate temperatures (1150°C in this case) interact, forming $TiSi_2$. Subsequent silicon atoms landing on the $TiSi_2$ surface have greater mobility than they would have on either the TiB_2 or bare substrates; as a consequence, the distance between seeds (crystallite growth centers) is relatively large. The crystallites then begin to grow in two dimensions, and this two-dimensional growth causes the formation of large initial seeds. The observation that enhanced growth requires the formation of a $TiSi_2$ phase places a lower limit on the substrate temperature and an upper limit on the rate of silicon deposition.

The *p-n* junctions in the polycrystalline silicon films on substrates coated with TiB_2 were formed by means of standard integrated circuit, diffusion, and masking techniques. Polycrystalline samples were observed to behave like single crystals with respect to oxidation, etching, and diffusion. The diffusion steps were not optimized for maximum cell efficiency; rather, the extensive literature on single-crystal solar cells was used as a guide. Other doping techniques for forming the *p-n* junction, appropriate for an all-vacuum process, have been shown to work, but they will not be discussed here. The need for the front pad to make contact with the back electrode (see Fig. 1e) introduces a negligibly small series resistance. In a cell made entirely by vacuum techniques, it would be possible to make direct contact with the TiB_2 layer. However, the configuration used is convenient because the silicon overlayer prevents oxidation of the TiB_2 layer during processing. In the final step, the top metal electrodes were vacuum deposited through masks.

Figure 2 is a planar view of devices having the layered structure illustrated in Fig. 1. The devices of various sizes are clearly visible on the 1 by ⅓ in. substrate. The device on the left has an area of approximately 1 cm^2.

Photovoltaic parameters were measured for various deposition conditions and fabrication procedures for polycrystalline film samples, for simultaneously processed single-crystal monitors, and for similarly processed epitaxial layers deposited under the same conditions on single-crystal substrates. The highest efficiency obtained so far in the polycrystalline films without an antireflection coating is about 3%. In general, as in single-crystal solar cells, antireflection coatings improve photovoltaic efficiency by about one-third,

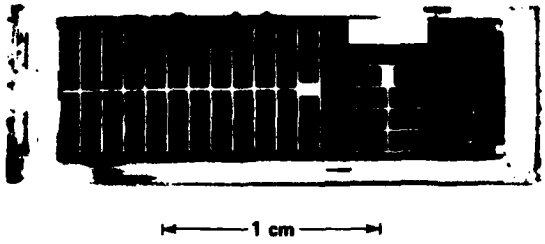

Fig. 2 Experimental thin-film silicon photovoltaic devices on 1 by ⅓ in. alumina substrate.

and this improvement has also been observed in the thin-film devices. Typical photovoltaic parameters for thin-film polycrystalline cells with an area of 2 mm^2 under standard (AM-1) illumination conditions are: short-circuit current density, J_{sc}, of 20 mA/cm^2; open-circuit voltage, V_{oc}, of 250 mV; and fill factor, *ff*, of 0.55. The fill factor, a measure of quality, depends on internal series and shunt resistances. For single crystal cells, the corresponding values are typically J_{sc} = 30 mA/cm^2, V_{oc} = 580 mV, and *ff* = *0.75*.

CONCLUSION

Progress has been made in developing thin-film structures for solar cells on insulating substrates that can be formed entirely by physical vapor deposition. The only portion of the devices not formed by vacuum deposition is the *n*-type region, which is formed by standard diffusion techniques. As mentioned earlier, techniques for forming the *n*-type region by vacuum deposition have been pursued successfully, but further development is required in order to refine the most appropriate methods. Considerable improvement in cell efficiencies will be achieved by better control over impurities coupled with the growth of larger silicon grains in the films.

REFERENCES

[1] For more detail see: C. Feldman, N. A. Blum, and F. G. Satkiewicz, "Vacuum Deposited Polycrystalline Silicon Solar Cells for Terrestrial Use," *IEEE Conf. Record*, No. 80CH1508-1, 391-396 (1980); and C. Feldman, C. H. Arrington III, N. A. Blum, and F. G. Satkiewicz, *Vacuum Deposited Polycrystalline Silicon Films for Solar Cell Applications, Final Technical Report*, Solar Energy Research Institute, Contract XS-9-8278-1 (Dec 1980).

[2] C. Feldman, F. G. Satkiewicz, and G. Jones, "Preparation and Electrical Properties of Stoichiometric TiB_2 Thin Films," *J. Less-Common Metals* **79**, 221-235 (1981).

[3] C. Feldman, F. G. Satkiewicz, and N. A. Blum, "The Behavior of TiB_2 Thin Film Electrodes in Polycrystalline Silicon Thin Film Solar Cells," presented at Seventh International Symp. on Boron, Borides, and Related Compounds, Uppsala, Sweden (9-11 Jun 1981) (to be published in *J. Less-Common Metals*).

This work was supported by Indirectly Funded R&D.

GEOLOGIC FAULTS AND EARTHQUAKES OF WESTERN CONNECTICUT AND SOUTHEASTERN NEW YORK

J. E. Tillman

Earthquakes of low to medium intensity (less than a magnitude of 4 on the Richter scale) are common in the area between the Hudson and the Housatonic Rivers. The source mechanism of the seismic events had been unknown because of the lack of mapped geologic faults in this region. Detailed structural and stratigraphic mapping in the Danbury Quadrangle and along two lineaments identified on satellite imagery and on magnetic surveys has resulted in the delineation of two major fault zones. The surface trace of one fault coincides with an alignment of historic earthquake epicenters.

BACKGROUND

One region in the eastern United States with a higher-than-average frequency of seismic events lies

along the northern Fall Line in Maryland, New Jersey, Pennsylvania, and New York and then, leaving the Fall Line, extends northeast into Connecticut.[1] The Ramapo Fault in New Jersey and New York is the best known structure along this trend; its relationship to seismicity has been the subject of investigation for a number of years.[2-4] However, many seismic events in this region, when accurately located, occur not precisely along the Ramapo but farther to the east in the Manhattan Prong (Fig. 1), an area with fewer previously mapped faults.[5,6] That region is densely populated and contains many critical facilities such as nuclear power plants, dams, large water supply reservoirs, aquaducts, hospitals, and major transportation arteries. Thus, a better understanding of the origin of the seismic events is important for adequate planning.

Although faults had not been mapped in earlier geologic investigations, studies of remotely sensed data from the Manhattan Prong have revealed the occurrence of major lineaments. References 7 and 8 examined LANDSAT, aeromagnetic, aeroradioactive, geologic, and topographic data and described the evidence for two northeast trending zones of lineaments — the Ridgefield and the Danbury Zones — which they were able to trace from the vicinity of the Pomperaug Valley in Connecticut to the Newark Basin in New York. Several LANDSAT and topographic lineaments were identified in that region[3,9]; when field checked, they coincided with zones of fracturing and faulting. The more important throughgoing of those zones were called the Saw Mill River-Danbury Lineament and the Pomperaug-Georgetown Lineament (Fig. 2).

In this project, a field program was initiated to determine if the LANDSAT, aeromagnetic, and topographic lineaments were, in fact, fault zones and, if they were, whether the geologic ages for their last

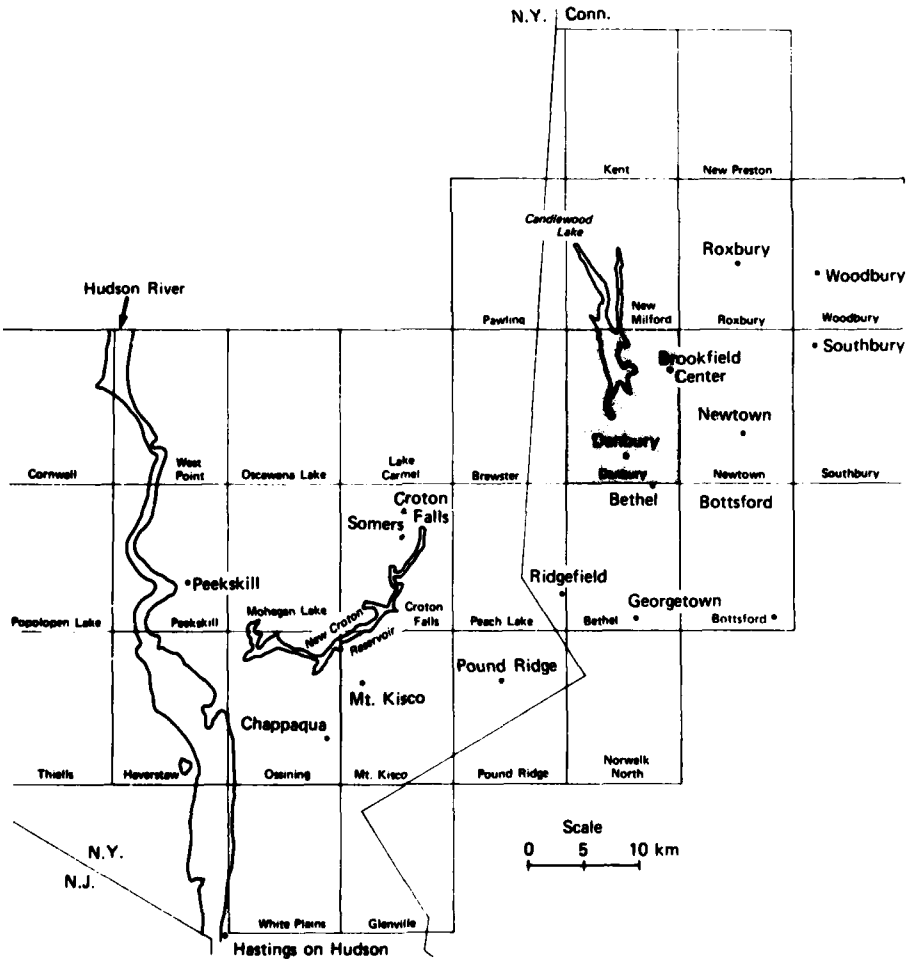

Fig. 1 Region of investigation into the possible source mechanisms of historic seismicity and location of the Danbury Quadrangle.

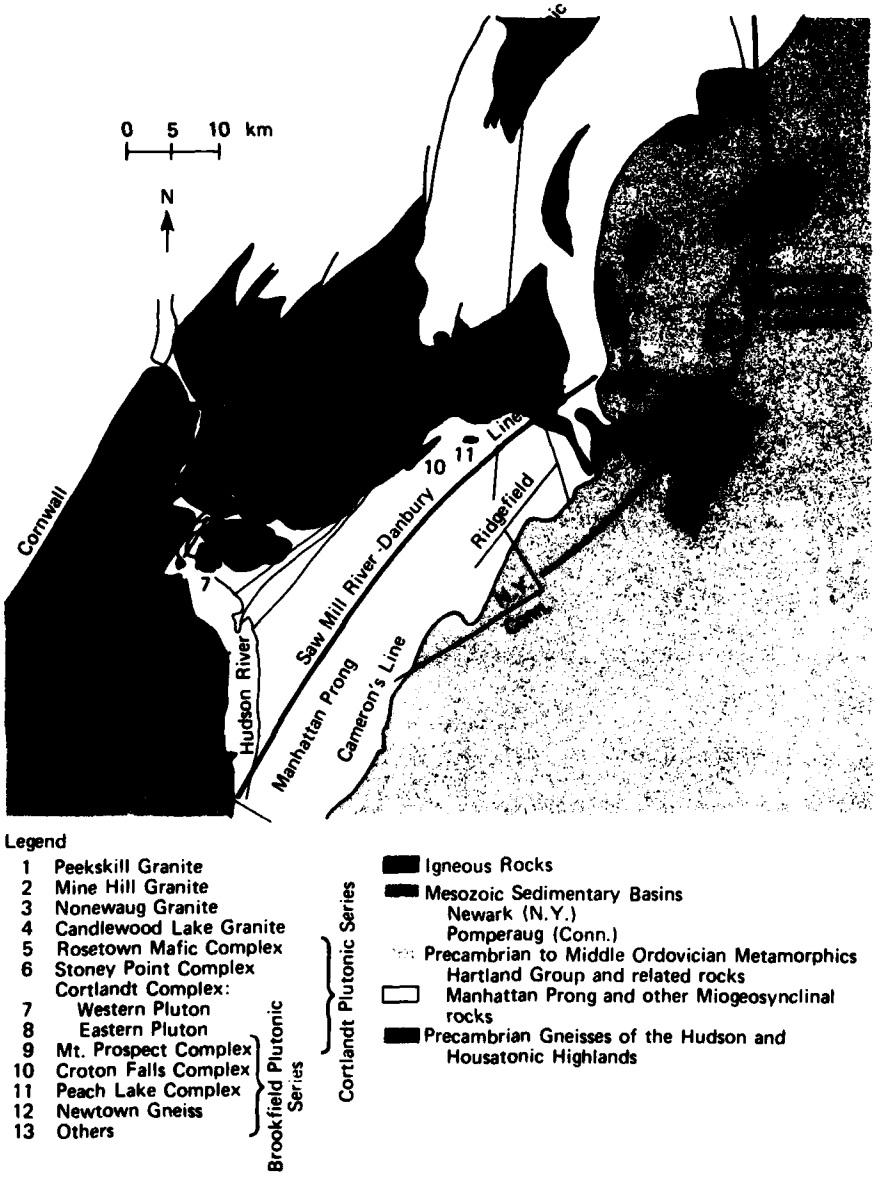

Fig. 2 Geologic setting and major faults of the northern Manhattan Prong.

movement allowed them to be considered as possible sources for the seismicity in the region. In the first phase of the project, a reconnaissance program identified locations for detailed field mapping and documentation. Linear zones where brittle deformation appeared to be concentrated were found to occur in several well-exposed outcrops and quarries at Woodbury, Southbury, Bottsford, Mt. Kisco, and Chappaqua. In the second phase, petrofabric analyses and structural mapping were performed at the outcrops to obtain more information on the lineaments. An example of an outcrop along one of the lineaments is shown in plan view in Fig. 3.

It was decided that the best way to show the style, sense, and magnitude of the displacement on one major lineament, the Saw Mill River-Danbury Lineament, was to map the stratigraphic relationships in the Danbury Quadrangle where an apparent 4 km dextral drag or offset of the Inwood Marble occurs.[7,10] The results of this work are discussed in Ref. 11.

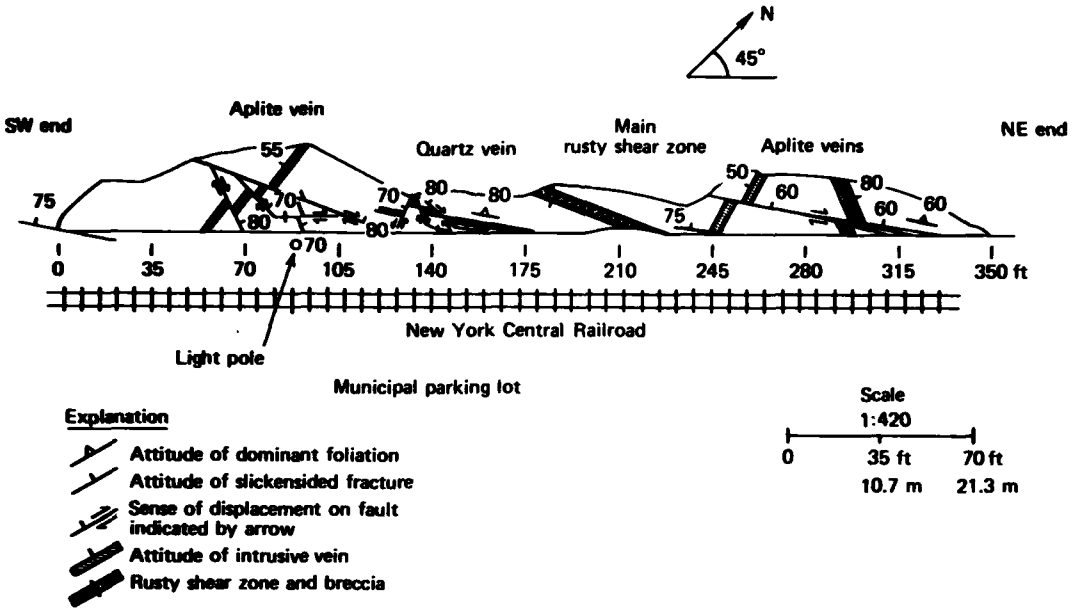

Fig. 3 Diagrammatic plan of the Fordham Gneiss exposure in the railroad cut in Mt. Kisco, N.Y.

DISCUSSION

Geology of the Danbury Quadrangle

The Danbury Quadrangle lies in western Connecticut (Fig. 1) astride Cameron's Line, the thrust contact between North American cratonic basement shelf deposits to the west and rocks with oceanic affinity to the east. This quadrangle also lies at the intersection of the dominant northeast trends, which are characteristic of the Manhattan Prong and the Central Appalachians, and the north-south trends, which are more common to western New England. The change in strike allows us to examine how the younger brittle structures affect the map patterns (Fig. 2).

The structure of the Danbury Quadrangle is complex. Several well-defined episodes of folding and faulting have occurred. The sequence of ductile and brittle deformation has been deciphered and used to generate a new geologic map for this area. However, the interpretation of the rock unit distribution and associated structural relationships is not unique. Previous interpretations[10] were rejected because of structural and stratigraphic inconsistencies and changes in stratigraphic correlation justified by additional outcrops and supported by a quadrangle aeromagnetic map. A purely multiple folding interpretation is also not chosen because of the many occurrences of thrust fault juxtaposition of units and the structurally sound, less complex thrust and fold interpretation that appears to satisfy all the data in this quadrangle.

In summary, the rocks now exposed in the quadrangle were initially thrust westward over Precambrian basement. Many small folds as well as the two map-scale basement cored antiforms are associated with that event. The event was followed by an episode of brittle deformation in the basement blocks and drag of the overlying metasedimentary units. The episode can best be explained as high-angle reverse faulting along the Danbury Fault Zone and parallel faults. It was followed by right-lateral strike-slip movements on intermediate to nearly vertical northeast striking fault zones. The youngest macroscopic faults in the area appear to be the northwest high-angle faults.

CONCLUSIONS

Brittle, crustal structures exist throughout western Connecticut and southeastern New York, and they may serve as seismic sources. The structures were active during several past tectonic events; there is no apparent reason why they cannot continue to be reactivated and utilized by future stress-release phenomena. The occurrence and partial extents of two of these features, the Saw Mill River-Danbury Fault Zone and the Pomperaug-Georgetown Fault Zone, have been mapped and described. These two zones are important, but there probably are others in the region that have not yet been mapped. Previous mapping did not always identify large faults because of poor exposure, lack of good remotely sensed optical and geophysical data, and an

emphasis on using ductile structures to explain rock distribution patterns.

Surface rupture associated with microseismicity and mesoseismicity in the area has not been reported and quite possibly may not occur because the stresses associated with these minor events diminish and reorient as they approach the surface of the earth. However, the details of the movement histories on these fault zones from the time of their initial formation in the Paleozoic through the Mesozoic and Cenozoic up to the present can be developed through careful analysis of surface and near-surface fault zone materials.[12] Such details are needed for a better understanding of intraplate seismicity in the eastern United States and can also be used in the seismic design of critical facilities, hazard mitigation planning, and groundwater exploration.

REFERENCES

[1] J. B. Hadley and J. F. Devine, "Seismotectonic map of the eastern United States," U.S.G.S. Miscellaneous Field Studies Map MF-620 (1974).

[2] Y. P. Aggarwaal and L. R. Sykes, "Earthquakes, faults, and nuclear power plants in southern New York and northern New Jersey," *Science* **200**, 425-429 (1978).

[3] J. E. Tillman, *Brittle Deformation of the Manhattan Prong*, JHU/APL QM-80-104 (Aug 1980).

[4] N. M. Ratcliffe, "Reassessment of the Ramapo Fault System as Control for Current Seismicity in the Ramapo Seismic Zone and the New York Recess," *Geol. Soc. Am. Abstr. with Prog.* **13**, No. 3 (1981).

[5] D. W. Fisher, Y. W. Isachsen, and L. V. Rickard, "Geologic map of New York," New York State Museum and Science Service Map and Chart Series No. 15 (1971).

[6] Y. W. Isachsen and W. G. McKendree, "Preliminary brittle structures map of New York," New York State Museum and Science Service Map and Chart Series No. 31 (1977).

[7] P. J. Barosh, M. H. Pease, Jr., R. W. Schnabel, K. F. Bell, and J. D. Peper, "Aeromagnetic lineament map of southern New England showing relation of lineaments to bedrock geology," U.S.G.S. Miscellaneous Field Studies Map MF-885 (1977).

[8] P. J. Barosh, "Interpretation of aeromagnetic data in southwestern Connecticut and evidence for faulting along the Northern Fall Line," in *Proc. 2nd International Conf. on Basement Tectonics* (1979).

[9] J. E. Tillman and H. S. Laird, "Dextral wrench tectonics and the controlled emplacement of Paleozoic plutons," *Geol. Soc. Am. Abstr. with Prog.* **9**, No. 3 (1977).

[10] J. W. Clark, *The Bedrock Geology of the Danbury Quadrangle*, Connecticut State Geological Survey Quadrangle Report No. 7 (1958).

[11] J. E. Tillman, *Fault Zones and Seismicity in Western Connecticut and Southeastern New York*, JHU/APL QM-81-126 (Oct 1981).

[12] J. E. Tillman and H. L. Barnes, "On Extending the Historic Record," *Bull. Seismol. Soc. Am.* (1980).

This work was supported by the Nuclear Regulatory Commission.

THE HAZARDOUS MATERIALS EMERGENCY RESPONSE GUIDEBOOK

A. V. Jensen and B. W. Hamill

An emergency response guidebook has been developed by APL for the U.S. Department of Transportation (DOT) to aid emergency services personnel responding to incidents involving spills of hazardous chemical materials during transport. The guidebook's content is the result of improvements in earlier guides and procedures; its format was determined experimentally in a study of the use by police personnel of several alternative versions. The guidebook provides the user with critical information about the health, fire, and explosion hazards of regulated materials and about handling the initial phases of spill, leak, and fire incidents involving those materials.

BACKGROUND

Since the early 1970's, DOT has sponsored a continuing modest project at APL to prepare recommendations in the form of single-page guides for use by emergency services personnel in the mitigation and management of spills that may occur during the transportation of bulk containers of hazardous chemicals. Reference 1, an early result of this project, has proved very popular since it was first prepared at the Laboratory in 1973 (and revised in 1974, Ref. 2). The preparation of the pamphlet had been undertaken by the Chemical Propulsion Information Agency, a DoD Information Analysis Center located at APL, as a spinoff from rela-

ted tasks on the proper handling of DoD chemical propellants in case of an emergency spill or catastrophic release of the materials. Many liquid propellants are toxic and all are powerful oxidizers or extremely flammable fuels.

Before the pamphlets were written, two dozen cards on liquid-propellant spills were prepared. They outlined the potential hazards of each material and recommended control procedures in a simple text and pictorial format. The cards were organized by chemical name, and a chart on each gave the recommended evacuation distances for spill puddles on hard earth or on concrete with spill areas of 200 to 800 sq ft. The evacuation data were produced by entering the desired maximum concentration levels and certain physical properties for the material into an in-house computer program written in Iverson's APL language. The program contained modules for projecting evaporation rates, converting units, and calculating a set of atmospheric dispersion isopleths based on D. B. Turner's *Workbook of Atmospheric Dispersion Estimates*[3] for volatile contaminants in air.

Worst-case atmospheric conditions corresponding to Turner's weather condition "D" were chosen because those conditions would conservatively predict dispersed concentrations of the spilled material for 85% of all possible weather conditions. The conservative isopleths (concentration outer boundaries), with the incorporation of a ±15° variability in wind direction and with a continuous point source (the spill puddle or leak), produced a series of three isopleths (Fig. 1). The isopleths could be smoothed to produce a circular isolation area of diameter, D, around the puddle or source that, when m- d with the outer bounds of the isopleths, produced a truncated isosceles triangle whose base represented the downwind width, B, at a downwind distance, A, from the incident (Fig. 2).

The simple diagram in Fig. 2 and a chart of values for D, A, and B provided the initial data for an on-scene public safety officer or range officer to clear an area at the scene of a spill of a volatile, toxic material. The officer was advised in the text that he was to continue to re-evaluate the observed effects on the population exposed to the material. The chart of values

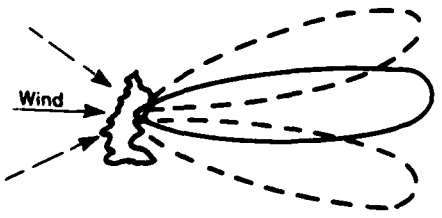

Fig. 1 Typical atmospheric dispersion isopleths near ground level.

covered a range of observable spill puddle areas from 200 to 800 sq ft, corresponding to spill areas resulting from failures of standard bulk transport tanks. The pamphlet was not intended to be a substitute for judgment on the part of personnel experienced in handling hazardous materials.

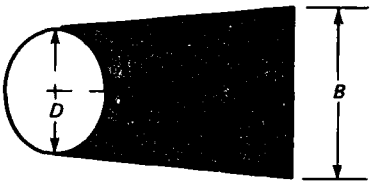

Fig. 2 Model representation of same isopleths as in Fig. 1.

DISCUSSION

The model and procedure described above were revised several times from 1973 to 1979 to produce hazardous-material action guides covering 43 products. More than a million copies of the "little red book"[4] were printed and distributed by DOT during that period, and numerous recipients requested a pamphlet with greater scope. A simple way to incorporate the more than 1700 additional regulated materials did not appear until DOT proposed that the United Nations four-digit identification number be appended to the proper name on shipping documents and that the same number be incorporated in placards and panels applied to bulk transport tanks and vehicles. With this simple universal code, a generic set of guide cards could be prepared. They could be cross-referenced by the shipping name and could cover the entire commodity list for both international and domestic shipments of hazardous materials. On the assumption that the identification numbers would be accepted, development of a new format for an all-inclusive guidebook was initiated in early 1979.

Formatting Experiment

An experiment was conducted to determine the best way to format the guidebook indexes and to organize the several sections[5] to ensure that personnel using the guidebook would be able to locate information quickly and accurately so that appropriate action could be taken. The subjects for the experiment were volunteer officers and patrolmen/agents of the Baltimore City Police Department.

Several possible formats for the identification number index and the alphabetical name index were considered, in combination with two alternative ways to organize the guidebook sections. The experiment required subjects to record the number of the correct guide to use for an incident involving each of 24 materi-

als identified by its United Nations identification number, by its chemical name, or by a placard of the type used to identify materials by DOT generic categories. The subjects timed themselves with stopwatches, under the supervision of the experimenter, as they performed each task. The resultant data comprised the elapsed times for looking up the three different kinds of items and the error rates.

The results of the experiment converged to favor one particular combination of guidebook organization and index format. Both indexes are in the front of the guidebook, and the guide sheets follow the second (alphabetical) index; the number index has the United Nations identification number at the left side of the entry, followed by the guide number and then the chemical name; the name index has the chemical name at the left, followed by the guide number and the identification number. This organization results in entries with the indexed information at the left margin, the relevant guide number immediately to the right of the indexed information, and extraneous information still farther to the right and out of the way.

It is noteworthy that the error rate for number items (2%) was lower than that for either placard items (4%) or name items (10%); this attests to the relatively better identifiability of cargoes bearing the identification numbers.

Guidebook Distribution and Use

The final product, DOT Publication P-5800.2 (Ref. 6), was published in late 1980 by DOT, and free distribution to public safety offices in the United States was begun in early 1981. The distribution of 700,000 copies is being accomplished by the International Association of Fire Chiefs under contract with DOT and is expected to be completed by the end of 1981. A copy of the guidebook is to be placed in each emergency services vehicle in the United States; additional copies are being provided for office and training use by the organizations operating the vehicles. Major safety product and label manufacturing firms have been given permission to reprint the guidebook without fees or royalties, and more than 200,000 copies have been sold in addition to the public sector's free distribution. Each booklet sells for about three dollars in five-copy lots, postpaid.

When the guidebook is used at an incident scene, the Chemical Manufacturers Association's Chemical Transportation Emergency Center (CHEMTREC) must be contacted for supplemental information in order to refine the guidebook's advice after the scene has been better defined and to connect the on-scene officials with responsible representatives of the shipper or manufacturer of the product involved. CHEMTREC maintains a 24-hour telephone-conferencing bridge system to bring expert advisors into a conference call and to coordinate the dispatch of special chemical response teams to assist at the scene. DOT has officially recognized CHEMTREC as the public service resource to be used in conjunction with the guidebook during the initial phases of an incident. The use of CHEMTREC does not eliminate government-mandated requirements for reporting to the EPA, U.S. Coast Guard, or local authorities, but CHEMTREC effectively coordinates efforts to minimize the immediate damage and to double check the on-scene commander's proposed response.

CONCLUSION

In summary, the *Hazardous Materials — 1980 Emergency Response Guidebook* is a valuable tool for all public safety services personnel who might be the first responders at a transportation incident involving regulated hazardous materials. It was and continues to be proposed as the source of immediate information to begin an evaluation of the potential hazard of an incident, and it has a useful on-scene life of twenty to thirty minutes. At the end of that time, the guide will have been used to help on-scene personnel evaluate the potential hazards, make the required judgments, and communicate accurately all pertinent details to appropriate shippers or manufacturers if the incident is serious enough to require specialized response teams.

A field evaluation of the current edition of the guidebook, planned for 1982, will determine how well prospective users of the guidebook can employ it under simulated conditions. Those results, together with information from actual incidents in which the guidebook was used, will provide a basis for future revisions and refinements of this APL product.

REFERENCES

[1] A. V. Jensen and H. R. Neumark, *Guide for Emergency Service for Hazardous Materials, Spills, Fire, Evacuation Area*, DOT Pamphlet, Office of Hazardous Materials (1973).

[2] A. V. Jensen and H. R. Neumark, *Emergency Services Guide for Selected Hazardous Materials, Spills, Fire, Evacuation Area*, DOT Pamphlet, Office of Hazardous Materials (1974).

[3] D. B. Turner, *Workbook of Atmospheric Dispersion Estimates*, Environmental Protection Agency, USGPO Stock No. 5503-0015 (1967).

[4] H. R. Neumark, *Hazardous Materials — Emergency Action Guide*, DOT Pamphlet, Office of Hazardous Materials Operations (1977).

[5] B. W. Hamill, "Experimental Document Design: Guidebook Organization and Index Formats," *Proc. Human Factors Society 24th Annual Meeting*, pp. 480-483 (1980).

[6] A. V. Jensen and H. R. Neumark, *Hazardous Materials — 1980 Emergency Response Guidebook*, DOT Publication P-5800.2, Materials Transportation Bureau (1980).

This work was supported by the U.S. Department of Transportation.

DECENTRALIZED ROUTING IN A LARGE AUTOMATED TRANSPORTATION NETWORK

A. J. Pue

The problem of efficiently routing vehicles from many origins to many destinations in a large Automated Guideway Transit network is formulated as an optimization problem by using a performance index based on total, time-averaged, travel time subject to the dynamic vehicle flow constraints of the network. An algorithm is designed so that all control computations can be performed in a completely decentralized manner where information exchange occurs only between physically adjacent wayside control computers.

BACKGROUND

Automated Guideway Transit (AGT) systems represent a developing transportation technology to serve urban regions as well as major activity centers such as airports, shopping districts, and universities. They are characterized by automatically controlled (driverless) vehicles of small to moderate size operating on dedicated guideway networks that have either on-line or off-line stations.

An urban-wide AGT network may be composed of hundreds of miles of connected guideway sections called links, joining up to a hundred stations (typically off-line) and containing hundreds of vehicles. Consequently, the problem of efficiently distributing and routing vehicles between many origins and destinations is of considerable importance in terms of customer acceptance, efficient operation, and energy use.

The network control function may be illustrated with the help of Fig. 1. Passengers arrive at the station loading platform and board a vehicle. The dispatched vehicle is controlled by a series of local wayside computers that communicate with the vehicle by means of sensors imbedded in the guideway as the vehicle merges into the mainline traffic and travels to its destination. Each wayside computer has jurisdiction over a region of the guideway network and passes control to adjacent wayside computers as the vehicle passes through jurisdictions.

From an economy and reliability viewpoint, it would be beneficial to design a decentralized routing control algorithm that uses the existing communications and computational capability required for vehicle control (illustrated by the series of interconnected wayside computers in Fig. 1). As each vehicle approaches a point where an alternate path may be taken (diverge point), the local wayside computer selects which outgoing link the vehicle should travel on. The computer makes this decision on-line and locally, based on information obtained from the adjacent wayside computers, thus utilizing the communication links already in place for vehicle spacing and velocity regulation. Most importantly, the algorithm must be structured so that local routing decisions satisfy a global network performance criterion. Consequently, the problem posed here is to develop a decentralized control strategy that accounts directly for network-wide dynamics and performance.

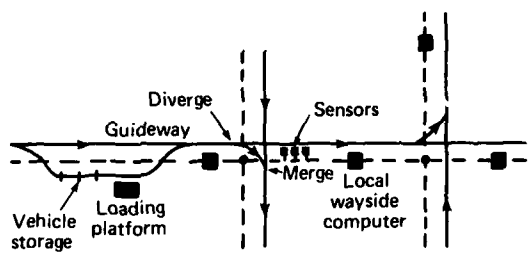

Fig. 1 Typical network section.

DISCUSSION

The fundamental routing problem may be viewed as a nonlinear multicommodity flow problem, one that has received wide attention in literature on nonlinear programming although primarily for the static case. Recently, more research has been devoted to the decomposition and efficient solution of large problems for both the static and dynamic situations (see Ref. 1 and references therein). In particular, applications have centered on automobile traffic, power, and computer communication networks.

For the specific application in automated transit systems, the main component describing the behavior and characteristics of a transportation network is vehicle flow. Flow is determined by operational policies, the intervehicle spacing control scheme, station geometries, and link connectivities that form the overall network design. Thus, the accurate modeling of vehicle flow and the attendent description of network dynamics are critical for the design of a successful routing-control law.

Research into developing traffic flow models has concentrated on the problem of automobile traffic in congested urban streets and freeways. Many models are based on the original continuum model of Lighthill and Whitham,[2] which was derived by using the analogy of

the continuity of fluid flow. That model forms the basis for many traffic flow models in the literature.

The model of an automated vehicle network does not contain the complicating factors of an urban traffic network such as passing, parked vehicles, and human behavior. The interactions between vehicles in an automated system may be described according to a well-defined longitudinal control law[3] that is based on accurate measurements of vehicle position and velocity. Thus, one could easily derive a microscopic traffic flow model based on discrete vehicle behavior. However, such a model would be of extremely high order and would lead to a complex and costly control algorithm. As a matter of judgment and practicality, aggregate models using macroscopic variables such as vehicle density are sufficient for the successful application of on-line routing-control laws. Such models have been derived in Ref. 4 for the vehicle-follower longitudinal control scheme. They have the same form as the fundamental traffic flow model but the vehicle flow into link i, q_i, is computed as a nonlinear function of the densities in adjacent links or

$$\dot{y}_i = [q_i(y_{i-1}, y_i) - q_{i+1}(y_i, y_{i+1})]/D_i \ , \qquad (1)$$

where y_{i-1}, y_{i+1} are the upstream and downstream link densities, respectively, D_i is the length of link i, and $\dot{y}_i$ is the derivative with respect to time.

The flow resulting from a particular vehicle type, j (each vehicle type is associated with a particular origin-destination station pair), is assumed to be the fractional portion of that vehicle type on a guideway section. If $x_{i,j}$ is the density of vehicle type j, and if y_i is the total density, then the flow resulting from type j is

$$q^j_{i+1} = [x_{i,j}/y_i]\, q_{i+1}(y_i, y_{i+1}) \ , \qquad (2)$$

where

$$y_i = \sum_j x_{i,j} \qquad (3)$$

and all densities are a function of time. Defining at time k the velocity function, $a_{i,i+1}(k) = q_{i+1}(y_i, y_{i+1})/y_i$, the density of vehicle type j on link i is given in discrete time by

$$x_{i,j}(k+1) = x_{i,j}(k) + T[a_{i-1,i}(k)x_{i-1,j}(k) - a_{i,i+1}(k)x_{i,j}(k)]/D_i \ , \qquad (4)$$

where T is the integration step size and D_i is the section length. This model has two features important to the development of decentralized control. First, note that the dynamics are linear in the vehicle type densities, $x_{i,j}(k)$. Thus, if the total density variables, $y_i(k)$, are treated as independent functions of time and not as functions of state, the flow equations are linear in state. Second, each vehicle type density, $x_{i,j}(k)$, depends only on upstream vehicle type densities; hence the subnetwork dynamics have what is termed a triangular structure

The model is extended to include links representing merge, diverge, and station elements.[4] For a diverge, a routing control variable, $0 \le u_{i,j}(k) \le 1$, is defined as the fraction of vehicle type j density routed onto outgoing link i. A total routing control variable, v_i, can be computed as

$$v_i = \sum_j u_{i,j}x_{i,j} \ . \qquad (5)$$

The approach taken to design the routing strategy was to formulate an optimization problem by using the above dynamic models of vehicle flow[4] and designing a performance (cost) index based on total time-averaged travel time in the network. If $\tau(x_i)$ is the travel time on link i, the total cost can be written as

$$\sum_{k=1}^{K} \sum_{i \in \ell} TD_i \tau(y_i(k))y_i(k)/t_f \ , \qquad (6)$$

where K is the number of time steps, ℓ is the set of network links, and t_f is the time period over which the optimization takes place. The cost (Eq. 6) would also include the time spent by passengers waiting at stations. The optimization problem then is to minimize Eq. 6 subject to the dynamic network flow constraints of the form defined by Eq. 4.

Minimization of Eq. 6 subject to the dynamic flow constraints of the network was accomplished by solving a dual optimization problem.[5] Duality is an optimization technique that converts a minimization problem into a corresponding maximization problem. It is commonly used when the resulting maximization problem is easier to solve than the original minimization problem. To apply this concept, the interconnection constraints of total density (Eq. 3) and total routing control (Eq. 5) are appended to Eq. 6 via Lagrange multipliers. Then, the problem-constraint dynamics decompose into j vehicle-type subnetwork constraints that are decoupled with respect to individual vehicle type density and routing-control variables. The total link density and total diverge-link-control variables are treated as additional control variables that act to interconnect the individual subnetwork dynamic constraints. The resulting optimization problem has a two-level structure consisting of a lower level minimization (with respect to u_i, v_i, y_i) and an upper level maximization (with respect to the Lagrange multipliers).

The principal benefit of applying the duality concept is to produce a dynamic constraint structure that allows a completely decentralized control computation. Because of the triangular structure of the subnetwork dynamics and the additive form of the cost function, the effects of each control variable on the dual-

function objective can be computed locally. To do this, the state equations are integrated in a distributed manner from origin to destination, where each link only needs to obtain information from adjacent upstream links. Information concerning future downstream congestion is obtained by integrating a subnetwork adjoint equation from destination to origin and backward in time.

The adjoint equation is used to express the performance index as a function of variables that are local to link i. It consists of transposed state dynamics; that is, if the state dynamics are upper triangular in structure, then the adjoint equation is lower triangular in structure. Thus, each adjoint variable depends on future downstream adjoint variables. This permits the adjoint equations to be integrated in a distributed manner, where each link obtains information from adjacent downstream links.

Using state and adjoint information, the algorithm is so structured that at the link level, routing, total control, and total density variables are computed to minimize the dual-function objective (lower level problem). Upper level coordinating control on each link is accomplished by computing Lagrange multipliers using subgradient optimization to maximize the dual function and to satisfy the interconnection constraints that total density be equal to the sum of individual type densities (Eq. 3) and that total control be equal to the sum of vehicle type controls (Eq. 5). Consequently, the control algorithm can be implemented so that wayside control computers only need to communicate with neighboring computers to solve the overall dual problem.

Convergence of the algorithm has been proven analytically, and its operation has been demonstrated by the simulation of a four-station, 58-link network[1] shown in Fig. 2. An example of algorithm performance is given in Fig. 3. The values of the cost function (Eq. 6) and the corresponding dual function are shown as a function of upper level iteration number. The network shown in Fig. 2 was initialized to a density of 0.015 vehicle per meter on each link and a set of routing control variables that gave a cost of 9641 s. For an optimization time of 30 s, the cost was reduced to the optimal value of 8908 s. Note that the final value of the dual function (which is maximized) corresponds to the final value of the cost function.

Because the computational cost for optimal control increases dramatically as the time scale is lengthened, suboptimal strategies are more appropriate for actual implementation. Several suboptimal strategies have been investigated[1] for the network example; results indicated that significant savings in computational cost are obtained with little sacrifice of performance. The results for the optimal and three suboptimal strategies, using the above numerical example, are given in Table 1. Run times are the computation times on an IBM 3033 for a 30 s optimization period and 20 upper-level iterations.

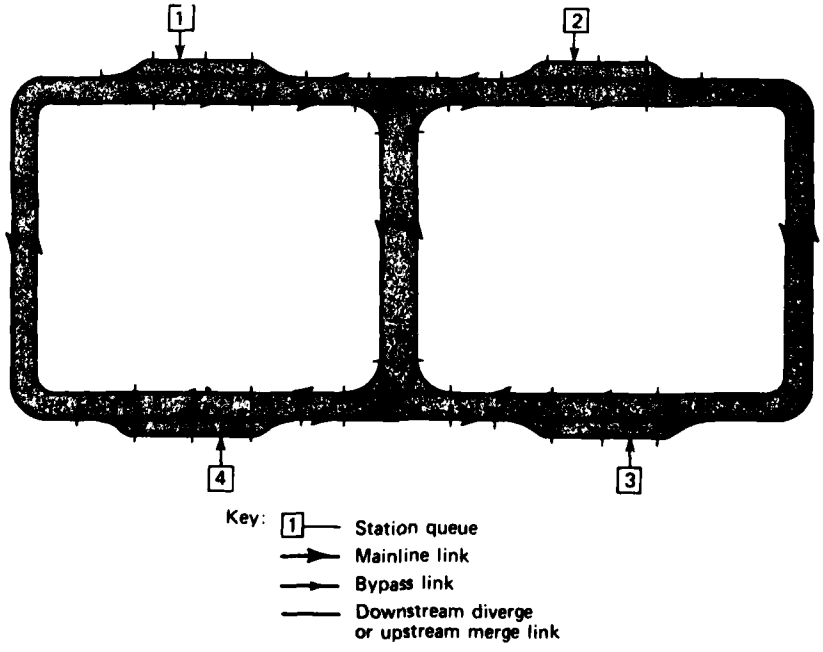

Fig. 2 Simulated network.

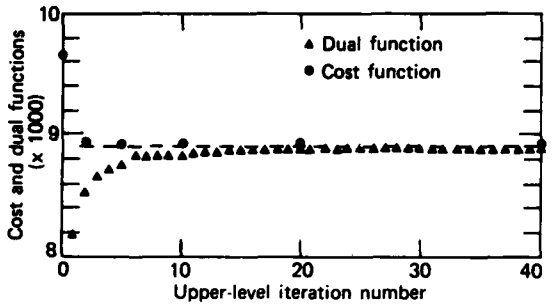

Fig. 3 Cost and dual functions.

REFERENCES

[1] A. J. Pue, "Vehicle Distribution and Routing in a Large Automated Transportation Network," Ph.D. Dissertation, Dept. of Electrical Engineering, Univ. Maryland (1981) (also JHU/APL TPR-046).
[2] M. J. Lighthill and G. B. Whitham, "On Kinematic Waves - II, A Theory of Traffic Flow on Long Crowded Roads," *Proc. R. Soc. (London)* **229A**, 317-345 (1955).

Table 1

SUBOPTIMAL COMPUTATIONAL RESULTS

	Final Cost	Run Time (s)
Optimal	8908	10.38
Suboptimal I	8918	3.91
Suboptimal II	8913	3.71
Suboptimal III	8941	2.39

[3] A. J. Pue, "A State-Constrained Approach to Vehicle-Follower Control for Short-Headway AGT Systems," *J. Dyn. Syst. Meas. Control* (Dec 1978).
[4] A. J. Pue, "Macroscopic Traffic Models for Vehicle-Follower Automated Transportation Systems," *Trans. Res.* **16B**, No. 2, 125-142 (1982).
[5] L. S. Lasdon, "Duality and Decomposition in Mathematical Programming," *IEEE Trans Syst. Man. Cybern.* **SSC-4**, No. 2 (Jul 1968).

This work was supported by the Urban Mass Transit Authority.

ATLANTIC CITY PARKING STUDY

R. C. Rand, D. L. Kershner, and R. A. Makofski

Traffic and parking forecasts traditionally have used time as the independent variable, requiring forecasts of future traffic flows, parking lots, parking requirements, road widening, etc. In some cases the driving force is not only separate from but almost independent of time. One such analysis is presented here, based on an actual application in Atlantic City and basically confirmed in 1981.

BACKGROUND

Most traffic studies are aimed toward the construction of a new highway or transit system; the results of the new construction are expected to become evident over a period of several years. Such a leisurely pace is not always the case; an example was Atlantic City several years ago when a large increase in trips as a result of the opening of the gambling casinos was evident but no major new construction was contemplated to ease the traffic and parking difficulties. To help meet the problem, Atlantic County officials asked APL to undertake the study of the traffic and parking problems and to make suitable recommendations.

Although Atlantic City had been known as a summer recreation city, the traffic was in no way comparable to that expected to be generated by the gambling casino industry. In addition, there are very limited airport facilities, virtually no train service, and only three bridges to the island on which Atlantic City is located.

DISCUSSION

The approach taken in this study to estimate the parking demand was to divide travelers into groups (Table 1) and to estimate the demand of each group separately. It immediately became apparent that the park-

ing required by some groups depended on the number of casinos operating, while the parking for other groups was largely independent of the number of casinos. In the former category, the parking required by casino-hotel employees, secondary employees, and visitors can be considered approximately linearly dependent on the number of casinos, N.

Table 1

TRAVELER GROUPS

Employee groups
Casino-hotel employees
Existing commercial, retail, and government employees
Secondary employees resulting from casino development
Visitor groups
Casino-hotel visitors
Beach recreation visitors (primarily interested in activities other than gambling)
Convention visitors
Business and shopping visitors (local residents)

Commercial, retail, and government employees were expected to continue to use existing facilities. The travel habits of those groups are rather well established and probably not easily changed. The numbers of beach and other recreation visitors are expected to decline as they compete for space with casino visitors. Many of them will be diverted to beaches outside Atlantic City. Almost all convention visitors are expected to be overnight guests and will have parking spaces at their hotels. (These spaces are not part of the parking supply considered in this study.) Since the casinos-hotels are close to the Convention Center, most internal trips will be by foot or jitney, and intracity automobile trips by this group should be minimal. Similarly, local residents entering the city for business and shopping are expected to time their visits for nonpeak hours and will usually be destined for locations outside the casino district.

This assumption leads to two useful approaches: the parking demand at any time depends linearly on N, and the slope of the line can be determined from a detailed analysis of a single casino. Although these assumptions may appear too strong, no detailed data were available at the time of the study, and local government and business personnel expressed no disagreement for $N < 10$. Furthermore, limited early observations confirmed the essential validity of the assumptions.

Parking demand models were developed to estimate the parking requirements, per casino, of the casino-hotel employees, secondary employees, and visitors. The models contained variables representing the total number of individuals in each group, the percent of those individuals arriving during the peak demand period, the percent using different transportation modes (modal split), and the average auto occupancy. The modal split and auto occupancy variables permit an assessment of the effects of transportation-related policies and improvements on parking demand. Variables representing the number of individuals in a group permit an examination of, for example, changes in staffing policies of the casinos.

In order to account for seasonal variations in demand for the visitor groups, a variable representing the ratio of daily visitors per casino to the annual average level (about 5000 visitors per casino per day) is included in the model of casino-hotel visitors. Three conditions were considered:

1. Average day (ratio = 1),
2. Peak day (ratio = 3.2, peak summer day), and
3. Design day (ratio = 2.0, average summer day).

The total parking demand is shown in Fig. 1 for the annual average day, design day, and peak day. The total demand estimates represent the sum of the parking demands of the individual traveler groups as computed by the parking models. The dashed curve in the figure represents the in-city parking available to serve the projected demand. The available parking consists of an estimated existing parking capacity of 17,350 spaces.

In Fig. 2, the design day demand is shown by traveler group. The available parking in the city is

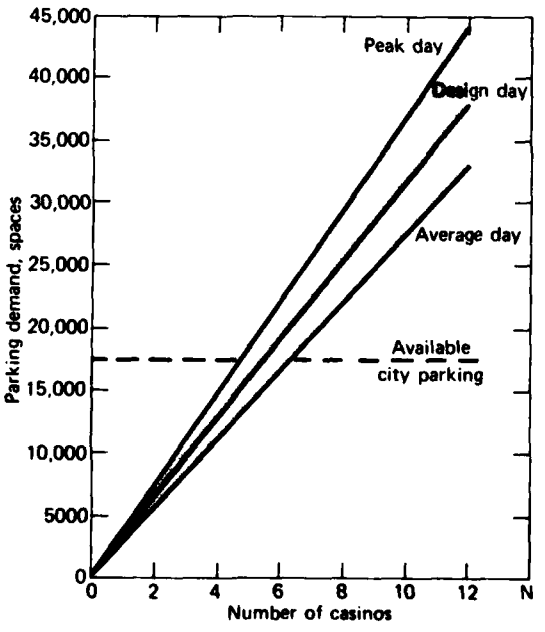

Fig. 1 Near-term parking demand.

sufficient to serve the demand for $N < 10$ if the casino-hotel employees use remote parking in the county or intercept facilities in the city. However, for $N \geq 15$, the casino-hotel employee group, which represents a large percentage of the total parking demand, will require 12,000 additional spaces. An additional 5000 spaces will be needed to serve the demand of the other traveler groups. The result is a total deficit of 17,000 spaces.

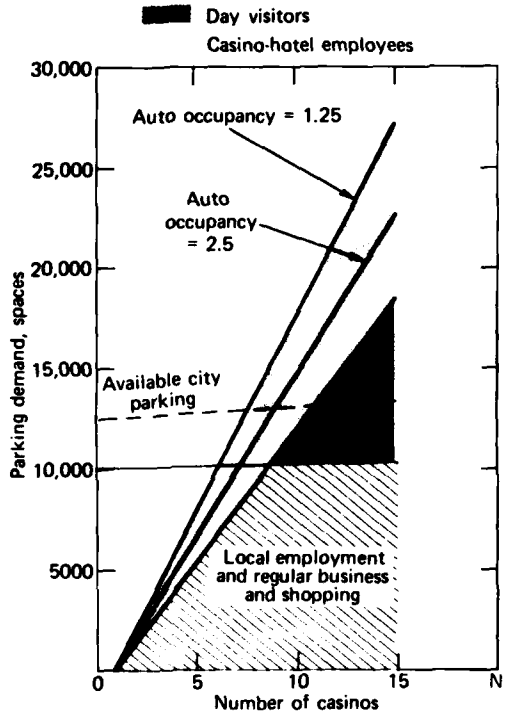

Fig. 2 Design day near-term parking demand, by group.

The curves for casino-hotel employees in Fig. 2 also show the effect of increasing the average auto occupancy for these employees from 1.25 (reported experience of one casino) to 2.5. By encouraging car and van pooling to raise the average occupancy to 2.5 persons per car, a parking deficit could be temporarily alleviated. Greater increases in ride sharing would, of course, reduce the deficit even further.

Although the above discussion makes the problem addressed seem like a straightforward computation, several factors actually required much extra effort. For one thing, although N was the obvious choice for an independent variable, time could not be completely ignored. The secondary employee category, for example, had a 2 year lag that required consideration. In addition, the present parking was complicated by a large number of "temporary" spaces owned by one of the casinos (the meaning of temporary was unclear; they are still temporary). Finally, the city's program for additional parking was uncertain and largely unscheduled.

The approach taken had the advantage of versatility so that forecasts could be corrected and updated as data became available.

CONCLUSIONS AND RECOMMENDATIONS

The situation depicted in Fig. 2 led to a recommendation to Atlantic County to provide and encourage intercept parking for casino employees and to promote car and van pooling. A second recommendation was to accelerate the rate of building city parking facilities over the planned rate of 1000 spaces per year.

In the fall of 1981, there were nine operating casinos, and our predictions had been basically confirmed, although no detailed data had been gathered. Probably the linear assumption will weaken with additional casinos, alleviating the predicted parking shortage to some extent, but the primary conclusion — that casino employees must be encouraged to keep cars off the island — is indisputable. Several casinos are already providing bus service from the mainland to the casinos.

REFERENCES

[1] "Planning for Twelve Million Annual Visitors to Atlantic City," *Traffic Q.* (Jan 1971).

[2] *City of Atlantic City, New Jersey Comprehensive Master Plan — Transportation Element*, Barton-Aschman Associates, Inc. (Oct 1978).

[3] *Atlantic City Intracity Circulation System and Transportation Center Feasibility Studies*, Gannett Fleming/Lisiewski Tarquine, Working Papers Nos. 1 and 6.

This work was supported by Atlantic County, New Jersey.

PATENTS

PATENTS ACTIVITIES

The APL Patents Office is responsible for ensuring compliance with contract and grant requirements relative to patent and data rights, as imposed by the various governmental agencies that sponsor work at the Laboratory. In addition to preparing formal disclosures of inventions for the appropriate sponsors, the Patents Office prepares and prosecutes patent applications on behalf of both the University and the Department of the Navy.

The following lists indicate the invention disclosures submitted to sponsors, the patent applications prepared and filed in the United States Patent Office, and the previously filed applications that were successfully prosecuted to issuance as patents, during Fiscal Year 1981.

INVENTION DISCLOSURES

W. H. Avery—*Flexible Cold Water Pipe*
W. H. Avery—*Platform-Cold Water Pipe Joint*
W. G. Bath, F. R. Castella, and S. F. Haase—*Apparatus for Filtering Range and Azimuth Measurement Data from a Plurality of Collocated Radars*
D. J. Buscher—*Quandit Serial Computer*
D. P. Crawford—*PC Card Extractor*
H. C. Davey—*Synchronous Multiband Signal Generator*
A. E. Davidoff—*Voice-Actuated Controller for the Handicapped*
O. J. Deters and M. H. Friedman—*A Simple, Directionally Sensitive Two-Component Laser Doppler Anemometer*
R. E. Fischell—*A Low Susceptibility Proof Mass for a Single Axis Drag Compensation System*
R. W. Flower—*Intraocular Pressure Monitor*
A. B. Fraser and T. R. Whyte—*Portable Submarine Dye System*
A. B. Fraser and V. T. Tolo (JHMI)—*Apparatus for Measuring, Recording, and Treating Spinal Curvature*
J. B. Garrison—*Digital Optical Correlator for Processing Synthetic Aperture Radar Data*
W. H. Guier, W. Schneider, and R. S. Carlson—*Computer Controlled Closed Loop Blood Pressure Control System*
F. K. Hill and R. W. Henderson—*Gimballing Cold Water Pipe Joint*
S. A. Kahn, R. L. Stewart, and S. G. Tolchin—*Local Area Communications Network*
E. H. Kidera—*A Motion-Compensated Launch/Recovery Crane for Towing of Oceanographic Instruments*
J. H. Kuck—*Analog Switch*
J. H. Kuck—*Methods of Eliminating Undesirable Transient Offset Voltage in the Clocking Signal Applied to a Towed Underwater Instrumentation Package*
S. J. Kundin—*Paravane Recovery Device*
R. E. Lee—*Transient Inline Particle Sampling Probe (TIPS)*
J. H. Loveless—*Optical Tachometer*
F. T. Marcellino—*Reverse Polarity and Negative Transient Detector for D.C. Bus Line*
J. C. Murphy—*Technique for Making Photoacoustic Spectroscopy (PAS) Measurements in the Time Domain*
R. J. Prengaman, R. E. Thurber, J. Phipps, and R. I. Greenberg—*Retrospective Data Processor*
D. N. Qualkinbush—*Depth Readout Circuit*
K. Reinitz—*Method of Radiation Hardening CMOS Circuitry by Substrate Biasing*
J. W. Sari and D. A. Bowser—*C-Pump (Compressed Pulse Underwater Electro-Magnetic Propagation in Conductive Media)*
J. A. Schetz, F. S. Billig, and S. Favin—*Analysis of Mixing and Combustion in a Scramjet Combustor*
W. Schneider, J. Loveless, and W. Seamone—*Computer-Aided Powered Manipulator*
G. Shoben—*Sliding Scale*
T. D. Smith—*Dissolved Gas Sensor*
J. D. Steinberg—*Cable Attachment Device*
D. F. Sterne, C. E. Crooke, and A. E. Davidoff—*Apparatus for Tactical Speech Synthesis*
R. J. Taylor—*Infrared Display Using Liquid Crystals*
D. M. Weintraub—*Energy Particle Weapon Employing a Negative Muon Beam*
T. Wyatt—*Method and Apparatus for Frequency Conversion by the Microlayer of the Ocean*

PATENT APPLICATIONS

J. G. Chubbuck and M. H. Epstein (JHMI)—*X-ray Readable Implantable Pressure Sensor*
R. E. Fischell—*A Low Susceptibility Proof Mass for a Single Axis Drag Compensation System*
A. B. Fraser—*Frequency Encoding Closed Loop Circuit with Transducer*
P. H. Gilbert—*Phase Demodulator*
E. J. Hoffman and J. C. Loessi—*Short-Circuit-Proof Connector Clip for a Multiterminal Circuit*
S. A. Kahn, R. L. Stewart, and S. G. Tolchin—*Local Area Communication Network*
C. A. Keller—*Fluid Level Measuring Device with Linear, High Resolution Output*
J. H. Loveless—*Motorized Wheelchair*
J. H. Loveless and W. Seamone—*Closed Loop Velocity Controller for Powered Wheelchair*
C. Philippides and W. H. Zinger—*Apparatus for Identifying Coded Information without Internal Clock Synchronization*
K. Reinitz—*A Solid State Magnetometer*
S. L. Sachs and F. K. Hill—*Ultrasonic Cleaning Method and Apparatus*

PATENTS ISSUED

J. G. Chubbuck and J. T. Turner—*Intracranial Pressure Implant*, No. 4,265,252
R. E. Fischell—*Charge Control Switch Responsive to Cell Casing Deflection*, No. 4, 275,739
R. C. Gipe and W. E. Engelkemier—*RF and IF Circuitry of an Uplink Receiver*, No. 4,287,604
J. H. Loveless and W. Seamone—*Chin Controller System for Powered Wheelchair*, No.4,260,035
S. R. Osborne—*Raster Scan Generator for Plan View Display*, No. 4,228,432
D. W. Rabenhorst—*Elastic Internal Flywheel Gimbal*, No. 4,244,240
S. L. Sachs and F. K. Hill—*Ultrasonic Cleaning Method and Apparatus for Heat Exchangers*, No. 4,244,749
D. J. Yost, A. Arrow, and R. L. Konigsberg—*High Angle-of-Attack Missile Control System for Aerodynamically Controlled Missiles*, No. 4,234,142

PUBLICATIONS AND PRESENTATIONS

B. I. Blum and S. G. Tolchin, "The Impact of Technology on Hospital Information Systems," in *Proc. Hawaii International Conf. on System Sciences*, Honolulu (8-9 Jan 1981).

N. A. Blum, K. Moorjani, T. O. Poehler, and F. G. Satkiewicz, "Hyperfine Field Distributions in Ferromagnetic Amorphous Fe_xB_{1-x} Thin Films," *J. Appl. Phys.* **52**, 1808-1810 (1981).

J. Bohandy and B. F. Kim, "Temperature Dependence of Mg Porphin, Cu Porphin, and Pd Porphin Luminescence," *J. Chem Phys.* 73, No. 11, 5477-5481 (1980).

C. O. Bostrom, "The APL Mission: Challenge for the 1980's," *Johns Hopkins APL Tech. Dig.* **1**, No. 4, 295-296 (1980).

R. W. Bruns and E. C. Jarrell, "RAM Guided Missile Weapon System," *Johns Hopkins APL Tech. Dig.* **2**, 200-206 (1981).

J. L. Calkins (JHMI) and B. F. Hochheimer (APL), "Retinal Light Exposure from Operation Microscopes," *Arch. Ophthalmol.* **97**, 2363-2367 (1981).

J. L. Calkins (JHMI) and B. F. Hochheimer (APL), "Retinal Light Exposure from Ophthalmoscopes, Slit Lamps, and Overhead Surgical Lamps: An Analysis of Potential Hazards," *Invest. Ophthalmol. Vis. Sci.* **19**, 1009-1015 (1980).

J. L. Calkins (JHMI), B. F. Hochheimer (APL), and W. J. Stark (JHMI), "Corneal Wound Healing: Holographic Stress-Test Analysis," *Invest. Ophthalmol. Vis. Sci.* **21**, 322-334 (1981).

J. L. Calkins (JHMI), B. F. Hochheimer (APL), and S. A. D'Anna (JHMI), "Potential Hazards from Specific Ophthalmic Devices," *Vision Res.* **20**, 1039-1053 (1980).

J. F. Carbary and S. M. Krimigis, "Low Energy Charged Particles at Saturn," *Johns Hopkins APL Tech. Dig.* **2**, No. 2, 87-89 (1981).

J. F. Carbary, S. M. Krimigis, and E. P. Keath (APL), G. Gloeckler (Univ. Maryland), W. I. Axford (Max-Planck Inst. Aeronomy), and T. P. Armstrong (Univ. Kansas), "Ion Anisotropies in the Outer Jovian Magnetosphere," *J. Geophys. Res.* **86**, 8285-8299 (1981).

F. R. Castella, "An Adaptive Two-Dimensional Kalman Tracking Filter," *IEEE Trans. Aerosp. Electron. Syst.* **AES-16**, No. 6, 822-829 (1980).

F. R. Castella, "Tracking Accuracies with Position and Rate Measurements," *IEEE Trans. Aerosp. Electron. Syst.* **AES-17**, 433-437 (1981).

R. D. Chapman, "Visibility of RMS Slope Variations on the Sea Surface," *Appl. Opt.* **20**, 1959-1966 (1981).

R. D. Chapman and G. B. Irani, "Errors in Estimating Slope Spectra from Wave Images," *Appl. Opt.* **20**, 3645-3652 (1981).

J. S. Chappell (JHU), A. N. Bloch (Exxon Co.), W. A. Bryden and M. Maxfield (JHU), T. O. Poehler (APL), and D. O. Cowan (JHU), "Degree of Charge Transfer in Organic Conductors by Infrared Spectroscopy," *J. Am. Chem. Soc.* **103**, 2442-2443 (1981).

H. K. Charles, Jr., "Ceramics in Photovoltaic Energy Conversion," *Ceram. Bull.* **59**, No. 12, 1201-1204 (1980).

L. -Y. Chiang (JHU), T. O. Poehler (APL), and A. N. Bloch and D. O. Cowan (JHU), "A Modified Synthesis of Tetraselenafulvalenes," *J. Chem. Soc. D*, No. 18, 866-867 (1980).

E. P. Cunningham, "Single-Parameter Terrain Classification for Terrain Following," *J. Aircr.* **17**, No. 12, 909-914 (1980).

S. A. D'Anna (JHMI) and B. F. Hochheimer (APL), "70mm Fluorescein Angiography and Color Fundus Photography," *J. Biol. Photogr.* **48**, 31-33 (1980).

R. B. Decker, "The Modulation of Low-Energy Proton Distributions by Propagating Interplanetary Shock Waves: A Numerical Simulation," *J. Geophys. Res.* **86**, 4537-4554 (1981).

R. B. Decker (APL), M. E. Pesses (Univ. Maryland), and S. M. Krimigis (APL), "Shock-Associated Low-Energy Ion Enhancements Observed by Voyagers 1 and 2," *J. Geophys. Res.* **86**, 8819-8831 (1981).

O. J. Deters and C. B. Bargeron (APL), G. M. Hutchins (JHMI), and F. F. Mark and M. H. Friedman (APL), "Arterial Intimal and Medial Thicknesses Correlate with Shear," in *Proc. 34th Annual Conf. on Engineering in Medicine and Biology* **23**, p. 303 (1981).

G. L. Dugger, R. W. Henderson, E. J. Francis, and W. H. Avery, "Projected Costs for Electricity and Products from OTEC Facilities and Plantships," *J. Energy* **5**, 231-235 (1981).

P. B. Edwards, "The JHU/APL Evening College Center," *Johns Hopkins APL Tech. Dig.* **1**, No. 4, 297-302 (1980).

L. W. Ehrlich, "An Ad-Hoc SOR Method," in *Elliptic Problem Solvers*, M. H. Schultz, ed., Academic Press, New York (1981); also, *J. Comput. Phys.* **44** (Nov 1981).

P. Esfandiari and P. H. E. Meijer (Catholic Univ.) and R. A. Farrell and S. Favin (APL) "New Generating Functions and Results for the Density Polynomials of the Lattice Gas," *Phys. Rev. B* **24**, 1298-1311 (1981).

L. F. Fehlner and T. W. Jerardi, "On the Conversion of Radionavigation Data to Geodetic Position," *Radionavig. J.*, 17-20 (1980-81).

L. F. Fehlner and T. W. Jerardi, "The Calibration of Loran-C at Sea," *Radionavig. J.*, 68-88 (1980-81).

C. Feldman, "Seventh International Symposium on Boron, Borides, and Related Compounds: A Trip Report," *Johns Hopkins APL Tech. Dig.* **2**, 222-223 (1981).

C. Feldman, F. G. Satkiewicz, and N. A. Blum, "The Behavior of TiB_2 Thin Film Electrodes in Polycrystalline Silicon Thin Film Solar Cells," *J. Less-Common Met.* **82**, 183-191 (1981).

C. Feldman, F. G. Satkiewicz, and G. Jones, "Preparation and Electrical Properties of Stoichiometric TiB_2 Thin Films," *J. Less-Common Met.* **79**, 221-225 (1981).

R. E. Fischell, "Microprocessor Application to an Artificial Pancreas," in *Proc. IEEE Computer Society Workshop on the Application of Personal Computing to Aid the Handicapped* (1980).

R. E. Fischell and R. B. Kershner, "Very Low Altitude Drag-Free Satellites," *Johns Hopkins APL Tech. Dig.* **1**, No. 4, 279-283 (1980).

R. W. Flower, "Choroidal Fluorescent Dye Filling Patterns: A Comparison of High Speed Indocyanine Green and Fluorescein Angiograms," *Int. Ophthalmol.* **2**, 143-149 (1980).

R. W. Flower, "The Role of Oxygen in the Retinopathy of Prematurity," *Johns Hopkins APL Tech. Dig.* **2**, 143-152 (1981).

R. W. Flower (APL) and A. Patz (JHMI), "Retinopathy of Prematurity and the Role of Oxygen," in *Oxygen and Living Processes: An Interdisciplinary Approach*, D. L. Gilbert, ed., Springer-Verlag, New York (1981).

R. W. Flower et al., "Retrolental Fibroplasia: Evidence for a Role of the Prostaglandin Cascade in the Pathogenesis of Oxygen-Induced Retinopathy in the Newborn Beagle," *Pediatr. Res.* **15**, 1293-1302 (1981).

S. N. Foner and R. L. Hudson, "Internal Energy Transfer in Molecule-Surface Collisions," *J. Chem. Phys.* **75**, 4727-4729 (1981).

S. N. Foner and R. L. Hudson, "Ionization Potential of the NH Free Radical by Mass Spectrometry: Production of Ground State and Electronically Excited NH by F-Atom Reactions," *J. Chem. Phys.* **74**, 5017-5021 (1981).

D. W. Fox, "A Method for Lower Bounds for Frequencies of Thin Skew Plates," in *Euromech. Colloq. No. 112: Bracketing of Continuous Structures*, A. Bosznay, ed., Hungarian Academy of Sciences, pp. 125-132 (1980).

D. W. Fox, "Two-Sided Rayleigh-Ritz Bounds," in *Euromech. Colloq. No. 112: Bracketing of Eigenfrequencies of Continuous Structures*, A. Bosznay, ed., Hungarian Academy of Sciences, pp. 121-124 (1980).

D. W. Fox, "Useful Technical Devices in Intermediate Problems," *Numerische Behandlung von Differentialgleichungen ISNM* **56**, 36-44 (1981).

D. W. Fox and V. G. Sigillito, "Bounds for Eigenvalues of Reinforced Plates," *Numerische Behandlung von Differentialgleichungen ISNM* **56**, 45-57 (1981).

D. W. Fox and J. R. Kuttler "Upper and Lower Bounds for Sloshing Frequencies by Intermediate Problems," *J. Appl. Math. Phys. (ZAMP)* **32**, 667-682 (1981).

D. W. Fox and V. G. Sigillito, "Sloshing Eigenvalues of Two-Dimensional Regions with Holes," *J. Appl. Math. Phys. (ZAMP)* **32**, 658-666 (1981).

M. H. Friedman, "Correlation of Human Arterial Morphology with Hemodynamic Measurements in Arterial Casts," in *Proc. Specialists' Meeting on Hemodynamics and the Arterial Wall*, Houston, pp. 86-89 (5-7 Nov 1980).

M. H. Friedman and C. B. Bargeron (APL), G. M. Hutchins (JHU), and F. F. Mark and O. J. Deters (APL), "Hemodynamic Measurements in Human Arterial Casts, and Their Correlation with Histology and Luminal Area," *J. Biomech. Eng.* **102**, 247-251 (Nov 1980).

M. H. Friedman (APL), G. M. Hutchins (JHMI), and C. B. Bargeron, O. J. Deters, and F. F. Mark (APL)," Correlation of Human Arterial Morphology with Hemodynamic Measurements in Arterial Casts," *J. Biomech. Eng.* **103**, 204-207 (1981).

M. H. Friedman (APL), G. M. Hutchins (JHMI), and C. B. Bargeron, O. J. Deters, and F. F. Mark (APL) "Correlation between Intimal Thickness and Fluid Shear in Human Arteries," *Atherosclerosis* **39**, 425-436 (1981).

M. H. Friedman and R. A. Meyer, "Transport across Homoporous and Heteroporous Membranes in Nonideal Nondilute Solutions. I. Inequality of Reflection Coefficients for Volume Flow and Solute Flow. II. Inequality of Phenomenological and Tracer Solute Permeabilities," *Biophys. J.* **34**, 535-557 (1981).

R. Fujii (Nat. Inst. Polar Res. Itabashi-ku, Japan), T. Iijima (Univ. Tokyo), T. A. Potemra (APL), and M. Sugiura (NASA/Goddard), "Seasonal Dependence of Large-Scale Birkeland Currents," *Geophys. Res. Lett.* **8**, 1103-1106 (1981).

D. S. Gann (JHMI) and W. H. Guier (APL), "A Simulation Approach to the Study of Neurohumoral Control of Blood Volume," in *Proc. 1981 Summer Computer Simulation Conf.*, pp. 419-420 (1981).

J. B. Garrison and R. E. Jenkins, "Automating Medical Image Analysis," *Johns Hopkins APL Tech. Dig.* **2**, 172-178 (1981).

W. J. Geckle and M. M. Feen, "Ionospheric Refraction Correction Model for Single-Frequency Doppler Navigation," in *Proc. IEEE Position Location and Navigation Symp.*, pp. 22-26 (1980).

R. E. Gibson, "A Systems Approach to the Management of Research and Development," *Johns Hopkins APL Tech. Dig.* **1**, No. 4, 252-263 (1980).

R. E. Gibson, "Leason Heberling Adams, 1887 - 1969," *Biogr. Mem. Nat. Acad. Sci.* **52**, 3-33 (1980).

R. E. Gibson, "The Hillebrand Award: The Early Years," *Capitol Chem.*, 6-9 (Mar 1981).

A. D. Goldfinger, "The Drag Balance: An Apparatus for Studying Atmosphere-Satellite Surface Interactions," *J. Spacecr. Rockets* **17**, No. 6. 565-566 (1980).

J. Goldhirsh, "Multiyear Slant-Path Rain Fade Statistics at 28.56 GHz for Wallops Island, Va.," *IEEE Trans. Antennas Propag.* **AP-28**, No. 6, 934-941 (1980).

B. L. Gotwols and G. B. Irani, "Optical Measurement of the Phase Velocity of Ocean Waves during the 1978 Wave Dynamics Experiment," *Johns Hopkins APL Tech. Dig.* **2**, 56-62 (1981).

R. A. Greenwald (APL) and A. D. M. Walker (Univ. Natal, South Africa), "Energetics of Long Period Resonant Hydromagnetic Waves," *Geophys. Res. Lett.* **7**, No. 10, 745-748 (1980).

C. Greifinger and P. S. Greifinger (R&D Assoc.) and L. W. Hart (APL), "Shielding of ELF Magnetic-Dipole Fields by Ferromagnetic Cylindrical Shells," *IEEE Trans. Electromagn. Compat.* **EMC-23**, 2-12 (1981).

D. U. Gubser and W. W. Fuller (NRL), T. O. Poehler (APL), D. O. Cowan and M. M. Lee (JHU), R. S. Potember (APL), L. Y. Chiang (JHU), and A. N. Bloch (Exxon Co.), "Magnetic Susceptibility and Resistive Transitions of Superconducting $(TMTSF)_2$-CLO_4: Critical Magnetic Fields, *Phys. Rev. B* **24**, 478-480 (1981).

G. Gucer (JHMI) and L. J. Viernstein (APL), "Continuous Recording of ICP in the Normal Monkey," in *Intracranial Pressure IV*, K. Shulman et al., eds., Springer-Verlag, Berlin (1980).

W. H. Guier, "A Model of the Vasculature for Use in Cardiovascular Simulations," in *Proc. 1981 Summer Computer Simulation Conf.*, pp. 427-431 (1981).

W. H. Guier and G. C. Weiffenbach, "The Early Days of Sputnik," *Johns Hopkins APL Tech. Dig.* **2**, 14-15 (1981).

G. Gustafsson (Kiruna Geophys. Inst., Sweden), T. A. Potemra and S. Favin (APL), and N. A. Saflekos (Boston College), "Distant Magnetic Field Effects Associated with Birkeland Currents (Made Possible by the Evaluation of Triad's Attitude Oscillations)," *J. Geophys. Res.* **86**, 9219-9223 (1981).

L. W. Hall, Jr. and D. T. Burton (APL) and L. H. Liden (JHU), "An Interpretative Literature Analysis Evaluating the Effects of Power Plant Chlorination on Freshwater Organisms," *CRC Crit. Rev. Toxicol.* **9**, 1-20 (1981).

L. W. Hall, Jr. (APL), G. R. Helz (Univ. Maryland), and D. T. Burton (APL), *Power Plant Chlorination, A Biological and Chemical Assessment*, Ann Arbor Science Pub., Inc. (1981).

D. C. Hamilton and G. Gloeckler (Univ. Maryland), S. M. Krimigis and C. O. Bostrom (APL), T. P. Armstrong (Univ. Kansas), W. I. Axford (Max-Planck Inst. Aeronomy), C. Y. Fan (Univ. Arizona), L. J. Lanzerotti (Bell Labs.), and D. M. Hunten (Univ. Arizona), "Detection of Energetic Hydrogen Molecules in Jupiter's Magnetosphere by Voyager 2: Evidence for an Ionospheric Plasma Source," *Geophys. Res. Lett.* **7**, No. 10, 813-816 (1980).

R. W. Hart, "Generalized Scalar Potentials for Linearized Three-Dimensional Flows with Vorticity," *Phys. Fluids* **24**, 1418-1420 (1981).

S. J. Healy, S. A. Kahn, R. L. Stewart, and S. G. Tolchin, "A Fiber-Optic Local Area Communication Network," *Johns Hopkins APL Tech. Dig.* **2**, 84-86 (1981).

H. I. Heaton, "Thermal Straining in a Magnetostrictive Optical Fiber Interferometer," *Appl. Opt.* **19**, 3719-3720 (1980).

M. L. Hill, T. R. Whyte, and R. O. Weiss (APL), R. Rubio (Army Atmospheric Sciences Lab.), and M. Isquierdo (Shellinger Labs.), "Use of Atmospheric Electric Fields for Vertical Stabilization and Terrain Avoidance," in *Proc. AIAA Guidance and Control Conf.*, pp. 401-410 (1981).

B. F. Hochheimer, "A Possible Cause of Chronic Cystic Maculopathy: The Operating Microscope," *Ann. Ophthalmol.* **13**, 153-155 (1981).

L. W. Hunter, "Transient Thermal Expansion of Solids during Inert Heating, Phase Change, and Surface Gasification," *J. Heat Transfer* **103**, 601-602 (1981).

L. W. Hunter and S. Favin, "Fire Propagation in a Thermally Thin Fuel-Lined Duct with a Parallel Well-Mixed Forced Flow," *Combust. Flame* **42**, 7-18 (1981).

L. W. Hunter and C. H. Hoshall, "An Ignition Test for Plastics," *Fire Mater.* **4**, No. 4, 201-202 (1980).

L. Hyvarinen (Oulu Univ., Finland) and R. W. Flower (APL), "Indocyanine Green Fluorescence Angiography," *Acta. Ophthalmol.* **58**, 528-538 (1980).

E. P. Irzinski, "A Coaxial Waveguide Commutator Feed for a Scanning Circular Phased Array Antenna," *IEEE Trans. Microwave Theory Tech.* **MTT-29**, 266-270 (1981).

C. K. Jen, "A Physicist's View of Science and Technology in China," *Johns Hopkins APL Tech. Dig.* **2**, 209-221 (1981).

T. W. Jerardi, "Robust Real Time Filtering of Loran Signals," *Radionavig. J.*, 35-45 (1980-81).

A. N. Jette and F. J. Adrian, "Valence Bond Study of Fluorine Hyperfine Interactions near Trapped Hydrogen Atoms in the Alkaline Earth Fluorides," *J. Phys. C: Solid State Phys.* **14**, 2319-2331 (1981).

R. I. Joseph (JHU) and R. C. Adams (APL), "Extension of Weakly Nonlinear Theory of Solitary Wave Propagation," *Phys. Fluids* **24**, No. 1, 15-22 (1981).

S. A. Kahn, R. L. Stewart, S. G. Tolchin, and S. J. Healy, "Functional and Logical Description of a New Fiber-Optic Contention Bus Network," in *Proc. COMPCON Fall 1980*, pp. 268-272 (1980).

R. B. Kershner, "The Arcane Art of Research and Development Management," *Johns Hopkins APL Tech. Dig.* **2**, 45-49 (1981).

R. B. Kershner, "Technical Innovations in the APL Space Department," *Johns Hopkins APL Tech. Dig.* **1**, No. 4, 264-278 (1980).

R. B. Kershner, "The Cost/Benefit Monster," *Johns Hopkins APL Tech. Dig.* **2**, 207-208 (1981).

D. L. Kershner, R. A. Makofski, and R. C. Rand, "Estimating the Demand for Parking in Atlantic City," *Traffic Q.* **35**, 589-608 (1981).

B. F. Kim and J. Bohandy, "Spectroscopy of Porphyrins," *Johns Hopkins APL Tech. Dig.* **2**, 153-163 (1981).

E. Kirsch (Max-Planck Inst. Aeronomy), S. M. Krimigis (APL), W. H. Ip (Max-Planck Inst. Aeronomy), and G. Gloeckler (Univ. Maryland), "X-Ray and Energetic Neutral Particle Emission from Saturn's Magnetosphere," *Nature* **292**, 718-721 (1981).

E. Kirsch (Max-Planck Inst. Aeronomy) and S. M. Krimigis, J. W. Kohl, and E. P. Keath (APL), "Upper Limits for X-Ray and Energetic Neutral Particle Emission from Jupiter: Voyager-1 Results," *Geophys. Res. Lett.* **8**, 169-172 (1981).

E. Kirsch (Max-Planck Inst. Aeronomy), S. M. Krimigis (APL), E. T. Sarris (Univ. Thrace), and R. P. Lepping (NASA/Goddard), "Detailed Study on Acceleration and Propagation of Energetic Protons and Electrons in the Magnetotail during Substorm Activity," *J. Geophys. Res.* **86**, No. A8, 6727-6738 (1981).

L. C. Kohlenstein, "On the Proportion of the Chesapeake Bay Stock of Striped Bass that Migrates into the Coastal Fishery," *Trans. Am. Fish. Soc.* **110**, 168-179 (1981).

S. Koslov, "Radiophobia: The Great American Syndrome," *Johns Hopkins APL Tech. Dig.* **2**, 102-121 (1981).

J. A. Krill and R. H. Andreo, "Vector Stochastic Variational Principles for Electromagnetic Wave Scattering," *IEEE Trans. Antennas Propag.* **AP28**, 770-776 (1980).

S. M. Krimigis, "A Post-Voyager View of Jupiter's Magnetosphere," *Endeavour* **5**, 50-60 (1981).

S. M. Krimigis (APL), T. P. Armstrong (Univ. Kansas), W. I. Axford (Max-Planck Inst. Aeronomy), C. O. Bostrom (APL), G. Gloeckler (Univ. Maryland), E. P. Keath (APL), L. J. Lanzerotti (Bell Labs.), J. F. Carbary (APL), D. C. Hamilton (Univ. Maryland), and E. C. Roelof (APL), "Low-Energy Charged Particles in Saturn's Magnetosphere: Results from Voyager 1," *Science* **212**, 225-231 (1981).

S. M. Krimigis, J. F. Carbary, E. P. Keath, and C. O. Bostrom (APL), W. I. Axford (Max-Planck Inst. Aeronomy), G. Gloeckler (Univ. Maryland), L. J. Lanzerotti (Bell Labs.), and T. P. Armstrong (Univ. Kansas), "Characteristics of Hot Plasma in the Jovian Magnetosphere: Results from the Voyager Spacecraft," *J. Geophys. Res.* **86**, 8227-8257 (1981).

J. R. Kuttler and V. G. Sigillito, "On Curve Veering," *J. Sound Vib.* **75**, 585-588 (1981).

J. R. Kuttler and V. G. Sigillito, "Upper and Lower Bounds for Frequencies of Trapezoidal and Triangular Plates," *J. Sound Vib.* **78**, 585-590 (1981).

J. R. Kuttler and V. G. Sigillito, "The *A Posteriori—A Priori* Method of Bounding Eigenvalues with Applications to the Eigenvalues of Clamped Rhombical Plates," in *Euromech. Colloq. No. 112: Bracketing of Eigenfrequencies of Continuous Structures*, A. Bosznay, ed., Hungarian Academy of Sciences, pp. 273-281 (1980).

J. R. Kuttler and V. G. Sigillito, "Upper and Lower Bounds for the Frequencies of Clamped Orthotropic Plates," *J. Sound Vib.* **73**, No. 2, 247-259 (1980).

R. Y. S. Lai (Univ. Wisconsin) and C. -M. Lee (APL), "Added Mass of a Spheroid Oscillating in a Linearly Stratified Fluid," *Int. J. Eng. Sci.* **19**, 1411-1420 (1981).

R. A. Langel, "Magsat Scientific Investigations," *Johns Hopkins APL Tech. Dig.* **1**, No. 3, 214-227 (1980).

L. J. Lanzerotti and C. G. Maclennan (Bell Labs.), T. P. Armstrong (Univ. Kansas), S. M. Krimigis (APL), and R. P. Lepping and N. F. Ness (NASA/Goddard), "Ion and Electron Angular Distributions in the Io Torus Region of the Jovian Magnetosphere," *J. Geophys. Res.* **86**, 8491-8496 (1981).

L. J. Lanzerotti and C. G. Maclennan (Bell Labs.), S. M. Krimigis (APL), T. P. Armstrong (Univ. Kansas), and K. Behannon and N. F. Ness (NASA/Goddard), "Statics of the Nightside Jovian Plasma Sheet," *Geophys. Res. Lett.* **7**, No. 10, 817-820 (1980).

L. J. Lanzerotti and C. G. Maclennan (Bell Labs.), R. P. Lepping (NASA-Goddard), and S. M. Krimigis (APL), "Intensity Variations in Plasma Flow at the Dawn Magnetopause," *Planet. Space Sci.* **28**, 1163-1169 (1980).

D. K. Larson, "Computer + Plotter = Direct-to-Art Design," *Microwaves* **20**, 91-97 (1981).

J. S. Lee and J. P. Doering (JHU), T. A. Potemra (APL), and L. H. Brace (NASA/Goddard), "Measurements of the Ambient Photoelectron Spectrum from Atmosphere Explorer: II, AE-E Measurements from 300 to 1000 km during Solar Minimum Conditions," *Planet. Space Sci.* **28**, 973-996 (1980).

C. S. Leffel, Jr., "The APL Satellite Refrigerator Program," *Johns Hopkins APL Tech. Dig.* **2**, 74-83 (1981).

J. J. Lentz, "Apportionment of Net Recharge in Landfill Covering Layer into Separate Components of Vertical Leakage and Horizontal Seepage," *Water Resour. Res.* **17**, 1231-1234 (1981).

A. L. Lew, R. C. Moore, J. R. Dozsa, and R. K. Burek, "The Magsat Telecommunications System," *Johns Hopkins APL Tech. Dig.* **1**, No. 3, 183-187 (1980).

A. T. Y. Lui (APL) and S. -I. Akasofu (Univ. Alaska), "Estimated North-South Component of the Electric Field in the Geomagnetotail Plasma Sheet," *Geophys. Res. Lett.* **7**, No. 11, 877-880 (1980).

A. T. Y. Lui and S. M. Krimigis, "Earthward Transport of Energetic Protons in the Earth's Plasma Sheet," *Geophys. Res. Lett.* **8**, 527-530 (1981).

A. T. Y. Lui and C. -I. Meng (APL), L. A. Frank and K. L. Ackerson (Univ. Iowa), and S. -I. Akasofu (Univ. Alaska), "Temperature Variation of the Plasma Sheet during Substorms," *Planet. Space Sci.* **29**, 837-842 (1981).

A. I. Mahan and C. V. Bitterli, "Reflection and Transmission of Plane Unbounded Electromagnetic Waves at an Absorbing-Nonabsorbing Interface with Numerical Calculations for an Ocean-Air Interface," *Appl. Optics* **20**, 3345-3359 (1981).

F. F. Mark, C. B. Bargeron, O. J. Deters, G. M. Hutchins, and M. H. Friedman, "Velocity Measurements of Pulsatile Flow through a Cast of an Asymmetric Human Aortic Bifurcation," in *Proc. ASME Biomechanics Symp.* **AMD-43**, pp. 47-50 (1981).

J. T. Massey and R. J. Johns, "A Short History of the Collaborative Biomedical Program," *Johns Hopkins APL Tech. Dig.* **2**, 141-142 (1981).

W. B. McCloskey, Jr., "The New Fisherman," *Johns Hopkins APL Tech. Dig.* **2**, 74-83 (1981).

E. E. McColligan (JHMI), B. I. Blum (APL), and R. E. Lenhard and M. B. Johnson (JHMI), "The Human Element in Computer Generated Patient Management Plans," in *Proc. 10th Annual Conf. of the Society for Computer Medicine* (1980).

C. -I. Meng, "Auroral Arcs Observed by DMSP Satellites," in *Physics of Auroral Arc Formation*, Geophysical Monograph Series **25**, pp. 67-79 (1981).

C. -I. Meng, "Electron Precipitation in the Midday Auroral Oval," *J. Geophys. Res.* **86**, 2149-2174 (1981).

C. -I. Meng, "Polar Cap Arcs and the Plasma Sheet," *Geophys. Res. Lett.* **8**, 273-276 (1981).

C. -I. Meng, "The Auroral Electron Precipitation during Extremely Quiet Geomagnetic Conditions," *J. Geophys. Res.* **86**, 4607-4627 (1981).

C. -I. Meng, A. T. Y. Lui, S. M. Krimigis, and S. Ismail, "Spatial Distribution of Energetic Particles in the Distant Magnetotail," *J. Geophys. Res.* **86**, 5682-5700 (1981).

R. A. Meyer (APL) and J. N. Campbell (JHMI), "Evidence for Two Distinct Classes of Unmyelinated Nociceptive Afferents in Monkey," *Brain Res.* **224**, 149-152 (1981).

R. A. Meyer (APL) and J. N. Campbell (JHMI), "Myelinated Nociceptive Afferents Account for the Hyperalgesia that Follows a Burn to the Hand," *Science* **213**, 1527-1529 (1981).

R. A. Meyer (APL) and J. N. Campbell (JHMI), "Peripheral Neural Coding of Pain Sensation," *Johns Hopkins APL Tech. Dig.* **2**, 164-171 (1981).

R. A. Meyer, E. C. Hills, and M. H. Friedman, "Tracer Permeabilities Underestimate Transmembrane Solute Flux under a Concentration Gradient," *J. Membrane Sci.* **8**, 247-253 (1981).

D. G. Mitchell and E. C. Roelof (APL), W. C. Feldman and S. J. Bame (Los Alamos Scientific Lab.), and D. J. Williams (NOAA), "Thermal Iron Ions in High Speed Solar Wind Streams, 2. Temperatures and Bulk Velocities," *Geophys. Res. Lett.* **8**, 827-830 (1981).

D. G. Mitchell and E. C. Roelof (APL) and J. H. Wolfe (NASA/Ames), "Latitude Dependence of Solar Wind Velocity Observed $\leq$ 1 AU," *J. Geophys. Res.* **86**, No. A1, 165-179 (1981).

F. M. Monaldo (APL) and R. S. Kasevich (Raytheon Co.), "Daylight Imagery of Ocean Surface Waves for Wave Spectra," *J. Phys. Oceanogr.* **11**, 272-283 (1981).

F. M. Monaldo (APL) and R. S. Kasevich (Raytheon Co.), "Measurement of Short-Wave Modulation Using Fine Time-Series Optical Spectra," *J. Phys. Oceanogr.* **11**, 1034-1036 (1981).

L. Monchick, "A Comment on the Inversion of Gas Transport Properties," *J. Chem. Phys.* **73**, No. 6, pp. 2929-2931 (1980).

L. Monchick, "Diffusion-Controlled Reactions in the Presence of Strong Electromagnetic Fields," *J. Chem. Phys.* **74**, 4519-4526 (1981).

L. Monchick, "Generalized Reorientation Cross Section for Cylindrically Symmetric Velocity Distributions," *J. Chem. Phys.* **75**, 3377-3383 (1981).

L. Monchick (APL) and J. Schaefer (Max-Planck Inst. Physics and Astrophysics), "Theoretical Studies of H_2-H_2 Collisions, II. Scattering and Transport Cross Sections of Hydrogen at Low Energies; Tests of a New *ab initio* Vibrator Potential," *J. Chem. Phys.* **73**, 6153-6161 (1980).

K. Moorjani, "The Fourth International Conference on Liquid and Amorphous Metals: A Trip Report," *Johns Hopkins APL Tech. Dig.* **1**, No. 4, 303-305 (1980).

K. Moorjani (APL), S. K. Ghatak (Indian Inst. Tech.), K. V. Rao and B. Kramer (Univ. Illinois), and H. S. Chen (Bell Labs.), "Spin Glass — Paramagnetic Phase Boundary in Amorphous Magnetic Alloys," *J. Phys.* **41**, No. C8, 718-722 (1980).

J. C. Murphy and L. C. Aamodt, "Optically Detected Photothermal Imaging," *Appl. Phys. Lett.* **38**, 196-198 (1981).

J. C. Murphy and L. C. Aamodt, "Signal Enhancement in Photothermal Imaging Produced by Three-Dimensional Flow," *Appl. Phys. Lett.* **39**, 519-521 (1981).

B. H. Nall, A. N. Jette, and C. B. Bargeron, "Electron Energy Loss Spectroscopy of a {111} Oriented Aluminum Single Crystal," *Surface Sci.* **110**, L606-L610 (1981).

J. B. Nelson, "Multivariant Technique for Multiclass Pattern Recognition: Comment," *Appl. Opt.* **20**, 8-9 (1981).

R. R. Newton, "Comments on 'Was Ptolemy a Fraud?' by Owen Gingerich," *Q. J. R. Astron. Soc.* **21**, 388-399 (1980).

R. R. Newton, "The Near-Term Potential of Doppler Location," *Johns Hopkins APL Tech. Dig.* **2**, 16-31 (1981).

R. R. Newton, "The Sources of Eratosthenes' Measurement of the Earth," *Q. J. R. Astron. Soc.* **21**, 379-387 (1980).

V. O'Brien, "Stagnation Regions of Separation," *Phys. Fluids* **24**, 1005-1009 (1981).

V. O'Brien, "The Flow of a Non-Newtonian Fluid Past Projections and Depressions," *ASME J. Appl. Mech.* **48**, 448-449 (1981).

V. O'Brien and L. W. Ehrlich, "Pulsatile Flow through a Constricted Artery," in *Biofluid Mechanics* **2**, D. J. Schneck, ed., Plenum Pub. Co. (1980).

V. O'Brien (APL), K. Sagawa and G. M. Hutchins (JHMI), and O. J. Deters, F. F. Mark, and L. W. Ehrlich (APL), "Flow Fields near Arterial Ring Occlusions," in *Proc. 34th Annual Conf. on Engineering in Medicine and Biology* **23**, p. 106 (1981).

G. W. Ousley, "Overview of the Magsat Program," *Johns Hopkins APL Tech. Dig.* **1**, No. 3, 171-174 (1980).

P. Pandolfini, G. L. Dugger, F. K. Hill, and W. H. Avery (APL) and H. D. Faust (Train Co.), "Alclad-Aluminum, Folded-Tube Heat Exchangers for Ocean Thermal Energy Conversion," in *Proc. 3rd Miami International Conf. on Alternative Energy Sources, Miami Beach*, p. 424 (Dec 1980).

J. G. Parker, "Acoustic Detection and Location of Leaks in Underground Natural Gas Distribution Lines," *Johns Hopkins APL Tech. Dig.* **2**, 122-123 (1981).

J. G. Parker and W. D. Stanbro, "Energy Transfer Processes Accompanying Laser Excitation of Hematoporphyrin in Various Solvents," *Johns Hopkins APL Tech. Dig.* **2**, 196-199 (1981).

L. Pasternack (JHU), D. M. Silver (APL), and D. R. Yarkony and P. J. Dagdigian (JHU), "Experimental and Theoretical Study of the CaI $4s3d\ ^1D$-$4s^2\ ^1S$ and $4s4p\ ^3P_1$ - $4s^2\ ^1S$ Forbidden Transitions," *J. Phys. B: Atom. Molec. Phys.* **13**, 2231-2241 (1980).

L. G. Phillips and S. L. Shadel, "Methane Recovery from Landfills," *Johns Hopkins APL Tech. Dig.* **2**, 63-68 (1981).

V. L. Pisacane and S. C. Dillon, "Determining Coordinates of the Rotational Pole Using Satellite Data from Four Sites," *J. Geophys. Res.* **86**, No. B2, 899-902 (1981).

R. S. Potember and T. O. Poehler, "Reversible Field Induced Phase Transition in Semiconducting Films of Copper and Silver Radical-Ion Salts," *J. Mater. Sci.* **7**, 389-390 (1981).

R. S. Potember and T. O. Poehler (APL), D. O. Cowan (JHU), P. Brant and F. L. Carter (NRL), and A. N. Bloch (Exxon Co.), "Vibrational and X-Ray Photoelectron Spectra of Semiconducting Copper-TCNQ Films," *Chemica Scripta* **17**, 219-221 (1981).

T. A. Potemra, "Hall Currents in the Aurora," in *The Hall Effect and Its Applications*, C. L. Chien and C. R. Westgate, eds., Plenum Pub. Co., pp. 399-415 (1980).

W. R. Powell, "An Analytical Expression for the Average Output Power of a Wind Machine," *Sol. Energy* **26**, 77-80 (1981).

L. L. Pryor, "Developing and Managing a Large Computer Program," *Johns Hopkins APL Tech. Dig.* **2**, 39-44 (1981).

H. A. Quigley (JHMI), R. W. Flower (APL), and E. M. Addicks and D. S. McLeod (JHMI), "The Mechanisms of Optic Nerve Damage in Experimental Acute Glaucoma," *Invest. Ophthalmol. Vis. Sci.* **19**, 505-517 (1980).

D. W. Rabenhorst, "Low Cost, High Performance, Dual Mode Car," in *1980 Flywheel Technology Symp.* (Supplement), pp. 68-80 (1980).

D. Richards and J. F. George (APL) and J. S. Seward (Seward Assoc.), "Design of 40-MW Grazing and Moored OTEC Pilot/Demonstration Plants," *J. Energy* **5**, 224-230 (1981).

D. Richards and L. L. Perini, "An OTEC Pilot Plant Heat Engine," *J. Energy Resour. Tech.* **103**, 172-179 (1981).

J. M. Ross, "A Successful Combination: Modular Oceanographic Laboratory Plus Offshore Mud Boat," *MTS J.* **14**, No. 3, 27-30 (1980).

J. Sanders (Univ. Minnesota), V. O'Brien (APL), and D. D. Joseph (Univ. Minnesota), "Stokes Flow in a Driven Sector by Two Different Methods," *Trans. ASME* **47**, 482-484 (1980)

E. T. Sarris, S. M. Krimigis, and T. Y. Lui (APL), K. L. Ackerson and L. A. Frank (Univ. Iowa), and D. J. Williams (NOAA), "Relationship between Energetic Particles and Plasmas in the Distant Plasma Sheet," *Geophys. Res. Lett.* **8**, 349-352 (1981).

F. W. Schenkel and R. J. Heins, "The Magsat Three Axis Arc Second Precision Attitude Transfer System," *J. Br. Interplanet. Soc. Space Tech.* **34**, 539-546 (1981).

J. A. Schetz, F. S. Billig, and S. Favin, "Analysis of Base Drag Reduction by Base and/or External Burning," *AIAA J.* **19**, 1145-1150 (1981).

J. A. Schetz, F. S. Billig, and S. Favin, "Scramjet Combustor Wall Boundary Layer Analysis," in *Proc. AIAA/SAE/ASME 17th Joint Propulsion Conf.*, pp. 1-10 (1981).

W. Schneider, W. Guier, R. S. Carlson, and L. A. Wenrich (APL) and K. Sagawa (JHMI), "Automatic Control of Phasic Aortic Pressure in the Experimental Animal," in *Proc. 1981 Summer Computer Simulation Conf.*, pp. 432-436 (1981).

W. Schneider (APL), G. Schmeisser (JHMI), and W. Seamone (APL), "A Computer-Aided Robotic Arm/Worktable System for the High-Level Quadriplegic," *Computer*, 41-47 (Jan 1981).

W. Seamone (APL) and G. Schmeisser (JHMI), "New Control Techniques for Wheelchair Mobility," *Johns Hopkins APL Tech. Dig.* **2**, 179-184 (1981).

W. Seamone (APL) and G. Schmeisser (JHMI), "Summary of JHU Research Project Activities," *Bull. Prosthetics Res.*, 10-35, 124-126 (1981).

W. Seamone (APL) and G. Schmeisser (JHMI), "System Trade-offs in Designing a Microcomputer Controlled Robotic Arm to Provide Functional Capabilities for the Handicapped," in *Proc. 1981 Summer Computer Simulation Conf.*, pp. 437-438 (1981).

K. E. Shade and M. C. Lucas, "The Mk 92 Fire Control System," *Johns Hopkins APL Tech. Dig.* **2**, 69-73 (1981).

V. G. Sigillito, "A Software Package for Elliptic Partial Differential Equations," in *Elliptic Problem Solvers*, M. H. Schultz, ed., Academic Press, New York (1981).

D. M. Silver and N. deHaas, "Temperature Dependence of the Reaction Rate for H + CF_3Br," *J. Chem. Phys.* **74**, 1745-1749 (1981).

J. H. Smart, "Direct Measurement of Vertical Shears in the Open Ocean," *Johns Hopkins APL Tech. Dig.* **1**, 284-288 (1980).

R. L. Stewart and S. G. Tolchin, "A Distributed Processing/Fiber-Optic Hospital Information System," in *Proc. 4th Symp. on Computer Applications in Medical Care*, pp. 1519-1524 (1980).

T. Thompson, "Performance of the Satrack/Global Positioning System, Trident I Missile Tracking System," in *Proc. IEEE Position Location and Navigation Symp.*, pp. 445-449 (1980).

J. E. Tillman, "Eastern Geothermal Resources: Should We Pursue Them?" *Science* **210**, No. 4470, 595-600 (1980).

S. G. Tolchin, B. I. Blum, and M. A. Butterfield, "A System Analysis Methodology for a Decentralized Health Care Information System," in *Proc. 4th Symp. on Computer Applications in Medical Care*, pp. 1479-1484 (1980).

S. G. Tolchin and R. L. Stewart, "The Distributed Processing Approach to Hospital Information Processing," *J. Med. Syst.* **5**, 345 (1981).

S. G. Tolchin, R. L. Stewart, S. A. Kahn, E. S. Bergan, and G. P. Gafke (APL) and D. W. Simborg, Q. E. Whiting-O'Keefe, M. G. Chadwick, and G. E. McCue (Univ. California) "Implementation of a Prototype Generalized Network Technology for Hospitals," in *Proc. Fifth Annual Symp. on Computer Applications in Medical Care*, pp. 1-10 (Nov 1981).

R. L. Trapp, "Automated Intrapulse RF Data Acquisition," in *Proc. IEEE SOUTHEASTCON*, pp. 508-512 (1981).

R. Turner, "The Glow-to-Arc Transition in a Pulsed High-Pressure Gas Discharge," *J. Appl. Phys.* **52**, 681-692 (1981).

J. F. Vickrey and C. L. Rino (SRI) and T. A. Potemra (APL), "Chatanika/Triad Observations of Unstable Ionization Enhancements in the Auroral F-Region," *Geophys. Res. Lett.* **7**, No. 10, 789-792 (1980).

P. J. Waltrup, F. S. Billig, and M. C. Evans, "Critical Considerations in the Design of Supersonic Combustion Ramjet (Scramjet) Engines," *J. Spacecr. Rockets* **18**, 350-356 (1981).

C. A. Wingate, Jr., T. B. Coughlin, and R. M. Sullivan, "An Ultra Stable Optical Bench for the Magnetic Survey Satellite," *Acta Astron.* **7**, 1389-1401 (1980).

T. Wyatt, "The Gestation of Transit as Perceived by One Participant," *Johns Hopkins APL Tech. Dig.* **2**, 32-38 (1981).

L. J. Zanetti and T. A. Potemra (APL), J. P. Doering and J. S. Lee (JHU), and R. A. Hoffman (NASA/Goddard), "Magnetic Field-Aligned Electron Distributions in the Dayside Cusp," *J. Geophys. Res.* **86**, 8957-8970 (1981).

R. D. Zwickl and E. C. Roelof, "Interplanetary Propagation of <1-MeV Protons in Nonimpulsive Energetic Particle Events," *J. Geophys. Res.* **86**, 5449-5471 (1981).

PRESENTATIONS

F. J. Adrian, "Surface Enhanced Raman Scattering (SERS): A Review and an Electrodynamic Mechanism," Howard Univ. Chemistry Dept. Seminar, Washington (6 Mar 1981).

R. H. Andreo, "Variational Methods for Wave Scattering from Random Systems," Wave Optics Lecture Series at NBS, Gaithersburg, Md. (23 Sep 1981).

W. H. Avery, "OTEC," Symp. on Current Energy-Related Research at the University, The Johns Hopkins Univ. Energy Research Inst., Baltimore (11 Jun 1981).

C. B. Bargeron, R. A. Farrell, and R. L. McCally (APL) and W. R. Green (JHMI), "CO_2 Laser Multiple Pulse Damage Thresholds in the Rabbit Cornea," Assoc. for Research in Vision and Ophthalmology, Sarasota (27 Apr-1 May 1981).

C. B. Bargeron, R. L. McCally, and R. A. Farrell, "CO_2-Laser Damage Thresholds in the Cornea: A Critical Temperature vs. a Damage Integral Mechanism," 4th International Congress for Eye Research, New York (28 Sep-3 Oct 1980).

G. A. Barnes, "Comparison of the Lift and Controllability at High Supersonic Speeds of Two Tail-Control Missile Configurations Differing in Wing Planform," 12th Navy Symp. on Aeroballistics, Carderock, Md. (12-14 May 1981).

R. W. Blevins, H. L. Donnelly, J. T. Stadter, R. O. Weiss, and L. Perez y Perez, "At-Sea Test of a Large Diameter Steel Cold Water Pipe," ASME Energy Sources Technology Conf., New Orleans (3-7 Feb 1980).

B. I. Blum, "A MUMPS Program Generator with a Relational Data Base Manager," MUMPS User's Group, Niagara Falls, N.Y. (15-19 Jun 1981).

B. I. Blum, "Program Generation with TEDIUM, An Illustration," Trends and Applications 1981 Conf., NBS, Gaithersburg, Md. (28 May 1981).

N. A. Blum, J. W. Leight, K. Moorjani, and F. G. Satkiewicz, "Mössbauer Study of Ferromagnetic Amorphous FeB and Fe_2B," American Physical Society Meeting, Phoenix (16-20 Mar 1981).

N. A. Blum, K. Moorjani, T. O. Poehler, and F. G. Satkiewicz, "Mössbauer Investigation of Sputtered Ferromagnetic Amorphous Fe_xB_{100-x} Alloys," Magnetism and Magnetic Materials Meeting, Atlanta (10-13 Nov 1981).

J. Bohandy and B. F. Kim, "Luminescence of Metalloporphins in Anthracene," American Physical Society Meeting, Phoenix (16 Mar 1981).

H. Bouver (APL) and R. E. Bargmann (Univ. Georgia), "A Comparison of Frequency Curves of Karl Pearson and Norman L. Johnson Using the Minimum χ^2," American Statistical Assoc., Houston (11-15 Aug 1980).

W. A. Bryden, J. P. Stokes, and K. O. Cowan (JHU), T. O. Poehler (APL), and A. N. Bloch (Exxon Co.), "Mott Transition in the Solid Solutions $HMTSF(TCNQ)_x(TCNQF_4)_{1-x}$," International Conf. on Low-Dimensional Conductors, Boulder, Colo. (12 Aug 1981).

D. T. Burton, "A Review of the Toxic Effects of Ozonated Waters to Fresh, Estuarine, and Marine Aquatic Organisms," Conf. on Ozone Treatment for Biofouling in Cooling Towers, Cincinnati (17 Jun 1981).

D. T. Burton and L. W. Hall, Jr., "Biofouling Control Procedures for Estuarine Power Plant Cooling Water Systems," Chlorine Conf., Mary Washington College, Fredericksburg, Va. (27-28 May 1981).

J. N. Campbell (JHMI), R. A. Meyer (APL), and S. R. Jaffe (JHMI), "Comparison of the Neural Mechanisms of Hyperalgesia in Glabrous and Hairy Skin," Third World Congress on Pain, Edinburgh (4-11 Sep 1981).

J. N. Campbell (JHMI), R. A. Meyer (APL), and S. M. Lancellota (JHMI), "Correlational Analysis of Hyperalgesia in Humans with Responses of Nociceptive Primary Afferents in the Monkey," 10th Annual Meeting, Society for Neuroscience, Cincinnati (Nov 1980).

L. Y. Chiang and P. Shu (JHU), T. O. Poehler (APL), D. O. Cowan (JHU), and A. N. Bloch (Exxon Co.), "Synthesis of Novel Organic Donors," International Conf. on Low-Dimensional Conductors, Boulder, Colo. (10 Aug 1981).

D. O. Cowan, L. Y. Chiang, P. Shu, K. Lerstrup, A. Kini, and M. Maxfield (JHU), T. O. Poehler (APL), and A. N. Bloch (Exxon Co.), "The Design, Synthesis and Characterization of the Molecular Components of Organic Conductors," International Conf. on Low-Dimensional Conductors, Boulder, Colo. (11 Aug 1981).

G. Dailey and R. C. Ballalieu, "Structural and Electrical Performance Considerations in the Design of Multiband Radomes," 12th Navy Symp. on Aeroballistics, Carderock, Md. (12-14 May 1981).

O. J. Deters, C. B. Bargeron, G. M. Hutchins, F. F. Mark, and M. H. Friedman, "Arterial Intimal and Medial Thicknesses Correlate with Shear," 34th Annual Conf. on Engineering in Medicine and Biology, Houston (21-23 Sep 1981).

W. P. Dey (Ecological Analysts), R. I. Baybutt (Whitehall Labs.), R. J. Klauda (APL), and J. C. Schneider (Florida Bureau of Marine Science and Tech.), "Early Life History of Striped Bass in the Hudson River Estuary," Conf. on Hudson River Fishes, Hyde Park, N.Y. (1-2 Sep 1981).

P. E. Dingwell and F. D. Weiskopf, "A Hot Film Anemometer for Ocean Turbulence," Oceans 81 Conf., Boston (16 Sep 1981).

G. L. Dugger, R. W. Henderson, E. J. Francis, and W. H. Avery, "Projected Costs for Electricity and Products from OTEC Facilities and Plantships," IECEC Conf., Seattle (Aug 1980).

G. L. Dugger, F. C. Paddison, and L. L. Perini, "Geothermal Enhanced OTEC (GEOTEC) Resources and Plant Concepts," 8th Ocean Energy Conf., Washington (Jun 1981).

G. L. Dugger, D. Richards, J. F. George, and W. H. Avery, "Ocean Thermal Energy Conversion," AEO-81-13, Seminar on Energy Options for Developing Countries, Madras (23-27 Feb 1981).

C. Feldman, "The Behavior of TiB_2 Thin Film Electrodes in Polycrystalline Silicon Thin Film Solar Cells," 7th International Symp. on Boron, Borides, and Related Compounds, Uppsala, Sweden (9-18 Jun 1981).

C. Feldman, "Vacuum Deposited Polycrystalline Silicon Solar Cells on Foreign Substrates," 5th International Thin Film Congress, Herzlia, Israel (21-25 Sep 1981).

R. E. Fischell, C. A. Blackburn, C. H. Fountain, A. F. Hogrefe, W. E. Radford, and J. R. Champion, "A Computer Controlled, Implantable, Insulin Delivery System," Third Congress, International Society for Artificial Organs, Paris (9 Jul 1981).

R. W. Flower, "RLF, the Retinopathy of Prematurity; A New Perspective," Anesthesiology and Critical Care Medicine Research Conf., JHMI, Baltimore (10 Apr 1981).

R. W. Flower et al., "Evidence for a Role of the Prostaglandin Cascade in the Pathogenesis of Oxygen Induced Retinopathy in the Newborn Beagle," Society for Pediatric Research, San Francisco (28 Apr-1 May 1981); Fortieth Clinical Meeting of the Wilmer Residents Assoc., Baltimore (6-8 May 1981).

D. W. Fox, "Bounds for Sloshing Eigenvalues by Conformal Mapping," SIAM 1981, Rensselaer Polytechnic Inst., Troy, N. Y. (10 Jun 1981).

D. W. Fox, "New Developments in Lower Bounds for Eigenvalues," Applied Mathematics Colloq., Institut für Angewandte Mathematik, Johannes Gutenberg Univ., Mainz, FRG (6 Oct 1980).

D. W. Fox and V. G. Sigillito, "Bounds for Sloshing Eigenvalues in a Slotted Region," SIAM 1981, Rensselaer Polytechnic Inst., Troy, N.Y. (10 Jun 1981).

E. J. Francis and G. L. Dugger, "Promising Applications of OTEC," 7th Energy Technology Conf., Washington (24-26 Mar 1980).

M. H. Friedman, "Biomedical Breakthroughs," Society of American Military Engineers, Baltimore (20 May 1981).

M. H. Friedman, "I. Biomedical Research and Development at the Applied Physics Laboratory. II. Fluid Mechanics of Atherogenesis," Washington Bioengineering Group,

Bethesda, Md. (19 May 1981).

M. H. Friedman, G. M. Hutchins, C. B. Bargeron, O. J. Deters, and F. F. Mark, "Negative Correlation of Intimal Thickness with Pulsatile Shear in Human Aortic Bifurcations," Federation of American Societies for Experimental Biology, Atlanta (12-17 Apr 1981).

M. H. Friedman and R. A. Meyer, "Membrane Reflection Coefficients for Volume Flow and Solute Flow Are Not Equal in Nonideal, Nondilute Solutions," Biophysics Society, Denver (23-25 Feb 1981).

R. M. Fristrom, "Chemical Factors in the Inhibition and Extinction of C-H-O Flames by Halogenated Compounds Interpreted with a Zone Flame Model," Meeting, Western States Section, The Combustion Institute, Los Angeles (20-21 Oct 1980).

J. B. Garrison and R. E. Jenkins, "Automating Medical Image Analysis," JHU/APL Colloq. (30 Jan 1980).

J. F. George and D. Richards, "Model Basin Tests of a Baseline 40 MW OTEC Pilot Plant," Eighth Ocean Energy Conf., Washington (7-11 Jun 1981).

A. P. Georgopoulos and J. F. Kalaska (JHMI) and J. T. Massey (APL), "Cortical Mechanisms of Two-Dimensional Aiming Arm Movements," Society for Neuroscience, Cincinnati (Nov 1980).

D. U. Gubser and W. W. Fuller (NRL), T. O. Poehler (APL), D. O. Cowan, M. M. Lee, and J. P. Stokes (JHU), and A. N. Bloch (Exxon Co.), "Magnetic and Resistive Transitions of Superconducting $(TMTSF)_2ClO_4$," International Conf. on Low-Dimensional Conductors, Boulder, Colo. (12 Aug 1981).

F. K. Hill, P. P. Pandolfini, G. L. Dugger, and W. H. Avery, "Biofouling Removed by Ultrasonic Radiation," Corrosion Conf., Toronto (6-10 Apr 1981).

T. B. Hoff and J. R. Young (Ecological Analysts) and R. J. Klauda (APL), "Distribution and Limited Morphometric Characteristics of Incidentally Caught Hudson River Shortnose Sturgeon," Conf. on Hudson River Fishes, Hyde Park, N.Y. (1-2 Sep 1981).

L. W. Hunter, "Fire Protection System Modelling: The Fire Resistance of Walls Penetrated by Electric Cables," 8th Water Reactor Safety Research Information Meeting, Gaithersburg, Md. (27-31 Oct 1980).

A. N. Jette, "Valence Bond Study of Hyperfine Interactions and Structure of Matrix Isolated $^2\Sigma$ Molecules," Seminar, Dept. Chemistry, Howard Univ. Washington (10 Apr 1981).

R. J. Johns (JHMI) and B. I. Blum (APL), "Using Hospital Clinical Information Systems to Control Cost as Well as to Improve Care," 8th Annual Northeast Bioengineering Conf., M.I.T. (Mar 1980).

B. F. Kim, J. Bohandy, and F. J. Adrian, "Vibronic Transition Moments," Symp. on Molecular Spectrosopy, Ohio State Univ., Columbus (18 Jun 1981).

R. J. Klauda (APL) and W. P. Dey, R. I. Baybutt, and J. W. Schneider (Texas Instruments), "Population Dynamics of the Early Life Stages of Striped Bass in the Hudson River Estuary," 37th Northeast Fish and Wildlife Conf., Virginia Beach (20-22 Apr 1981).

R. J. Klauda (APL) and P. H. Muessig (Ecological Analysts), "Fisheries Data Sets Compiled by Utility-Sponsored Research in the Hudson River Estuary," Conf. on Hudson River Fishes, Hyde Park, N.Y. (1-2 Sep 1981).

L. C. Kohlenstein, "Planning Strategy for Power Plant Siting," Symp. on Current Energy-Related Research at the University, The Johns Hopkins Univ. Energy Research Inst., Baltimore (11 Jun 1981).

J. A. Krill, R. H. Andreo, and R. A. Farrell, "Variational and Exact Solutions for Electromagnetic Scattering from Two Randomly Separated Cylinders," 1981 CSL Scientific Conf. on Obscuration and Aerosol Research, Aberdeen Proving Ground, Md. (25 Jun 1981).

H. A. Kues (APL) and L. W. Hirst and S. A. D'Anna (JHMI), "A Specular Microscopic Study of the Effects of Microwave Radiation on the Cornea," Fortieth Scientific Meeting, Residents Assoc. of the Wilmer Ophthalmological Inst., Baltimore (6 May 1981).

H. A. Kues (APL) and L. W. Hirst and S. A. D'Anna (JHMI), "An in Vivo Specular Microscopic Study of the Effects of Microwave Radiation on the Rabbit Corneal Endothelium," 3rd Annual Conf., Bioelectromagnetics Society Meeting, Washington (10-12 Aug 1981).

J. R. Kuttler, "Bounds for Sloshing Eigenvalues by Conformal Mapping II," SIAM 1981, Rensselaer Polytechnic Inst., Troy, N.Y. (10 Jun 1981).

M. D. Lasky, "Math and Engineering," Math and Science Career Symp. for Gifted Girls, The Johns Hopkins Univ. (27 Mar 1981).

M. M. Lee and J. P. Stokes (JHU), T. O. Poehler (APL), D. O. Cowan (JHU), A. N. Bloch (Exxon Co.), and D. U. Gubser and W. W. Fuller (NRL), "Synthesis and Study of Electrochemically Grown Salts of Organic π-Donors," International Conf. on Low-Dimensional Conductors, Boulder, Colo. (12 Aug 1981).

R. E. Lee, R. Turner, and F. S. Billig, "Particulate Measurements in the APL Fuel-Rich Ramjet Combustor Supersonic-Exhaust Flow," Meeting, Western States Section, The Combustion Institute, Los Angeles (20-21 Oct 1980).

C. S. Leffel, Jr., "A Two-Year-Life Refrigerator in Space," JHU/APL Colloq. (15 May 1981).

R. E. Lenhard (JHMI) and B. I. Blum (APL), "Educational Applications of a Computer Based Clinical Information System," Meeting, American Assoc. for Cancer Education, Louisville (2-4 Oct 1980).

E. F. Lucero, "Approximate Method for Predicting Supersonic Normal Force Coefficient of Very-Low-Aspect Ratio Lifting Surfaces," 12th Navy Symp. on Aeroballistics, Carderock, Md. (12-14 May 1981).

R. A. Makofski, "Transportation in Atlantic City: The Casinos Give Better Odds," JHU/APL Colloq. (10 Oct 1980).

F. F. Mark, M. H. Friedman, C. B. Bargeron, and O. J. Deters, "Pulsatile Flow Velocity Measurements in a Cast of the Aortic Bifurcation," Joint ASME/ASCE Mechanics Conf., Univ. Colorado (22-24 Jun 1981).

J. T. Massey (APL) and A. P. Georgopoulos and J. F. Kalaska (JHMI), "Visually Guided Discrete Arm Movements in Two (X-Y) Dimensions, I. Changes during Motor Learning, II. The Effects of Spatial and Temporal Uncertainty, III. All or None or Modifiable?" 64th Annual Meeting, Federation of American Societies for Experimental Biology, Anaheim (Apr 1980).

M. T. Mattson (Normandeau Assoc.), T. J. Chambers (Texas Instruments), R. M. Shapot (Normandeau Assoc.), and R. J. Klauda (APL), "Optimum Deployment of a 3.0 m Beam Trawl for Quantitative Fisheries Sampling in the Hudson River Estuary," Conf. on Hudson River Fishes, Hyde Park, N.Y. (1-2 Sep 1981).

R. L. McCally and R. A. Farrell, "Corneal Structure Deduced from Small Angle Light Scattering and Birefringence Properties," Meeting, Assoc. for Research in Vision and Ophthalmology, Sarasota (27 Apr-1 May 1981).

R. L. McCally and R. A. Farrell, "Structural Implications of the Small Angle Light Scattering and Birefringence Properties of the Cornea," American Physical Society Meeting, Phoenix (16-20 Mar 1981).

J. B. McLaren (Ecological Analysts), R. J. Klauda (APL), and T. B. Hoff (Ecological Analysts), "Striped Bass Commercial Fishery of the Hudson River," Conf. on Hudson River Fishes, Hyde Park, N.Y. (1-2 Sep 1981).

R. A. Meyer, "Peripheral Neural Coding of Pain Sensation,"

Biennial Meeting of the Johns Hopkins Medical and Surgical Assoc., Baltimore (Jun 1981).

R. A. Meyer and M. H. Friedman, "Inequality of Membrane Reflection Coefficients for Solute and Volume Flow," 65th Annual Meeting of the Federation of American Societies for Experimental Biology, Atlanta (12-17 Apr 1981).

L. Monchick, "Anisotropic Molecular Forces and Their Influence on Transport Properties, Kinetic Coefficients and Other Molecular Cross Sections," Natuurkunde Colloq., Katholieke Univ. Nijmegen, The Netherlands (24 Nov 1980).

L. Monchick, "Modern Kinetic Theory of Polyatomic Molecules and Non-Spherical Molecular Forces," Theoretical Physics Seminar, Univ. Utrecht, The Netherlands (5 Nov 1980).

L. Monchick, "Molecular Collisions and Their Correlation with Molecular Forces," Werkbespreking Groep Molecuulfysica, Univ. Leiden, The Netherlands (4 Nov 1980).

L. Monchick, "New Developments in the Theory of Diffusion Controlled Reactions," Seminar der Statische Physik, Univ. Erlangen-Nürnberg, West Germany (20 Nov 1980).

L. Monchick, "Transport Properties of Anisotropic Molecules," 3rd European Conf. On Low Energy Molecular Collisions, Oxford Univ. (4 Sep 1980).

K. Moorjani, "Amorphous Solids," Univ. Delhi, India (5 Aug 1981); Saha Inst. Nuclear Sciences, Calcutta (18 Aug. 1981).

K. Moorjani, "Magnetic Glasses," Centre National de la Recherche Scientifique, Grenoble, France (23 Jun 1981); Indian Inst. Technology, Kharagpur, India (12 Aug 1981).

K. Moorjani, "Spin Glasses," Centre National de la Recherche Scientifique, Grenoble, France (30 Jun 1981).

K. Moorjani, "Magnetism in Disordered Solids," Seminar, Center for Materials Research, The Johns Hopkins Univ., Baltimore (8 Oct 1980).

R. E. Moos (CH2M Hill), R. J. Klauda (APL), and R. E. Schmidt (Hudosonia Ltd.), "Movements of Atlantic Tomcod in the Hudson River Estuary and Adjacent Waters," Conf. on Hudson River Fishes, Hyde Park, N.Y. (1-2 Sep 1981).

J. C. Murphy, "Photoacoustic Spectroscopy and Photothermal Microscopy," Physics Dept. Seminar, Martin Marietta Labs., Baltimore (10 Dec 1980).

V. O'Brien, "Blood Flow Dynamics," Advanced Biomechanics Seminar, The Johns Hopkins Univ. (8 Dec 1981).

V. O'Brien, "Bounds and Estimates of Second Normal Stress Difference in Rectilinear Flow," Numerical Simulation Workshop, Ross Priory, Scotland (19 May 1981).

V. O'Brien, "Flow Fields near Arterial Ring Occlusions," Biomechanics Seminar, The Johns Hopkins Univ. (18 Sep 1981).

V. O'Brien, "Flow in an Occluded Artery Model," Fluid Dynamics Division Meeting, American Physical Society, Cornell Univ., Ithaca (25 Nov 1980).

V. O'Brien, "Physics and Chemistry," Math and Science Career Symp. for Gifted Girls, The Johns Hopkins Univ., Baltimore (27 Mar 1981).

V. O'Brien, "(Pulsatile) Blood Flow," Biomedical Engineering Seminar, The Johns Hopkins Univ., Baltimore (17 Nov 1980).

V. O'Brien, O. J. Deters, F. F. Mark, and L. W. Ehrlich (APL) and K. Sagawa and G. M. Hutchins (JHMI), "Flow Fields near Arterial Ring Occlusions," Homewood Fluid Mechanics and Biomedical Engineering Seminar, The Johns Hopkins Univ., Baltimore (18 Sep 1981)

V. O'Brien and L. W. Ehrlich, "Pulsatile Flow through a Constricted Artery," 2nd Mid-Atlantic Conf. on Biofluid Mechanics, Virginia Polytechnic Inst. and State Univ. (4-6 May 1980).

J. S. O'Connor, "Development Testing of a Concrete Cold Water Pipe for Ocean Thermal Energy Conversion Systems," 3rd International Conf. on Alternate Energy Systems, Bal Harbour, Fla. (17 Dec 1980).

J. S. O'Connor, "Scale Model Structural Testing of a Lightweight Concrete Cold Water Pipe for OTEC Systems," 5th International Symp. on Concrete Technology, Univ. Nuevo Leon, Monterrey, Mexico (25 Mar 1981).

J. S. O'Connor, "The Development of a Lightweight Concrete for Ocean Thermal Energy Conversion (OTEC) Systems," International Conf. on the Performance of Concrete in the Marine Environment, St. Andrews, New Brunswick (19 Aug 1980).

D. K. Pace, "Battle Group Anti-Air Warfare Coordination Data Link Analysis," 46th Symp., Military Operations Research Society, Naval War College, Newport, R. I. (2-4 Dec 1980).

D. K. Pace, "Data Link Support for Battle Group Anti-Air Warfare Coordination (BGAAWC)," 47th Military Operations Research Soc. Symp., Fort McNair, Washington (7-9 Jul 1981).

D. K. Pace, "Opportunities for Analysis in Response to Battle Group Anti-Air Warfare Coordination," 2nd Aegis Analysts Meeting, RCA, Moorestown, N. J. (19-20 Nov 1980); 46th Symp., Military Operations Research Society, Naval War College, Newport, R.I. (2-4 Dec 1980).

P. P. Pandolfini, J. L. Keirsey, G. L. Dugger, and W. H. Avery (APL) and H. D. Foust (Trane Co.), "Alclad-Aluminum Folded-Tube Heat Exchangers for Ocean Thermal Energy Conversion," 3rd Miami International Conf. on Alternative Energy Sources, Miami Beach (15-17 Dec 1980).

P. P. Pandolfini, J. L. Keirsey, J. Funk, and R. T. Cusick, "Tests of the APL/JHU Folded Tube OTEC Heat Exchanger Core Unit," ASME Meeting, Chicago (16-18 Nov 1980).

T. E. Phillips, K. Moorjani, J. C. Murphy, and T. O. Poehler, "TiO_2-VO_2 Alloys — Reduced Bandgap Effects in the Photoelectrolysis of Water," American Physical Society Meeting, Phoenix (16-20 Mar 1981); Electrochemical Society Meeting, Denver (14 Oct 1981).

K. A. Plantz, "Battle Group Impact on Advanced Surface-to-Air Missile Design," 47th Military Operations Research Society Symp., Washington (7-9 Jul 1981).

T. O. Poehler (APL) and F. Wudl and D. Nalewajek (JHU), "Microwave Conductivity of Solid Solutions $[(TMTSF)_{1-x}(TMDTF)_x]_2PF_6$," American Physical Society Meeting, Phoenix (16-20 Mar 1981).

R. S. Potember, "Electrical Switching and Memory Phenomena in Organic Charge Transfer Complexes," Colloq., Univ. Southern Calif. (2 Dec 1980).

R. S. Potember, "Electrical Switching and Memory Phenomena in Organic Chafge Transfer Salts," Chemistry Dept. Colloq., Princeton Univ. (4 Feb 1981).

R. S. Potember, "Electrical Switching and Memory Phenomena in Semiconducting Charge Transfer Salts," Colloq., Univ. California, Berkeley (27 Jan 1981).

R. S. Potember, "Switching and Memory Effect in Charge-Transfer Complexes," Meeting, Design of Molecular Systems for Electronic Devices, Institute of Molecular Science, Okazaki, Japan (29 Nov 1980).

R. S. Potember (APL), D. O. Cowan (JHU), and T. O. Poehler (APL), "Properties of a New Polyaromatic Conductor," American Physical Society Meeting, Phoenix (16-20 Mar 1981).

R. S. Potember and T. O. Poehler, "Reversible Field Induced Phase Transition in Semiconducting Films of Copper and Silver Metal-Organic Radical-Ion Salts," 3rd Conf. on Electrical and Related Properties of Organic Solids, Wdzydze, Poland (19 Jun 1981).

R. S. Potember and T. O. Poehler (APL), A. N. Bloch (Exxon Co.), and P. Brant and F. L. Carter (NRL), "Spectroscopic Properties of Semiconducting Cu-TCNQ Films," International Conf. on Low-Dimensional Conductors, Boulder, Colo. (11 Aug 1981).

R. S. Potember and T. O. Poehler (APL) and D. O. Cowan and A. N. Bloch (JHU), "Spectroscopic and Electrochemical Properties of Semiconducting Cu-TCNQ Films," American Physical Society Meeting, Phoenix (16-20 Mar 1981).

W. R. Powell, "Energy Storage," Symp. on Current Energy Related Research at the University, The Johns Hopkins Univ. Energy Research Inst., Baltimore (11 Jun 1981).

S. E. Riblett and D. O. Cowan (JHU), T. O Poehler (APL), and A. N. Bloch (Exxon Co.), "Photoconductivity and Related Studies on Organic Semiconductors," International Conf. on Low-Dimensional Conductors, Boulder, Colo. (11 Aug 1981).

D. Richards, J. F. George, and J. S. Seward, "Design of 40-MW Grazing and Moored OTEC Pilot/Demonstration Plants," IECEC Conf., Seattle (Aug 1980).

J. C. W. Rogers, "Downstream Boundary Conditions for Incompressible Flows," Applied Mathematics Colloq., New York Univ. (3 Oct 1980); Mathematics Seminar, Univ. Arizona (20 Oct 1980); Thermo- and Gas-Dynamics Div. Seminar, NASA-Ames (28 Oct 1980); Applied Mathematics Colloq., Univ. Wisconsin, Madison (24 Mar 1981).

J. C. W. Rogers, "Numerical Solution of a Gasification Problem," Seminar, Fachbereich 19, Freie Univ., Berlin (11 Nov 1980); Numerische Behandlung Freier Randwertaufgaben, Oberwolfach, FRG (20 Nov 1980).

J. C. W. Rogers, "Numerical Solution of Hyperbolic and Parabolic Conservation Laws," Mathematics Colloq., Univ. California, Davis (21 Oct 1980); Numerical Analysis Seminar, Stanford Univ. (22 Oct 1980); Mathematics Seminar, Polytechnic Inst. of New York (29 Oct 1980); Applied Mathematics Colloq., Univ. Delaware (4 Dec 1980).

J. C. W. Rogers, "Solution of Free Boundary Problems of Hyperbolic and Parabolic Type," Applied Mathematics Seminar, Brookhaven National Labs., Upton, N.Y. (4 Jun 1981).

J. C. W. Rogers, "Solution of Stefan and Ablation Problems," Applied Mathematics Seminar, Aberdeen Proving Ground, Md. (28 Apr 1981).

J. C. W. Rogers, "The Stefan Problem with Surface Tension," Meeting on Free Boundary Problems, Montecatini, Italy (22 Jun 1981).

F. G. Satkiewicz, "Characterization of Polycrystalline, Thin-Film Silicon Solar Cells by Secondary Ion Mass Spectrometry," Gordon Research Conf. on Thin Films and Solid Surfaces, New London, N. H. (13-17 Jul 1981).

F. G. Satkiewicz, "Thin Films and Solid Surfaces," Gordon Research Conf., New London, N. H. (13-17 Jul 1981).

R. E. Schmidt (Hudsonia Ltd.), R. J. Klauda (APL), and J. M. Bartels (Hudsonia Ltd.), "Distribution and Movements of the Early Life Stages of Three *Alosa* spp. in the Hudson River Estuary with Comments on Mechanisms that Reduce Interspecific Competition," Conf. on Hudson River Fishes, Hyde Park, N.Y. (1-2 Sep 1981).

W. Seamone, "Work Table/Robotic Arm," Interagency Conf. on Employment of the Handicapped, Washington (12 Feb 1981).

W. Seamone and W. Schneider, "JHU/APL Robotic Arm/Worktable," Robotics Conf., sponsored by the Veterans Administration, Stanford Univ. (27 Aug 1981).

A. A. Shoukas, K. Sagawa, and W. L. Maughan (JHMI) and W. Ebert and J. B. Garrison (APL), "Multiple Marker Implantation for Biplane Cine Ventriculography," 53rd Scientific Session, American Heart Assoc., Miami Beach (17-20 Nov 1980).

W. J. Sternberger (APL), W. E. Woodward (NOAA), and P. A. Heinmiller (Univ. Rhode Island), "Remote Sonar Sensing of At-Sea Oil Layer Thicknesses," Oceans 81 Conf., Boston (16-18 Sep 1981).

J. P. Stokes, W. A. Bryden, J. S. Chappell, T. J. Emge, and D. O. Cowan (JHU), T. O. Poehler (APL), T. J. Kristenmacher (JHU), and A. N. Bloch (Exxon Co.), "(TMTSF) (2,5-TCNQBr$_2$): Structure and Physical Properties," International Conf. on Low-Dimensional Conductors, Boulder, Colo. (12 Aug 1981).

B. Stuckey, "Hard Kill/Soft Kill Effectiveness Analysis," 47th Military Operations Research Society Symp., Washington (7-9 Jul 1981).

R. Thorensen, K. M. Joseph, and J. J. Winterhalter (Magnavox) and J. R. Champion (APL), "Navstar GPS Receiver for Satellite Applications," AGARD 31st Guidance and Control Panel Symp., London (14-17 Oct 1980).

L. E. Tisserand, "Aerodynamics of a Rolling Airframe Missile," 12th Navy Symp. on Aeroballistics, Carderock, Md. (12-14 May 1981).

J. L. Weiss (JHMI) and R. E. Jenkins and J. B. Garrison (APL), "An Automated High-Speed Contouring System for 2-D Echocardiography," Annual Conf. on Clinical Research, Washington (Jan 1980).

AUTHOR INDEX

AUTHOR INDEX

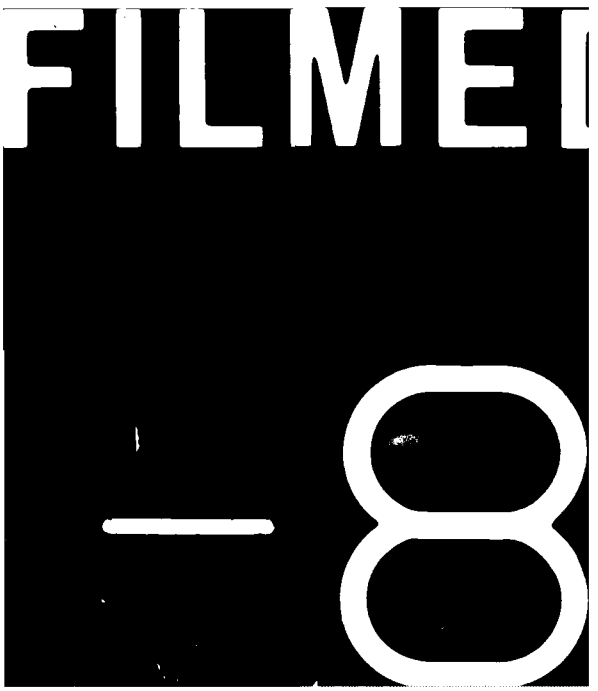
FILME
8